Enabling yeast replication in extreme cold and heat

Laman Trip, D.S.

DOI
10.4233/uuid:ff7b419c-aba7-49ed-99dd-c427762abf84

Publication date
2022

Document Version
Final published version

Citation (APA)
Laman Trip, D. S. (2022). *Enabling yeast replication in extreme cold and heat*. [Dissertation (TU Delft), Delft University of Technology]. https://doi.org/10.4233/uuid:ff7b419c-aba7-49ed-99dd-c427762abf84

Important note
To cite this publication, please use the final published version (if applicable).
Please check the document version above.

ENABLING YEAST REPLICATION IN EXTREME COLD AND HEAT

ENABLING YEAST REPLICATION IN EXTREME COLD AND HEAT

Dissertation

for the purpose of obtaining the degree of doctor
at Delft University of Technology,
by the authority of the Rector Magnificus prof. dr. ir. T. H. J. J. van der Hagen,
chair of the Board for Doctorates,
to be defended publicly on
Wednesday 8 June 2022 at 15:00 o'clock,

by

Diederik Scato LAMAN TRIP

Master of Science in Mathematics, Leiden University, The Netherlands,
born in Haarlem, The Netherlands.

This dissertation has been approved by the promotors.

Composition of the doctoral committee:

Rector Magnificus,	*chair*
Prof. dr. H. O. Youk,	University of Massachusetts, *promotor*
Prof. dr. Y. M. Blanter,	Delft University of Technology, *promotor*
Dr. G. E. Bokinsky,	Delft University of Technology, *copromotor*
Independent members:	
Prof. dr. P. A. S. Daran-Lapujade,	Delft University of Technology
Prof. dr. J. Garcia-Ojalvo,	Universitat Pompeu Fabra
Prof. dr. S. Mukherji,	Washington University in St. Louis
Dr. S. M. Depken,	Delft University of Technology
Prof. dr. N. H. Dekker,	Delft University of Technology, *reserve member*

Keywords: Yeast, temperature, reactive oxygen species, glutathione, proliferation, cooperation, lifespan, design principles, systems biology, aging, climate change

Funding: This work was supported by the European Research Council (ERC) and the Netherlands Organisation for Scientific Research (NWO)

Printed by Gildeprint

Casimir PhD Series, 2022-11

ISBN 978-90-8593-522-3

An electronic version of this dissertation is available at
`http://repository.tudelft.nl/`.

CONTENTS

SUMMARY

Open questions are whether life can be enabled in uninhabitable environments, and whether there is a limit to how much one can tune the speed of proliferation. Answering such questions has broad implications. It may reveal whether we can live in unforeseen habitats, whether we can slow down aging, and whether there are limits to lifespan. In this dissertation, we explore such questions for the budding yeast by changing the temperature. We will use temperature, a physical parameter, as a knob to tune the speed of cellular life. Temperature affects all organisms and habitats, and is of contemporary interest in light of climate change. Indeed, cells of microbes, plants and cold-blooded animals often endure temperatures that can be considered extreme. For reference, budding yeast lives comfortably at 30 °C and has a doubling time of roughly 1.5 hours – the time a cell needs to grow and divide into two cells. During our studies, we will elucidate the common principles that govern the life of yeast at extreme temperatures – how a cell survives, grows, replicates, ages, and dies. We combine models, experiments and measurements of single cells and at a molecular level, and integrate these into a systems-level view of the life of yeast at extreme temperatures.

In **Chapter 2**, we reveal how yeast cells – conventionally viewed as autonomous organisms – help each other and their future generations to survive and replicate at high temperatures (38 °C – 41 °C). Cells do so by exporting an antioxidant (glutathione) to their environment, which serves a common good for the population. We demonstrate that such cooperation yields surprising behaviors: at the same high temperature, a population can continuously grow, never grow, or grow after an unpredictable amount of time (hours to days), depending on its population density. Moreover, cells in a population that never grows can collectively delay their approach to extinction. We summarize these behaviors in a "phase diagram" that reveals when populations grow, and when they go extinct as function of temperature and population density. We show that cells can only survive and proliferate at high temperatures when the population exports sufficient glutathione to its environment. Thus, the habitability of temperature for yeast emerges from the community instead of from the individual. This study is one of the first demonstrations of cells cooperatively fighting rising temperatures.

In **Chapter 3**, we uncover unbeatable "speed limits" for the life of yeast at near-freezing temperatures (0 °C – 5 °C). These speed limits are the slowest and fastest possible speeds for yeast to grow and replicate – a cell does not survive if it replicates slower

than the minimum speed at each temperature. We show that cells die and cannot replicate at near-freezing temperatures primarily because of Reactive Oxygen Species (ROS). Removing these ROS largely prevents deaths and enables cells to replicate. We use this intervention to reconstruct the life of a typical yeast cell at near-freezing temperatures. By observing individual cells from their birth to their death, we reveal months-long lifespans, weeks-long cell-cycle durations, and the dynamics of transcription and protein synthesis. These measurements together uncover the origin of the speed limits: they emerge from an interplay between the protein-synthesis rate and the abundance of intracellular ROS. We demonstrate that tuning this interplay can accelerate a cell's life and enable more cells to proliferate at near-freezing temperatures. To our knowledge, this study establishes one of the first fundamental constraints to slowing down a biological clock.

Together, these studies uncover quantitative, fundamental principles of cellular life. They establish that yeast cells, by working together, can thrive in habitats that are considered unlivable, and that there are limits to how much one can tune their speed of life. Our discoveries raise the question of whether such principles and limits generalize to other microbes and cells of other organisms. Moreover, they encourage further studies of temperature's role in an organism's speed of replicating, aging and lifespan.

SAMENVATTING

Open vraagstukken zijn of we leven mogelijk kunnen maken in onbewoonbare gebieden, en of er grenzen zijn aan het beïnvloeden van de snelheid van voortplanting. De antwoorden op zulke vragen kunnen verstrekkende gevolgen hebben. Het kan aantonen of we kunnen leven in gebieden die we niet voor mogelijk hielden, of we veroudering kunnen vertragen, en of er grenzen zijn aan ouderdom. In deze dissertatie onderzoeken we zulke vragen voor bakkersgist door de temperatuur te veranderen. We gebruiken de temperatuur, een fysische parameter, als een knop om de snelheid van het leven van cellen aan te passen. Temperatuur heeft effect op alle organismen en leefgebieden, en is actueel vanwege klimaatverandering. Cellen van micro-organismen, planten en koudbloedige dieren worden bijvoorbeeld vaak blootgesteld aan extreme temperaturen. Ter illustratie leeft bakkersgist het liefste bij 30 °C en heeft dan een delingstijd van ongeveer 1.5 uur – de tijd die een cel nodig heeft om te groeien, in tweeën te delen, en zich daarmee voort te planten. Tijdens deze studies onthullen we algemene principes die het leven van gist bepalen bij extreme temperaturen – hoe een cel kan overleven, groeien, delen, ouder worden en sterven. We combineren modellen, experimenten en metingen van individuele cellen en op een moleculair niveau, en verenigen alles in een systematisch beeld van het leven van gist bij extreme temperaturen.

In **Hoofdstuk 2** onthullen we hoe gistcellen – die gezien worden als zelfstandige organismen – elkaar en toekomstige generaties helpen te overleven en te delen bij hoge temperaturen (38 °C – 41 °C). De cellen doen dit door collectief een antioxidant (glutathion) uit te scheiden, wat het algemeen nut dient van de populatie. We laten zien dat deze samenwerking tot verrassend gedrag leidt: bij dezelfde, hoge temperatuur kan een populatie continu groeien, niet groeien, of groeien na een onvoorspelbare tijd van uren tot dagen, afhankelijk van het aantal cellen in de populatie (de dichtheid). Bovendien kunnen cellen in een populatie die niet groeit, samen hun uitsterven vertragen. We vatten dit gedrag samen in een "fasediagram", dat als functie van de temperatuur en de dichtheid van cellen illustreert welke populaties kunnen groeien en welke zullen uitsterven. We tonen aan dat cellen alleen kunnen overleven en delen bij hoge temperaturen als de populatie genoeg glutathion uitscheidt in zijn omgeving. De leefbaarheid van hoge temperaturen wordt voor gist dus bepaald door de gemeenschap en niet door het individu. Dit onderzoek is een van de eerste voorbeelden van cellen die samen tegen stijgende temperaturen vechten.

In **Hoofdstuk 3** ontdekken we onoverkomelijke "snelheidslimieten"voor het leven van gist bij lage temperaturen (0 °C – 5 °C). Deze snelheidslimieten zijn de minimum en maximum snelheden waarmee gist kan groeien en delen – een cel kan niet overleven als zij zich langzamer deelt dan de minimum snelheid. We tonen aan dat reactieve zuurstof componenten (ROS) de voornaamste reden zijn dat cellen zich niet kunnen delen en, als gevolg, overlijden bij lage temperaturen. Het verwijderen van deze ROS voorkomt celdood en maakt celdeling mogelijk. We gebruiken deze interventie om het leven van een typische gistcel bij lage temperaturen te reconstrueren. Door individuele gistcellen van hun geboorte tot hun dood te observeren, onthullen we een maandenlange levensduur, wekenlange fasen van de celcyclus, en de dynamiek van transcriptie en eiwit synthese. Deze metingen leggen samen de oorsprong van de snelheidslimieten bloot: deze ontstaan uit een wisselwerking tussen de snelheid van eiwit synthese en de hoeveelheid ROS in een cel. Door deze wisselwerking te manipuleren, laten we zien dat het leven van een cel versnelt kan worden en dat meer cellen zich kunnen delen bij lage temperaturen. Dit onderzoek stelt een van de eerste fundamentele beperkingen vast voor het vertragen van een biologische klok.

Samen beschrijven deze onderzoeken kwantitatieve, fundamentele principes voor het leven van cellen. Ze tonen aan dat gistcellen kunnen gedijen in leefomgevingen die we niet mogelijk achtten, en dat er limieten zijn aan het beïnvloeden van de snelheid van het leven. Deze ontdekkingen roepen nieuwe vragen op, bijvoorbeeld of zulke principes ook voor andere micro-organismen en voor cellen van organismen in het algemeen gelden. Bovendien zijn deze ontdekkingen een aanmoediging voor verdere studies naar de rol van temperatuur in de snelheid van voortplanting, veroudering en de levensduur van een organisme.

1

INTRODUCTION

Temperature is perhaps the most important physical parameter affecting all cellular life [1]. Indeed, cell replications become slower when the temperature changes to less optimal values, and cells seize to replicate and may die if the temperature goes outside the range of a cell's habitable temperatures (Fig. 1.1a) [1]. Thus, we can use temperature as a knob to tune the speed of cellular life. A fundamental question is how environmental conditions such as temperature and countless biochemical reactions dictate the speed at which an organism's life progresses – how fast a cell moves through its cell cycle, how fast a cell approaches death, and whether a cell can live in a given habitat at all. Answering this question is important for understanding a cell's ability to proliferate and whether limits exist for the speed of proliferation, slowing down aging and extending lifespan. We explore these ideas for the budding yeast *Saccharomyces cerevisiae* by changing temperature.

The conventional views on proliferation at extreme temperatures. A reasonable requirement for cells to remain alive and proliferate is liquid water, thereby setting the boundaries for livable temperatures at earth's surface roughly between the formation of ice at 0 °C and the boiling of water at 100 °C, with microorganisms such as yeast typically having a habitable range spanning 40 °C [1]. The textbook view on unicellular microbial life states that sufficiently extreme temperatures, outside the habitable range, prevent yeast from proliferating through failure of key intracellular factors or processes. However, the known factors or processes that fail and the reasons why they fail are very different at high and low temperatures. At high temperatures, the conventional view states

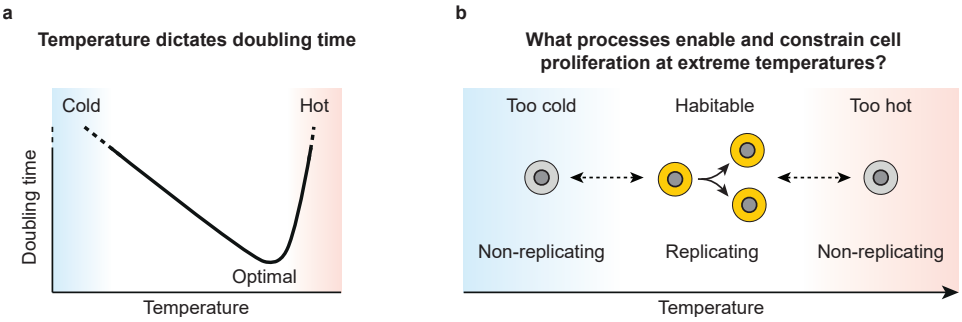

Figure 1.1: Temperature dictates the speed of replications, with proliferation stopping as temperature becomes too extreme. **(a)** As physical parameter, temperature dictates a cell's doubling time. Cell replications slow down when the temperature changes to sub-optimal values and cells stop replicating and may die when temperature becomes too extreme (too hot or too cold to be habitable [1]). **(b)** Question central to this dissertation: what biophysical processes enable and constrain cell proliferation at extreme temperature?

that crucial proteins unfold and heat-induced damages occur that prevent proliferation [2–6]. At near-freezing temperatures, popular views argue that cells cannot proliferate because essential processes occur too slowly to sustain life [1, 7–9], and due to physical damages such as stiff membranes and oxidative damages [1, 9–16].

Each of these views proposes specific genes, stress responses and mechanisms as reasons that cells fail to proliferate. However, beyond such particular mechanisms, we still poorly understand the principles that together dictate and constrain yeast's life at extreme temperatures [2–5, 10, 11, 17, 18]. A temperature that prohibits proliferation of one cell could still permit proliferation of another, genetically identical cell – for example through stochastic cell-to-cell variations leading to different responses to environmental conditions and stress [19–23]. Moreover, the behavior of one cell also affects the lives of other cells, since cells share their extracellular environment and, at the very minimum, consume from the same pool of available nutrients. Thus we currently lack a systems-level view for life that shows how the environment and multiple intracellular processes collectively determine how a cell survives, grows, replicates, ages and dies at extreme temperatures. We sought to uncover such a systems-level view and re-examine the conventional picture, leading to the theme that is central to this dissertation (Fig. 1.1b):

What biophysical processes enable and constrain cell proliferation at extreme temperatures?

Uncovering design principles that govern cellular life at extreme temperatures. In this dissertation, we quantify the effect of extreme temperatures on budding yeast on the single-cell and genome-wide level, and combine our findings into a unified, systems-level view.

In **Chapter 2**, we show that cells work together to collectively survive and replicate at high temperatures. As a surprising consequence, a population only grows at high temperatures when there are enough cells working together: for the same temperature, a yeast population can exponentially grow, never grow or grow after an unpredictable amount of time, depending on its population density. The populations that never grow collectively delay their approach to extinction. These features arise from yeasts secreting and extracellularly accumulating glutathione, an ubiquitous antioxidant. We show that secreting glutathione is both necessary and sufficient for yeasts to collectively survive and proliferate at high temperatures. A mathematical model recapitulates all these features. Finally, we demonstrate that cells can, in fact, replicate at high temperatures that would conventionally be considered unlivable.

In **Chapter 3**, at near-freezing temperatures, we show that yeast exhibits a collective growth using glutathione that is similar to high temperatures. We show that cells die and cannot replicate at near-freezing temperatures primarily because of abundant intracellular Reactive Oxygen Species (ROS). Removing these ROS largely prevents deaths, and enables and accelerates cell replication. By removing ROS, we measure single cells' lifespans, days-to-months-long cell-cycle durations, protein-synthesis rates, and genome-wide transcription rates. A mathematical model that integrates these measurements reveals that the protein-synthesis rate and ROS abundance together impose speed limits for life at near-freezing temperatures – shortest and longest possible doubling times. Consequently, a cell must replicate at a minimum speed or face a certain death at near-freezing temperatures.

Together, these studies establish common design principles for a cell's survival and proliferation at extreme temperature.

2

COLLECTIVE GROWTH AND SURVIVAL AT HIGH TEMPERATURES

The conventional view is that high temperatures cause microbes to replicate slowly or die. In this view, microbes autonomously combat heat-induced damages. Yet, microbes co-exist with each other, raising the underexplored and timely question of whether they can cooperatively combat heat-induced damages at high temperatures. Here we use budding yeast to show that cells can help each other and their future generations survive and replicate at high temperatures. As a surprising consequence, even for the same temperature, a yeast population can either exponentially grow, never grow, or grow after unpredictable durations (hours-to-days) of stasis, depending on its population density. Through the same mechanism, yeasts collectively delay and can eventually stop their approach to extinction, with higher population-densities stopping faster. These features arise from yeasts secreting and extracellularly accumulating glutathione - a ubiquitous heat-damage-preventing antioxidant. We show that secreting glutathione, which eliminates harmful extracellular chemicals, is both necessary and sufficient for yeasts to collectively survive high temperatures. A mathematical model, generally applicable to any cells that cooperatively replicate by secreting molecules, recapitulates all these features. Our study demonstrates how organisms can cooperatively define and extend the boundaries of life-permitting temperatures.

This chapter has been published as: D. S. Laman Trip, H. Youk, *Yeasts collectively extend the limits of habitable temperatures by secreting glutathione*, **Nature Microbiology**, 5, 7, p. 943-954 (2020)

2.1. INTRODUCTION

Microbes live in a range of "habitable temperatures" [1, 24, 25]. The conventional view is that increasing the temperature above some optimal value causes microbes to take more time to replicate and that once the temperature goes beyond the habitable range – into an "unlivable temperature" regime – microbes cannot replicate and they die [1, 24–26] (Figs. 2.1a-b). In this textbook view, a microbe's ability to replicate at high temperatures hinges on whether the cell, by itself, can combat heat-induced damages such as misfolded proteins [2–5]. A cell is unable to combat these damages at sufficiently high temperatures, leading to its death (Fig. 2.1c). Yet a microbe often lives with other cells instead of alone, enabling them to work together for their collective survival [27–31]. Given the timeliness of understanding how the rising global temperatures affect organisms, we used the budding yeast, *Saccharomyces cerevisiae*, to re-examine the conventional picture – one in which yeasts autonomously combat heat shocks – to investigate whether microbes can also collectively combat high temperatures to avoid becoming extinct (Fig. 2.1d).

As our starting point, we reproduced the well-known, textbook picture of how temperature affects microbial growths by measuring the population-level growth rates for a laboratory-standard ("wild-type") strain of haploid budding yeast in liquid cultures [6, 26, 32, 33] (Fig. 2.1b, Supplementary Figs. S2.1-S2.2). In this picture, the population growth rate is zero for temperatures of 40 °C and higher (Fig. 2.1b, Supplementary Fig. S2.1). Despite being evidently true – as we reproduced it here – we discovered that this textbook picture is misleading and requires a revision. Here, we revise this picture with experiments and a mathematical model, which reveal that, at sufficiently high temperatures, yeasts secrete and extracellularly accumulate glutathione – a major antioxidant for many species – that cleanses the extracellular environment of harmful reactive oxygen species whose high reactivity is damaging for cells. Thus, we discovered that yeasts help each other and their future generations to replicate, survive, and avoid becoming extinct at high temperatures (Fig. 2.1d). Our work thereby demonstrates the habitability of a temperature for a single-celled organism emerging as a community-level property, determined by interactions among the members of the microbial community.

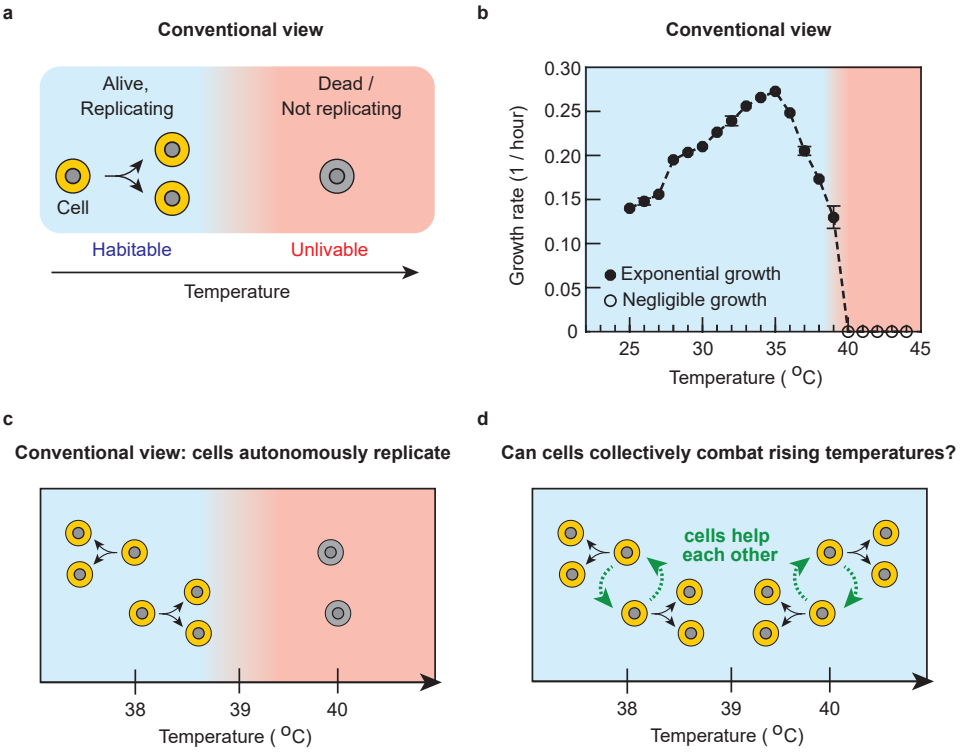

Figure 2.1: Conventional, cell-autonomous view of temperature-dependent cell-replication. **(a)** The conventional view states that cells autonomously replicate at "habitable temperatures" (blue region) and that at sufficiently high temperatures (i.e., "unlivable temperatures"), cells fail to replicate and can eventually die (red region). **(b)** Growth rate as a function of temperature for populations of wild-type yeast cells. Black data points in the blue region are for populations with sustained, exponential growth over time and white data points in the red region are for populations with negligible, non-exponential growth (error bars represent the mean with s.e.m., having $n = 3$ replicates per data point). The boundary between blue and red regions is near 39 °C. (Also see Supplementary Figs. S2.1-S2.2). **(c)** The conventional view (explained in (a)) applied to budding yeast, based on the data in (b). **(d)** Question that we investigated in our study: can microbes collectively combat rising temperatures so that they can turn a temperature that is unlivable (e.g., 40 °C shown in (c)) into a habitable temperature?

2.2. RESULTS

Population-density determines replicability of cells and habitability of temperature. We re-examined the conventional, cell-autonomous picture by incubating populations of wild-type yeasts in liquid media at a conventionally-defined habitable temperature (~38 °C), unlivable temperature (~40 °C), and a transition temperature in between the two (~39 °C). This time, and in contrast with the conventional picture (Supplementary Fig. S2.1), we precisely set the initial population-density (# of cells / mL) and studied its effect on population growth. With a flow cytometer, we counted the integer number of cells per volume to determine the population densities over time. These experiments revealed surprising behaviors. Specifically, at the supposedly habitable temperature of ~38 °C, none of the replicate populations that started with a relatively low population-density (initially ~200 cells / mL) grew at all during ~12 days of incubation except for a small, transient growth that occurred for a few hours right after the transfer from 30 °C (Fig. 2.2a – red curves). At the same temperature (~38 °C), setting the population-density to be just five times larger (initially ~1,000 cells / mL) yielded a population whose behavior was completely unpredictable: it could either grow until it reached the carrying capacity (i.e., $\sim 10^7$ cells / mL) or not grow at all after the initial transient-growth (Fig. 2.2a – green curves). When the population did grow, it could wait four days, eight days, or some other, unpredictable time before starting to grow (Fig. 2.2a – multiple green curves). Still, at the same temperature (~38 °C), setting the population-density to be again just five times larger (initially ~5,000 cells / mL) yielded populations that always grew exponentially and identically over time up to the carrying capacity (Fig. 2.2a – blue curves). Thus, at the supposedly "habitable" temperature of 38 °C, only the largest of the three initial densities led to the deterministic growth that the conventional picture states should be exhibited by every population [1, 6, 32, 33]. The same three, population-density-dependent growth behaviors also occur near the upper limit of the habitable temperatures (~39 °C) (Fig. 2.2b). Moreover, we found that populations with sufficiently many cells can grow at ~40 °C – a supposedly "unlivable" temperature (Fig. 2.2c – blue curves). These results show that in order to determine whether a yeast-population grows or not, one must know both the temperature and its initial density.

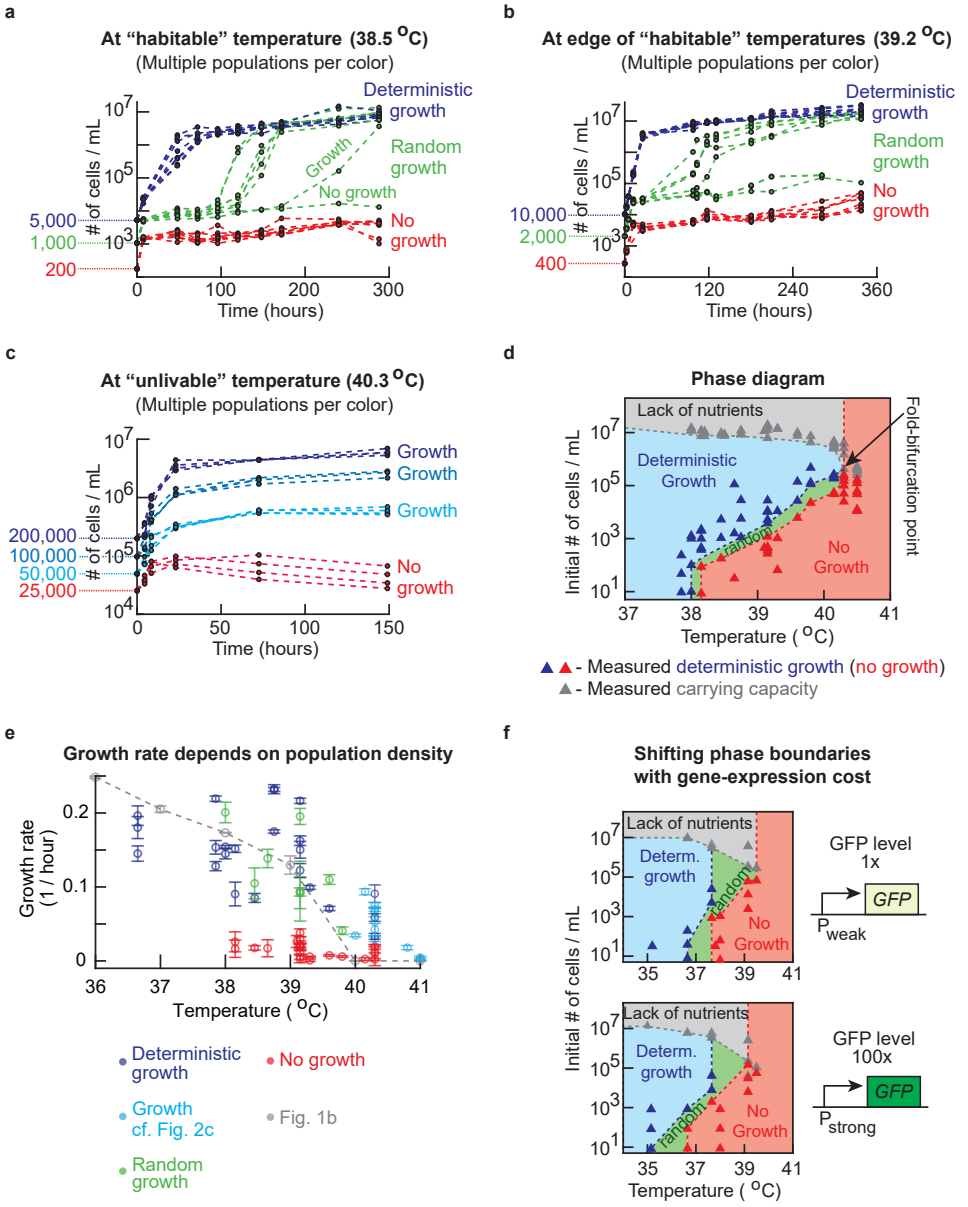

Figure 2.2: Population-density determines replicability of cells and habitability of each temperature. **(a-c)** Population-density (number of cells / mL) measured over time with a flow cytometer for populations of wild-type yeast of differing initial population-densities at **(a)** a conventionally-defined habitable temperature (38.4 °C), **(b)** near the edge of conventionally-defined habitable and unlivable temperatures (39.2 °C) and **(c)** at a conventionally-defined unlivable temperature (40.3 °C). Figure 2.1b sets the conventional definition of temperature's habitability. Each color in (a-b) shows $n = 8$ populations that start with the same density. Red curves show no population growth beyond initial transient growth (i.e., "no growth"). Green curves show unpredictable growth (i.e., "random growth"). ***(caption continues on the next page)***

Figure 2.2 ***(caption continued from the previous page):*** Blue curves show deterministic, exponential growth where all populations grow identically (i.e., "deterministic growth"). Each color in (c) shows $n = 4$ populations with the same initial density. All colors except red show growth by ~10-fold. **(d)** Phase diagram constructed from measurements. Colors of regions and triangles represent the behaviors mentioned in (a-b) – blue marks deterministic growth, green marks random-growth, red marks no-growth, and grey marks populations not growing as they have more cells than the carrying capacity. Each triangle represents an experiment of the type shown in (a-c). (Also see Supplementary Figs. S2.3-S2.4 for details). **(e)** Growth rates of populations in the no-growth phase (red), random-growth phase (green) and deterministic-growth phase (blue) as a function of temperature. Error bars represent the mean with s.e.m., having $n = 6$ or more replicates per data point for temperatures below 40 °C, and $n = 3$ biological replicates for temperatures above 40 °C. Grey data are from Figure 2.1b. **(f)** Phase diagrams constructed for engineered yeast strains that constitutively express GFP at the indicated levels (1x and 100x). Triangles indicate experimental data. Compare the 1x-GFP strain with the 100x-GFP strain only, since genetic background of the GFP-expressing strains is slightly different from the wild-type. (Also see Supplementary Fig. S2.5).

Phase diagram summarizes population-level behavior across temperatures. By incubating liquid cultures of populations with differing initial densities at multiple temperatures, we constructed a "phase diagram" of population behaviors (Fig. 2.2d and Supplementary Figs. S2.3-S2.4). The phase diagram, summarizing the population-level growth behaviors, consists of four phases – deterministic growth, random growth, no-growth, and no-growth due to insufficient nutrients – as a function of the initial population-density and temperature. It reveals that the conventional picture (Figs. 2.1b-c) mistakenly arises because one typically sets the initial population-density to lie within some narrow range when studying population growth. This leads to, for example, the growth rate appearing to decrease as the temperature increases within a given range (e.g., 36.5 °C 39 °C) (Fig. 2.1b). But, in fact, for the same temperature range, we found that the populations' growth rates – when they grew – were poorly correlated with temperature and could highly vary among populations even for the same temperature if we widely varied the initial population-density (Fig. 2.2e). The phase boundary between the deterministic-growth and random-growth phases (Fig. 2.2d) describes the minimum, initial population-density to guarantee that a population grew at each temperature. Conversely, the phase boundary between the random-growth and no-growth phases (Fig. 2.2d) describes the maximum, initial population-density to guarantee that a population never grew at each temperature. Both of these values are highly sensitive to temperature (e.g., a ~100-fold change when going from 39 °C to 40 °C (Fig. 2.2d)). The random-growth phase may be seen as a hybrid of the deterministic-growth and no-growth phases. A small change of either can transform a no-growth into a deterministic-growth and vice-versa (Fig. 2.2a). Intriguingly, all phase boundaries converge at a single point (a "fold-bifurcation point") located at 40.3 °C, leading to only the no-growth phase at temperatures beyond 40.3 °C (Fig. 2.2d). Specifically, at temperatures above 40.3 °C, populations can grow but stop growing before reaching

the carrying capacity, with their final population-densities depending on their initial population-densities. The term "fold-bifurcation point" comes from dynamical systems theory and is the point in the phase diagram where a stable fixed point (the carrying capacity) merges with an unstable fixed point (the upper boundary of the no-growth phase).

Expressing a superfluous gene reshapes phase diagram. We discovered that forcing yeasts to constitutively express the Green Fluorescent Protein (GFP), which serves no function for cell growth, shifts the phase boundaries (Fig. 2.2f, Supplementary Fig. S2.5). In particular, reducing the expression of GFP could shift the phase boundaries by several degrees Celsius, suggesting that the cost of expressing superfluous genes can markedly alter the phase diagram. In light of previous studies [34, 35], this may be due to expressing GFP shifting intracellular resources away from performing roles that are for cell growth, while these resources may be especially crucial for surviving high temperatures. While these experiments revealed genetic means for reshaping the phase diagram, we leave the molecular mechanisms that underlie the shape of the phase boundaries for future studies.

A few cells initiate population growth in random-growth phase and transiently replicating sub-populations exist in non-growing populations. We turned to single-cell-level measurements for further insights. The wild-type strain has a mutated *ade2* gene that causes a cell to accumulate a red pigment, which can only be removed through dilution by cell division [36]. Thus, we could use a flow cytometer's red-fluorescence detector to determine which cells had been replicating and which cells had not (Supplementary Fig. S2.6). For a deterministically growing population, we discovered that, after a short transient growth associated with the transfer from 30 °C to the high temperature, the number of replicating cells exponentially increased over time up to the carrying capacity (Supplementary Fig. S2.6). In contrast, for random-growth and no-growth populations, the number of replicating cells typically decreased until very few remained ($\sim 1-5\%$ of population). Subsequently, the number of replicating cells either spontaneously increased by orders of magnitude after an unpredictable hours or days (random-growth) or remained sustainably low and fluctuated by few-folds over nearly a week (no-growth) (Supplementary Fig. S2.6). These fluctuations were sufficiently small that the total cell density remained nearly constant. These results establish that a small sub-population of transiently replicating cells exist in random-growth and no-growth populations, and that the fraction of replicating cells in these populations could stably remain in low numbers (e.g., ~1% of total population). We will later return to these features with a mathematical model that recapitulates them.

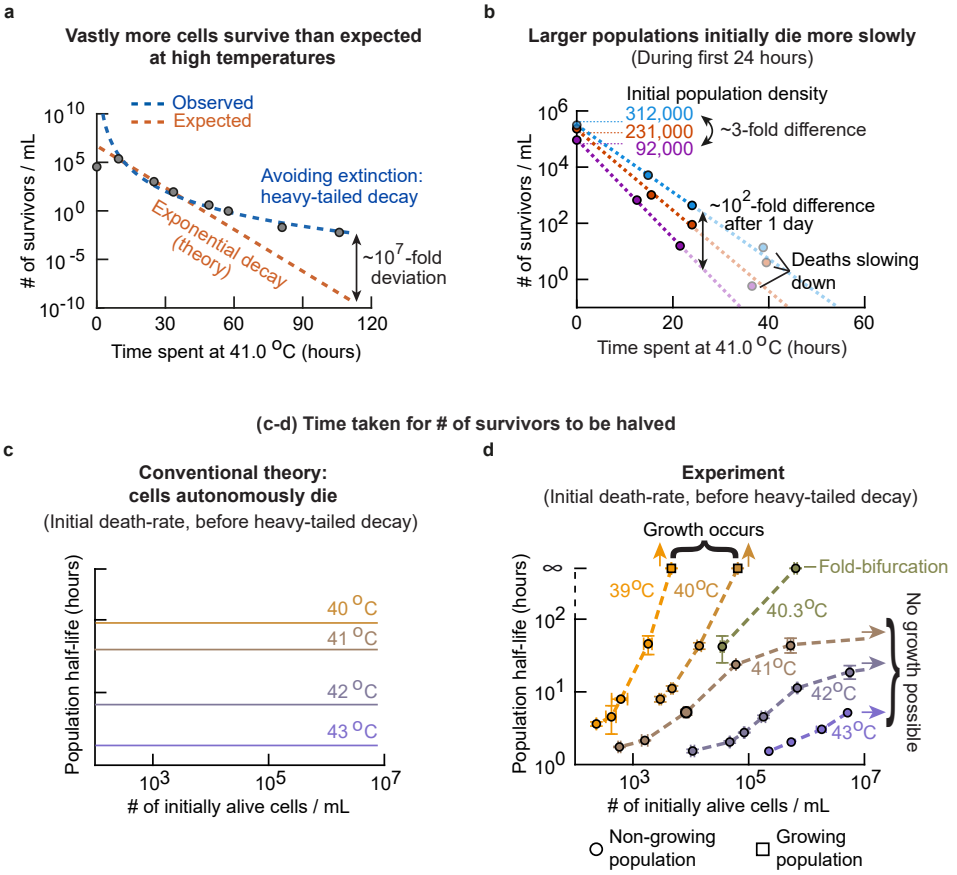

Figure 2.3: Cells collectively combat death to avoid population extinction at high temperatures. **(a)** The number of survivors / mL (circles) over time in a non-growing, wild-type population at 41.0 °C. Orange line is an exponentially decaying function fitted to the first three data points (between 10 and 40 hours). Blue curve is a power-law function fitted to the same data points. (Also see Supplementary Fig. S2.7). **(b)** Number of survivors / mL for three populations of differing initial densities at 41.0 °C, measured as in (a). Initial densities after transient growth were ~92,000 cells / mL (purple), ~231,000 cells / mL (orange), and ~312,000 cells / mL (blue). Dashed lines represent an exponentially decreasing function fitted to the first three time points. (Also see Supplementary Fig. S2.7). **(c)** Cartoon illustrating the conventional view which states that cells autonomously die and that every cell has the same probability of dying per unit time. This means that the population half-life is independent of the initial population-density at each temperature. Different colors represent different temperatures. **(d)** Population half-life as a function of initial density, based on fitting an exponentially decreasing function to the number of survivors / mL measured during the first 24 hours of incubation (after ~20 hours of transient growth due to cells coming from 30 °C and adjusting to the new temperature). Each color shows the half-lives of populations at different temperatures, indicating 39.2 °C, 40 °C, 40.3 °C, 40.8 °C, 42 °C and 43 °C. Error bars represent the mean with s.e.m., having $n = 3$ replicates per data point. Circles represent populations in the no-growth phase. The two squares (at 39.2 °C and 40 °C) represent populations that grew due to having sufficient population-densities to trigger their own growths (Fig. 2.2d).

Cells collectively combat extinctions at high temperatures. We next asked whether cell death, like cell replication, also depends on the initial population-density. At several temperatures, we measured how the number of surviving cells changed over time for no-growth populations (Supplementary Fig. S2.7). Surprisingly, these measurements deviated qualitatively from the textbook picture in which microbes such as yeasts autonomously die and in which the number of survivors should exponentially decrease over time [26] (Fig. 2.3a – orange line). Yet, we discovered that the number of survivors decreases over time in a heavy-tailed (power-law-like) manner (Fig. 2.3a – blue curve). In other words, the population continuously decelerates, and eventually would cease, its approach to extinction. For example, after three days at 41 °C, the number of survivors in a population deviated by $\sim 10^7$-fold from the expected value dictated by the conventional theory (Fig. 2.3a – last time point; Supplementary Fig. S2.7). Moreover, we discovered that the rate at which cells die at high temperatures depends on the initial population-density (Fig. 2.3b and Supplementary Fig. S2.7). Specifically, the number of survivors appears to exponentially decrease during the first day before it noticeably enters a heavy-tailed decay regime on later days (Fig. 2.3b). Hence, we can assign a constant rate of decay to each population to describe how the number of survivors initially decreases (e.g., during the first day at a high temperature). We found that this rate ("initial death-rate") decreases as the initial population-density increases, such that the number of survivors decreases more slowly for higher initial population-densities (Fig. 2.3b – three dashed lines). These results suggest a highly non-linear, cooperative effect that cells have on each other's survival.

Temperature of the fold-bifurcation point separates two extinction-avoidance regimes. We next measured the initial death-rate at multiple temperatures for populations of differing initial densities. The population half-life, which is derived from the initial death-rate and is the time taken for the number of survivors to be halved, should be independent of the initial population-density, according to the conventional view in which yeasts autonomously die (Fig. 2.3c). Instead, we discovered that increasing the initial population-density always increases the population half-life and that the temperature determines how sensitively the population half-life depends on the initial population-density (Fig. 2.3d). Specifically, a population half-life has two regimes of sensitivities. Temperatures below 40.3 °C exhibit the first regime. Here, the population half-life is highly sensitive to the initial population-density: it increases from hours to days if the initial population-density nearly doubles (Fig. 2.3d – yellow curves for 39 °C and 40 °C). Moreover, as the initial population-density keeps increasing, the population half-life keeps increasing and eventually becomes infinite. This is because a sufficiently high-density population grows at these temperatures (Fig. 2.2d). Temperatures above

40.3 °C exhibit the second regime: increasing the initial population-density above some value hardly changes the population half-life, and eventually plateaus at a finite value as the initial population-density keeps increasing (Fig. 2.3d – purple curves for 41 °C ~ 43 °C). This occurs because populations cannot grow regardless of their initial densities at these temperatures (Fig. 2.2d). At the fold-bifurcation point (Fig. 2.2d), the density of survivors can remain at a nearly constant value (i.e., the population half-life is infinite because the initial death-rate is zero). The fold-bifurcation point is the only place in the phase diagram (at 40.3 °C with $\sim 1 \cdot 10^5$ cells / mL) at which a non-growing population's half-life is infinite. In other words, a population at the fold-bifurcation point can constantly maintain its density of survivors, apparently indefinitely, unless fluctuations cause its demise. Taken together, our results establish that a yeast's death depends on the other cells in the population. Moreover, we determined that neither heat-resistant mutants nor "persister-like" cells such as those seen in antibiotic persistence [37] can explain our data on cell deaths (Supplementary Fig. S2.8).

Extracellular factor dictates cell replication at high temperatures. We next sought to uncover the mechanisms that underlie the density-dependent cell replication and death of yeasts. As a start, we determined that cells isolated from a growing culture and put into a fresh medium do not grow, whereas the liquid medium isolated from an exponentially growing population and transplanting a fresh population of cells into it causes that population to grow, even though the phase diagram indicated that the population initially had too few cells for it to grow (Fig. 2.4a-c, Supplementary Figs. S2.9-S2.10). These results suggested that some factor(s) dictating population growth reside in the extracellular – not intracellular – environment. Moreover, we confirmed that depletion of any of the nutrients does not cause a population to grow (Supplementary Figs. S2.10-S2.11), indicating that it is the secretion of some factor(s) at high temperatures that induces population growth.

Yeast cells secrete glutathione to help each other replicate at high temperatures. By performing a transcriptome analysis (RNA-seq) on wild-type yeast populations at different locations in the phase diagram (Supplementary Fig. S2.12), we uncovered gene-expression profiles that are similar to those of yeasts undergoing environmental stresses [38, 39]. We hypothesized that yeast cells at high temperatures may be stressed due to reactive oxygen species, which are known to be abundant at high temperatures [40–42] and damaging for cells [43–45]. Given that antioxidants inactivate reactive oxygen species, we further hypothesized that the cells may be secreting antioxidants at high temperatures.

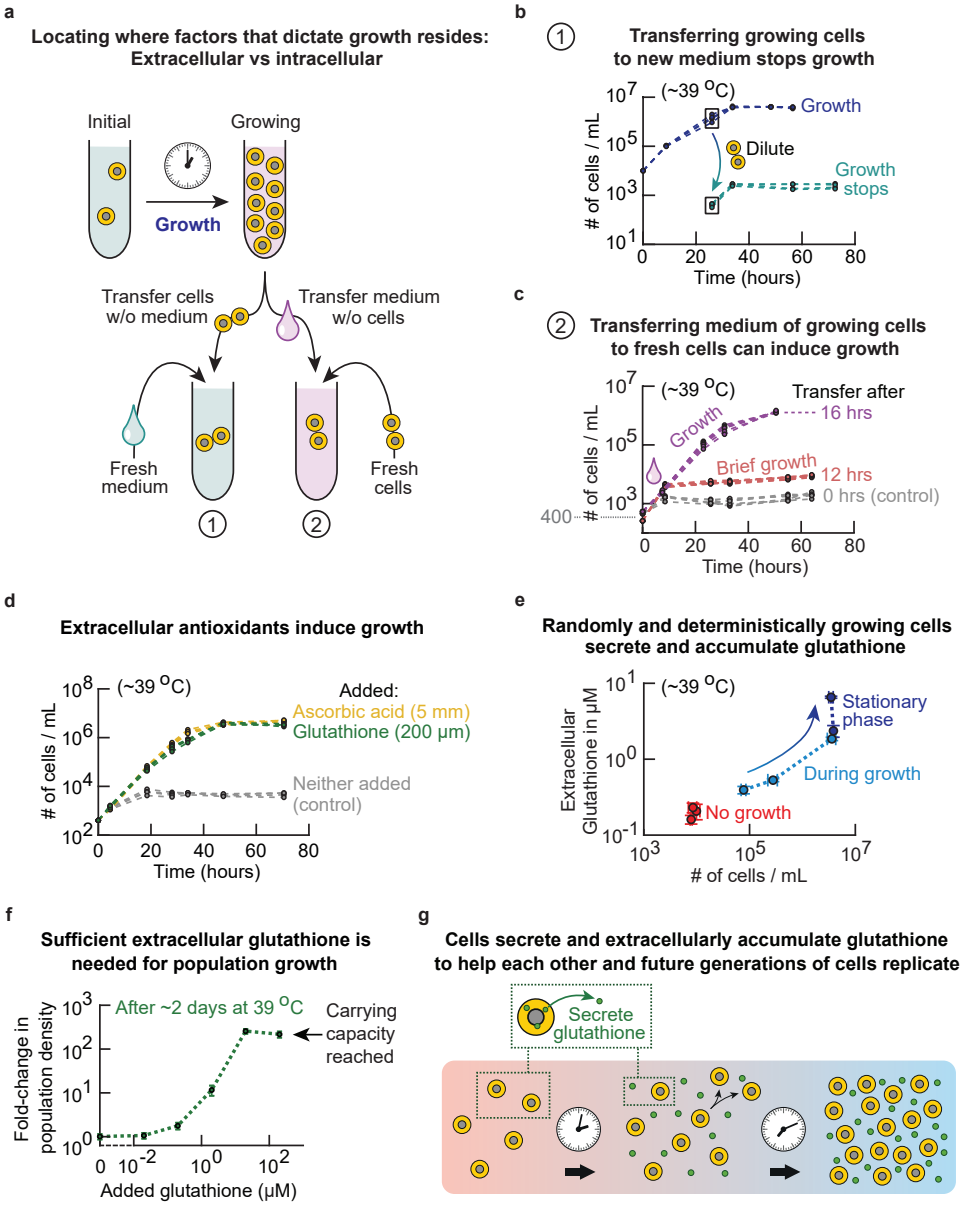

Figure 2.4: Cells secrete and extracellularly accumulate glutathione to help each other and future generations of cells replicate at high temperatures. **(a)** Schematic description of experiments in (b) and (c) to determine whether intracellular ("1") or extracellular ("2") factors dictate population growth. **(b)** At 39.2 °C. Labelled "1" in (a): wild-type cells were transferred (boxed data point) from log-phase populations (blue curves, initially ~10.000 cells / mL) to fresh medium (green curves, initially ~400 cells / mL). Each color shows $n = 4$ replicate populations. (Also see Supplementary Fig. S2.9). **(c)** At 39.2 °C. Labelled "2" in (a): fresh cells from 30 °C were incubated in a growth medium that previously harbored log-phase cells at ~39 °C for 0 hours (grey curves), 12 hours (red curves) or 16 hours (purple curves). Each color shows at least $n = 6$ replicate populations. (Also see Supplementary Fig. S2.10). ***(caption continues on the next page)***

Figure 2.4 ***(caption continued from the previous page)*****: (d)** No-growth populations (initially ~400 cells / mL) at 39.2 °C. Adding either ascorbic acid (5 mM – yellow curves) or glutathione (200 μM – green curves) to the growth medium induces population growths. Without adding either one, populations do not grow (grey curves). Each color shows $n = 4$ replicate populations. **(e)** At 39.2 °C. The measured concentrations of total extracellular glutathione as a function of the population-density over time for no-growth (red curve, initially ~400 cells / mL), random-growth (light blue curve, initially ~2,000 cells / mL), and deterministic-growth populations (dark blue curve, initially ~10,000 cells / mL). Error bars represent the mean with s.e.m., having $n = 3$ replicates per data point. The arrow shows both the population-density and concentration of extracellular glutathione increasing together over time. (Also see Supplementary Fig. S2.13). **(f)** At 39.2 °C. Sensitivity of no-growth populations (initially ~400 cells / mL) to (reduced) glutathione added into the growth medium, as a function of glutathione concentration. Error bars represent the mean with s.e.m., having $n = 4$ replicates per data point. Shown here is the fold-change in the population-density after two days of incubation. **(g)** Cartoon illustrating the mechanism deduced in (a-f). Yeasts secrete and extracellularly accumulate glutathione at high temperatures, inducing population growth when its concentration reaches at least a threshold amount (~0.3 μM from (f)).

Indeed, studies have found that heat-shocked yeasts produce and maintain elevated levels of intracellular glutathione [40, 41], a tripeptide that is yeast's primary antioxidant [40, 46, 47], besides having other essential roles [48]. Although much is known about glutathione's intracellular roles in yeast [46–51], little is known about whether yeast cells secrete glutathione and why and when they would do so, aside from a few examples such as yeasts secreting glutathione to defend against harmful extracellular arsenite [52].

Supporting our hypothesis is the fact that yeast is known to secrete small amounts of glutathione in stationary-phase at 30 °C (after diauxic shift) [53], and that we found that medium coming from such populations induced growth at high temperatures (Supplementary Fig. S2.10). Indeed, we discovered that adding high concentrations of either glutathione or ascorbic acid – both antioxidants [46] – to the growth medium caused growth of populations that, without the added antioxidants, could not have grown by themselves because they had too few cells (Fig. 2.4d). Hence, extracellular antioxidants – glutathione and ascorbic acids – are sufficient for inducing population growth at high temperatures. Focusing on glutathione, we found that random-growth and deterministic-growth populations continuously secreted and extracellular accumulated glutathione during log-phase growth and stationary-phase at high temperatures (Fig. 2.4e and Supplementary Fig. S2.13). But we detected only small concentrations of extracellular glutathione that barely increased over time for no-growth populations at high temperatures. Moreover, consistent with the density-dependent growth only occurring for temperatures above ~36 °C being caused by glutathione, we found that yeasts secreted glutathione at temperatures above ~36 °Cbut not below it (Fig. 2.2d and Supplementary Fig. S2.13). Furthermore, we had to add sufficiently high concentrations of glutathione to induce growth of a population that could not grow by itself (Fig. 2.4f). Specifically, if the extracellular glutathione concentration was below ~0.3 μM, populations hardly grew. But extracellular glutathione concentrations above ~0.3 μM

induced population growth up to the carrying capacity. Consistent with these findings, when we did not add any glutathione at high temperatures, no-growth populations had accumulated less than ~0.3 μM of extracellular glutathione whereas the growing population had accumulated more than ~0.3 μM of extracellular glutathione (Fig. 2.4d). In summary, we established that yeast secretes and extracellularly accumulates glutathione at high temperatures, which induces population growth above a threshold concentration of ~0.3 μM (Fig. 2.4g).

Mathematical model recapitulates experimental data. To explain our data, we developed a stochastic, mathematical model that contained just one free parameter (Supplementary Theory S2.6). In this model, each alive cell secretes glutathione at a constant rate and in each time step, with some probability, takes one of three actions: a cell replicates, dies or stays alive without replicating (Fig. 2.5a). The probability of dying is fixed and linearly increases with temperature. Given that populations require at least a threshold glutathione-concentration for growth (Fig. 2.4f), the probability of replicating non-linearly increases with the extracellular glutathione concentration in our model (Fig. 2.5b). The only free parameter, which requires fitting to our data, is the extracellular glutathione concentration at which the probability of replicating is half its maximum (Fig. 2.5b – blue curve). All other parameters are directly read-off from our data (Supplementary Theory S2.6).

Our model recapitulates all the main experimental data (Figs. 2.5c-f and Supplementary Fig. S2.14). The model's main idea is that in order to avoid becoming extinct at a high temperature, the population – which initially lacks any extracellular glutathione and thus starts with a zero probability of a cell replicating – must keep accumulating extracellular glutathione to keep increasing the probability of replication up to and above the probability of a cell dying – which is fixed by the temperature (Supplementary Fig. S2.14). Populations achieve this if and only if they starts with sufficiently many cells. Populations with too few cells go extinct and belong to the no-growth phase because they have insufficient time to accumulate enough extracellular glutathione: the probability of replicating increases until the last cell dies but always remains below the probability of dying. Populations with intermediate densities may grow or approach extinction (i.e., exhibits the random-growth phase) because the glutathione concentration nears the threshold concentration by the time there are very few surviving cells, whose stochastic replication or death subsequently determine whether or not the probability of replicating exceeds that of dying. At temperatures above ~40.3 °C – where the fold-bifurcation is – the probability of dying exceeds the maximum possible probability of replicating, meaning that only the no-growth phase exists at these temperatures (Fig. 2.5b – grey dashed line). In the no-growth phase, the continuous accumulation of extracellular glutathione results

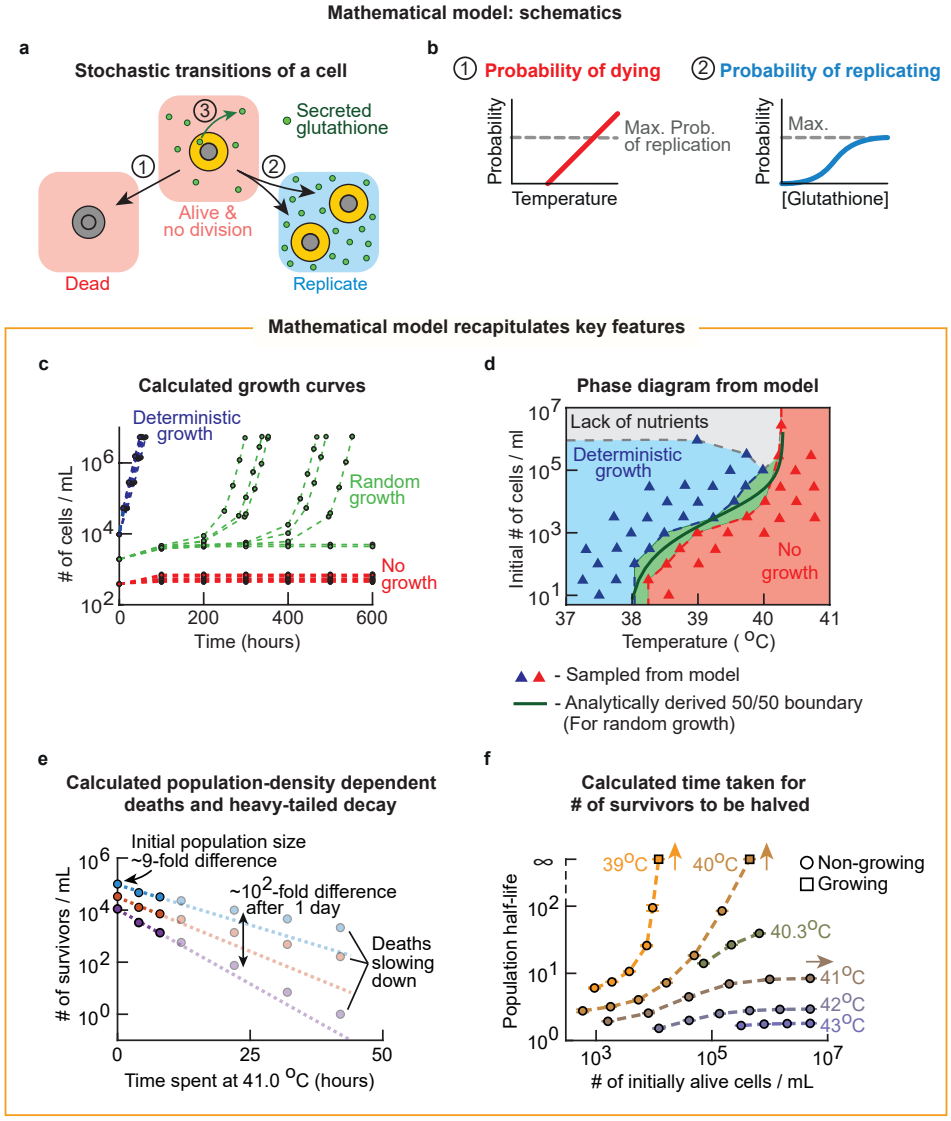

Figure 2.5: Mathematical model with one free parameter recapitulates all the main experimental data. (a-b) Description of the mathematical model (full description in Supplementary Theory S2.6). **(a)** A cell (yellow circle) can be in three states. In each time step, any alive cell either stays alive without replicating, replicates, or dies. Alive cells constantly secrete glutathione (green circles). **(b)** Schematic description of the probabilities that describe each of the transitions between states shown in (a). *Left panel:* probability of a cell dying (red line) is fixed by the temperature and does not change over time. It linearly increases with temperature and, beyond some temperature, it exceeds the maximum allowed value for the probability of a cell replicating (grey line). *Right panel:* probability of a cell replicating (blue curve) non-linearly increases with the concentration of the extracellular glutathione. **(c-f)** Results generated by the model described in (a-b) with a single fixed set of parameters for all panels. Model recapitulates: **(c)** the population-growth curves (compare with Fig. 2.2a), **(d)** the phase diagram (compare with Fig. 2.2d), ***(caption continues on the next page)***

Figure 2.5 ***(caption continued from the previous page)*****: (e)** population-density dependent deaths (compare with Fig. 2.2b), **(f)** population half-life (based on cell deaths during the first day of incubation – compare with Figure 2.3d), the number of survivors decaying over time as a heavy-tailed function (Supplementary Fig. S2.15), and single-cell-level data on growths (compare Supplementary Fig. S2.6 with Supplementary Fig. S2.14). The number of replicate simulations matches that of the respective experiments. (Also see Supplementary Figs. S2.15-S2.16 for further simulations and an extended model that includes limited availability of nutrients).

in populations decelerating their approach to extinction over time, leading to the heavy-tailed function describing the number of survivors decreasing over time and populations with higher initial densities more slowly approaching extinction (Supplementary Fig. S2.15). Taken together, our minimal model recapitulates all the main features of our experimental data (Figs. 2.5c-f).

Extracellular glutathione is necessary and sufficient for surviving high temperatures. To address whether extracellular glutathione is necessary – not only sufficient (Fig. 2.4e-f) – for yeast cells to survive high temperatures, we used a "masking agent" (1-Methyl-2-vinylpyridinium, M2VP) that specifically inactivates extracellular glutathione, without interfering with the intracellular glutathione or any other processes (Supplementary Fig. S2.17) [54, 55]. Adding the masking agent stopped deterministically growing populations at high temperatures (Fig. 2.6a). Thus, glutathione is both necessary and sufficient – glutathione is the only responsible molecule – for inducing cell replication at high temperatures (above ~36.7 °C).

Manipulating synthesis, import, and export of glutathione at high temperatures. To gain further insights, we constructed mutants that were either unable to synthesize glutathione (*gsh1*Δ-strain) (Fig. 2.6b) [56], or unable to import glutathione (i.e., *hgt1*Δ-strain) [57], or had severely reduced ability to secrete glutathione (*gex1,2*Δ-*adp1*Δ-strain) [58, 59]. We found that the mutant that cannot synthesize glutathione (*gsh1*Δ-strain) confirmed our earlier conclusion that the wild-type cells secrete glutathione only at high temperatures (above ~36 °C) (Supplementary Fig. S2.18). We also found that the mutant that cannot import glutathione (*hgt1*Δ-strain) had the same population-density-dependent growths at high temperatures as the wild-type strain (Fig. 2.6c). Thus, yeast cells do not need to import extracellular glutathione in order to replicate at high temperatures. This means that glutathione's extracellular action alone is responsible for promoting replication at high temperatures. Consistent with glutathione's extracellular action – not its intracellular action – promoting cell replication, we found that reducing the export of glutathione reduced the populations' ability to grow at high temperatures. Specifically, we found that the mutant with significantly reduced abilities to secrete glutathione

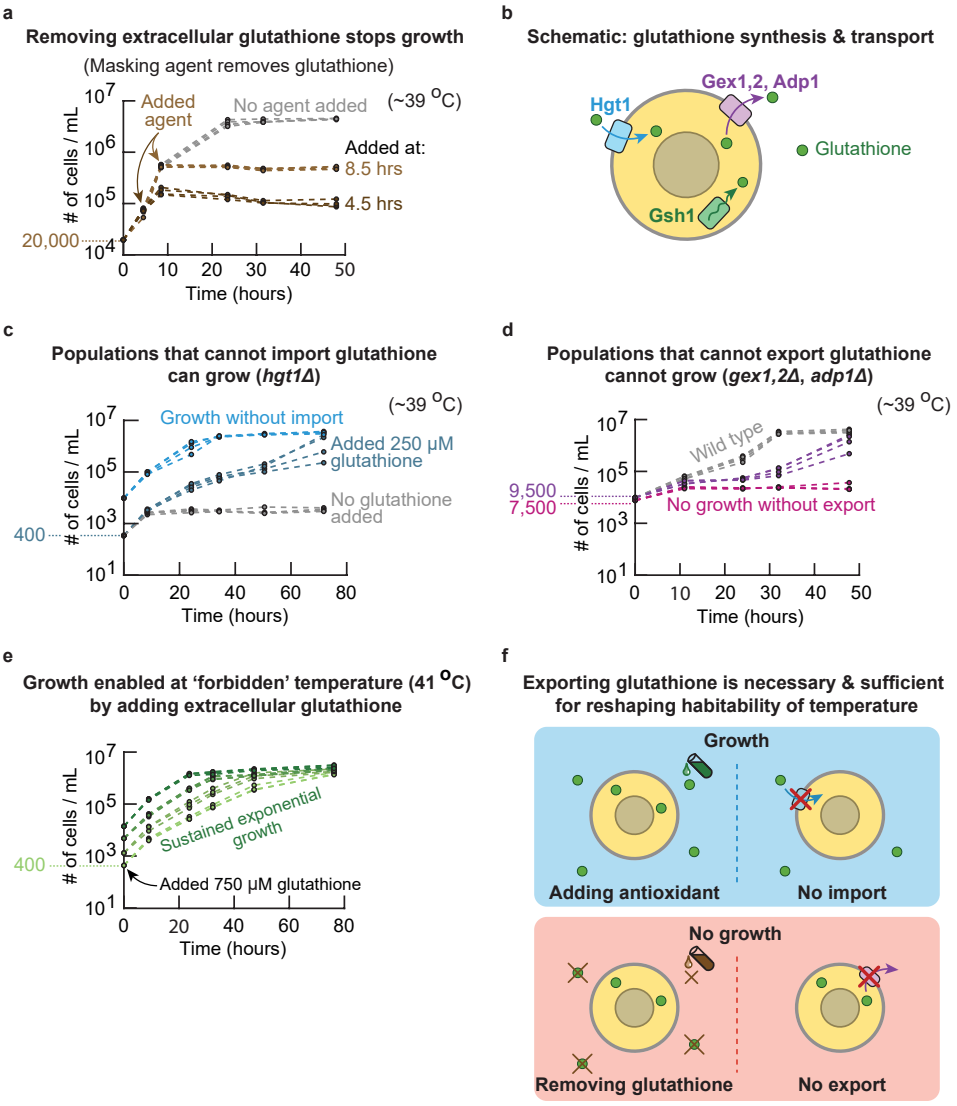

Figure 2.6: Budding yeast exports glutathione, whose extracellular role – not intracellular roles - as an antioxidant enables cells to survive high temperatures. **(a)** At 39.2 °C. Wild-type populations (all initially ~20,000 cells / mL) that should deterministically grow if left alone. A masking agent (M2VP) that inactivates extracellular glutathione was added after 4.5 hours (dark brown curves) or 8.5 hours (light brown curves) of incubation. Grey curves shows populations that did not receive the masking reagent. Each color shows $n = 4$ replicate populations. (Also see Supplementary Fig. S2.17). **(b)** Schematic showing how the budding yeast synthesizes, imports, and exports glutathione. Glutathione is intracellularly synthesized via an enzyme encoded by *GSH1*. Glutathione is imported by a proton-coupled glutathione-importer encoded by *HGT1*. Glutathione is exported by numerous exporters (not all shown), including proton antiporters encoded by *GEX1,2* and an ATP-dependent exporter encoded by *ADP1*. **(c)** At 39.2 °C. Light blue curves show deterministically growing populations of a mutant strain (*hgt1*Δ-strain) that cannot import glutathione (initially ~10,000 cells / mL). ***(caption continues on the next page)***

Figure 2.6 ***(caption continued from the previous page)*:** Grey curves show mutant populations (initially ~400 cells / mL) incubated without any glutathione added. Dark blue curves show mutant populations (initially ~400 cells / mL) incubated with 250 µM added glutathione. Each color shows $n = 4$ replicate populations. **(d)** At 39.2 °C. Populations of a mutant strain that lacks some of the main glutathione exporters (*gex1,2*Δ-*adp1*Δ-strain) (initially ~9,500 cells/mL (purple curves) or ~7,500 cells / mL (pink curves)). Wild-type populations shown as a comparison (grey curves, initially ~9,500 cells / mL). Each color shows $n = 4$ replicate populations. (Also see Supplementary Fig. S2.18). **(e)** At 41 °C. Wild-type populations of various initial densities (from ~400 cells / mL (lightest green curves) to ~14,000 cells / mL (darkest green curves)) grown in medium supplemented with 750 µM of glutathione. Each color shows at least $n = 3$ replicate populations. **(f)** Cartoon illustrating mechanisms deduced in (a-e). Exporting glutathione is necessary and sufficient for budding yeasts to reshape the habitability of temperature. For yeasts to survive and replicate at high temperatures, extracellular glutathione is (1) necessary since blocking glutathione or blocking glutathione-export stops population growth and is (2) sufficient since adding glutathione or blocking glutathione-import enables populations to grow.

(*gex1,2*Δ-*adp1*Δ-strain) was less able to replicate than the wild-type strain (Fig. 2.6d), requiring a higher initial densities for growth. Moreover, we found that the mutant with a reduced glutathione-export (*gex1,2*Δ-*adp1*Δ-strain) still secreted measurable amounts of glutathione at high temperatures, which was not due to glutathione passively leaking out through cell membranes (Supplementary Fig. S2.19), suggesting that additional glutathione exporters may exist at high temperatures.

Yeasts can replicate at "unlivable" temperatures. We established that no population can avoid extinction at temperatures above 40.3 °C (Fig. 2.2d), because the cells die too fast to accumulate enough extracellular glutathione. Hence, we reasoned that giving sufficiently high concentrations of glutathione to populations at the start of incubation at extremely high temperatures may help them accumulate enough glutathione before extinction. Indeed, for example at 41 °C, we could rescue populations with as few as 400 cells / mL from extinction, with the populations growing exponentially until reaching a carrying capacity (Fig. 2.6e).

2.3. DISCUSSION

By showing that secreting and extracellularly accumulating glutathione is necessary and sufficient for yeast cells and their future generations to survive and replicate at high temperature (Fig. 2.6f), our work revises the textbook view of cells autonomously combating heat-induced damages. A common explanation for why cells, including from budding yeast, are unable to replicate at high temperatures is that essential proteins unfold at high temperatures [3]. Our work suggests that this explanation requires revisions. In fact, we found that cells with enough extracellular glutathione can replicate at extremely high temperatures for which such proteins would unfold (i.e., above 41 °C – Fig. 2.6e, Supplementary Fig. S2.15). Glutathione, an antioxidant essential

for many organisms, including humans [46], is central to diverse processes [47–52]. Our work extends the relatively little known extracellular functions of glutathione in yeast [52, 53] by showing that cells must secrete sufficient amounts of glutathione at high temperatures during log-phase growth and stationary phases. The glutathione extracellular accumulates and, we found, exists mainly (for no-growth populations) or with elevated levels (for growth populations) in the oxidized form (Supplementary Fig. S2.13) [53]. This suggests that cells collectively "clean up" their environment by reducing harmful, extracellular reactive oxygen species and thereby help each other and their future generations replicate and survive high temperatures.

Researchers have observed fold-bifurcation points, like the one in our study (Fig. 2.2d), in other microbial populations on the verge of extinctions such as those in which yeast cells collectively hydrolyze extracellular sucrose [60–62]. These dynamical systems typically exhibit features familiar from phase transitions such as "critical slowing down" [61], that in our study could emerge as the yeast-population's half-life being infinite at the fold-bifurcation point (Fig. 2.3d). By uncovering a phase diagram for cell replication, our work may aid in advancing theories of non-equilibrium statistical mechanics [63] that pertain to biologically realistic, self-replicating systems that drive and maintain themselves out of thermal equilibrium. Moreover, investigating how organisms can collectively combat high temperatures, as in our study, may suggest ways to help organisms combat climate change and help us understand how climate change impacts unicellular life and multicellular communities.

2.4. METHODS

Growth media and strains. The "wild-type", haploid yeast strain that we used is from Euroscarf with the official strain name "20000A". It is isogenic to another laboratory-standard haploid yeast "W303a", and has the following genotype: *MATa; his3-11_15; leu2-3_112; ura3-1; trp1Δ2; ade2-1; can1-100*. We built the two strains that constitutively expressed GFP by first using PCR to insert a functional *ADE2* gene into the locus of the defective *ade2* gene in the wild-type strain, by a homologous recombination, so that the red pigments that would have accumulated without the *ADE2* insertion no longer existed (i.e., the strain can now synthesize adenine). We could thus detect their GFP fluorescence without interferences from the red pigments. After replacing the defective *ade2* locus with a functional *ADE2*, we constructed the 1x-GFP and 100x-GFP strains (see GFP-expression levels in Supplementary Fig. S2.5a) by integrating a single-copy of a linearized yeast-integrating plasmid. Specifically, the 1x-GFP strain had its GFP expression controlled by the constitutive promoter of yeast's *KEX2* gene (621 bases upstream

of its ORF) which was on a yeast-integration plasmid [64] that constitutively expressed *HIS3* (from *C. glabrata*) and integrated into the non-functional *his3* locus of the wild-type strain by a homologous recombination. The 100x-GFP strain had its GFP expression controlled by a strong constitutive promoter pGPD1 [64] which was on the same plasmid as the one for the 1x-GFP strain except that the *KEX2* promoter was swapped with the *GDP1* promoter. We cultured all yeasts in defined, minimal medium that consisted of (all from Formedium): Yeast Nitrogen Base (YNB) medium, Complete Supplement Mixture (CSM) that contained all the essential amino acids and vitamins, and glucose at a saturating concentration (2% = 2 g per 100 mL). The agar pads, which we used for growing yeast colonies, contained 2% agar (VWR Chemicals), Yeast Extract and Peptone (YEP) (Melford Biolaboratories Ltd.), and 2% glucose.

Growth experiments. In a typical growth experiment, we first picked a single yeast colony from an agar plate and then incubated it at 30 °C for ~14 hours in 5 mL of minimal medium, which contained all the essential amino acids and a saturating concentration of glucose (2%). Afterwards, we took an aliquot of a defined volume from the 5 mL culture (typically 20 μL), and then flowed it through a flow cytometer to determine the 5 mL culture's population-density (# of cells / mL). We then serially diluted the culture into fresh minimal medium to a desired initial population-density for a growth experiment at various temperatures. Specifically, we distributed 5 mL of diluted cells to individual wells in a "brick" with twenty-four 10 mL wells (Whatman: "24-well x 10 mL assay collection & analysis microplate"). This ensured that we had 8 identical replicate cultures for each initial population-density (e.g., in Figure 2.2a-c). We sealed each brick with a breathable film (Diversified Biotech: Breathe-Easy), covered it with a custom-made Styrofoam-cap for insulation, and incubated it in a compressor-cooled, high-precision thermostatic incubators (Memmert ICP260) that stably maintained their target temperature throughout the course of our growth-experiments, with a typical standard deviation of 0.017 °C over time (deviation measured over several days; Supplementary Fig. S2.2). Throughout the incubation, the cultures in the brick were constantly shaken at 400 rpm on a plate shaker (Eppendorf MixMate) that we kept in the incubator. To measure the population-density, we took a small aliquot (typically 50 μL) from a well, diluted it with PBS (Fisher Bioreagents) into a 96-well plate (Sarstedt, Cat. No. 9020411), and then flowed it through the flow cytometer which gave us the # of cells / mL. We determined the growth rates by measuring the maximum slope of the log-population-density after their initial, transient growth.

Flow cytometry. The flow cytometer that we used was a BD FACSCelesta with a High-Throughput Sampler and lasers with the following wave lengths: 405 nm (violet), 488 nm

(blue), and 561 nm (yellow/green). We calibrated the FSC and SSC gates to detect only yeast cells (FSC-PMT = 681 V, SSC-PMT = 264 V, GFP-PMT = 485 V, mCherry-PMT = 498 V. As a control, flowing PBS yielded no detected events). The number of cells per mL that we plotted in our growth experiments is proportional to the number of events (yeast cells) that the flow cytometer measured in an aliquot of cells with a defined volume. We measured the GFP fluorescence with a FIT-C channel and the "red cells" (Supplementary Fig. S2.6) with a mCherry channel. We analysed the flow cytometer data with a custom MATLAB script (MathWorks).

Measuring number of surviving cells. For Figures 2.3a-b and Supplementary Figs. S2.7-S2.8, we prepared 250 mL cultures of wild-type cells in 500 mL Erlenmeyer flasks. We placed a constantly spinning magnetic stir-bar at the bottom of the flasks and placed each flask on top of spinning magnets at 220 rpm (Labnet Accuplate) inside the thermostatic incubators (Memmert ICP260) that we set at the desired high temperatures. For Figure 2.3d, we prepared a brick with cultures as described in "growth Experiments" in order to have multiple replicate populations and to compare the different population-densities. For every time point we ensured that these populations were not growing (i.e., all populations were in the no-growth phase after a transient growth) by using the flow cytometer to measure the cell densities over time to verify that their population-densities indeed remained constant over time. For the first 48 hours of incubation, we measured the number of Colony Forming Units (CFUs) by taking out a small volume aliquot from the liquid cultures at high temperatures and distributed droplets from a serial dilution of the aliquot across an agar pad (2% glucose with YEP) that we then incubated in 30 °C for several days until (no) colonies appeared. When there were few surviving cells per mL – especially for the last time points in each experiment – we determined, in parallel to the plating method, the number of CFUs by transferring an appropriate volume of the liquid cultures from the incubator to an Erlenmeyer flask and then diluting it with the same volume of fresh minimal medium. We then sealed this flask with a breathable film (Diversified Biotech: Breathe-Easy) and then left it still without stirring, on a benchtop at ~24 – 30 °C – we checked that slightly lower temperatures did not affect the colony-forming abilities. This method allowed any surviving cells to settle down to the bottom of the flask and form colonies. We counted the number of colonies at the bottom of the flask, that we plotted as the last time points in each experiment (Fig. 2.3a, Supplementary Figs. S2.7-S2.8).

Cell-transfer experiments. We prepared a 24-well brick with liquid cultures, in the deterministic-growth phase (e.g., initially 10,000 cells / mL) at a desired temperature (e.g., at 39.2 °C). We incubated the brick containing these liquid cultures in the thermo-

static incubators as described in "growth experiments". After ~48 hours of incubation, we took aliquots of these cultures that were growing in mid-log phase (verified through flow cytometry) and diluted each of them into fresh 5 mL minimal media that were in 24-well bricks. These newly created populations were in the no-growth phase at the same temperature as the original population that they came from (initially ~400 cells / mL at 39.2 °C). We sealed the 24-well brick with a breathable film (Diversified Biotech: Breathe-Easy) and then incubated them at the same temperature as the original population. We performed the growth experiments with these new populations as described in "growth experiments".

Medium-transfer experiments. Details are also in Supplementary Fig. S2.10. At a given temperature, we first grew populations in the deterministic-growth phase (e.g., initially 30,000 cells / mL at 39.2 °C). We used a flow cytometer to measure the population-densities at different times so that we knew in which part of deterministic growth they were (e.g., mid-log phase). We then transferred each liquid culture to a 50 mL tube (Sarstedt) and centrifuged it so that the cells formed a pellet at the bottom of the tube. We then took the resulting supernatant, without the cell pellet, and flowed it through a filter paper with 0.2 µm diameter pores (VWR; 150 mL Filter Upper Cup) to remove any residual cells from the supernatant. After filtering, we flowed an aliquot of the filtered media through a flow cytometer to verify that there were no cells left in the filtered media. We incubated fresh cells into these filtered media (instead of into fresh minimal medium) and proceeded with a growth experiment at a desired temperature as described in "growth experiments".

Measuring the depletion of extracellular nutrients. Details are also in Supplementary Fig. S2.11. We prepared various growth media by diluting the minimal medium (SC medium) by various amounts with water. These diluted SC-media were each supplemented with a 2% glucose. Next, we incubated fresh cells in these diluted SC-media at the desired temperature (e.g., 39.2 °C) as described in "growth experiments". We compared populations of cells that initially had 400 cells / mL (corresponding to a no-growth phase; Fig. 2.2d) with populations that initially had 10,000 cells / mL (corresponding to a deterministic-growth phase; Fig. 2.2d) in order to confirm that cells were still able to grow in these media. Similarly, we also varied the amounts of glucose that we supplemented to SC-media to test whether populations could grow.

RNA-seq. For each temperature that we studied, we collected cells in 50 mL tubes and spun them in a pre-cooled centrifuge. We then extracted RNA from each cell-pellet with a RiboPure Yeast Kit (Ambion, Life Technologies) as described by its protocol. Next, we

prepared the cDNA library with the 3' mRNA-Seq library preparation kit (Quant-Seq, Lexogen) as described by its protocol. Afterwards, we loaded the cDNA library on an Illumina MiSeq with the MiSeq Reagent Kit c2 (Illumina) as described by its protocol. We analysed the resulting RNA-Seq data as previously described [65]. In short, we performed the read alignment with TopHat, read assembly with Cufflinks, and analysis of differential gene-expressions with Cuffdiff. We used the reference genome for *S. cerevisiae* from Ensembl assembly R64-1-1). We categorized the genes by the Gene Ontologies with AmiGO2 and manually checked them with the Saccharomyces Genome Database (SGD).

Measuring concentration of extracellular glutathione. To quantify the concentration of extracellular glutathione, we removed cells from the liquid media by flowing the liquid cultures that contained cells through a 0.45 μm pore filter (VWR, cellulose-acetate membrane). To ensure and verify that there were no cells remaining in the filtered media, we flowed the filtered media through a flow cytometer. The flow cytometer indeed did not detect any cells in the filtered media. We then measured concentrations of glutathione in the filtered media as described in the manufacturers' protocol (Sigma Aldrich, Cat. No. 38185 'quantification kit for oxidized and reduced glutathione'). We used "BMG Labtech Spectrostar Nano" to measure the optical absorbance at 415 nm. As a background for all measurements (blank), we subtracted the absorbance that we obtained by applying the assay to fresh minimal medium which did not contain any glutathione (the background absorbance could come from, for example, cysteine in the minimal medium). We subsequently determined the concentrations of extracellular glutathione by using a calibration curve that we constructed by measuring the absorbance at 415 nm for known amounts of glutathione that we added by hand into a buffer provided by the manufacturer.

Glutathione masking experiment. We incubated a brick of liquid cultures that were in the deterministic-growth phase (initially ~20.000 cells / mL) at 39.2 °C. After some time (e.g., ~8.5 hours), we added 750 μM of 1-Methyl-2-vinylpyridinium (M2VP, Sigma Aldrich, Cat. No. 69701), a thiol scavenging agent that rapidly masks reduced glutathione [55]. We then proceeded with the experiment as described in "growth experiments". Identical replicate cultures that did not receive M2VP were used as a reference.

Mutant yeasts. We constructed mutant strains that could not synthesize glutathione or could not import or export glutathione. Primers were designed with a $50-60$ bp sequence that was either homologous to the $50-60$ bp that is upstream of the desired gene's start codon or downstream of the desired gene's stop codon. These primers were

used to amplify a selection marker by PCR, resulting in a PCR product that contained a selection marker and whose ends were homologous to the flanking regions of the gene to be knocked out. The wild-type strain was grown overnight at 30 °C in a 5 mL YPD in a rotator set at 40 rpm, and was then transformed with the PCR fragment using standard methods of yeast cloning. The glutathione biosynthesis mutant (*gsh1*Δ-strain) was constructed by removing the *GSH1* gene from the wild-type strain. The import mutant (*hgt1*Δ-strain) was constructed by removing the *HGT1* gene. The export mutant (*gex1,2*Δ-*adp1*Δ-strain) was constructed by removing, sequentially, the *GEX1* gene, then the *GEX2* gene, and then the *ADP1* gene. The resulting transformants were grown on YPD selection plates, and knockouts were verified by PCR.

Measuring integrity of cell membrane. Cells of the *gex1,2*Δ-*adp1*Δ-strain were incubated in liquid medium at 39.2 °C (initially ~$3,000 - 10,000$ cells / mL; corresponds to a random-growth phase). We took aliquots of these cultures and then stained them with 1 μg / mL of propidium iodide (Thermo Fisher Scientific, Cat. No. P3566). We then flowed these stained aliquots through a flow cytometer. The flow cytometer measured the number of cells that were unstained by the propidium iodide (i.e., cells whose membranes were intact [66]).

Mathematical model. Derivations of equations, a detailed description of the mathematical model, and the parameter values used for simulations are in the Supplementary Theory S2.6.

S2.5. SUPPLEMENTARY FIGURES

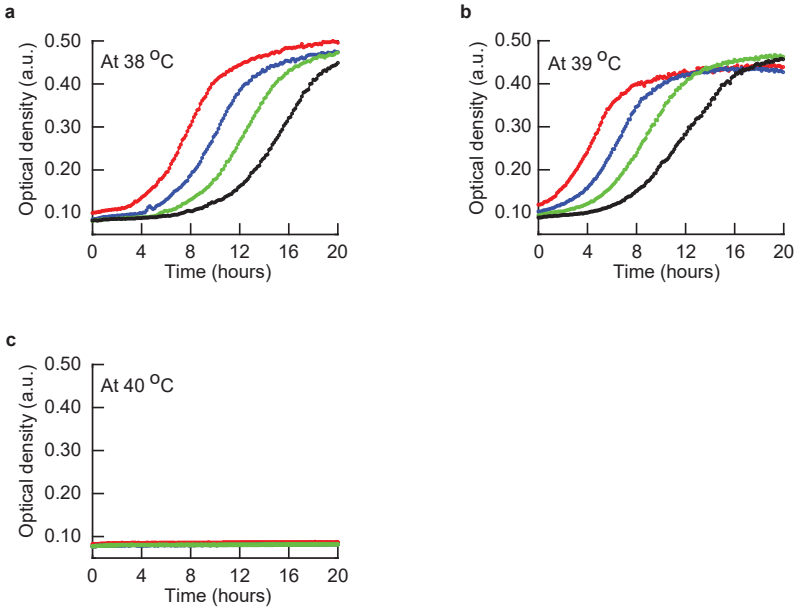

Figure S2.1: Conventional view of temperature-dependent cell-growth for populations of wild-type yeast defines habitable and inhabitable temperatures (Related to Figure 2.1b). (a-c) To obtain the conventional picture (Fig. 2.1b), we performed laboratory-standard growth experiments in which we used a plate reader (BioTek Synergy HTX microplate plate reader, model S1LFA) to measure the Optical Density (OD) of liquid cultures of wild-type yeast cells over time (up to 20 hours shown here). The OD represents the optical absorption of light at a wavelength of 600 nm and is directly proportional to the number of cells per volume, OD = 0.10 corresponds to approximately 10^6 cells / mL. The plate reader cannot detect sufficiently small ODs (i.e., OD < 0.08). We show here data for 38 °C **(a)**, 39 °C **(b)**, and 40 °C **(c)**. Populations are representative for $n = 3$ replicates. For each temperature, the different colors represent cell-populations with distinct starting ODs. To obtain these starting ODs for a given temperature, we diluted cells from a single liquid culture of cells that grew overnight at 30 °C (also for growth experiments that appear in later figures). The starting ODs are approximately 0.10 (red curves), 0.05 (blue curves), 0.025 (green curves), and 0.0125 (black curves). Blue, green, and black curves start with ODs – obtained by serial dilutions of denser cultures – that are below the lowest OD that the plate reader can detect whereas the red curves start with ODs above it. All cultures at 38 °C and 39 °C reach their carrying capacities (i.e., the ODs plateau over time in (a-b)). None of the populations grew at 40 °C (i.e., the OD remains flat over time in (c)).

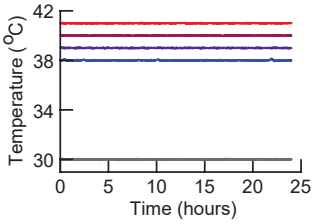

Figure S2.2: Temperature remains stable during all our growth experiments (Related to Figure 2.2). In all our growth experiments (performed with liquid cultures of cells incubated in compressor-cooled, high-precision thermostatic incubators (Memmert ICPs)), the incubators maintained their target temperature throughout the course of the experiments, with a typical standard deviation of 0.017 °C over time (deviation measured over several days). As representative examples of a continuous measurement, shown here are temperatures recorded by the incubator's sensor, zoomed to 24 hours for five separate growth experiments: Starting from the top, the curves are for 41 °C (red curve), 40 °C (purple curve), 39 °C (dark blue curve), 38 °C (light blue curve) and 30 °C (grey curve). We also verified and aligned the incubators' temperatures by using a different thermocouple device. Thus, we measured temperature values with two different thermocouple devices and the temperature remained stable and constant over the course of each growth-experiment.

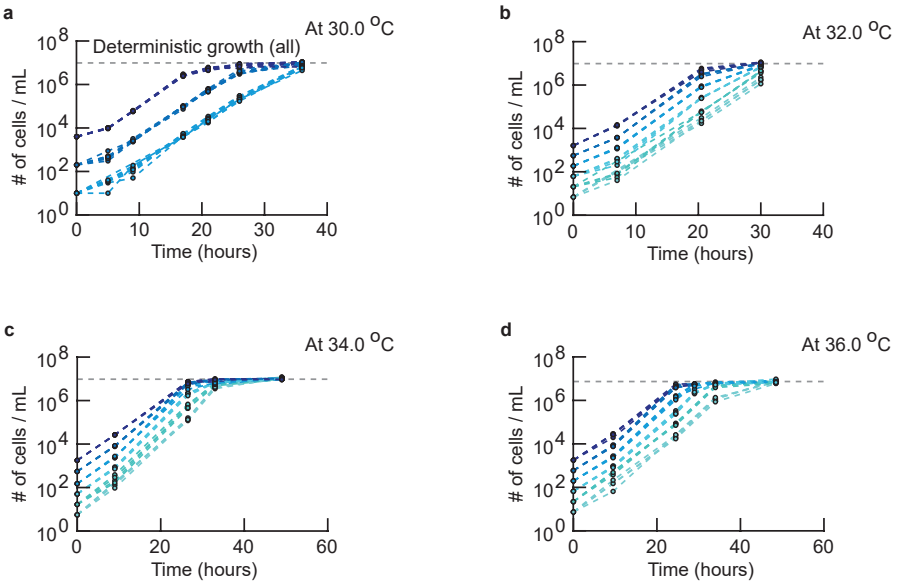

Figure S2.3: If the temperature is at or below 36 °C, every population of wild-type cells deterministically grows regardless of the initial population-density (i.e., all populations grow to reach a carrying capacity) (Related to Figures 2.2a-d). (a-d) Population-density (number of cells / mL) measured over time with a flow cytometer (Methods 2.4). Each curve shows a population of wild-type cells that started with a desired initial density. The initial population-densities vary over ~1,000-fold, from very dilute (initially ~10 cells / mL) to less dilute (initially ~1,000 cells / mL). Horizontal, grey line at the top of each plot shows the carrying capacity that we estimated by averaging the density of each population after it eventually stops growing (we used only the populations with the highest initial densities for this estimate). Sample data shown for 30.0 °C **(a)**, 32.0 °C **(b)**, 34.0 °C **(c)**, and 36.0 °C **(d)**. Different colors represent different initial population-densities. For each color, there are $n = 8$ (a) or $n = 6$ (b-d) replicate populations (biological replicates). For every initial density, every replicate population exponentially grew in an identical manner until they reached a carrying capacity. Here, "identical manner" means that all curves of the same color perfectly overlap within each panel (compare this with populations that exhibit random growths in Supplementary Fig. S2.4). In other words, every initial population-density, regardless of how low they were, led to a deterministic growth for temperatures at or below 36.0 °C. These results show that the no-growth and random-growth phases do not exist below 36 °C. Only deterministic growth exists for wild-type cells at temperatures below 36 °C, consistent with the wild-type strain's phase diagram (Figure 2.2d).

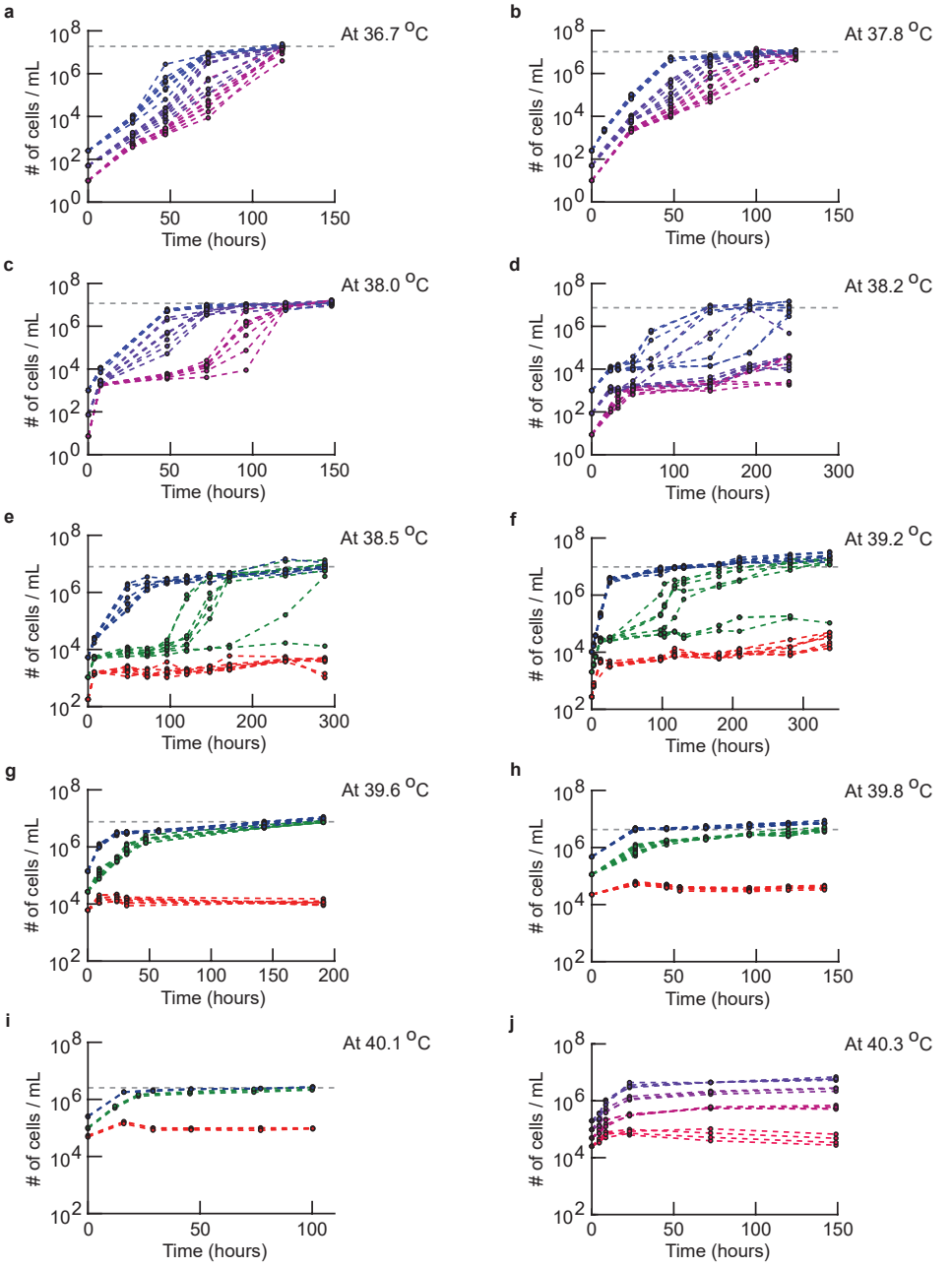

Figure S2.4: If the temperature is above 36 °C, the growth of wild-type cells depends on the initial population-density (Related to Figures 2.2a-e). (a-j) Population-density (number of cells / mL) measured over time with a flow cytometer for populations of the wild-type cells with differing initial densities. Grey line shows the carrying capacity that we estimated by averaging the final densities of the populations that grew. We only used the populations that started with the lowest initial densities for this estimate. ***(caption continues on the next page)***

Figure S2.4 ***(caption continued from the previous page):*** Sample data shown for 36.7 °C **(a)**, 37.8 °C **(b)**, 38.0 °C **(c)**, 38.2 °C **(d)**, 38.5 °C **(e)** and 39.2 °C **(f)** – (e-f) were copied here from Fig. 2.2a-b for completeness. Further sample data shown for 39.6 °C **(g)**, 39.8 °C **(h)**, 40.1 °C **(i)** and 40.3 °C **(j)** ((j) was also copied from Fig. 2.2c). Different colors represent different initial population-densities. Each color shows multiple biological replicates ($n = 8$ (a-h), $n = 3$ (i) or $n = 4$ (j)). To show multiple starting densities for populations having the same growth phase, we used here a color scheme that is different from the one used in Figures 2.2a-c. Based on the growth experiments whose sample data are shown here, we constructed the phase diagram for the wild-type cells (Fig. 2.2d). To construct the phase diagram, we determined whether a given initial population-density belongs to a deterministic growth phase, or a random growth phase, or a no-growth phase. Specifically, an initial population-density belongs a deterministic growth phase in the phase diagram if every replicate population, all of which start at the same density, exponentially grows over time in an identical manner (i.e., all curves of the same color overlap – collapse into a single curve – in the plots above). As an example, Supplementary Fig. S2.3 shows all initial population-densities leading to a deterministic growth at temperatures below 36 °C. An initial population-density belongs to the no-growth phase in the phase diagram if none of the replicate populations grow after an initial, transient growth that typically lasts at most ~10 hours due to the effect of the cells having just been transferred from 30 °C to their new temperature. As an example, in (g), the lowest initial population-density (red curves) belongs to the no-growth phase. An initial population-density belongs to a random-growth phase in the phase diagram (Fig. 2.2d) if the curves of the same color – representing replicate populations – do not overlap or when some replicate populations do grow while others do not. Here, the replicate populations do not overlap due to each population growing at distinct rates or starting to grow – after a stasis – at different times after the transient growth stops, causing these populations to reach a carrying capacity at vastly different times (i.e., different by tens to hundreds of hours) despite all replicate populations having the same initial density. As an example, an intermediate initial population-density in (e) – represented by green curves – leads to random growth. Finally, we determined the phase boundaries in the phase diagram (Figure 2.2d). Specifically, we drew the boundary that divides the deterministic-growth and random-growth phases by connecting the data points that represent the lowest measured initial population-density that yielded a deterministic growth for each temperature (i.e., the minimum number of cells per unit volume necessary to guarantee that a population grew at each temperature). We drew the boundary that divides the random-growth and no-growth phases by connecting the data points that represent the highest measured initial population-densities that yielded a no-growth phase for each temperature (i.e., the maximum number of cells per unit volume necessary to guarantee that a population would not grow at each temperature). Finally, we determined the temperature above which a population-level growth is no longer possible by determining the lowest temperature at which populations that start with different densities always reach different final densities when they stop growing (i.e., populations never grow to the carrying capacity where one or more essential nutrients has been depleted). As an example, at 40.3 °C (j), populations with different initial densities never reach the same density when they stop growing.

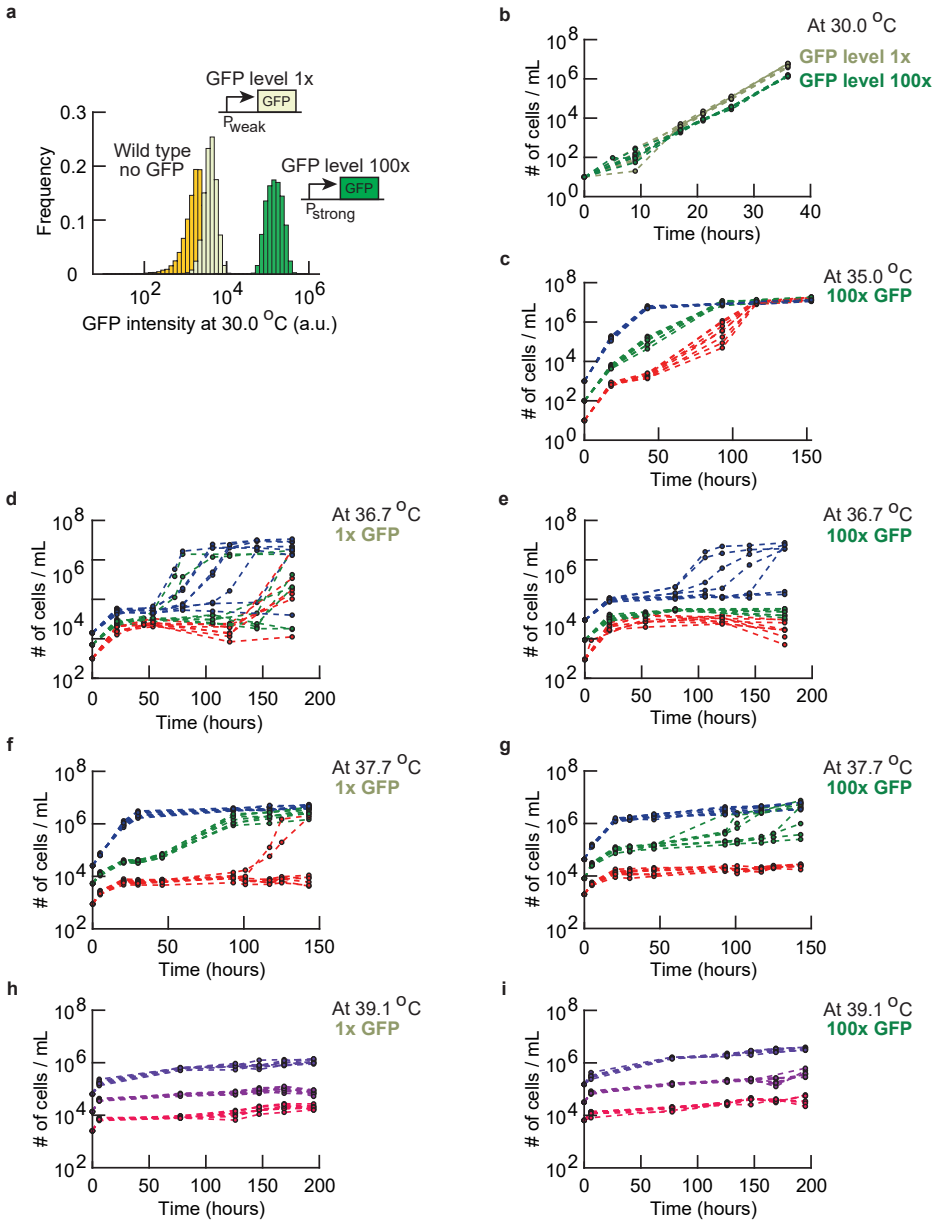

Figure S2.5: Cost of expressing a gene (GFP) alters how an initial population-density affects whether a population grows or not at high temperatures (Related to Figure 2.2f). Characterization of the two yeast strains ("1x-GFP" and "100x-GFP" strains) that constitutively express GFP. **(a)** A histogram of GFP-expression levels of the two engineered yeasts and the wild-type strain as measured by a flow cytometer. The 1x-GFP cells have a higher average fluorescence than the wild-type cells whereas the 100x-GFP cells have ~100-fold higher average fluorescence than the 1x-GFP cells. **(b-i)** As with the wild-type strain (Supplementary Fig. S2.3-S2.4), we performed growth experiments in which we used a flow cytometer to measure the population-density (number of cells / mL) for the 1x-GFP and 100x-GFP strains. ***(caption continues on the next page)***

Figure S2.5 ***(caption continued from the previous page)*****:** (**b**) Populations of the GFP expressing strains at 30 °C for the 1x-GFP strain (light green curves) and the 100x-GFP strain (dark green curves). Further sample data shown for the 1x-GFP strain (**d**, **f**, and **h**) and for the 100x GFP strain (**c**, **e**, **g**, and **i**). Each strain was incubated at different temperatures, at 35.0 °C (**c**, 100x GFP strain only), at 36.7 °C (**d-e**), at 37.7 °C (**f-g**) and at 39.1 °C (**h-i**). Different colors represent different initial population-densities. Each color shows multiple replicate populations ($n = 6$ (b) or $n = 8$ (c-i)). To distinguish deterministic, random, and no-growth phases for the 1x-GFP and 100x-GFP strains, we used criteria that are similar to the ones that used for the wild-type strain (Figure 2.2d; described in Supplementary Fig. S2.4). Here, for a given temperature, we classified an initial population-density as belonging to the deterministic-growth phase if at least six out eight replicate populations (biological replicates) that started with this density exponentially grew (note that for the wild-type cells, all eight out of eight replicate populations must have exponentially grown for the initial population-density to be classified as yielding a deterministic growth). Conversely, for a given temperature, we classified an initial population-density as belonging to the no-growth phase if six out of eight populations with the same initial population-density did not grow (for the wild-type strain, all eight populations had to not grow). These slight differences in the definitions of the phases between the wild-type and the GFP-expressing strains do not qualitatively change the main features of the phase diagrams (Figure 2.2f). These measurements show that, at a given temperature, expressing more of a spurious gene (GFP) requires a population to start with a higher initial density of cells in order to be able to deterministically grow.

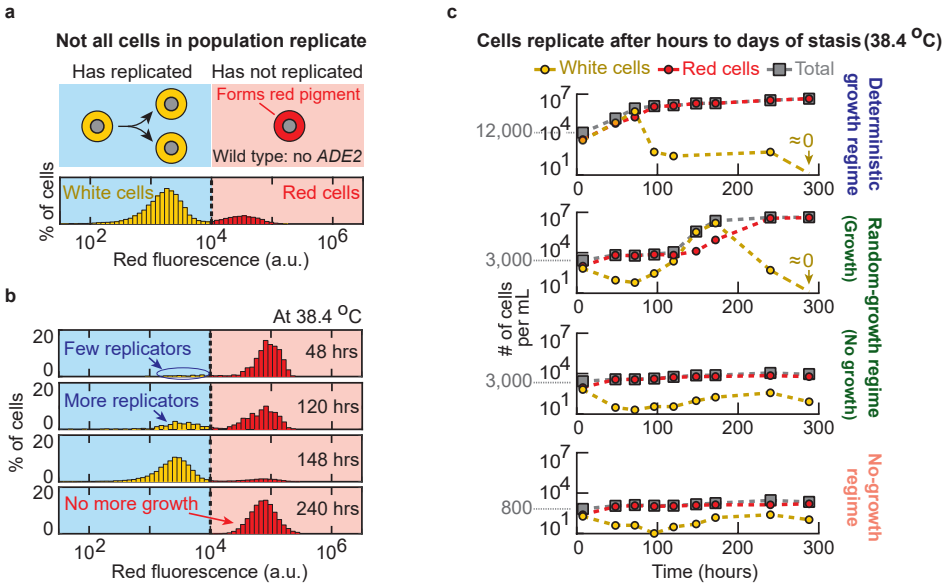

Figure S2.6: Few cells stochastically and transiently replicate within populations that are in either no-growth or random-growth phase (Related to Figures 2.2a-d). **(a)** The wild-type strain lacks a functional *ADE2* gene for synthesizing adenine. Since we incubated yeasts in the minimal medium with all the essential nutrients – including adenine – the wild-type cells were still capable of growing. But having a defective *ade2* gene turns yeast cells red if they have not divided for some time because they have accumulated red pigments – these are by-products of the not-fully-repressed and defective adenine-biosynthesis. The cells can only dilute away the red pigments through cell divisions. The histogram shows percentages of red cells (non-replicating cells) and "white cells" (non-red, replicating cells) in a population, determined by a flow cytometer's red-fluorescence detector that quantified redness of individual cells. **(b)** Percentage of white and red cells over time measured with the flow cytometer for a population of wild-type cells. Time shows hours of incubation at 38.4 °C. These histograms show example time courses for a population that grew at a high temperature. **(c)** Density of white and red cells in a liquid culture, at various times for the three different growth regimes as indicated by the phase diagram (Figure 2.2d). Random-growth phase shows two population behaviors – one growing (second row) and one not growing (third row).

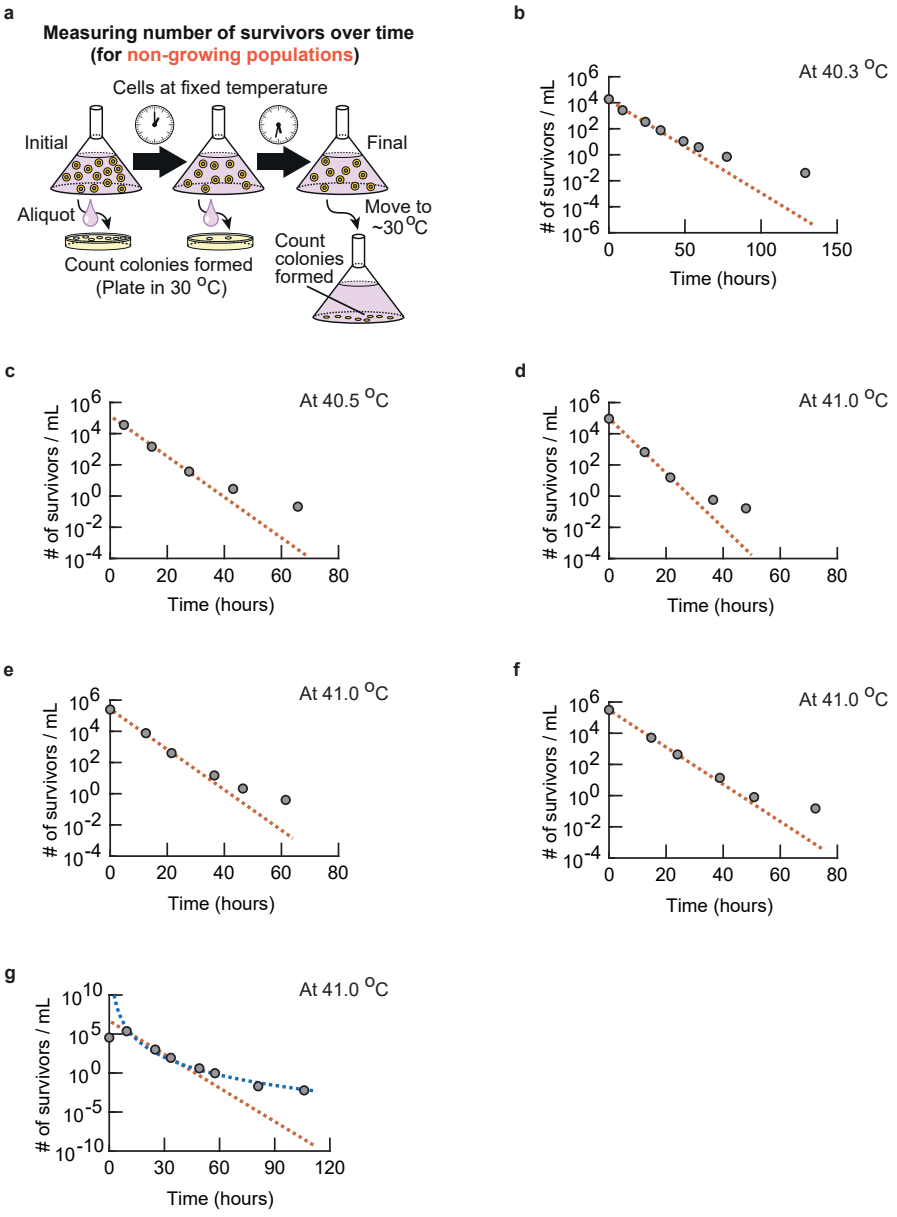

Figure S2.7: Unconventional deaths at high temperatures: number of survivors at high temperatures decreases over time as a heavy-tailed function and deviates by orders of magnitude from the conventionally expected number of survivors (Related to Figures 2.3a-b). (a) Schematic description of how we measured the number of surviving wild-type cells over time in a population that was incubated at a high temperature and that could not grow because it was in the no-growth phase according to the phase diagram (Figure 2.2d). In short, at various times, we took an aliquot from a liquid culture of non-growing population that was kept at a high temperature. ***(caption continues on the next page)***

Figure S2.7 ***(caption continued from the previous page)*****:** We then serially diluted this aliquot by known amounts – this was to ensure that we could have countable numbers of colonies if there were any survivors in the aliquot – and spread the droplets containing the serially diluted cells on an agar pad which we incubated at 30 °C. After a few days, we counted the number of colonies that formed (colony forming units) on the agar pad at 30 °C. By counting the number of colony-forming units and knowing the dilutions and volumes of the aliquots that we took out at various times, we determined the "number of survivors / mL" that we plotted in (b-g) and in Figures 2.3a-b. For the last several time points of each of these experiments, aside from counting the number of colony forming units, we additionally verified our results by using a complementary method to count the number of survivors per volume. This was necessary since taking an aliquot whose volume is only a fraction of the total volume of the liquid culture would have yielded very few colonies on the agar pad, since there was typically less than one survivor per mL in the liquid cultures. Thus, we additionally took out an appropriate volume (typically tens of mL) from the liquid culture which was incubated at a high temperature, transferred it to an Erlenmeyer flask, and then left the flask at ~30 °C for several days without shaking it. All the surviving cells in this liquid sample that we took out settled down to the bottom of the flask and formed colonies. Finally, to measure the last time points in (b-g) and Figure 2.3a-b, we moved the flask that contained the entire remaining liquid culture (i.e., the entire population) from a high temperature to ~30 °C to ensure that we counted all remaining survivors using the "settling-to-the-bottom" method. Both methods – directly counting the colonies formed on agar after spreading a serially diluted aliquot of the liquid culture and counting the colonies formed by surviving cells that settled down to the bottom of a flask – yielded the same results. **(b-g)** We used the method in (a) to measure the number of surviving wild-type cells per mL at 40.3 °C **(b)**, 40.5 °C **(c)** and 41.0 °C **(d-g)**. In (b-f), the brown dashed lines represent an exponentially decaying function that we fitted to the first three time points (i.e., data points for the first day of incubation at a high temperature). For (g), the brown dashed lines represent an exponentially decaying function that we fitted to the data points that lie within 10 - 50 hours. The blue dashed curve is a power-law function fitted to the same data points as the ones that we used to fit the exponentially decaying functions. In (b-g), we found that the data points vastly deviate from the brown dashed line (i.e., the final time point deviates by at least $\sim 10^4$ cells / mL). Thus, contrary to the conventional view of cell death at high temperatures, the number of survivors does not exponentially decrease over time (i.e., cell death is not fixed by a single rate constant). Instead, it decreases over time as a heavy-tailed function.

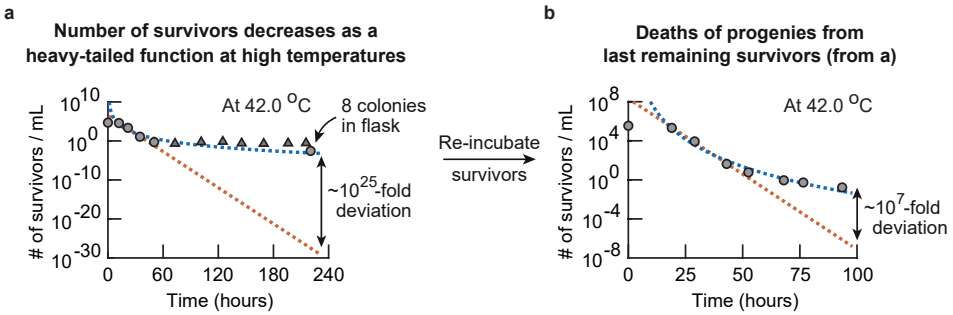

Figure S2.8: Number of survivors decreasing over time as a heavy-tailed function is not due to heat-tolerant mutants or persistor-like cells existing within a population (Related to Figures 2.3a-b). (a-b) The number of survivors / mL over time for populations of wild-type cells kept in the no-growth phase at 42.0 °C. The brown dashed lines represent an exponentially decaying function that we fitted to the data points that lie between 10 and 50 hours. The blue dashed curves are a power-law function that we fitted to the same data points. (Also see Supplementary Fig. S2.7). **(a)** The number of surviving wild-type cells. Triangles are overestimates (i.e., the aliquots taken from the liquid culture at 42 °C did not yield any colonies on agar at 30 °C, so there could not have been more survivors in the liquid culture than values represented by the triangles). Eight colonies formed at the last time point (~220 hours – the last circle). **(b)** We took one of these eight colonies – progenies of the survivors from the last time point in (a) – and used the cells from this colony to repeat the experiment. The number of survivors in this new experiment also decreased over time as a heavy-tailed function at 42 °C. This result eliminates the possibility that the survivors of the high temperature in the first experiment (a) are either heat-tolerant mutants or persistor-like cells that behave similarly to persistors of antibiotic treatments. To see this, suppose that the survivors at the last time point in (a) were heat-tolerant mutants or persistor-like cells. Then the starting population in (b) must be a pure population of these heat-tolerant mutants or persistor-like cells, that would have died at a slower rate than all the other cells of the wild-type population that started in (a). It then follows that the number of survivors/mL in (b) should decrease as a single, slowly decaying exponential function rather than decreasing over time as a heavy-tailed function. Thus, by contradiction, the survivors at high temperatures are not heat-tolerant mutants or persistor-like cells.

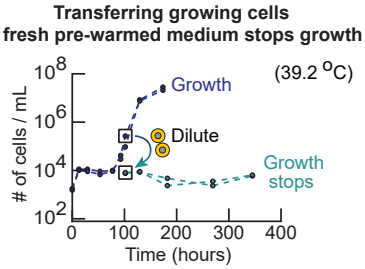

Figure S2.9: Transferring cells growing at ~39 °C to a fresh medium that was pre-warmed to 39 °C before the transfer stops cell growth (Related to Figure 2.4a). All experiments done at 39.2 °C. Two overlapping blue curves show two populations of wild-type cells that started with the same initial density. At this initial population-density, these two populations are in the random-growth phase at 39.2 °C. After ~100 hours of incubation at 39.2 °C, we took some of the cells in these populations, which were growing in mid-log phase (marked by the boxed blue data points), and transferred them into a fresh minimal medium that we pre-warmed to 39.2 °C. The transfer was such that the newly created population, in the fresh medium, started with the same number of cells / mL as the population-density that the original populations had after their transient growth and before they started to grow (~10,000 cells / mL as shown). A population that starts with ~10,000 cells / mL at this temperature (39.2 °C) would be in the deterministic-growth phase according to the phase diagram (Figure 2.2d). We incubated the newly created liquid cultures at the same temperature as the original populations and measured their population densities over time (green curves show two replicate populations). Both new populations did not grow at all (flat green curves), indicating that cells that were growing at the high temperature did not continue to grow when transferred to fresh medium at the same high temperature. The fact that these populations of transferred cells (green curves) did not grow does not contradict the phase diagram (Figure 2.2d) since, for constructing the phase diagram, we transferred cells from 30 °C to a new (higher) temperature whereas for the experiment described here, we transferred cells from 39.2 °C to 39.2 °C.

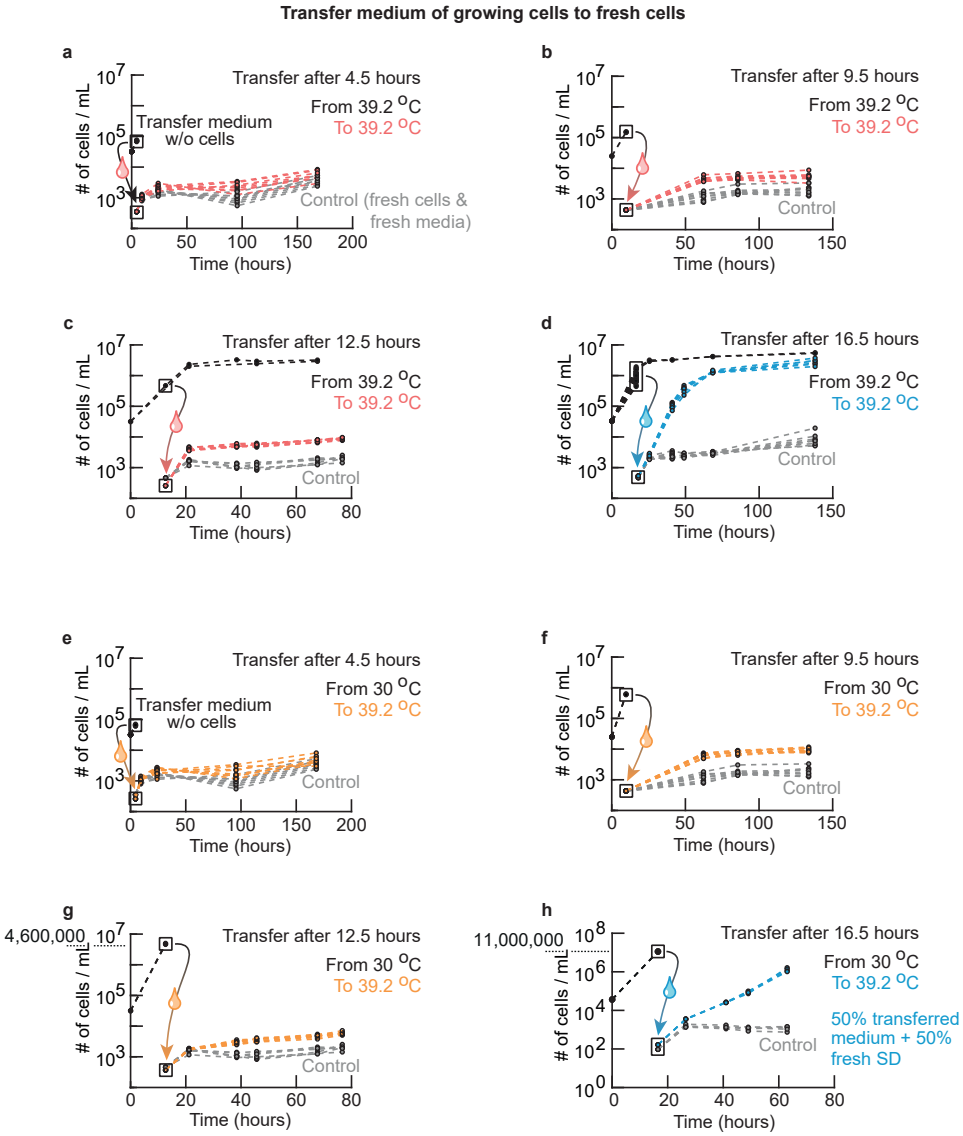

Figure S2.10: Density-dependent growth of cells at high temperatures is due to the cells collectively altering their shared extracellular environment (Related to Figures 2.4b-c). (a-d) All black curves all represent a population of wild-type cells that started with ~30,000 cells / mL and that was deterministically growing at 39.2 °C. We let such a population grow for 4.5 hours **(a)**, 9.5 hours **(b)**, 12.5 hours **(c)**, or 16.5 hours **(d)** before we flowed the liquid cultures of these growing cells through filter papers that had 200 nm diameter pores. This resulted in a complete, physical separation of the cells from their liquid growth media. We confirmed the complete separation by flowing the filtered media through a flow cytometer: we detected no cells in them at all. We then transplanted fresh cells into each of these filtered media. This created new populations (all initially ~400 cells / mL) which we also incubated at 39.2 °C. We then measured the densities of these newly created populations over time (red curves for (a-c) and blue curves for (d)). ***(caption continues on the next page)***

Figure S2.10 ***(caption continued from the previous page)*:** As a control, we also incubated fresh cells in fresh medium – rather than in one of the filtered media – at the same density (initially ~400 cells / mL). We then measured the control population's density over time (grey curves in (a-d)). For each color in (a-d), there are $n = 8$ (a-c) or $n = 6$ (d) replicate populations. Red curves in (a-c) show no appreciable growth beyond transient growth while the blue curves in (d) show populations that deterministically grew and reached the carrying capacity. These results (a-d) show that growing cells at a high temperature (e.g., 39.2 °C) gradually alter their extracellular growth medium – for example, by potentially secreting a factor – in such a way that the medium can induce growth of populations that cannot grow by themselves (without inheriting the changed medium) because their initial densities are too low (e.g., ~400 cells / mL). **(e-h)** We used the same protocol as in (a-d) except that this time, we grew the wild-type cells at 30.0 °C instead of at 39.2 °C before taking away their growth media for creating the new populations that we incubated at 39.2 °C. Specifically, we grew the wild-type cells – starting again at ~30,000 cells / mL (black curves) – for 4.5 hours **(e)**, 9.5 hours **(f)**, 12.5 hours **(g)**, or 16.5 hours **(h)** before taking away their liquid media and transplanting fresh, wild-type cells into them by using the same filtration method as in (a-d). We incubated the newly created populations (initially ~400 cells / mL) at 39.2 °C as in (a-d). Orange curves in (e-g) show these population densities over time at 39.2 °C. Grey curves in (e-h) show control populations which are identical to the control populations in (a-d). For each color in (e-h), there are $n = 8$ (e-g) or $n = 4$ (h) replicate populations. Beyond the initial, transient growth, none of the orange curves (e-g) show any sustained exponential growth (i.e., no population reached the carrying capacity). The results in (e-g) show that, unlike the media taken from the cells that were growing at a high temperature (39.2 °C), the media taken from cells growing at the conventional temperature (30 °C) does not contain the right factors for inducing growth of populations at a high temperature (39.2 °C). (h) Populations incubated at 30 °C were in a stationary phase after 16.5 hours of log-phase growth that depleted essential nutrients, which caused the populations to undergo a diauxic shift. We took out the growth medium of these stationary populations and supplemented it with 50 % fresh medium to replenish the depleted nutrients. We then transplanted fresh cells into this mix of fresh and depleted medium, and incubated the newly created population at 39.2 °C. Blue curves show all replicate populations growing at 39.2 °C. These results (e-h) show that some factors that yeasts secrete during a stationary phase at 30 °C after a diauxic shift – and perhaps during a diauxic shift – also can induce population growth at high temperatures (e.g., at 39.2 °C).

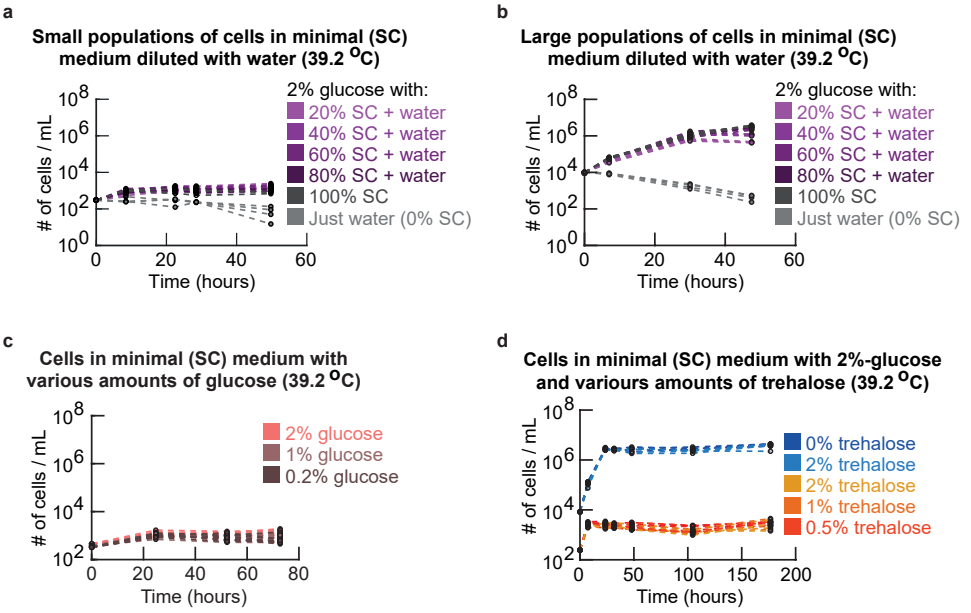

Figure S2.11: Population-density dependent growth at high temperatures is not due to cells depleting essential nutrients from the extracellular medium (Related to Figure 2.4c). All at 39.2 °C. **(a-b)** Minimal medium (called "SC medium") contains all essential amino acids and nitrogenous bases. Wild-type cells were incubated in SC medium that we diluted with water by various amounts as indicated (note: "100% SC" means no dilution, "50% SC" means that we used water to dilute all contents of SC by half, etc.). We supplemented all media, regardless of by how much they were diluted, with a saturating concentration (2%) of glucose. Growth curves show how population densities change for cells incubated in a 20%-SC medium (i.e., 20% SC + 80% water, supplemented with 2% glucose), 40%-, 60%-, 80%-, and a 100%-SC medium. Different colors represent different dilutions of SC. Light grey curves show populations incubated in just water with 2% glucose (i.e., no SC, and therefore no nutrients at all except for glucose). **(a)** All curves start at ~400 cells / mL. None of the populations grew. **(b)** All curves start at ~10,000 cells / mL. All populations, except for those without any essential amino acids (0% SC), grow deterministically until they reach their respective carrying capacities. Thus, the 20% to 100% SC all contain sufficient nutrients for a population to grow. Together, (a) and (b) show that population growth is not caused by depletion of some extracellular components in the SC-medium (i.e., these results suggest that cells secrete some factors that induce population growth at high temperatures). **(c)** Complementary to (a). Wild-type populations (initially ~400 cells / mL) were incubated at 39.2 °C in minimal medium (100%-SC medium) with various concentrations of glucose. Shown here are cells incubated in SC + 2% glucose, SC + 1% glucose, and SC + 0.2% glucose. None of these populations grew. Thus, population-density dependent growth that we observed is not due to the depletion of glucose. (a-c) together establish that it is not a depletion of any of the nutrients in the media that cause the observed population-density dependent behaviors. This is further supported by the fact that media that has been depleted of nutrients by wild-type populations in log-phase at 30 °C also does not induce population growth at high temperature (Supplementary Fig. S2.10e-g). **(d)** Wild-type cells incubated in minimal medium supplemented with various concentrations of trehalose at two different initial population-densities (one that is too low for population-level growth (~400 cells / mL) and one that is sufficiently high for population-level growth (~10,000 cells / mL)). These data show that trehalose neither inhibits (at 10,000 cells / mL) nor induces (at 400 cells / mL) population growth. These results show that trehalose plays no role in aiding or preventing populations growth at high temperatures. For each color in (a-d), there are $n = 4$ (a-b,d) or $n = 8$ (c) replicate populations.

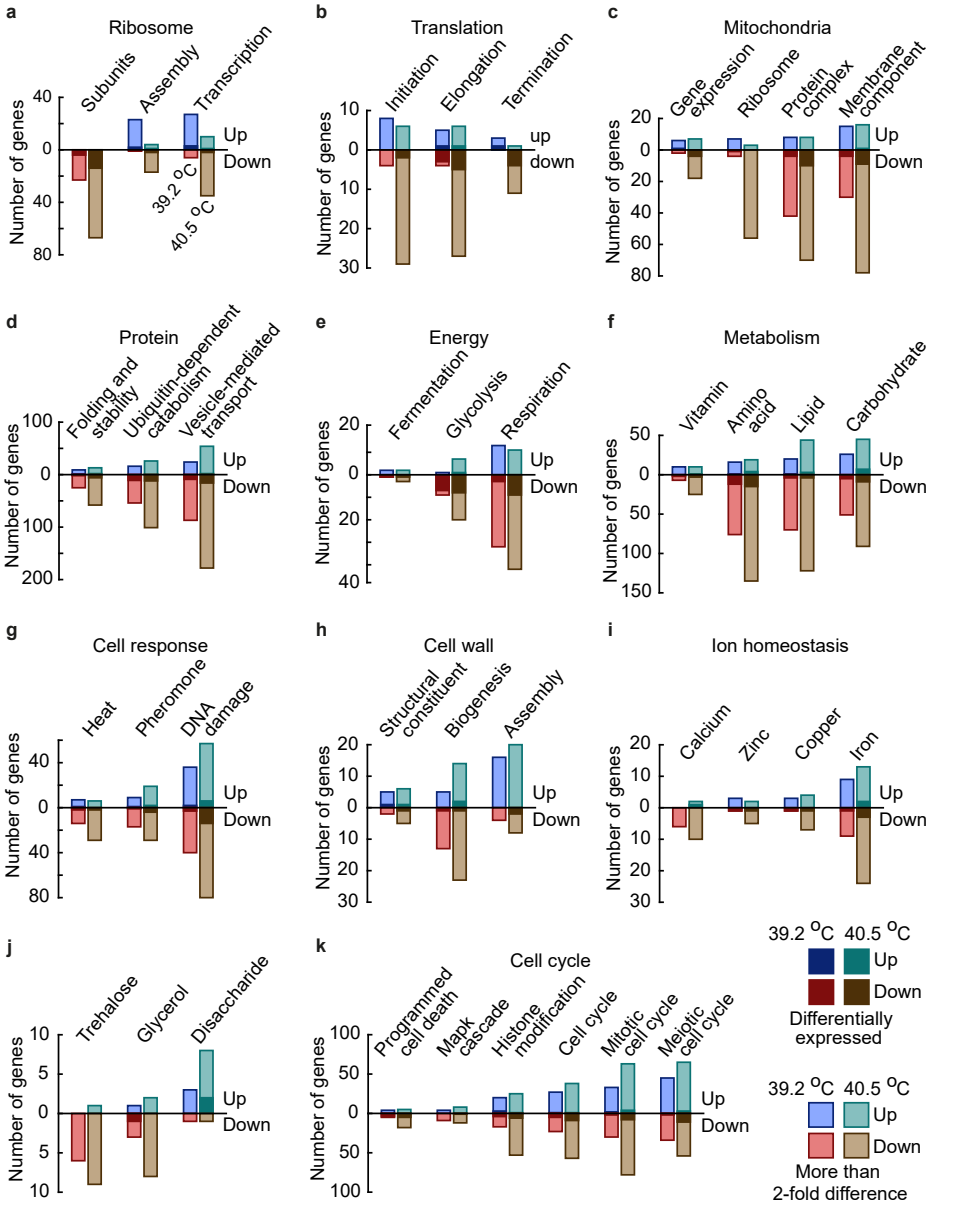

Figure S2.12: Transcriptome (RNA-seq) analysis reveals the effects of high temperatures on gene expression in deterministic-growth and no-growth phases (Related to Figures 2.4d-f). Transcriptome (RNA-seq) analysis of wild-type yeast cells in mid-log phase growth at 39.2 °C after 75 hours and 100 hours of incubation (initial population-density: ~11,000 cells / mL) and in no-growth-phase at 40.5 °C after 72 hours of incubation (initial population-density: ~48,000 cells / mL). Genes were categorized based on the Gene Ontology (GO) annotations. Shown here are the number of genes that are up-regulated (blue) and down-regulated (red) for the respective categories. Genes are classified as up- or down-regulated relative to their expression level in growing populations at 30 °C. ***(caption continues on the next page)***

Figure S2.12 ***(caption continued from the previous page)*****:** For the analysis, we averaged the expression levels of $n = 3$ (at 39.2 °C and 30 °C) or $n = 2$ (at 40.5 °C) biological replicates. The gene counts only include genes whose expression level differed by at least a 2-fold from their expression levels at 30 °C (shown in light colors) and genes that were differentially expressed (shown in dark colors, corrected for multiple testing). **(a)** Genes associated with the ribosome. Notably, ribosomal protein subunits were down-regulated. Ribosome assembly, polymerases I and III and transcription of rRNA were up-regulated for deterministically growing cells at 39.2 °C while they were down-regulated for cells in the no-growth phase at 40.5 °C. **(b-c)** Genes associated with translation **(b)** and the mitochondrial genes **(c)**. Almost all differentially expressed genes were down-regulated. The ribosomal genes of mitochondria were up-regulated for deterministically growing cells at 39.2 °C and down-regulated for the no-growth-phase cells at 40.5 °C compared to their expression levels at 30 °C. **(d-f)** Genes associated with protein processing **(d)**, genes associated with the central carbon metabolism **(e)** and other metabolic activity **(f)**. Many genes were significantly differentially expressed. Most notably, genes of the glycolysis and respiration were down-regulated at high temperatures. **(g-h)** Genes for cellular responses to heat and DNA damage **(g)** and genes associated with the cell wall **(h)**. Strikingly, cell wall assembly was up-regulated for both the deterministically growing cells and the no-growth-phase cells at high temperatures relative to their expression levels at 30 °C. **(i-j)** Genes associated with ion homeostasis **(i)** and other carbohydrates **(j)**. Most genes involved in the turnover of trehalose (a metabolite involved in thermotolerance) were down-regulated compared to their expression levels at 30 °C. Genes associated with metabolism of disaccharides such as maltose were up-regulated, even though the minimal growth medium lacked disaccharides and our wild-type strain is unable to grow on maltose. **(k)** Genes associated with the cell cycle. Summarizing **(a-k)**. Our transcriptome analysis revealed that the global gene-expression levels were predominantly down-regulated for both deterministically growing cells (at 39.2 °C) and no-growth-phase cells (at 40.5 °C) compared to the expression levels for growing cells at 30 °C. This global down-regulation was more pronounced for the no-growth-phase cells at 40.5 °C than for the growing cells at 39.2 °C. Interestingly, the central carbon metabolism was down-regulated for both the no-growth-phase and deterministically growing cells. Similarly, the synthesis of ribosomal subunits was also down-regulated even for the deterministically growing cells at 39.2 °C. In contrast, genes involved in the ribosomal transcription and assembly, the mitochondrial ribosome, and translation termination were up-regulated for the deterministically growing cells at 39.2 °C, while they were down-regulated for the no-growth-phase cells at 40.5 °C.

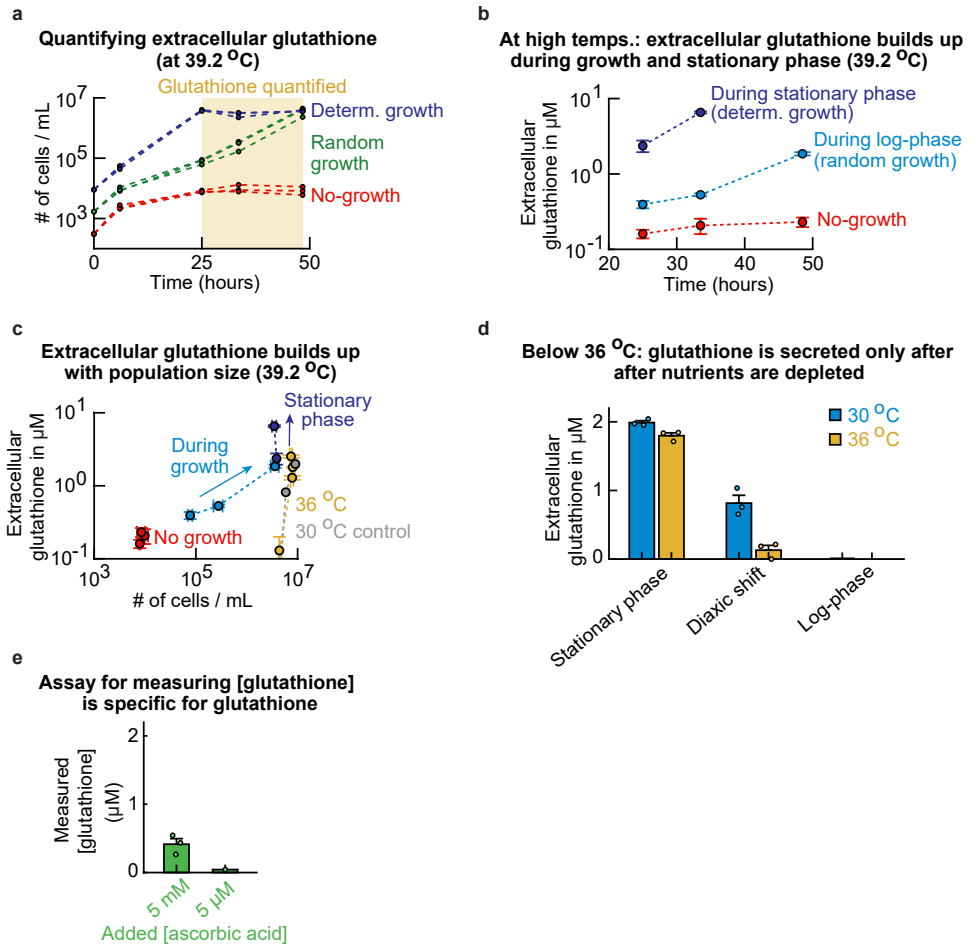

Figure S2.13: At high temperatures, cells in random-growth and deterministic-growth populations secrete glutathione while in log-phase growth and in stationary phase (Related to Figure 2.4e). **(a)** Populations with different starting densities at 39.2 °C ($n = 3$). **(b-c)** For each of the populations in (a), we measured the extracellular glutathione concentration after 25 hours, 33 hours and 48 hours of incubation at 39.2 °C (i.e., the time points in the yellow region in (a)). Error bars represent the mean with s.e.m., having $n = 3$ replicates per data point. **(b)** To quantify the extracellular glutathione concentration, we separated the cells from their media by using a filter that removes the cells (a filter with 0.45 µm pores and a cellulose-acetate membrane). To ensure and verify that there were no cells left in the filtered media, we flowed the filtered media through a flow cytometer. The flow cytometer did not detect any cells in the filtered media. We measured the glutathione concentration in the filtered media that we took from each population shown in (a) with a commercial assay kit (Methods 2.4). The extracellular glutathione concentration remained constant over time at a very low level for the no-growth populations (red curves). The extracellular glutathione concentration increased over time during the log-phase growth (light blue curves). The extracellular glutathione concentration kept increasing over time after a population had stopped growing and was in stationary phase because it had reached a carrying capacity (dark blue curves). To check whether most of the extracellular glutathione was in the oxidized or the reduced form, we also determined the concentration of oxidized glutathione in the filtered media taken from a population that was incubated for 48 hours at 39.2 °C. ***(caption continues on the next page)***

Figure S2.13 ***(caption continued from the previous page)*****:** For populations growing in log-phase (light blue in (b)), we found that most of the extracellular glutathione was in the reduced form (77% ± 3% (mean with s.e.m., $n = 3$), approximately 3 : 1 ratio of reduced-to-oxidized form). For the non-growing populations in the no-growth phase (red in (b)), we found that most of the extracellular glutathione was in the oxidized form (25% ± 24% (mean with s.e.m., $n = 3$), approximately 1 : 3 ratio of reduced-to-oxidized form). Hence, growing populations maintain an extracellular environment with more reduced glutathione than oxidized glutathione (note that the reduced form of glutathione, not the oxidized form, is able to reduce reactive oxygen species). **(c)** By combining the results of (a) and (b), we determined the extracellular glutathione concentration as a function of the population-density. This result shows that the no-growth-phase populations maintain, over time, a nearly constant population-density as well as a nearly constant extracellular glutathione concentration (red curve). While a population is growing in log-phase, the extracellular glutathione concentration keeps increasing while the population-density is increasing over time (light blue curve). The glutathione concentration continues to increase after the population has reached the carrying capacity and stops growing (i.e., during stationary phase) (dark blue curve). Also shown are the extracellular glutathione concentrations for populations at 30 °C (grey curve) and at 36 °C (yellow curve). Glutathione is only detectable after the population enters a stationary phase at temperatures below 36 °C (i.e., no secretion of glutathione during log-phase growth). **(d)** As a control, we measured the concentration of the extracellular glutathione for populations incubated at 30 °C (blue bars) and 36 °C (yellow bars). We did not measure any extracellular glutathione for populations that were growing in log-phase at these temperatures (unlike in the case of higher temperatures such as 39.2 °C – see (c)). But as soon as these cells depleted glucose, they started to secrete glutathione, resulting in the glutathione accumulating in the extracellular medium over time while the cells were in stationary phase at 30 °C and 36 °C. This observation matches the fact that the media that we transferred from a population that was in stationary phase at 30 °C (16 hours after incubation in 30 °C) induced population growth at 39.2 °C (Supplementary Fig. S2.10h). Moreover, these results show that cells only secrete glutathione during and after log-phase growth at temperatures above 36 °C, consistent with our observation that the growth of wild-type cells depends on the initial population-density only for temperatures above 36 °C(Supplementary Figs. S2.3-S2.4). **(e)** Testing the specificity of the commercial glutathione assay kit used in (b-d). We added either a low or beyond-saturating (physiologically unrealistic) concentration of ascorbic acid into fresh minimal medium and then subjected these ascorbic-acid containing media to the glutathione assay kit. Note that ascorbic acid is also an antioxidant but one that the budding yeast does not produce. For physiological concentrations of ascorbic acid (e.g., 5 μM shown), the glutathione assay kit did not show any readings (i.e., it did not falsely report that glutathione was present). It only reported a false signal (i.e., presence of glutathione) for the non-physiological ascorbic-acid concentration of 5 mM – the kit falsely reported ~0.4 μM of non-existent glutathione. Note that 0.4 μM is much lower than the > 1 μM glutathione that we observed in the filtered media of cultures grown at the high temperatures. Thus, for our purpose, we can say that the glutathione assay kit is specific for detecting glutathione with negligible false positive readings due to the components of minimal media or other antioxidants. For each condition in (d-e), the error bars represent the mean with s.e.m., having $n = 3$ biological replicates. Dots show raw data.

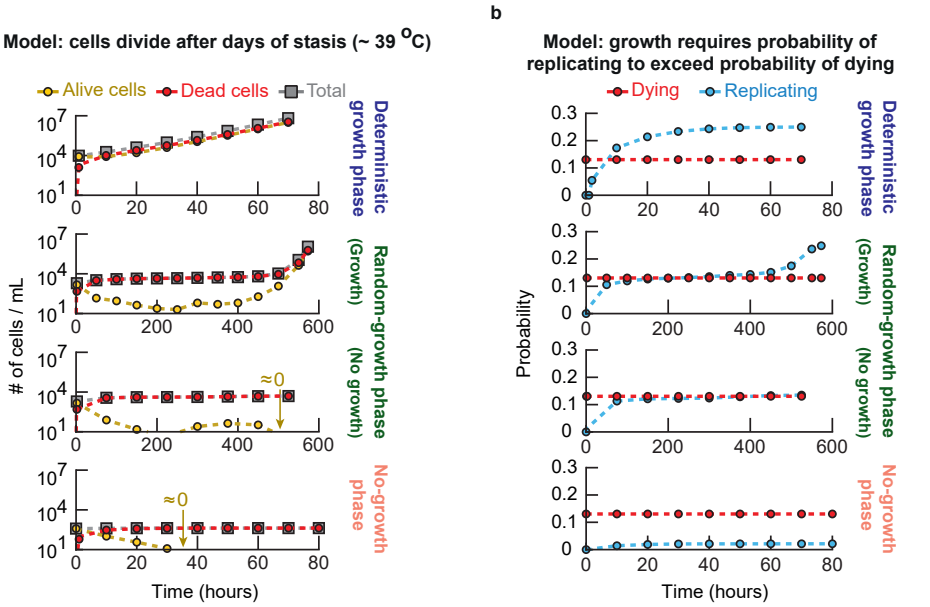

Figure S2.14: Mathematical model reproduces the sustained population of few replicating cells in random-growth and no-growth phases (Related to Supplementary Fig. S2.6). Simulations with the mathematical model. **(a)** The number of alive (yellow) and dead cells (red) over time. The same, fixed set of parameters was used as in Figure 2.5. Depending on the initial population-density, the number of alive cells grows exponentially (top row – deterministic-growth phase) or decreases exponentially until extinction (bottom row – no-growth phase). For intermediate population-densities (2nd and 3rd rows – random-growth), the population is very sensitive to the stochastic transitions of very few alive cells (at ~300 hours). Based on whether these cells stay alive without replicating, replicate, or die in the next time steps, the population can eventually either expand and exponentially grow (2nd row) or go extinct (3rd row). **(b)** The probability of replicating (blue) and the probability of dying (red) as a function of time for the same simulated populations as in (a). The probability of dying per unit time is fixed by temperature and identical for all populations, while the probability of replicating is initially zero and increases over time as the alive cells always secrete glutathione (Figure 2.5b). The probability of replicating quickly exceeds the probability of dying for high initial population-densities (top row), leading to deterministic growth. For intermediate initial population-densities (2nd and 3rd rows), the number of alive cells initially decreases over time as the probability of replicating continuously approaches – but stays smaller than – the probability of dying. Simultaneously, this decreasing pool of alive cells keeps secreting glutathione until, after ~300 hours, the probability of replicating is very close to the probability of dying and very few alive cells are left in the population. Here, the probability of replicating either exceeds the probability of dying – leading to exponential growth (2nd row) – or remains smaller than the probability of dying – leading to extinction (3rd row). This results in random-growth. For low initial population-densities (bottom row), the probability of replicating remains well below the probability of dying. Here, the population goes extinct before the alive cells can secrete sufficient glutathione to increase the probability of replicating, leading to no-growth.

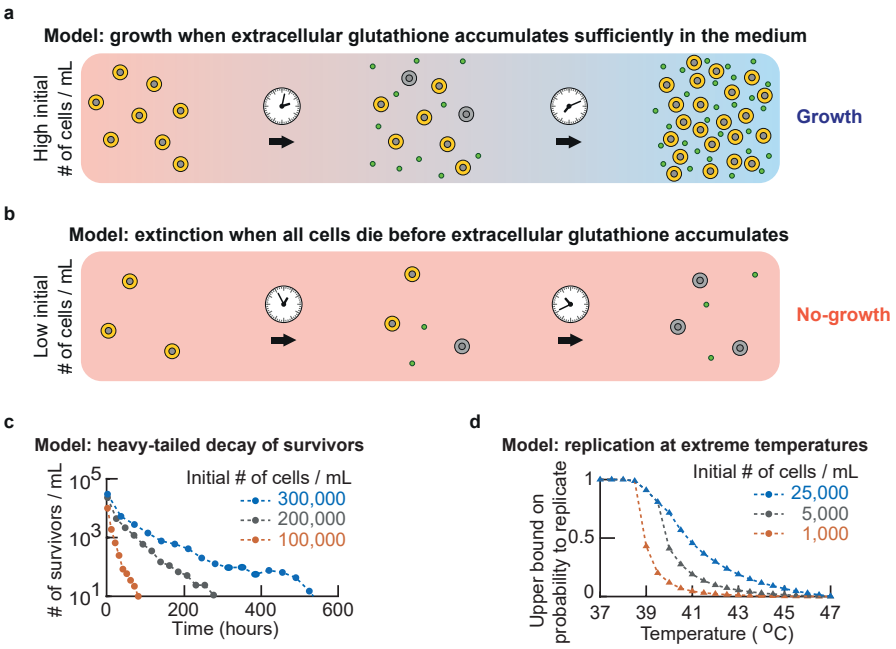

Figure S2.15: Mathematical model reproduces heavy-tailed decay of number of survivors and predicts that cells can replicate at extremely high temperatures (Related to Figure 2.5 and Supplementary Fig. S2.14). (a-b) Schematic summary that outlines the main features of the model. All cell populations eventually either grow exponentially **(a)** or go extinct **(b)**. **(c)** Only the no-growth phase exists in the population-level phase diagram for temperatures above 40.3 °C. Populations are unable to grow because the maximum probability of replicating is always lower than the probability of dying for these temperatures. Thus, over time, a decreasing number of alive cells continuously accumulates extracellular glutathione, which in turn increases the probability of replicating for those alive cells. Consequently, there is balance between a constant probability of dying and an initially lower probability of replicating that keeps approaching the probability of dying, evermore closing the gap between the two values (Supplementary Fig. S2.14). A competition between the two elements results in the population whose approach to extinction continuously slows down over time, leading to the number of survivors decreasing over time as a heavy-tailed (power-law-like) function (Supplementary Theory S2.6). **(d)** Finally, a consequence of our model, which recapitulates all the main features of the experimental data, is that cells could potentially replicate at extremely high temperatures (e.g., 45 °C) albeit with vanishingly low probability.

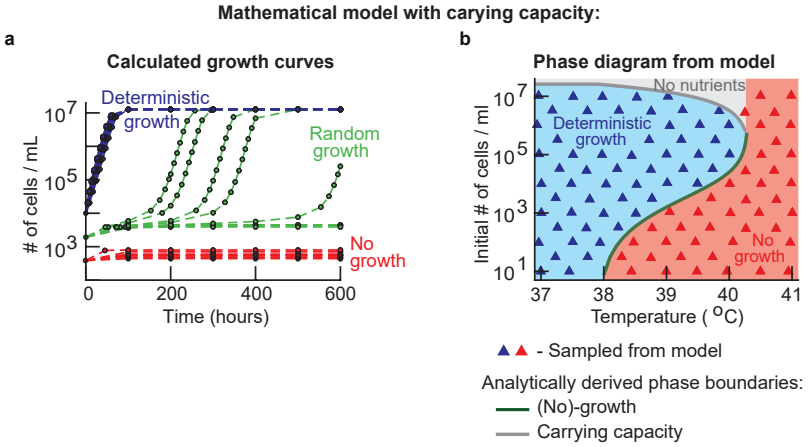

Figure S2.16: Extended mathematical model including a carrying capacity reproduces the fold-bifurcation (Related to Figure 2.5 and Supplementary Fig. S2.15). The carrying capacity was estimated by fixing the available nutrients for growth at 37 °C to permit a maximum density of $1.88 \cdot 10^7$ cells / mL (Fig. 2.2d and Supplementary Theory S2.6). All other parameters are identical to the ones in Fig. 2.5 and Supplementary Fig. S2.15. The extended model recapitulates **(a)** the population growth curves (compare with Figs. 2.2a and 2.5c), and **(b)** the phase diagram with analytically derived phase boundaries for growth (green solid line) and the carrying capacity (grey solid line) (compare with Figs. 2.2d and 2.5d). Although the carrying capacity is not necessary to describe the growth of cell populations at high temperatures, this extended model completes the description of all observed behaviors at high temperatures. The fold-bifurcation emerges as the phase boundary for growth (an unstable boundary where random growth occurs) meets and annihilates the phase boundary for the carrying capacity (a stable boundary beyond which populations are unable to grow).

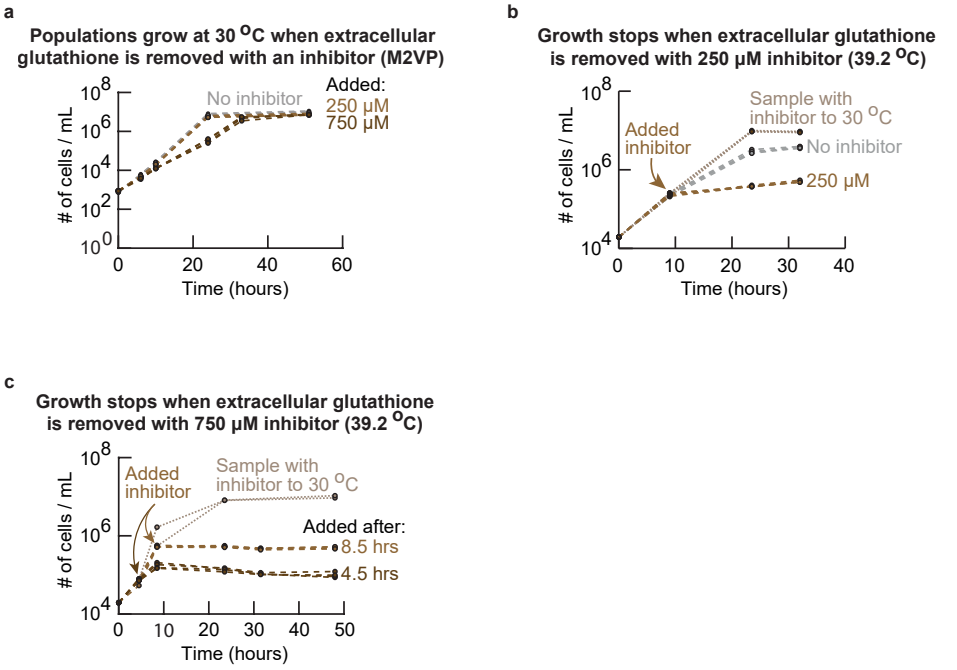

Figure S2.17: Chemically masking reduced glutathione in the extracellular environment stops population growth at high temperatures (Related to Figure 2.6a). **(a)** We used a thiol scavenging agent, 1-methyl-2-venylpyridinium (M2VP), to rapidly scavenge and mask all reduced glutathione (Methods 2.4). Wild-type populations at 30 °C were incubated with the masking agent at 0 µM, 250 µM and 750 µM. These populations exponentially grew at 30 °C. These results show that the masking agent (M2VP) does not interfere with intracellular processes and only scavenges extracellular glutathione (note that log-phase cells do not secrete glutathione at 30 °C). **(b-c)** At 39.2 °C. Deterministically growing populations at 39.2 °C were subjected to 250 µM of the masking reagent after ~10 hours of incubation **(b)** or 750 µM of the masking reagent after ~4.5 hours or ~8.5 hours of incubation **(c)**. All populations stopped growing after the masking agent was added. These results show that removing extracellular, reduced glutathione stops all growths at a high temperature. Aliquots of these populations, from 39.2 °C, were transferred to 30 °C after the masking agent was added (dotted light brown curves). These populations continued to exponentially grow to the carrying capacity at 30 °C. These results show that the masking agent stops population growth by specifically masking the extracellular glutathione that the cells secrete at high temperatures. For (a-c), all colors show $n = 4$ replicate populations.

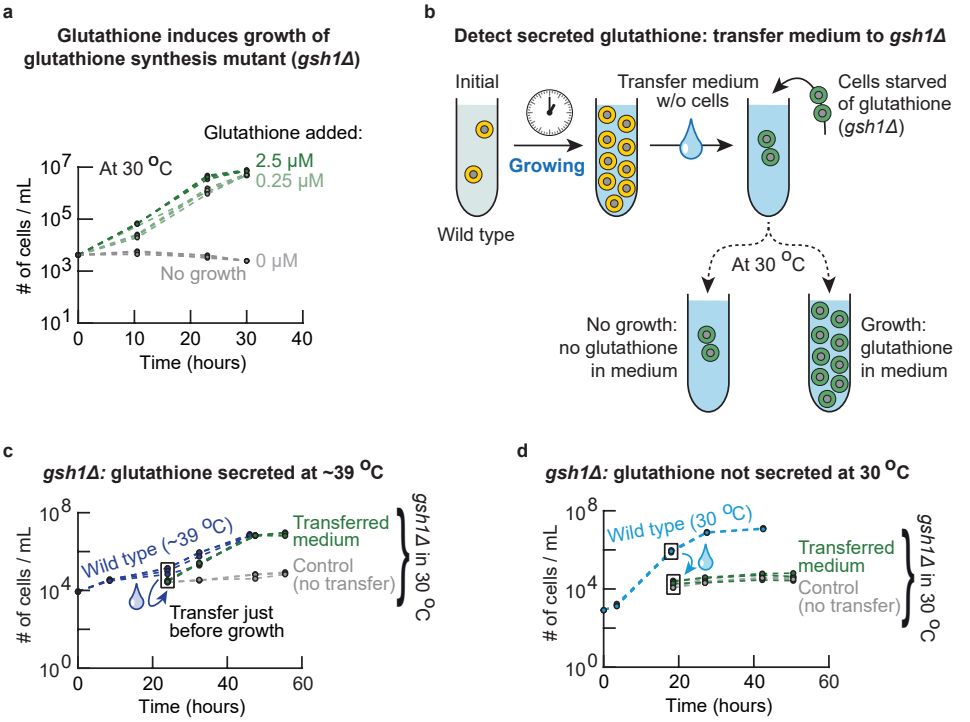

Figure S2.18: Mutant strain that cannot synthesize glutathione (*gsh1*Δ-mutant) detects glutathione secreted by wild-type yeast at high temperatures (Related to Figure 2.4e and Supplementary Fig. S2.13). (a) We constructed a mutant strain that could not synthesize glutathione by knocking out, in the wild-type strain, the *GSH1* gene which is essential for glutathione biosynthesis (Methods 2.4). Glutathione has essential intracellular roles in yeast, so the *gsh1*Δ-mutant can only grow in media that we supplement with glutathione [55]. To check this, we incubated cells of the *gsh1*Δ-mutant that we had starved of gluthatione in SD-medium, to which we then added 0 μM, 0.25 μM or 2.5 μM glutathione. These cells did not grow in medium without any glutathione (0 μM) but they grew in media with very small amounts of glutathione (i.e., more than 0.25 μM of extracellular glutathione). **(b)** We used the *gsh1*Δ-mutant strain to detect glutathione secreted by wild-type cells at high temperatures. We separated the growth media from cells grown at a fixed temperature by flowing the liquid cultures through 0.45 μM pore filters. We confirmed that there were no cells left behind in the filtered media by flowing the media through a flow cytometer. We then transplanted *gsh1*Δ-mutant cells that were starved of glutathione into these filtered media at 30 °C. Subsequently, we measured the population densities of the *gsh1*Δ cells over time at 30.0 °C. **(c-d)** For example, we took the growth media from wild-type cells, just before growth at 39.2 °C **(c)** or during late log-phase growth at 30.0 °C **(d)**. We then gave these filtered media to *gsh1*Δ-cells and incubated them at 30.0 °C (green curves). As a control, we incubated populations of *gsh1*Δ-cells at the same starting density in fresh medium without any glutathione (grey curves). Only the media taken from cells incubated at high temperatures (39.2 °C) was able to induce growth of *gsh1*Δ-cells. For all colors in each panel, there are $n = 4$ (a) or $n = 3$ (c-d) replicate populations. This result supports our finding that wild-type cells secrete glutathione at micromolar concentrations at high temperatures above 36 °C (Supplementary Fig. S2.13).

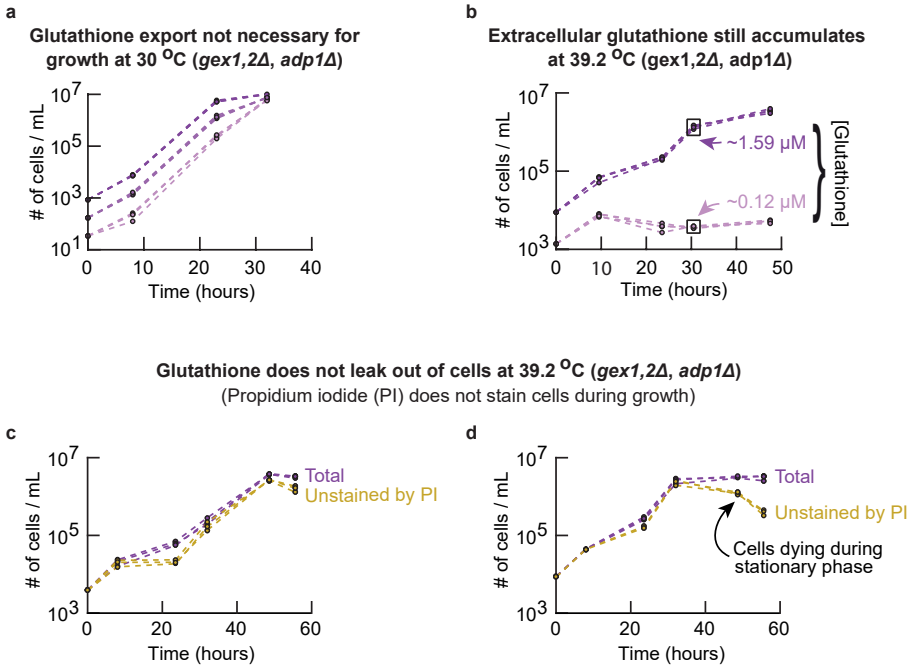

Figure S2.19: Mutants with reduced glutathione-export (*gex1,2*Δ-*adp1*Δ-mutant) still secrete glutathione at high temperatures, which is not due to glutathione passively leaking out through cell membranes (Related to Figure 2.6d). We constructed a mutant strain by knocking out, in the wild-type strain, three genes that encode major glutathione exporters: *GEX1*, *GEX2* and *ADP1* (Methods 2.4). **(a)** Population-density over time for populations of the export mutant strain, starting with different initial densities at 30 °C ($n = 4$ biological replicates). Growth of the mutant at 30 °C is not impaired compared to the wild type such that glutathione export is not necessary at 30 °C. **(b)** Populations of the mutant strain with different starting densities at 39.2 °C ($n = 3$ biological replicates). For each population, we measured the extracellular glutathione concentration after ~30 hours of incubation (boxed data points). These measurements show that growing populations of the mutant strain still secrete glutathione to the extracellular medium at high temperatures (1.59 ± 0.004 μM, mean with s.e.m.) while non-growing populations do not (0.12 ± 0.003 μM). **(c-d)** Population-density over time for the export mutant with different starting densities at 39.2 °C (purple curves, $n = 3$ biological replicates). For each population and for every time point, we took an aliquot of the liquid culture and incubated it with 1 μg / mL of propidium iodide for 20 minutes at room temperature. We measured the number of cells that were not stained by the propidium iodide with a flow cytometer (yellow curves). Cells stained by propidium iodide have lost their membrane integrity – propidium iodide flows into the cells and stains their DNA if and only if their membranes are damaged [66]. The fact that almost all the cells in the populations were unstained by the PI (i.e., the purple and yellow curves nearly perfectly overlap in (c-d)) shows that glutathione does not simply leak out of the mutant cells – their membrane integrity was maintained during their growths at the high temperature. In other words, the mutant strain exports glutathione through other export mechanisms besides those mediated by the three genes that we knocked out.

S2.6. SUPPLEMENTARY THEORY

S2.6.1. MODEL SUMMARY

We summarize here the most important analytical results on the model for yeast growth, before providing the mathematical argumentation and derivations. The simplest stochastic model for yeast growth at high temperature is that cells replicate and cells die with fixed probabilities per unit time. In such a linear model, the average behavior of the population is independent of population size. Since the population density dictates whether a population grows or not, any such linear model is unable to reproduce the behavior of yeast that we observed experimentally.
The presence or emergence of cells with a heritable trait, such as persister-like cells or heat-tolerant mutants that can replicate at high temperatures and pass this property on to their offspring, is also unable to explain our data. In our experiments, we use $c = 8$ replicate populations per condition, and the largest initial population size is $k = 25$-fold larger than the smallest one. An upper bound for the probability to observe the outcome of our experiments if the mechanism were a heritable trait is then given by (Section S2.6.3),

$$P_{c,k} \leq k^c \cdot \left(\frac{1}{k+1}\right)^{c+\frac{c}{k}} = 0.26. \tag{S2.1}$$

We were able to reproduce these results many times (Fig. 2.2a-c and Supplementary Figs. S2.3-S2.5), such that a model with a mechanism based on heritable traits cannot explain our experimental observations. Hence, we need a non-linear, stochastic model to reproduce the data. To this end we use experimental observations (Fig. 2.4a-g). Our data suggests that cells secrete gluathione that allows for cell growth when glutathione accumulates sufficiently (Fig. 2.4a-g and Supplementary Figs. S2.9-S2.13). We therefore extend the simplest model by assuming that the probability of replicating depends on the concentration of extracellular glutathione, which cells secrete at a constant rate.

The full model is as follows. Let A_t be the population-size of alive cells at a time t with initial population-size A_0. Per unit time, any cell dies with probability $p_d(T)$ that linearly increases with the temperature T. Moreover, cells replicate with probability $p_a(t)$ per unit time, where $p_a(t)$ is given by a maximum probability of replicating μ that is scaled by a Hill function depending on the concentration of the extracellular glutathione m_t and a constant $k(T)$. Finally, the glutathione accumulates extracellularly through secretion by alive cells at a rate $r_m(T)$. We describe the total population size at time t with N_t, and let $N_{\text{birth}}(t)$ and $N_{\text{death}}(t)$ be the number of births and deaths of cells at time t. Then the

stochastic model describing yeast growth at high temperature is given by,

$$\begin{aligned} N_{\text{birth}}(t) &\sim \text{Binom}\big(A_t, p_a(t)\big), \\ N_{\text{death}}(t) &\sim \text{Binom}\big(A_t, p_d(T)\big), \\ A_{t+1} &= A_t + N_{\text{birth}}(t) - N_{\text{death}}(t), \\ p_a(t) &= \mu \cdot \frac{m_t}{k(T) + m_t}, \\ m_{t+1} &= m_t + r_m(T) A_t, \end{aligned} \tag{S2.2}$$

where A_0 is the initial population-size, and the initial probability of replicating is given by $p_a(0) = 0$. The total population size changes according to,

$$N_{t+1} = N_t + N_{\text{birth}}(t). \tag{S2.3}$$

This model reproduces all the main features that we observed experimentally (Fig. 2.5 and Supplementary Fig. S2.14-S2.16). All simulations in all figures were performed with one single set of parameters, choosing the temperature T and initial population-size A_0 appropriately. The parameters used to fit the model to our experimental data are the maximum probability of replicating ($\mu = 0.25$; approximating some maximum growth rate of wild-type yeast), constant $K = k(T)/r_m(T) = 30{,}000$ (chosen such that order of magnitude of the phase boundary matches the boundary we found experimentally; Fig. 2.2d) and the probability of dying depending on temperature, $p_d(T) = \mu \cdot \frac{T - T_{\min}}{T_{\max} - T_{\min}}$ with $T_{\min} = 37.9\,^\circ\text{C}$ and $T_{\max} = 40.2\,^\circ\text{C}$ (chosen such that the endpoints of the phase boundary match the boundary we found experimentally; Fig. 2.2d).

A deterministic approximation of the stochastic model allows us to derive an analytical expression for the phase boundary between the deterministic growth phase and the no-growth phase (Section S2.6.6). The analytical expression for the phase boundary is given by (simplified equation S2.48),

$$A_0 \propto \frac{K \cdot p_d^2(T)}{\mu - p_d(T)}. \tag{S2.4}$$

Hence, the initial population-size required for growth diverges as the probability of dying approaches the probability of replicating in the model. Finally, the deterministic approximation is used to show that, in the no-growth regime where the population does not grow, the number of survivors in a population is not appropriately described by any exponential decay (Section S2.6.7). Instead, the rate at which the number of survivors changes continuously decreases. This is the result of the probability of replicating approaching the probability of dying. Therefore the decay of the number of survivors fol-

lows a heavy-tailed function, as we also find in our experiments (Fig. 2.3a-b and Supplementary Fig. S2.7).

S2.6.2. DESCRIPTION OF A LINEAR MODEL

First, we consider the simplest stochastic model for yeast growth at high temperature. We assume that all cells are identical and independent (i.i.d.). Let A_t be a random variable representing be the number of alive cells at a time t. Per unit time, cells replicate with probability p_a and cells die with a probability $p_d(T)$ that is monotonically increasing with temperature T. Then $\{A_t\}_{t\geq 0}$ is a discrete-time Markov process describing yeast growth at high temperatures. Let N_t be the total population size at time t and describe the number of births and deaths with $N_{\text{birth}}(t)$ and $N_{\text{death}}(t)$ respectively. This model is described by,

$$\begin{aligned} N_{\text{birth}}(t) &\sim \text{Binom}\big(A_t, p_a\big), \\ N_{\text{death}}(t) &\sim \text{Binom}\big(A_t, p_d(T)\big), \\ A_{t+1} &= A_t + N_{\text{birth}}(t) - N_{\text{death}}(t). \end{aligned} \tag{S2.5}$$

with the total population size changing according to,

$$N_{t+1} = N_t + N_{\text{birth}}(t). \tag{S2.6}$$

We can approximate this stochastic model as follows. As both cell replication and cell death follow a Binomial distribution with parameters p_a and $p_d(T)$ respectively, we have,

$$\mathbb{E}[A_{t+1}] = A_t + p_a A_t - p_d(T) A_t. \tag{S2.7}$$

By approximation, for large A_t, we then obtain the following linear differential equation for system,

$$\begin{aligned} A_{t+1} - A_t &\approx \Big(p_a - p_d(T)\Big) \cdot A_t \\ \frac{dA}{dt} &\approx \Big(p_a - p_d(T)\Big) \cdot A. \end{aligned} \tag{S2.8}$$

It follows that, for a sufficiently large initial population of replicating cells A_0, the number of alive cells in the population can be deterministically approximated by,

$$A(t) = A_0 \cdot \exp\Big((p_a - p_d(T)) \cdot t\Big). \tag{S2.9}$$

S2.6.3. NECESSITY OF A NON-LINEAR MODEL

Here we demonstrate that we need a non-linear model to describe yeast growth at high temperatures. To see this, suppose we have a linear model (e.g., as in Section S2.6.2). The parameters of this model are fixed (i.e., there is no emergence of heritable traits such as persister-like cells or mutants), and all cells are autonomous (independent). In our experiments, we find that, at 39°C, populations with initially 400 cells / mL never grow, while populations with initially 10,000 cells / mL always grow (Fig. 2.2b). Suppose that we use a linear model to simulate the behavior of these populations. Thus, we simulate a population having initially 400 cells / mL many times (say 25 replicates), all of which would not grow by assumption. Since the cells are autonomous, we can combine these twenty-five populations into one single, larger population without changing the outcome, because each cell is autonomous. Thus, we would have a population with initially $25 \cdot 400 = 10,000$ cells / mL, and we would obtain the same no-growth. This is because the cells were autonomous. This contradict our experimental results, as we found that the population of initially 10,000 cells / mL always grows (at 39 °C). Such argument demonstrates that a linear model with fixed parameters is unable to reproduce our experimental data.

This can also directly be seen from the linear model (Section S2.6.2). The behavior of the model (equation S2.9) is completely independent of the initial population-size of replicating cells A_0. When $p_a > p_d(T)$, the population would grow exponentially. In contrast, growth is impossible if $p_a < p_d(T)$ and the population would go extinct. Hence, yeast growth ceases at the temperature where the probability of dying p_d exceeds the probability of replicating p_a for populations of any size. Thus, such a linear model (Section S2.6.2) is unable explain our experimental data.

The arguments above do not consider populations growing through emergence of cells with a heritable trait (e.g., persisters or heat-tolerant mutants). Here we consider growth at high temperatures being enabled by such heritable traits. In such mechanisms, rare cells emerge or exist in the population whose probability of replicating exceed the probability of dying ($p_d(T) < p_a$), and who are responsible for a lineage of replicating cells in the population, leading to population growth. For convenience, we will refer to cells that can give rise to a whole lineage of replicating cells as "persisters" here. These persisters must exist in sufficiently low numbers in low density populations to not have these populations grow. At the same time, these persisters must occur frequently enough such that high density populations always grow. As soon as a population has a persister cell, it will grow until it reaches a carrying capacity due to the persister cell yielding a sub-population of cells that replicate. Next, we demonstrate that, regardless of the frequency at which the persisters initially are present or later emerge in a population, the

probability that such a mechanism reproduces our data is too small to be consistent with our data.

Experimentally we observe populations of cells of some initial size N_0 that never grow (Fig. 2.2a-c and Supplementary Figs. S2.3-S2.5). Moreover, in our experiments we use a $k = 25$-fold difference in initial population size between the lowest and highest initial densities. Thus, the largest populations initially have $k \cdot N_0$ cells and always grow. We therefore consider populations of cells with initially N_0 or $k \cdot N_0$ cells. We assume that these cells are identical and independent (i.i.d.), and that they are unable to replicate at high temperature ($p_d(T) > p_a$). Let $p_g > 0$ be the probability that a cell is or will become a persister cell. A persistor cell can replicate at high temperatures ($p_d(T) < p_a$), and leads to population growth because it passes this ability on to its offspring. Then the probability that a culture with an initial population of size N_0 will never grow is the probability that none of the cells becomes a persister cell, given by,

$$P_{\text{no growth}}(N_0) = (1 - p_g)^{N_0}. \tag{S2.10}$$

Moreover, the probability that the culture of initial size $k \cdot N_0$ will eventually grow is the probability that some cell becomes a persister cell, given by,

$$P_{\text{growth}}(k \cdot N_0) = 1 - (1 - p_g)^{k \cdot N_0}. \tag{S2.11}$$

Hence, the probability to observe c cultures of initial size N_0 that never grow and c cultures of initial size $k \cdot N_0$ that all grow, is given by,

$$\begin{aligned} P_c(N_0) &= \left(P_{\text{no growth}}(N_0)\right)^c \cdot \left(P_{\text{growth}}(k \cdot N_0)\right)^c \\ &= \left((1 - p_g)^{N_0}\right)^c \cdot \left(1 - (1 - p_g)^{k \cdot N_0}\right)^c. \end{aligned} \tag{S2.12}$$

Here $P_c(N_0)$ gives the probability to observe the outcome we observe in our experiments: all cultures of a small initial size do not grow, while all cultures of a large initial size do grow. To maximize the probability of observing this outcome, we want to maximize $P_c(N_0)$ for its only free variable, the probability to be or to become a persistor cell p_g. To simplify notation, let $x := (1 - p_g)^{N_0}$. Then, from equation S2.12,

$$\begin{aligned} P_c(N_0) &= x^c \cdot (1 - x^k)^c \\ &= \left(x - x^{k+1}\right)^c. \end{aligned} \tag{S2.13}$$

Taking the derivative to maximize $P_c(N_0)$ yields,

$$\begin{aligned}\frac{dP_c}{dp_g} &= \frac{dP_c}{dx}\cdot\frac{dx}{dp_g}\\ &= c\left(x-x^{k+1}\right)^{c-1}\cdot\left(1-(k+1)x^k\right)\\ &\quad\cdot N_0(1-p_g)^{N_0-1}\cdot(-1).\end{aligned} \tag{S2.14}$$

Notice that $\frac{dP_c}{dp_g}$ is zero for the trivial solutions $p_g = 0$ and $p_g = 1$ (none or all of the cells are persistor cells). The nontrivial solution of $\frac{dP_c}{dp_g} = 0$ is given by $1-(k+1)x^k = 0$, which yields the following solution maximizing $P_c(N_0)$ for p_g,

$$x = \left(\frac{1}{k+1}\right)^{\frac{1}{k}}. \tag{S2.15}$$

Therefore, the probability $P_c(N_0)$ that describes the outcome we observe in our experiments is maximized for,

$$(1-p_g)^{N_0} = \left(\frac{1}{k+1}\right)^{\frac{1}{k}}, \tag{S2.16}$$

and the probability p_g – the probability of being a persister cell – that maximizes the probability of observing our experimental outcome is given by,

$$p_g = 1-\left(\frac{1}{k+1}\right)^{\frac{1}{kN_0}}. \tag{S2.17}$$

Finally, by substituting equation S2.17 into equation S2.12 the actual probability $P_c(N_0)$ that describes the experimentally observed outcome is bounded from above by,

$$\begin{aligned}P_c(N_0) &\leq \left(\frac{1}{k+1}\right)^{\frac{c}{k}}\cdot\left(1-\frac{1}{k+1}\right)^c\\ &= k^c\cdot\left(\frac{1}{k+1}\right)^{c+\frac{c}{k}}.\end{aligned} \tag{S2.18}$$

This upper bound only depends on the number of replicate populations c per initial population size and the dilution factor k between the different population sizes. We used $c = 8$ replicate populations for each initial density and a $k = 25$-fold difference between the largest and smallest initial populations in our experiments. Thus, an upper bound for the probability to observe the outcomes of our experiments via persistor cells is given by $P_c(N_0) \leq 0.26$ (S2.18). We repeatedly made these experimental observations (Fig. 2.2a-c and Supplementary Figs. S2.3-S2.5), such that the presence or emergence of persister cells is unable to explain our observations.

S2.6.4. DEFINITION OF NON-LINEAR MODEL

A linear model such as in equation S2.9 is insufficient to describe the behavior of our yeast cells at high temperatures. Moreover, our data suggests that cells secrete glutathione that accumulates extracellularly and that allows for cell replication when a sufficient concentration has been reached (Fig. 2.4a-g and Supplementary Fig. S2.13). We can therefore safely assume that the cells are not independent (not autonomous). Here, we extend the linear model with the secretion of glutathione and a probability of replicating that depends on the extracellular glutathione concentration.

Similar to the linear model (equation S2.9), let A_t be the population size of alive cells at time t. Per unit time, a cell dies with probability $p_d(T)$ depending on the temperature T. In contrast with the linear model, we now assume that the probability of replicating is not a constant based on our observation that population-sizes can remain constant while still containing alive cells (Fig. 2.2a-b). Thus, we assume that cells replicate with probability $p_a(t)$, where $p_a(t)$ is given by some maximum probability of replicating μ that is scaled by a Hill function, which depends on the current concentration of extracellular glutathione m_t and a constant $k(T)$. The extracellular glutathione accumulates through secretion by alive cells with a secretion rate $r_m(T)$. As before, we describe the total population size at time t with N_t and let $N_{\text{birth}}(t)$ and $N_{\text{death}}(t)$ be the number of births and deaths of cells at time t. Then the non-linear, stochastic model is described by,

$$\begin{aligned} N_{\text{birth}}(t) &\sim \text{Binom}\big(A_t, p_a(t)\big), \\ N_{\text{death}}(t) &\sim \text{Binom}\big(A_t, p_d(T)\big), \\ A_{t+1} &= A_t + N_{\text{birth}}(t) - N_{\text{death}}(t), \\ p_a(t) &= \mu \cdot \frac{m_t}{k(T) + m_t}, \\ m_{t+1} &= m_t + r_m(T) A_t, \end{aligned} \tag{S2.19}$$

with the total population size changing according to,

$$N_{t+1} = N_t + N_{\text{birth}}(t). \tag{S2.20}$$

The behavior of this non-linear model is completely different from the linear model (Section S2.6.2). Here, the probability of replicating $p_a(t)$ increases monotonically over time as function of the number of alive cells. Initially the probability of replicating is zero and there is no guarantee that any population of cells will grow unless the cells accumulate sufficient extracellular glutathione such that $p_a(\tau) > p_d(T)$ for some time $\tau > 0$. This non-linear model (the equations in S2.19) is studied in more detail with simulations (Fig.

2.5 and Supplementary Fig. S2.14) and analytically through an approximation in the following sections.

S2.6.5. DETERMINISTIC APPROXIMATION OF THE NON-LINEAR MODEL

Here, we analytically study the non-linear model (equations in S2.19), for which we use a deterministic approximation to gain insight into some key features of the model. In the non-linear model, both cell replication and cell death follow a Binomial distribution, such that the number of alive cells at the next time step can be estimated by,

$$\mathbb{E}[A_{t+1}] = A_t + p_a(t)A_t - p_d(T)A_t. \tag{S2.21}$$

By approximation, we then obtain the following deterministic, non-linear system of equations:

$$\begin{aligned} A_{t+1} &= A_t + p_a(t)A_t - p_d(T)A_t, \\ p_a(t) &= \mu \cdot \frac{m_t}{k(T) + m_t}, \\ m_{t+1} &= m_t + r_m(T)A_t. \end{aligned} \tag{S2.22}$$

First, we rewrite this system into a more convenient form. We rescale the extracellular glutathione concentration through $M_t = m_t / r_m(T)$ and also rewrite $K(T) = k(T)/r_m(T)$. Here, $K(T)$ represents the constant $k(T)$ relative to the glutathione synthesis rate $r_m(T)$. Thus we obtain the following simplified, deterministic approximation of the stochastic model describing population behavior at high temperatures,

$$\begin{aligned} A_{t+1} &= A_t \cdot \Big(1 + p_a(t) - p_d(T)\Big) \\ p_a(t) &= \mu \cdot \frac{M_t}{K(T) + M_t} \\ M_{t+1} &= M_t + A_t. \end{aligned} \tag{S2.23}$$

Interpretation of the deterministic approximation. The relative change of the number of alive cells in the population is determined by the factor $1 + p_a(t) - p_d(T)$ which depends on time (through the probability of replicating) and on temperature (through the probability of dying). The number of alive cells increases on average when $p_a(t) > p_d(T)$ and the number of alive cells decreases on average when $p_a(t) < p_d(T)$. Notice that $p_a(t) \leq \mu$ for all $t > 0$ by choice of the Hill function. Moreover, as $p_a(0) = 0$, the population of alive cells in the population initially decreases exponentially (roughly decreases with a factor $1 - p_d(T)$ per unit time). For the maximum probability of replicating μ and

the probability of dying p_d we distinguish two cases:

- $p_d < \mu$: In the limit of the extracellular glutathione concentration ($M_t \to \infty$) we find that $p_a(t) \to \mu$. Then $p_a(t) > p_d$ for some $t > 0$. The population can grow exponentially.

- $p_d > \mu$: The probability of dying always exceeds the maximum probability of replicating, and the population of alive cells decreases on average. The population is guaranteed to go extinct.

The probability of dying depends linearly on the temperature. The qualitative behavior of the model is fixed for a given probability of dying. Without loss of generality, a sensible assumption is to let the probability of dying for a cell increase when the temperature increases. Since we know that all populations grow at $T = 37.9\,^{\circ}\text{C}$ and all populations do not grow at $T = 40.2\,^{\circ}\text{C}$ (Fig. 2.2d), the simplest assumption is to have the probability of dying linearly increase between these two values, such that $p_d(40.2) = \mu$. Any non-linear, but still monotonically increasing probability of dying as function of temperature yields the same qualitative behavior of the model, but displays these behaviors at different temperatures.

The glutathione secretion rate is constant. Instead of being a constant, one can set the glutathione secretion rate $r_m(T)$ to be dependent on, for example, the population size A_t or the current glutathione concentration m_t. Such modifications change the threshold $K(T)$ (equation in S2.23), which in turn changes the location of the steepest increase of the Hill function in the probability of replicating $p_a(t)$. Thus, choosing such modifications change how the probability of replicating changes over time in the model. However, the qualitative behavior of the model does not change upon a different, sensible, choices for the glutathione secretion rate $r_m(T)$ or the threshold $K(T)$. For example, we could set $r_m(T)$ to be linearly dependent on the population size A_t – such that larger populations secrete more glutathione. Conversely, we could set the secretion rate $r_m(T)$, for example, inversely proportional to the glutathione concentration m_t – lower glutathione concentrations trigger a higher secretion rate. These choices for non-constant parameters in the model make the growth ability of populations more or less sensitive to their initial densities, but do not change the qualitative behavior of populations (i.e., the existence of no-growth, random growth and deterministic growth). We therefore choose the simplest assumptions for our model by having the parameters $r_m(T)$ and $K(T)$ constant for a given temperature.

S2.6.6. ANALYTICAL DESCRIPTION OF THE PHASE BOUNDARY FOR GROWTH

Here we derive a description of the phase boundary in our model (Fig. 2.5). In contrast to the linear model for growth (equation S2.9), the non-linear model (equations in S2.19) allows for a population of cells with $p_a(0) < p_d(T)$ to grow for some $t > 0$ due to the accumulation of extracellular glutathione. Although this non-linear model (from the equations in S2.19) is stochastic, we can use the deterministic approximation (equations in S2.23) to gain some insight into the shape of the phase boundary for growth and study how the behavior of the model depends on the parameters. Notice that any cell population of the model eventually either grows or goes extinct due to the accumulation of glutathione. Without loss of generality, assume that there exists some $\epsilon > 0$ such that a cell population would (on average) grow when $p_a(t) > \epsilon p_d$ for some $t > 0$. Equivalently, a cell population would go extinct if $p_a(t) \leq \epsilon p_d$ for all $t > 0$. Note that $\epsilon = 1$ would suffice. For now, we ignore the dependence of cell populations on the temperature, and write $K = K(T)$ and $p_d = p_d(T)$ for simplicity. The approach here is as follows. First we derive upper and lower bound for the number of alive cells in a population, followed by upper and lower bounds for the concentration of the extracellular glutathione. Finally, all these bounds are used to derive an approximate description of the phase boundary for growth in the phase diagram (Fig. 2.5).

Bounds for the number of alive cells in a population. First, we determine a lower and upper bound for the number of alive cells when the population is not growing ($1 + p_a(t) - p_d(T) < 1$ for the equations in S2.23). Notice that, by recursive substitution of the equations in S2.23,

$$A_{t+1} = A_0 \cdot \prod_{s=0}^{t} \Big(1 + p_a(s) - p_d\Big), \tag{S2.24}$$

where A_0 is the initial number of alive cells at time $t = 0$. Moreover, the probability of replicating is bounded by $p_a(s) \geq 0$ for all $s \geq 0$, such that,

$$\begin{aligned} A_t &= A_0 \cdot \prod_{s=0}^{t-1} \Big(1 + p_a(s) - p_d\Big) \\ &\geq A_0 \cdot \prod_{s=0}^{t-1} \Big(1 - p_d\Big) \\ &= A_0 \cdot \Big(1 - p_d\Big)^t. \end{aligned} \tag{S2.25}$$

Next, suppose that the cell population goes extinct. Then $p_a(s) < \epsilon p_d$ for all $s > 0$ and some $0 < \epsilon \leq 1$ by assumption and,

$$\begin{aligned} A_t &= A_0 \cdot \prod_{s=0}^{t-1} \Big(1 + p_a(s) - p_d\Big) \\ &< A_0 \cdot \prod_{s=0}^{t-1} \Big(1 - p_d(1-\epsilon)\Big) \\ &= A_0 \cdot \Big(1 - p_d(1-\epsilon)\Big)^t. \end{aligned} \tag{S2.26}$$

Thus, using equations S2.25 and S2.26, when a cell population will go extinct, the number of alive cells in the population at time t is bounded by,

$$A_0 \cdot \Big(1 - p_d\Big)^t \leq A_t < A_0 \cdot \Big(1 - p_d(1-\epsilon)\Big)^t. \tag{S2.27}$$

Bounds for the concentration of extracellular glutathione. Next, we determine a lower and upper bound on the concentration of extracellular glutathione when the population of cells is not growing, similarly to the bound of the number of alive cells above. Recursive substitution of M_t and using equation S2.24 yields,

$$\begin{aligned} M_{t+1} &= \sum_{s=0}^{t} A_s \\ &= A_0 + \sum_{s=1}^{t} A_s \\ &= A_0 + A_0 \sum_{s=1}^{t} \prod_{k=0}^{s-1} \Big(1 + p_a(k) - p_d\Big). \end{aligned} \tag{S2.28}$$

Recall that we can bound the probability of replicating by $p_a(k) \geq 0$, such that,

$$\begin{aligned} M_{t+1} &\geq A_0 + A_0 \sum_{s=1}^{t} \prod_{k=0}^{s-1} \Big(1 - p_d\Big) \\ &= A_0 + A_0 \sum_{s=1}^{t} \Big(1 - p_d\Big)^s \\ &= A_0 \cdot \sum_{s=0}^{t} \Big(1 - p_d\Big)^s. \end{aligned} \tag{S2.29}$$

Equation S2.29 represents the first $t+1$ terms of a geometric series that converges as its ratio satisfies $|1-p_d(T)|<1$ (the phase boundary exists when $0<p_d(T)<1$). Hence,

$$M_{t+1} \geq A_0 \cdot \frac{1-\left(1-p_d\right)^{t+1}}{p_d}. \tag{S2.30}$$

Similarly, we seek an upper bound on the concentration of the extracellular glutathione. Suppose, that $p_a(k)<\epsilon p_d$ for all $k>0$ and some $0<\epsilon\leq 1$, such that the population goes extinct by assumption. Then, starting from equation S2.28, and substituting $p_a(k)<\epsilon p_d$ and simplifying as in equation S2.29,

$$\begin{aligned} M_{t+1} &= A_0 + A_0 \sum_{s=1}^{t} \prod_{k=0}^{s-1} \left(1+p_a(k)-p_d\right) \\ &< A_0 + A_0 \sum_{s=1}^{t} \prod_{k=0}^{s-1} \left(1-p_d(1-\epsilon)\right) \\ &= A_0 \sum_{s=0}^{t} \left(1-p_d(1-\epsilon)\right)^s. \end{aligned} \tag{S2.31}$$

Again substituting the known sum of a geometric series, we obtain,

$$M_{t+1} < A_0 \cdot \frac{1-\left(1-p_d(1-\epsilon)\right)^{t+1}}{p_d(1-\epsilon)}. \tag{S2.32}$$

Thus, when the cell population goes extinct, equations S2.30 and S2.32 yield the following bounds for the concentration of the extracellular glutathione M_t at time t,

$$A_0 \cdot \frac{1-\left(1-p_d\right)^{t}}{p_d} \leq M_t < A_0 \cdot \frac{1-\left(1-p_d(1-\epsilon)\right)^{t}}{p_d(1-\epsilon)}. \tag{S2.33}$$

Deriving the boundary between the growth and extinction regimes. The bounds from equations S2.27 and S2.33 provided us with estimates for the number of alive cells in the population and of the extracellular glutathione concentration when the population would go extinct. These bounds are usefull, as they provide the extracellular glutathione concentration and number of alive cells that any such population are expected to be able to achieve. Using these bounds, we seek a contradiction next. Assuming that a population wil go extinction, we seek the lowest initial number of alive cells A_0 for which the probability of replicating still exceeds the probability of dying before extinction. Hence, on average, the population does not go extinct since – even in the worst case – these populations would accumulate sufficient extracellular glutathione to grow.

More specifically, we first determine a lower bound on the probability of replicating $p_a(t)$ at the time when cell population is not yet extinct, as a function of the initial number of alive cells A_0. Here, the cell population is not yet extinct when (from equation S2.27),

$$A_t \geq A_0 \cdot (1 - p_d)^t \geq 1. \tag{S2.34}$$

Let τ be the time of extinction. Then, by solving equation S2.34, the time of extinction is lower bounded by,

$$\tau > \frac{\log(1/A_0)}{\log(1 - p_d)}. \tag{S2.35}$$

Substituting equation S2.35 in the lower bound for the extracellular glutathione concentration (equation S2.33) yields,

$$\begin{aligned} M_\tau &\geq A_0 \cdot \frac{1 - \left(1 - p_d\right)^\tau}{p_d} \\ &> \frac{A_0 - 1}{p_d}. \end{aligned} \tag{S2.36}$$

Thus, the extracellular glutathione concentration right before extinction is lower bounded by equation S2.36. Finally, substitution of equation S2.36 into the probability of replicating in our model (equation in S2.23) gives, as $p_a(t)$ is monotonically increasing in M_t,

$$p_a(\tau) > \mu \cdot \frac{A_0 - 1}{K p_d + A_0 - 1}. \tag{S2.37}$$

Recall that we assume that the population grows when $p_a(t) > \epsilon p_d$ for some $t > 0$. Therefore, the population will grow when (from equation S2.37),

$$p_a(\tau) > \mu \cdot \frac{A_0 - 1}{K p_d + A_0 - 1} > \epsilon p_d, \tag{S2.38}$$

Solving equation S2.38 for A_0 yields the following lower bound on the initial number of alive cells that always result in population growth,

$$A_0 - 1 > K \cdot \frac{\epsilon p_d^2}{\mu - \epsilon p_d}. \tag{S2.39}$$

In short, the above equation was derived as follows. We assumed that a population would go extinct, and determined the minimum concentration of extracellular glu-

tathione it would produce. This concentration yields a lower bound for the probability of replicating at the time of extinction. Finally, we derived a lower bound on the population size (equation S2.39) for which this probability of replicating exceeds the probability of dying, such that the population would still grow. Thus, any population that satisfies equation S2.39 cannot go extinct.

Next, again using equations S2.27 and S2.33, we determined an upper bound for the initial number of alive cells A_0 for which the population goes extinct. Recall that the population wuold go extinct when $p_a(t) \leq \epsilon p_d$ for all $t > 0$ and some $0 < \epsilon \leq 1$. Specifically, when τ is the time of extinction, we require that $p_a(\tau) \leq \epsilon p_d$ since $p_a(t)$ is monotonically increasing. The number of alive cells is bounded from above by equation S2.27 when the population goes extinct,

$$A_t < A_0\Big(1 - p_d(1-\epsilon)\Big)^t. \tag{S2.40}$$

Then the population is extinct for τ solving,

$$A_0 \cdot \Big(1 - p_d(1-\epsilon)\Big)^\tau < 1. \tag{S2.41}$$

Let τ be the time of extinction. Then, by solving equation S2.41 we obtain an upper bound for the time of extinction,

$$\tau < \frac{\log(1/A_0)}{\log\big(1 - p_d(1-\epsilon)\big)}. \tag{S2.42}$$

Substitution of S2.42 into the upper bound of the extracellular glutathione concentration when the population goes extinct (equation S2.33) yields,

$$\begin{aligned} M_\tau &< A_0 \cdot \frac{1 - \big(1 - p_d(1-\epsilon)\big)^\tau}{p_d(1-\epsilon)} \\ &< \frac{A_0 - 1}{p_d(1-\epsilon)}. \end{aligned} \tag{S2.43}$$

The bound in equation S2.43 gives an upper bound on the amount of extracellular glutathione a given population can accumulate at the time of extinction. Finally, substituting equation S2.43 into the probability of replicating yields,

$$p_a(\tau) < \mu \cdot \frac{A_0 - 1}{K p_d(1-\epsilon) + A_0 - 1}. \tag{S2.44}$$

Recall that we assume that the cell population would go extinct when $p_a(\tau) \leq \epsilon p_d$. Thus,

the population indeed goes extinct if, by substituting into equation S2.44,

$$p_a(\tau) < \mu \cdot \frac{A_0 - 1}{K p_d (1-\epsilon) + A_0 - 1} < \epsilon p_d. \tag{S2.45}$$

Solving equation S2.45 for A_0 yields the following upper bound on the initial number of alive cells that guarantees that the population goes extinct,

$$A_0 - 1 < K \cdot \frac{\epsilon(1-\epsilon)p_d^2}{\mu - \epsilon p_d}. \tag{S2.46}$$

In summary, we now found deterministic boundaries for the initial number of alive cells that, on average, guarantee extinction (equation S2.46) and population growth (equation S2.39). Growth and extinction are unpredictable for any initial number of alive cells in between. Thus, the random phase in our phase diagram (Fig. 2.5) is described by equations S2.39 and S2.46,

$$K \cdot \frac{\epsilon(1-\epsilon)p_d^2}{\mu - \epsilon p_d} < A_0 - 1 < K \cdot \frac{\epsilon p_d^2}{\mu - \epsilon p_d}. \tag{S2.47}$$

The interpretation of these bounds is as follows. Suppose that we want populations to grow when $p_a(t) > \epsilon p_d$ for some $t > 0$ and to go extinct when $p_a(t) \leq \epsilon p_d$ for all $t > 0$, with some $0 < \epsilon \leq 1$. Then the initial number of alive cells that describes the phase boundary scales according to equation S2.47,

$$A_0 \propto 1 + K(T) \cdot \frac{p_d^2(T)}{\mu - p_d(T)} \tag{S2.48}$$

Moreover, for the populations that go extinct, a lower bound for the extinction time is given by equation S2.35.

S2.6.7. HEAVY-TAILED DECAY TO EXTINCTION

Finally, we consider the death and extinction of populations at high temperatures. More specifically, we study the rate of death of the alive cells in the population. A common assumption is that the number of alive cells follows some exponential decay over time. This is indeed the case when the probability of replicating $p_a(t)$ is constant, since $1 + p_a(t) - p_d(T)$ is then a constant for each temperature (equations in S2.23). In contrast, the probability of replicating $p_a(t)$ in our model is monotonically increasing over time as a result of the accumulation of extracellular glutathione.

The rate of death for extinction-bound populations. First, we derive the rate at which the number of alive cells in the population decreases. To this end, notice that the number of alive cells in the population is approximated by the deterministic equations in S2.23,

$$A_{t+1} = \Big(1 + p_a(t) - p_d(T)\Big) \cdot A_t. \tag{S2.49}$$

We will only be interested in the rate at which the number of alive cells decreases at times very close to some time $t' > 0$. We therefore assume that $p_a(t)$ is temporarily a constant close to time t', such that $p_a(t) = p_a(t') := p_{a,t'}$. The probability of replicating $p_a(t)$ is thus independent of time for t near t'. For insight, we further approximate equation S2.49 with the following linear differential equation,

$$\begin{aligned} \frac{dA}{dt} &\approx \frac{A_{t+1} - A_t}{t+1-t} \\ &= A_{t+1} - A_t \\ &= -\Big(p_d(T) - p_a(t')\Big) \cdot A_t. \end{aligned} \tag{S2.50}$$

Solving this differential equation yields,

$$A_t = A_{t'} \cdot \exp\Big(-(p_d(T) - p_a(t'))(t - t')\Big), \tag{S2.51}$$

where $A_{t'}$ is the number of alive cells at the time t'. For $p_d(T) - p_a(t') > 0$, the above equation shows that the population A_t near time t' indeed exponentially shrinks with rate $p_d(T) - p_a(t')$. Thus, close to any time t', the number of alive cells in the population decreases exponentially with some characteristic rate $p_d(T) - p_a(t')$. However, this rate is monotonically decreasing as t' increases. This is because, over time, the probability of replicating increases towards the probability of dying through the accumulation of extracellular glutathione. To see how the probability of replicating increases towards the probability of dying, reconsider equation S2.51. We note that the rate at which the number of alive cells in the population decreases, given by $p_d(T) - p_a(t')$, increases from,

$$p_d - p_a(0) = p_d, \tag{S2.52}$$

at time $t = 0$ to, at the time of extinction (using the lower bound for the probability of replicating in equation S2.38),

$$p_d - p_a(\tau) \leq p_d - \mu \cdot \frac{A_0 - 1}{K p_d + A_0 - 1}. \tag{S2.53}$$

For sufficiently large populations ($A_0 \to \infty$), we then have $p_d - p_a(\tau) \to p_d - \mu$. Thus, the rate at which the number of alive cells decreases is initially p_d and decreases to some smaller value when the population goes extinct, down to $p_d - \mu \geq 0$ for sufficiently large populations. This shows that the rate at which the number of alive cells decreases is not constant, and can even become zero in cases where the maximum probability of replicating is equal to the probability of dying ($\mu = p_d$). In those cases, subject to fluctuations, the number of births on average matches the number of deaths in the population. Thus, our model explains how secretion of glutathione leads to a heavy-tailed decay of the number of alive cells in the population. We study this heavy-tailed decay in more detail next.

Extinction-bound populations do not follow exponential decay. Next we will show that the decreasing number of alive cells in an extinction-bound population cannot be bounded with an exponential function if sufficiently large populations grow at that same temperature. First we consider the decay of the number of alive cells A_t. For a given temperature, our model states that (equation in S2.23),

$$A_{t+1} = A_t \cdot \Big(1 + p_a(t) - p_d\Big), \tag{S2.54}$$

such that the decreasing number of alive cells is given by recursively substituting equation S2.54 (equation S2.26),

$$A_t = A_0 \cdot \prod_{s=0}^{t-1} \Big(1 + p_a(s) - p_d\Big). \tag{S2.55}$$

Now suppose that the number of alive cells A_t in the population decreases exponentially or faster. We can then find an upper bound for the number of alive cells in the population using some exponential function. Let $0 < \alpha < 1$ be some constant and assume that the number of alive cells in the population decreases at least exponentially,

$$A_t \leq A_0 \cdot \alpha^t. \tag{S2.56}$$

For A_t to be exponentially bounded, both equations S2.55 and S2.56 require that, for all $t > 0$,

$$A_0 \cdot \prod_{s=0}^{t-1} \Big(1 + p_a(s) - p_d\Big) \leq A_0 \cdot \alpha^t. \tag{S2.57}$$

Taking the logarithm and eliminating common terms yields the following condition for the decreasing number of alive cells to be exponentially bounded. For some constant

$0 < \alpha < 1$, we need,

$$\frac{1}{t}\sum_{s=0}^{t-1}\log\big(1+p_a(s)-p_d\big) \le \log(\alpha), \qquad \text{for all } t>0. \tag{S2.58}$$

In words, for the decay of $A(t)$ to be exponentially bounded, we need $\log(1+p_a(t)-p_d)$ to be on average remain smaller than $\log(\alpha)$ for some fixed $0<\alpha<1$. Recall the probability of replicating $p_a(t)$ is monotonically increasing in time. Therefore we have $p_a(t) \ge p_a(\tau)$ for all $t \ge \tau$ and $\tau > 0$. We can now split the function $p_a(t)$ into two time regimes for which we have a lower bound of the value $p_a(t)$: we can use the bound $p_a(t) \ge 0$ for $t < \tau$ and the bound $p_a(t) \ge p_a(\tau)$ for $t \ge \tau$. Thus, we can further bound the left hand side of condition S2.58 as,

$$\begin{aligned}
&\frac{1}{t}\sum_{s=0}^{t-1}\log\big(1+p_a(s)-p_d\big)\\
&\quad\ge \frac{1}{t}\sum_{s=0}^{\tau}\log(1-p_d) + \frac{1}{t}\sum_{s=\tau}^{t-1}\log(1+p_a(\tau)-p_d)\\
&\quad= \frac{\tau}{t}\log(1-p_d) + (1-\frac{\tau}{t})\log(1+p_a(\tau)-p_d).
\end{aligned} \tag{S2.59}$$

Substitution of the lower bound of equation S2.59 into equation S2.58 yields the following condition for the decreasing number of alive cells to be bounded by an exponential function,

$$\frac{\tau}{t}\log(1-p_d) + (1-\frac{\tau}{t})\log(1+p_a(\tau)-p_d) \le \log(\alpha), \tag{S2.60}$$

for all $t > \tau$. With $0 < \alpha < 1$, we can distinguish the following cases:

- $p_d < \mu$: These parameters allow for growth in our model (experimentally, for $T < 40.2°$C). We can choose any A_0 such that, eventually, $p_a(\tau) \ge p_d$ for some $\tau > 0$. Then $1 + p_a(\tau) - p_d > 1$ and $\log(1 + p_a(\tau) - p_d) > 0$. Substitution into equation S2.60 yields,

  $$\frac{\tau}{t}\log(1-p_d) < \frac{\tau}{t}\log(1-p_d) + (1-\frac{\tau}{t})\log(1+p_a(\tau)-p_d).$$

  We notice that $\frac{\tau}{t}\log(1-p_d) \to 0$ as $t \to \infty$ for τ fixed. Thus, for large enough populations and after sufficient time, the condition in equation S2.60 yields $0 \le \log(\alpha)$ which cannot be satisfied for $0 < \alpha < 1$. Thus, the decreasing number of alive cells in the population cannot be bounded by a single exponential function when $p_d < \mu$.

- $p_d > \mu$: The probability of dying is higher than the maxium probability of repli-

cating. No population can achieve $p_a(t) \geq p_d$ and all populations are guaranteed to go extinct. At time of extinction τ, we have $p_a(\tau) < p_d$ such that there exists some $1 > \alpha > 0$ for which the decay of the population of alive cells is exponentially bounded (we can choose $\alpha = 1 + p_a(\tau) - p_d$ in equation S2.57). However, the rate at which the number of alive cells decreases also monotonically decreases over time up to the point of extinction, starting with rate $p_d(T)$ at time $t = 0$ decreasing to $p_d(T) - p_a(\tau)$ at the time of extinction.

Overall, the number of alive cells in the population does not decrease exponentially over time. Instead, the decrease of the number of alive cells is heavy-tailed as a result of the probability of replicating approaching the probability of dying over time. When populations can grow ($p_d < \mu$), this heavy-tailed decay cannot be bounded by a single exponential function. Hence, the change of the number of alive cells in the population cannot be appropriately modeled by an exponential function. Experimentally, we find that the decay of the population of alive cells is indeed heavy-tailed (Fig. 2.3a-b and Supplementary Fig. S2.7), and appropriately described by a power-law function.

S2.6.8. LIMITED NUTRIENTS REVEALS ANALYTICAL FOLD-BIFURCATION POINT

As a last addition to the model, we describe the carrying capacity for the full stochastic model (equations in S2.19) and derive the analytical expression for the phase boundary at the carrying capacity. The carrying capacity describes the boundary in the phase diagram where nutrients become the limiting factor for cell replication. Cells can replicate at densities below the carrying capacity (sufficient nutrients) and cell replication stops and populations are unable to grow at densities above the carrying capacity (insufficient nutrients, Fig. 2.2d). To derive the carrying capacity, we assume that the temperature is such that $\mu > p_d(T)$ (growth is possible) and that we start with enough cells for the population to grow. The required number of alive cells is analytically approximated by the phase boundary for growth (equation S2.48, omitting the temperature dependence of $p_d(T)$ and assuming that $r_m(T) = 1$, with $K = k(T)$ independent of temperature for convenience),

$$A_0 \geq \frac{K p_d^2}{\mu - p_d}. \tag{S2.61}$$

Assuming equation S2.61, a population will accumulate enough extracellular glutathione to eventually reach a probability of replicating that satisfies $p_b(t) \approx \mu > p_d(T)$ and thereby grow. We can therefore safely assume that for some sufficiently small $\epsilon > 0$ and sufficiently long time $\tau > 0$, the number of alive cells can be bounded from below

by,

$$A_t \geq A_0 \cdot (1+\epsilon)^{t-\tau}, \qquad \text{for all } t \geq \tau. \tag{S2.62}$$

We further assume that there is a finite pool of nutrients R and that every alive cell in the population consumes one unit of nutrients from this pool per unit time, such that the number of consumed nutrients at time t is given by $\sum_{s=0}^{t-1} A_s = M_t$ – equal to the total number of units of accumulated glutathione, since each cell also secretes one unit of glutathione per unit time. Then the number of available nutrients after time t is given by $R - M_t$. For simplicity, we let the probability of replicating scale linearly with the number of remaining nutrients such that,

$$p_b(t) \propto \frac{R - M_t}{R}. \tag{S2.63}$$

Then the amount of consumed nutrients is bounded from below by (using equation S2.62),

$$\begin{aligned} M_t > \sum_{s=\tau}^{t} A_s &\geq \sum_{s=0}^{t-\tau} A_0 \cdot \Big(1+\epsilon\Big)^s \\ &= A_0 \cdot \frac{(1+\epsilon)^{t-\tau+1} - 1}{\epsilon}. \end{aligned} \tag{S2.64}$$

Since the number of consumed nutrients cannot exceed the carrying capacity R, we seek the time $t' > 0$ when the population runs out of nutrients. Solving equation S2.64 for the time t' at which nutrients have been fully depleted ($M_{t'} \geq R$), yields,

$$t' \geq \tau - 1 + \log\Big(\frac{\epsilon R}{A_0} + 1\Big) / \log(1+\epsilon). \tag{S2.65}$$

Then the maximum density A_∞ that can be achieved for a given amount of nutrients R is bounded from below by substituting the lower bound for the time where nutrients have been depleted (equation S2.65) into the lower bound for the population size (equation S2.62),

$$\begin{aligned} A_\infty \geq A_{t'} &\geq A_0 \cdot (1+\epsilon)^{t'-\tau} \\ &\geq \epsilon R + A_0. \end{aligned} \tag{S2.66}$$

Similarly, still assuming that the temperature is such that $\mu > p_d(T)$, the population density can be bounded from above by (recall that we grow with at most rate $\mu - p_d$, equation

S2.23),

$$A_t \leq A_0 \cdot (1+\mu-p_d)^t. \tag{S2.67}$$

Using the fact that $M_t = \sum_{s=0}^{t-1} A_s$, the number of consumed nutrients can be bounded from above by,

$$\begin{aligned} M_t &\leq A_0 \cdot \sum_{s=0}^{t-1} (1+\mu-p_d)^s \\ &= A_0 \cdot \frac{(1+\mu-p_d)^t - 1}{\mu - p_d}. \end{aligned} \tag{S2.68}$$

Solving equation S2.68 for $M_{t'} \leq R$ yields the minimum time $\tau > 0$ where the population still has nutrients available,

$$t' \leq \log\Big(\frac{(\mu-p_d)R}{A_0} + 1\Big) / \log(1+\mu-p_d). \tag{S2.69}$$

Finally, the maximum density A_∞ that can be reached for an available amount of nutrients R is upper bounded by substituting the upper bound for the time when nutrients are still available (equation S2.69) into the upper bound for the population size of the fastest possible growing population (equation S2.67),

$$A_\infty \leq A_\tau \leq (\mu-p_d)R + A_0. \tag{S2.70}$$

Combining the lower and upper bounds from equations S2.66 and S2.70 for the maximum possible population density that can be reached yields,

$$\epsilon R + A_0 \leq A_\infty \leq (\mu-p_d)R + A_0. \tag{S2.71}$$

with $\epsilon > 0$ and $\epsilon < \mu - p_d$. Thus, without loss of generality, using the phase boundary for growth to express A_0 (equation S2.61), we find the phase boundary at the carrying capacity,

$$A_\infty \propto (\mu-p_d)R + \frac{K p_d^2}{\mu - p_d}. \tag{S2.72}$$

When $p_d(T) \to \mu$ by increasing the temperature to the fold-bifurcation point, we obtain $A_\infty \to A_0$ since the first term in equation S2.72 becomes negligible compared to the second term in equation S2.72. We thereby find that the two phase boundaries will meet and annihilate each other at the fold-bifurcation.

3

SPEED LIMITS OF CELLULAR LIFE AT LOW TEMPERATURES

Microbes often live in frigid environments with slow intracellular processes. However, little is known about how slowly life can progress or the constraints that govern a cell's slow progression in life – how it proliferates, ages and dies. Here we use budding yeast to quantitatively establish principles that govern cell proliferation at near-freezing temperatures (0 °C – 5 °C). We discovered that ROS is the primary determinant of yeast's ability to survive and divide at near-freezing temperatures, with cells secreting glutathione to prevent death and enable cell replication. Observing days-to-months-long cell-cycle progression in individual cells revealed that ROS inhibits the S-G2-M (replicative) phases while elongating G1 (growth) phase up to a threshold duration, beyond which cells are unable to replicate and die due to an unsustainably large size. This threshold G1-duration is set by an interplay between ROS and the global gene-expression speed, which we quantified through the rates of genome-wide transcription and protein synthesis at frigid temperatures. A mathematical model demonstrates that the protein-synthesis rate and ROS together impose speed limits for life at near-freezing temperatures – the shortest and longest possible doubling times. Progressing through the cell cycle more slowly than the low-speed limit ensures death. This work establishes a quantitative foundation for understanding the fundamental limits of cellular life at near-freezing temperatures.

The content of this chapter has been submitted as: D. S. Laman Trip, T. Maire, H. Youk, *Fundamental limits to progression of cellular life in frigid environments*, In review (2022)

3.1. INTRODUCTION

Organisms that cannot regulate their internal temperatures – microbes, plants, and cold-blooded animals – often live in frigid environments without freezing. The cellular processes of these organisms, such as gene expression and cell division, are extremely slow but evidently progress at these near-freezing temperatures (0 °C - 5 °C) [1]. How they do so remains poorly understood [10, 11, 17, 18], raising fundamental questions about the limitations of cellular life. Central among them are how slowly a cell's life can proceed without stopping – how slowly a cell can move through its cell cycle and how slowly a cell approaches death. Beyond their relevance to near-freezing temperatures, these questions are central to understanding cellular life's limitations, whether one can slow a biological clock to an arbitrarily low, non-zero speed and whether doing so extends lifespan. We quantitatively address these questions for the budding yeast, *Saccharomyces cerevisiae*, at near-freezing temperatures by combining mathematical modeling with measurements at single-cell and genome-wide levels.

Conflicting observations argue both for and against the possibility of yeasts proliferating at near-freezing temperatures. Two popular views argue that budding yeast stops replicating at near-freezing temperatures. One proposes that essential processes such as transcription, translation, and molecular transport are too slow for sustaining proliferation at near-freezing temperatures [1, 7–9]. The other, complementary view proposes that yeast cannot proliferate at near-freezing temperatures due to physical damages caused by cell membranes becoming too rigid, proteins denaturing, oxidative stresses and others [1, 9–16]. Yeast can repair such damages by, for example, expressing genes to fluidify membranes, (re-)fold proteins with chaparones and respond to oxidative damages [1, 8, 14, 15]. But at sufficiently low temperatures (below 10 °C), the damage is thought to reduce proliferation [14], and eventually (at ~5 °C) becomes too severe for yeasts to divide [10, 14, 67]. These studies suggest that yeast cells cannot proliferate and are likely to die at an undetermined, sufficiently low temperature.

In contrast, daily experience tells us that some yeast cells in an isogenic colony can proliferate, albeit slowly, when stored in a refrigerator, and that fungal colonies can appear on refrigerated foods after months. Moreover, cellular processes can remain active at near-freezing temperatures despite being slow [8, 10, 17, 18, 67]. However, these observations do not quantitatively reveal limits to cellular life at near-freezing temperatures. Here, we show that few cells in an isogenic population of budding yeast can proliferate at near-freezing temperatures, and that Reactive Oxygen Species (ROS) are both the primary inhibitors of cell replication and primary causes of cell deaths. By re-

moving ROS, we enable cells to survive and replicate at near-freezing temperatures, so that populations that previously would have gone extinct can now grow. We observed single cells proliferating at unusual timescales for yeast (e.g., months), and determined the durations of extremely slow cell-cycle events, rates of protein synthesis, and rates of genome-wide transcription at near-freezing temperatures. By combining these findings, our study reveals an interplay between ROS and the rate of gene-expression that quantitatively determines both the likelihood and the speed limits of cell-cycle progression (i.e., fastest and slowest possible doubling time) at near-freezing temperatures. These results show that there is a precise speed-range for sustaining a yeast cell's life at near-freezing temperatures, and provides an approach for uncovering similar speed limits for other organisms. More generally, our findings establish a quantitative foundation for understanding fundamental limits to slowing down life, aging of cells and extending lifespans.

3.2. RESULTS

Cells help each other survive and replicate at near-freezing temperatures. To examine how yeast cells proliferate at near-freezing temperatures, we prepared liquid cultures of a laboratory-standard yeast strain ("wild type" *Saccharomyces cerevisiae*) at various population densities (from 10 cells/mL to 100,000 cells/mL). We incubated these cultures at various fixed temperatures (4.0 °C to 14.0 °C) in high-precision thermostatic incubators that maintained a desired temperature within ±0.1 °C (Supplementary Fig. S3.1). During ~60 days of incubation, we regularly took aliquots from each culture to measure its population density with a flow cytometer (Methods 3.4). At temperatures above 6.0 °C, every population always slowly grew to reach the carrying capacity (Supplementary Figs. S3.2). But at 5.0 °C, surprisingly, only populations that started with more than 1,000 cells/mL grew (Fig. 3.1a – blue curves) whereas populations that started with less than 1,000 cells/mL never grew (Fig. 3.1a – red curves). Strikingly, at 4.7 °C – just 0.3 °C below 5.0 °C – no population grew regardless of its initial density (Supplementary Figs. S3.2). In fact, not a single population grew at temperatures below 4.7 °C during the two months regardless of their initial density. Combining these measurements yielded a "phase diagram" that indicates for which initial densities a population could grow at each temperature (Fig. 3.1b). The phase diagram showed that density-dependent growth only occured within a narrow ~1 °C window between 5 °C and 6 °C and that 5 °C is the lowest temperature at which populations can grow. Outside the density-dependent regime, above 6.0 °C where populations always grow, the doubling time is independent of initial density and diverges as the temperature decreases (Supplementary Fig. S3.3). Still outside the density-dependent regime,

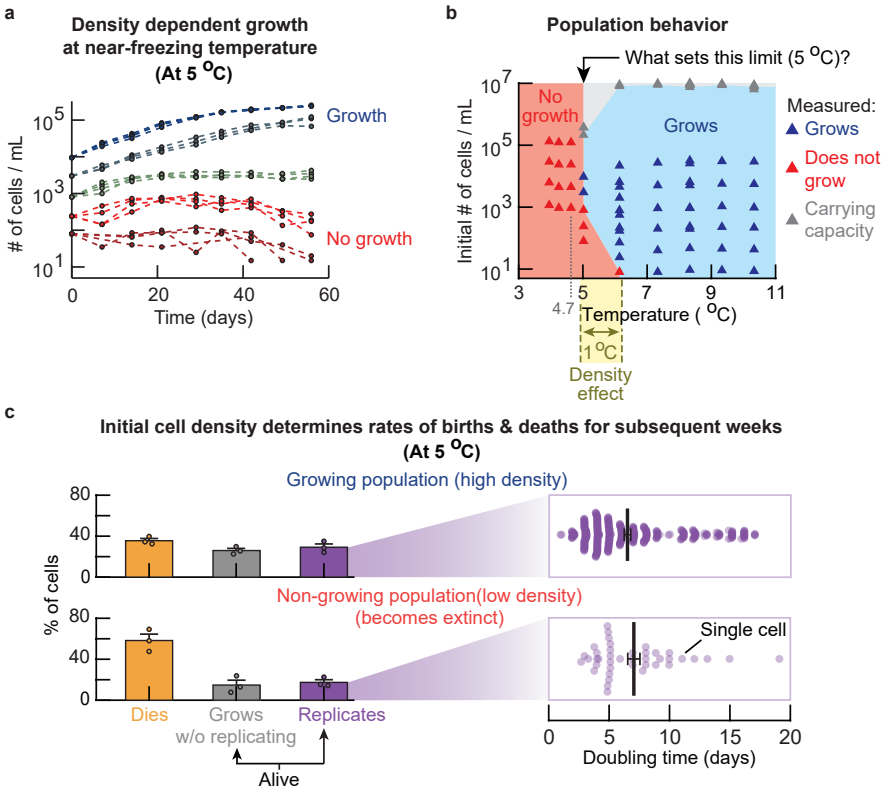

Figure 3.1: Cell proliferation, survival, and death are dependent on population density at lowest possible temperature (5 °C) at which populations grow. **(a)** At 5.0 °C. Population density (number of cells / mL) of wild-type yeast measured over time with a flow cytometer. Each curve shows a different population. Blue curves show "growth" (> 10-fold increase in population density). Red curves show "no growth". Each color has $n = 4$ replicate populations .(Also see Supplementary Fig. S3.1). **(b)** Phase diagram that summarizes all growth experiments of type shown in (a). Triangles represent every a population growing (blue), not growing (red), or a carrying capacity (grey). Regions are colored according to population behavior. Each triangle represents at least $n = 4$ biological replicates exhibiting identical behavior. (Also see Supplementary Figs. S3.2-S3.5). **(c)** *Left:* Single-cell behavior at 5.0 °C for high-density populations (initially ~6,250 cells / mL; growing) and low-density populations (initially ~250 cells / mL; non-growing). A cell either dies (orange bars), is alive and replicates (purple bars) or stays alive and grows without replicating (grey bars). In high-density populations, 29.2 ± 3.1% (mean with s.e.m.) of cells replicates, 35.6 ± 2.2% dies and 26.0 ± 2.1% grows without replicating. In low-density populations, 17.4 ± 2.6% of cells replicates, 58.3 ± 6.2% dies and 14.8 ± 4.8% grows without replicating. Remaining percentage of cells were conflicting in one of these categories (e.g., replicated and died during the time-lapse). Error bars show mean with s.e.m., having $n = 3$ biological replicates per condition. Dots show mean percentage of each population. *Right:* Single-cell doubling times for cells in high-density populations (top) and low-density populations (bottom). Doubling time is 6.5 ± 0.3 days (mean with s.e.m.) in high-density populations and 7.1 ± 0.5 days in low-density populations. Doubling times are the time interval between the mother cell forming a bud and either the daughter cell or mother cell forming a new bud. Data also includes cells whose divisions were unfinished at the end of the time-lapse. Error bar shows mean with s.e.m., with $n = 3$ biological replicates.
In all figures, the populations were pre-incubated for two weeks at the given temperature before the start of measurements other than cell densities.

below 5.0 °C where populations never grow, the doubling time exceeds the average lifespan of cells such that cells may survive but do not replicate (Supplementary Figs. S3.4-S3.5). Aas we will show, the phase diagram hides yeast's true ability to replicate at even lower temperatures (e.g., 1 °C).

To better understand the origin of the density-dependent growth at 5 °C, we used a wide-field microscope to continuously monitor single cells in "low-density" (~250 cells/mL) and "high-density" (~6,250 cells/mL) populations for ~20 days at 5 °C (Methods 3.4). The high-density populations grew to the carrying capacity whereas the low-density populations did not grow at 5 °C. For each cell, we determined whether it eventually died, stayed alive and replicated, or stayed alive without replicating (i.e., continuously grew in size) during the 20 days (Fig. 3.1c). We found that most cells in the high-density populations survived (36% died) whereas most cells in the low-density populations died (58%). Additionally, the low-density populations had less cells replicating (17%) than the high-density populations (29%). Hence, the low-density population was approaching extinction. In both populations, the replicating cells had doubling times that ranged from ~2 days to over 17 days (Fig. 3.1c). Moreover, the distributions of single-cell doubling times were nearly identical with comparable averages, being 6.5 days for the high-density population and 7.1 days for the low-density populations (Fig. 3.1c). Together, these results establish that density-dependent growth at 5 °C arises from cells collectively determining their survival and proliferation (Supplementary Theory S3.6).

Cells collectively remove Reactive Oxygen Species (ROS) by secreting glutathione in frigid environments. We sought to explain how cells in higher density populations are more likely to replicate. A common suggestion for cells being unable to replicate at near-freezing temperatures is that the gene-expression machineries may be too slow or impaired [1, 7]. However, we found that non-replicating cells could synthesize proteins at similar levels as replicating cells at 5 °C (Supplementary Fig. S3.6). We also discovered that the supernatant of high-density populations induced the growth of low-density populations that would have gone extinct without the supernatant (Supplementary Fig. S3.7). Hence, cells were likely secreting molecules that promotes their replication. One candidate molecule was trehalose – a cryoprotectant known to accumulate in cells and whose abundance correlates with viability at low temperatures [17]. However, we found that trehalose is not responsible for sustained replication at 5 °C (Supplementary Fig. S3.7) [68]. Motivated by our previous work (Chapter 2), we hypothesized that yeast could be secreting glutathione, a key antioxidant that reduces Reactive Oxygen Species (ROS) [40, 46, 47]. ROS can damage cellular components (e.g., nucleic acids [43, 69], proteins [44, 69], and cell membranes [45]) and are known to do so at near-freezing temperatures

[14–16]. Indeed, at 5 °C, we detected glutathione accumulating in the growth medium of high-density, growing populations but not for low-density, non-growing populations (Fig. 3.2a, Supplementary Fig. S3.8). In fact, growing populations secreted and extracellularly accumulated glutathione at every temperature below 8 °C (Supplementary Fig. S3.9). Moreover, by measuring intracellular ROS concentrations in live, single cells using fluorescent reporter dyes, we found that cells in the high-density populations typically had less intracellular ROS than cells in low-density populations (e.g., ~10-fold less superoxides on average) (Fig. 3.2b). Altogether, these results show that cells in high-density populations secrete more glutathione and have less intracellular ROS than cells in non-growing populations.

Adding reduced glutathione (GSH) enables and accelerates cell replication. We reasoned that cells were cooperatively reducing their intracellular ROS concentrations by using the extracellular pool of glutathione that they built together. To verify this, we added high concentrations (50 μM) of reduced glutathione (GSH) to the growth media of low-density populations at 5 °C. The added GSH caused the low-density populations to grow (Fig. 3.2c – green), whereas the same, low-density populations did not grow without added GSH (Fig. 3.2c – red). Moreover, the added GSH decreased the ROS concentrations in cells of the low-density populations (Fig. 3.2d – green) to nearly the same values as in cells of the high-density populations (Fig. 3.2b – blue; Supplementary Fig. S3.10). Hence, GSH alone – through its antioxidant action and above a ~1 μM concentration (Supplementary Figs. S3.11-S3.12) – is sufficient to decrease the intracellular ROS concentration and induce cell proliferation at 5 °C.

We also discovered that adding more extracellular GSH accelerates population growth at 5 °C (Fig. 3.2e). For example, without added GSH, low-density populations did not grow at all (Fig. 3.2e – red), while sufficiently high-density populations doubled in density once every 7 – 10 days while accumulating up to ~0.1 μM of extracellular GSH (Fig. 3.2e – blue). Low-density populations whose growth media were supplemented by GSH, doubled in density between once every 6 days (with 1 μM of GSH) and every 3 days (with 1 mM of GSH) (Fig. 3.2e – green). Thus, we could accelerate and tune the speed of cell replication by varying the amounts of extracellular GSH. We further confirmed this by monitoring single cells over weeks with a microscope. We found that adding GSH to the low-density populations more than tripled the percentage of cells that replicated (from 17% to 70%) and shortened the average single-cell doubling time by more than half (from 7.1 days to 2.9 days) (Supplementary Fig. S3.13).

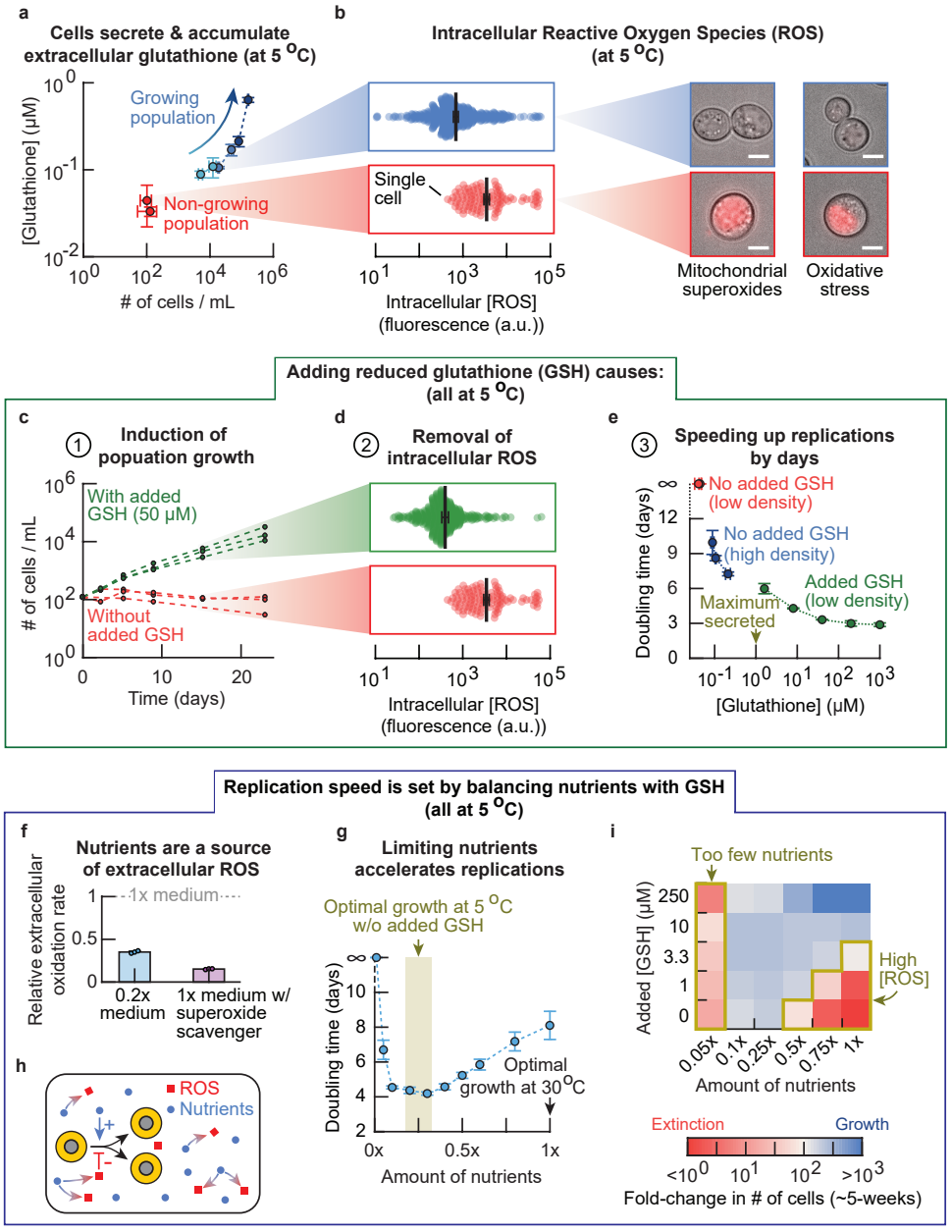

Figure 3.2: Glutathione enables and accelerates cell replications at near-freezing temperatures by removing ROS. All at 5.0 °C. **(a)** Measured extracellular glutathione concentration for low-density (non-growing) populations (red dots, initially ~300 cells / mL) and high-density (growing) populations (blue dots, initially > 900 cells / mL). Arrow indicates direction of time of incubation. Each data point has $n = 3$ biological replicates. (Also see Supplementary Figs. S3.7-S3.9). **(b)** Intracellular ROS abundance (mitochondrial superoxides) after two weeks of incubation in cells from high-density populations (blue dots, initially ~6,250 cells / mL) or low-density populations (red dots, initially ~250 cells / mL). ***(caption continues on the next page)***

Figure 3.2 ***(caption continued from the previous page)*:** Error bars show mean with s.e.m. of the average fluorescence in $n = 3$ biological replicates. Images show representative examples of intracellular ROS in cells from high-density populations (top row) or low-density populations (bottom row). Cells were stained to indicate mitochondrial superoxides (left column) or general cellular ROS (right column). Images are a composite of brightfield image with fluorescence of ROS-responsive dye. Scale bar is 5 μm. **(c)** Population-density over time of cells incubated with (green curves) and without (red curves) 250 μM reduced glutathione ("GSH"). Initially ~120 cells / mL. (Also see Supplementary Figs. S3.11-S3.12). **(d)** Intracellular ROS abundance in single cells from low-density populations (initially ~250 cells / mL) after two weeks of incubation without (blue dots) or with (green dots) 250 μM added GSH. Error bars show mean with s.e.m. of the average fluorescence in $n = 3$ biological replicates. (Also see Supplementary Fig. S3.10).**(e)** Doubling time as function of glutathione concentration for populations without any added GSH ([glutahione] measured) at low density (red curve), high density (blue curve), or with various amounts of added GSH (green curve, initially ~250 cells / mL). Each data point has $n = 4$ biological replicates. (Also see Supplementary Fig. S3.12). **(f)** Extracellular oxidation rate relative to the oxidation rate in plain 1x-medium, for 0.2x medium (blue bar) or 1x-medium that contained 100 μM superoxide scavenger (Trolox; purple bar). (Also see Supplementary Fig. S3.14). **(g)** Doubling time as function of the amount of non-sugar nutrients in the medium (initially ~190 cells / mL). Optimum doubling time of 4.2 ± 0.1 days (mean with s.e.m.) is achieved at ~0.3x non-sugar nutrients. Each data point has $n = 3$ biological replicates. **(h)** Summarizing (f-g): Non-sugar nutrients (i.e., the amino acids, vitamins and trace elements) have opposing effects on cell replication by simultaneously generating ROS and fueling replications at near-freezing temperatures. **(i)** Combining (c-h): Sensitivity of populations to abundance of non-sugar nutrients and GSH in the growth medium. Heatmap shows the measured fold-change of the population density after five weeks of incubation (initially ~210 cells / mL). Each condition shows the average fold-change of $n = 3$ replicate populations. (Also see Supplementary Figs. S3.15-S3.16). In all panels, the error bars represent mean with s.e.m..

In summary, we found that extracellular GSH has three major effects at near-freezing temperatures: *i)* removing intracellular ROS by acting as an antioxidant, *ii)* making cells more likely to replicate while decreasing their doubling time, and *iii)* enabling enough cells to survive and replicate to cause population growth. These results also establish that cells at 5 °C are not replicating as fast as possible, and that adding GSH unlocks faster proliferation.

Cell-replication speed is set by balancing amounts of GSH and ROS-generating nutrients. To further tune cells' ROS concentrations and quantify how ROS affects proliferation, we sought to identify and control a major source of ROS. Given that cells secrete glutathione, we hypothesized that ROS were created in the extracellular environment of cells. The growth medium that we used was a well-defined, minimal medium ("1x medium") consisting of 2% glucose and "non-sugar" nutrients (i.e., essential amino acids, vitamins, etc.). To infer the rate at which the growth medium generates ROS, we measured the fluorescence of oxidation-responsive dyes over time in media at 5 °C without cells (i.e., the oxidation rate). The oxidation rate is a proxy for the ROS-creation rate, as demonstrated by the observation that adding scavengers of ROS (e.g., scavengers of superoxides) to the 1x medium caused a ~6-fold decrease in the oxidation rate (Fig. 3.2f – purple bar). Moreover, decreasing the amount of non-sugar nutrients by 80% decreased the oxidation rate by ~3-fold (Fig. 3.2f – blue bar; Supplementary Fig. S3.14) and short-

ened the population's doubling time from ~8 days to ~4 days at 5 °C (Fig. 3.2g). Decreasing the amount of non-sugar nutrients further, however, sharply increased the population doubling time (Fig. 3.2g). This result demonstrates the opposing effects of nutrients, both fueling and inhibiting cell replication (Fig. 3.2h). Finally, by widely varying the concentrations of added GSH and non-sugar nutrients in the growth medium, we measured the extend to which we could inhibit or enable cell replication in low-density populations at 5 °C (Fig. 3.2i; Supplementary Figs. S3.15-S3.16). Together, these experiments establish that non-sugar nutrients are a major generator of ROS and that GSH can counteract ROS. Thus, ROS – from a balance between nutrients and GSH – dictate whether and how fast a population can grow at near-freezing temperatures.

ROS prevents cell replication and promotes death. Having identified ROS as a primary inhibitor of population growth, we sought to elucidate how ROS affects a cell's life – its ability to divide, grow, and survive. To achieve this, we used a wide-field microscope to continuously monitor single cells for ~3 weeks at 5 °C. At the start of the 3-week period, we used a fluorescent ROS-reporter dye to determine the ROS concentration in each cell (as in Fig. 3.2b), and subsequently determined which of the following events occurred over the next 3 weeks: A cell either successfully separated from its mother cell to begin its life ("begins life"), replicated ("replicates"), grew in size without replicating ("grows", without bud formation), or died by bursting open ("dies") (Fig. 3.3a). Hardly any cell remained stationary in its size and nearly all cells that died did so by bursting. By determining what percentage of cells underwent each of the four events within a given range of ROS concentrations, we found the probability of each event occurring as a function of ROS abundance. We did so for cells in high-density populations that accumulated GSH themselves (0.1 μM – 1 μM; Fig. 3.2a – blue) and for low-density populations with abundant added GSH (250 μM). In all populations, the cells with more ROS were less likely to replicate and more likely to die (Fig. 3.3b – purple and red curves respectively). Strikingly, despite the abundant GSH in low-density populations, there was virtually a zero chance of replicating for cells with more than a certain "threshold concentration" of ROS (Fig. 3.3b – bottom panel; purple curve ends at ~6,000 a.u. of ROS). The cells with ROS concentrations above this threshold did not replicate but could still increase in size or, more likely, die. In contrast, cells in the populations with added GSH were virtually assured to replicate if they had less than the threshold concentration of ROS (Fig. 3.3b – bottom panel; purple curve below ~6,000 a.u. of ROS).

Larger cells are more likely to die and less likely to divide regardless of their ROS level. From the continuous monitoring of cells we found no dependence between the abundance of intracellular ROS and the cell size (maximum cross-sectional area)

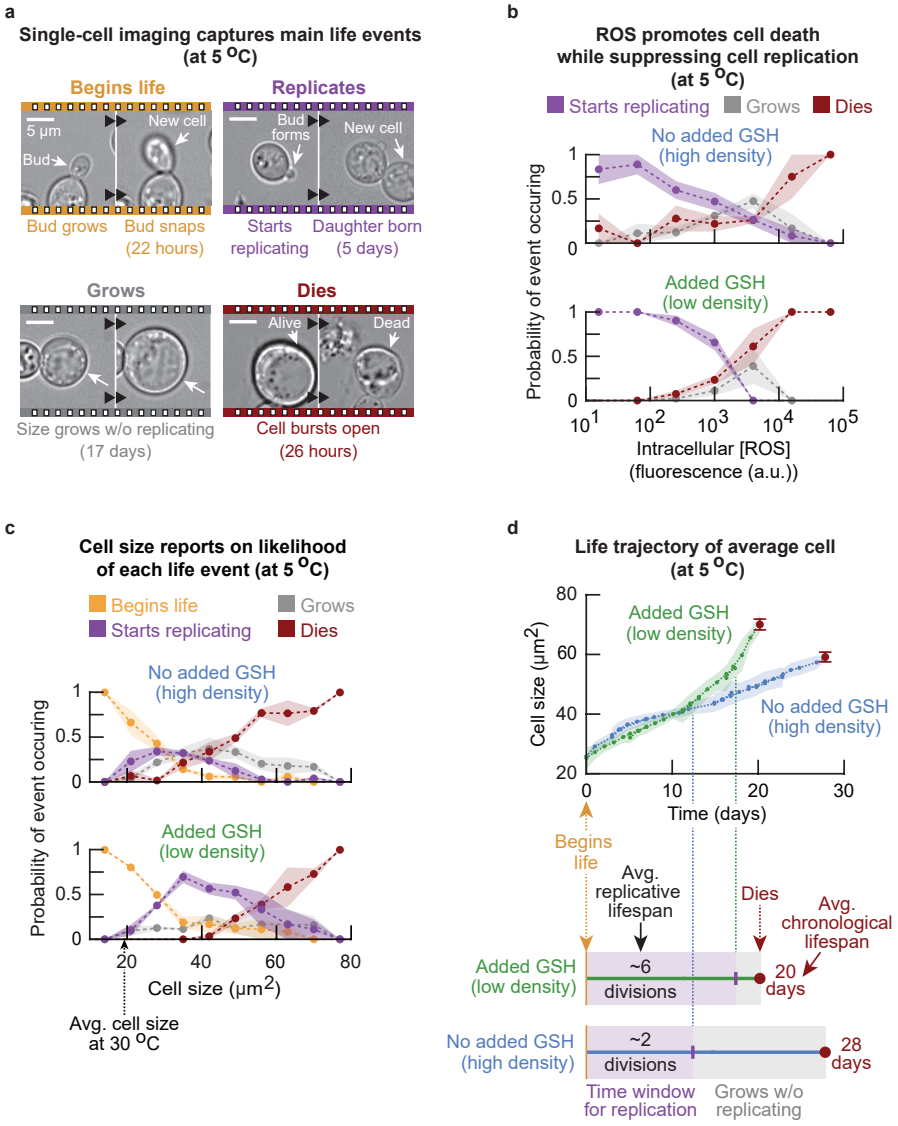

Figure 3.3: Glutathione shortens chronological lifespan and increases replicative lifespan at near-freezing temperatures. All at 5.0 °C. **(a)** Snapshots from time-lapse movies of single cells at 5.0 °C (initially ~8,000 cells / mL). Each cell exhibits one of four events: "Begins life" (just-born daughter cell after cytokinesis), "Replicates", "Grows" (grows in size without replicating), or "Dies" (by bursting open). Populations were incubated for two weeks at 5.0 °C before the start of the movies to remove transient effects. Scale bar is 5 µm. **(b)** Probability of each event occurring as function of the intracellular ROS (mitochondrial superoxide) concentration at 5.0 °C, showing the probability that a cell starts replicating (purple), grows without replicating (grey), or dies (red). Populations were incubated either without (top, initially ~6,250 cells / mL) or with (bottom, initially ~250 cells / mL) 250 µM added GSH. Dots show the mean, and shaded area represents the s.e.m. of average probabilities from $n = 3$ biological replicates. **(c)** Probability of each event occurring as a function of cell size. Shown are populations that were incubated either without (top, initially ~8,000 cells / mL) or with (bottom, initially ~420 cells / mL) 250 µM added GSH. ***(caption continues on the next page)***

Figure 3.3 ***(caption continued from the previous page)*:** Dots show the mean and shaded area shows the s.e.m. of average probabilities from $n = 3$ biological replicates. (Also see Supplementary Fig. S3.18-S3.19). **(d)** *Top:* Life trajectory of cells. Shown is average cell size over time at 5.0 °C without (blue curve, $n = 330$ cells) and with (green curve, $n = 175$ cells) 250 μM added GSH. Dots show the mean of the average cell size for each replicate. Red dot indicates average size at the time just before death. Shaded area and error bars represent s.e.m. of $n = 3$ biological replicates. *Bottom:* Timeline of cells. A cell begins life, may replicate and/or grow without replicating and eventually dies. The time window for replications (12 days without any added GSH, 18 days with added GSH) transitions into the time window for growth without replicating at the cell size where the probability of replicating decreases below the probability of growing or dying in (c). The average replicative age (2 divisions without any added GSH, 6 divisions with added GSH) is the time window for replications divided by the average single-cell doubling time (Supplementary Fig. S3.13). The average chronological age (28 days without any added GSH, 20 days with added GSH) was determined from the life trajectory and average cell size just before death. (Also see Supplementary Figs. S3.21-S3.23).

(Supplementary Fig. S3.17). Hence, we reasoned that cell size may yield additional information that is not provided by ROS. Motivated by this, we used the same type of single-cell movies at 5 °C as before to measure how likely each event – being born, replicating, growing in size without replicating, or dying – occurred as a function of cell size (Fig. 3.3c). As before, we compared high-density populations that grew without added GSH with low-density populations having abundant added GSH (250 μM). In both populations, we found that larger cells were less likely to replicate and more likely to die (Fig. 3.3c – red and purple curves respectively). Moreover, we found that increasing the amount of extracellular GSH – decreasing the average abundance of ROS in cells (Fig. 3.2d) – greatly increased the probability of replicating for cells of nearly every size. Indeed, cells in populations with abundant ROS were unlikely to ever replicate because they were born too large (Supplementary Fig. S3.18), while reducing the average ROS level caused even some of the largest cells to give birth to daughters (Fig. 3.3c – compare two purple curves). Together, these results establish that the cell size and ROS abundance independently tune the probability of replicating at 5 °C, with larger cells and cells with more ROS being less likely to replicate.

ROS shortens replicative lifespan but increases chronological lifespan. By continuously monitoring cells to find their probability of replicating, we found that the cell size continuously increases throughout a cell's life at 5 °C (Supplementary Figs. S3.19-S3.20). It also revealed the typical sizes of newborn ($< 30\ \mu m^2$) and dying cells ($> 60\ \mu m^2$). Thus, we could plot the average cell size as a function of time, starting with the typical size at birth and ending with the typical size at death (Supplementary Figs. S3.21-S3.22). Additionally, by using the probabilities of each event occurring for each cell size, we could construct a timeline that described the number of days that a cell typically lived (i.e., chronological lifespan) and the typical number of time that a cell divided before dying (i.e., replicative lifespan). We reconstructed these typical timelines for cells in high-

density populations without added GSH (Fig. 3.3d – blue curve), and for cells in low-density populations with 250 μM added GSH (Fig. 3.3d – green curve). The timelines revealed that having more GSH – and thereby less intracellular ROS – caused a typical cell to grow in size more rapidly (Fig. 3.3d – top panel). These cells died sooner by reaching a burst-prone size earlier in life. Hence, having less ROS shortens the chronological lifespan (Fig. 3.3d; Supplementary Fig. S3.23).

For the replicative abilities during the life of cells, we have found that older cells are less likely to replicate at 5 °C since cells continuously grow in size and larger cells are less likely to replicate (Fig. 3.3c-d). A cell thus loses its replicative ability as it ages. Moreover, we found that GSH promotes cell replication for cells of al sizes (Fig. 3.3c). As a consequence, the timelines show that a cell can replicate throughout almost its entire life with abundant GSH (first ~18 days of a 20-day lifespan), whereas it can replicate only within the first half of its life without added GSH (first ~12 days of a 28-day lifespan). Finally, the timelines show that having more GSH caused a three-fold increase in the replicative lifespan, from 2 divisions without added GSH to 6 divisions with added GSH (Fig. 3.3d – bottom two lines). This is a consequence of GSH shortening doubling times and enabling older cells to replicate (Figs. 3.2e and 3.3c). Altogether, these results establish that extracellular GSH accelerates the life of cells at near-freezing temperatures by speeding up cell replication, increasing the replicative lifespan and shortening the chronological lifespan of cells.

ROS elongate G1 (size growth) duration and inhibit G1-to-S transition. To discover how ROS inhibit cell replication at near-freezing temperatures, we engineered a yeast strain by fusing GFP to a histone (H2B) and mCherry to Whi5, a well-known regulator of the G1-to-S transition. For this strain, the fluorescence of H2B-GFP represents the amount of histones and is a proxy for the amount of DNA in a cell [70–72]), and migration of Whi5-mCherry fluorescence from the nucleus to the cytoplasm marks the G1-to-S transition [70, 73–76] (Supplementary Fig. S3.24). We monitored single cells of this engineered strain for nearly one month at 5 °C. Regardless of the extracellular GSH concentration, we found that replicating cells typically took one day to double their GFP level (the DNA duplicated) after Whi5-mCherry exited their nuclei (Fig. 3.4a). Additionally, in both populations, we found that the cells that never replicated continuously increased in size, while their GFP level (amount of DNA) did not change and Whi5-mCherry remained localized in their nuclei (Fig. 3.4b). Hence, the non-replicating cells were typically stuck in G1 at near-freezing temperatures.

By further monitoring individual cells replicating, we determined the average duration of all major cell-cycle events and how ROS affected each duration at 5 °C (Fig. 3.4c-d; Supplementary Fig. S3.25-S3.26). These measurements revealed that having more extra-

cellular GSH – and thereby lower ROS abundance in cells – caused more cells to exit G1 (Supplementary Fig. S3.25). Having more extracellular GSH also shortened G1 duration, from an average of 32 hours for cells that accumulated GSH by themselves to 15 hours for cells with 250 μM added GSH (Fig. 3.4c-d – green and blue data). Thus, cells with more intracellular ROS spent more time in G1 phase and are less likely to divide (i.e., less likely to enter S phase) [77–79]. This explains why a cell with an above-threshold concentration of ROS does not replicate: such a cell does not leave G1 and increases in size for many days, typically more than 6 days, until growing further becomes impossible and the cell dies by bursting (Fig. 3.4d – red and grey arrows). This suggests – and we will confirm – that a cell must exit G1 within a certain time window to complete a cell cycle and that this window is set by the threshold concentration of ROS.

ROS do not affect duration of S-G2-M (replicative) phases. Reconstructing the cell cycle also revealed that ROS did not affect the duration S-G2-M phases at 5 °C (Supplementary Fig. S3.26). Indeed we found that, regardless of extracellular GSH concentration, a replicating cell typically took ~25 hours to duplicate its chromosomes, ~6 hours for G2 phase, and ~22 hours for mitosis and cytokinesis combined (Fig. 3.4d – brown arrows). Hence, a typical cell took just over 2 days for the combined S-G2-M (replicative) phases of the cell cycle at 5 °C, regardless of ROS abundance. This establishes that the widely varying doubling times of individual cells that we previously noted (Fig. 3.1c) are due to the variation of the G1 duration in replicating cells. Including the G1 phase, the total cell-cycle duration (i.e., the doubling time) was 2.8 days for cells in populations with added GSH at 5 °C. This closely matches the 2.9 days that we measured as the average single-cell doubling time of the wild-type strain in the presence of added GSH (Supplementary Fig. S3.13).

Finally, by monitoring cells that replicated more than once, we discovered that a cell completes its current cell cycle more slowly than a previous cell cycle (Supplementary Fig. S3.27). This result shows that the duration of G1 elongates for consecutive replications. Thus, the doubling time of a single cell increases as a cell ages at 5 °C and the observed variation of G1 durations can, at least partially, be attributed to age differences of cells in the populations. Specifically, a newborn typically spent less than 12 hours in G1 (Fig. 3.4d – green arrow), whereas older cells could spend 16 days in G1 and eventually burst (Fig. 3.4d – red arrow; also see Fig. 3.3d). Altogether, these results establish that ROS and age elongate the G1 duration by inhibiting the G1-to-S transition and that GSH, through removing ROS, shortens G1 duration by promoting the G1-to-S transition. A cell thus loses its replicative ability as it ages by becoming unable to exit G1 at near-freezing temperatures (Fig. 3.3-3.4).

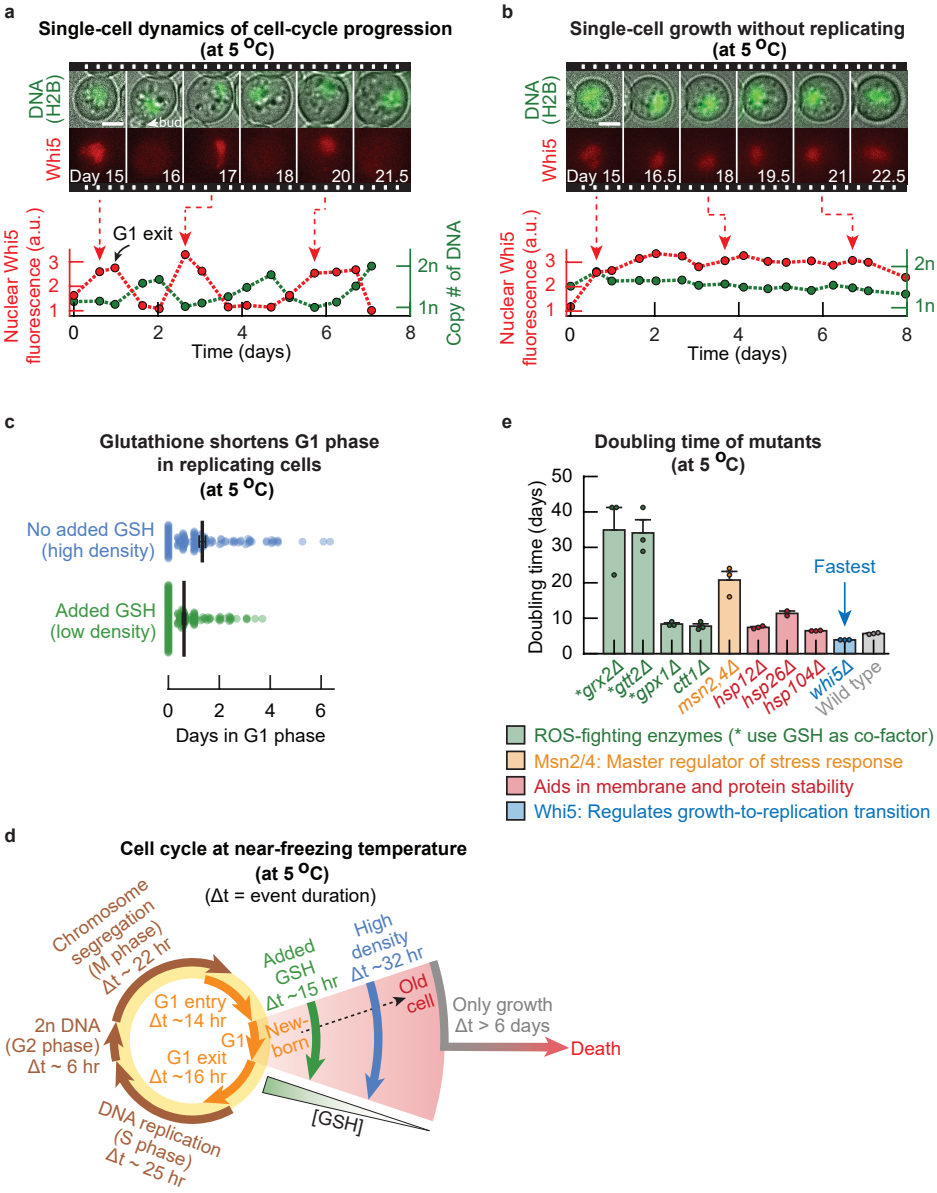

Figure 3.4: Reconstructing and tuning cell-cycle durations with ROS and mutations at near-freezing temperatures. All at 5.0 °C. **(a-b)** Single-cell dynamics of cell-cycle progression **(a)** and growth without replicating **(b)**. Cells were incubated for two weeks at 5.0 °C before the start of the measurements to remove any transient effects. Movie strips show composite of brightfield image with DNA (top row, H2B-GFP) or Whi5 (bottom row, Whi5-mCherry). Graphs show the normalized amount of nuclear Whi5 (red, left y-axis) and the copy number of DNA (green, right y-axis). Scale bars are 3 µm. (Also see Supplementary Fig. S3.24). **(c)** Distributions of G1 duration in replicating cells without (blue dots, initially ~6,250 cells / mL) or with (green dots, initially ~1,250 cells / mL) 250 µM added GSH. Average G1 duration is 32.0±3.0 hours (mean with s.e.m.) without and 14.7±1.5 hours with added GSH. Error bars show mean with s.e.m., having $n = 3$ replicate populations. Dots show data aggregated from all replicates. (Also see Supplementary Fig. S3.25). ***(caption continues on the next page)***

Figure 3.4 ***(caption continued from the previous page)*****: (d)** Duration of cell-cycle phases. Only the duration of G1 depends on ROS and age (orange arrows), but not S phase (~25 hours), G2 phase (~6 hours) or M phase (~22 hours) (brown arrows). Starting from newborns, G1 duration increases for cells in populations with 250 μM added GSH (~15 hours, green arrow), to cells in populations without added GSH (~32 hours, blue arrow), to over 6 days for non-replicating cells (grey/red arrow). (Also see Supplementary Figs. S3.24-S3.27). **(e)** Doubling time of mutant strains (all initially ~6,250 cells / mL). Mutants were a knockout of: ROS-fighting enzymes that use GSH as a co-factor (*grx2*Δ (doubling time 35 days), *gtt2*Δ (34 days), *gpx1*Δ (8 days); green bars) or without GSH as co-factor (*ctt1*Δ (8 days); green bar), master regulators of the general stress response (*msn2,4*Δ (21 days); orange bar), heat-shock proteins (*hsp12*Δ (7 days), *hsp26*Δ (11 days), *hsp104*Δ (7 days); red bars) or a G1-to-S transition regulator (*whi5*Δ (4 days); blue bar). Wild type is shown as a comparison (6 days, grey bar). Error bars show the mean with s.e.m. of $n = 3$ biological replicates. Dots show raw data. (Also see Supplementary Figs. S3.28-S3.31).

Mutations that hinder or promote cell replication by controlling the G1-to-S transition in frigid environments. To further explore how ROS prevents cell replication by elongating G1 duration and inhibiting the G1-to-S transition at near-freezing temperatures, we constructed mutant strains that each had one gene deleted. Several mutants were knockouts of ROS-defense genes that are known to be induced at near-freezing temperatures [8, 11, 14, 39]. Two of these mutants (*grx2*Δ, *gtt2*Δ) lacked a ROS-reducing enzyme that uses GSH as a co-factor. High-density populations of these mutants had a doubling time of ~35 days at 5 °C, compared to ~6 days for the wild type at the same density (Fig. 3.4e – compare left two green bars with grey bar). Hence, disrupting the ROS-reducing ability severely inhibits cell replication at 5 °C (Supplementary Fig. S3.28).

A mutant without the Msn2 and Msn4 stress-response regulators [80–82], had a doubling time that exceeded 20 days even when receiving ample GSH (Supplementary Fig. S3.29). Thus, a subset of genes controlled by Msn2,4 is essential for cell replication at near-freezing temperatures regardless of the presense of extracellular GSH. One example of Msn2,4-regulated genes is *GRX2* [83], whose knockout we have found to not grow. In contrast, genes for heat-shock proteins that are known to be expressed at low temperatures and are also controlled by Msn2,4 [11, 17, 39, 84, 85], were not necessary for population growth at 5 °C (Fig. 3.4e – red bars; Supplementary Fig. S3.30).

Another way to promote cell replication, besides promoting the G1-to-S transition through removing ROS, may be enabling cells with abundant ROS to exit G1. Indeed, we found that knocking out Whi5 (*whi5*Δ), an important regulator of the G1-to-S transition, caused populations to grow faster than the wild-type strain at the same density (Fig. 3.4e – blue bar), having a doubling time of less than 4 days at 5 °C. Moreover, monitoring single cells revealed that *whi5*Δ cells were typically smaller than the wild-type cells and that *whi5*Δ and wild-type cells had nearly the same, wide distribution of single-cell ROS

concentrations at 5 °C (Supplementary Fig. S3.31). These results show that deleting Whi5 shortens G1 duration and enables more cells with abundant ROS to enter S phase at 5 °C. Overall, we can enable and accelerate cell replication at near-freezing temperatures by promoting the G1-to-S transition in two ways: by either removing intracellular ROS (adding GSH) or by removing a G1-to-S regulator when having abundant ROS (deleting Whi5).

Existence of speed limits for completing the cell cycle in frigid environments. By monitoring individual cells for two months at 1 °C, we further confirmed that promoting the G1-to-S transition is the key to enabling more cells to replicate at near-freezing temperatures. Specifically, we found that extracellular GSH did not remove intracellular ROS at 1 °C, and thus did not aid replications with less than 2% of all cells completing an entire cell cycle (Supplementary Figs. S3.33-S3.32). However, we found that *whi5*Δ cells were ~2.5 times more likely to replicate (undergo G1-to-S transition, as marked by bud formation) than wild-type cells at the same population-density at 1 °C (26% and 11% respectively) (Fig. 3.5a). On average, the replicating cells took ~28 days to complete the S-G2-M phases, and cells typically spent at least 51 days in G1 phase at 1 °C (Fig. 3.5a). Thus, some rare cells can still replicate at 1 °C with months-long cell-cycle events, although cell replication becomes increasingly rare as the temperature approaches the freezing of water.

Taken together, our findings suggest that a cell cannot take an arbitrarily long time to replicate at a given near-freezing temperature. This is because we have shown that longer doubling times are caused by extended G1 durations which in turn result from higher ROS concentrations. But once the intracellular ROS increases to an above-threshold concentration, a cell becomes unable to replicate and will grow and eventually die by bursting open. Thus, we hypothesized that there must be a longest possible doubling time at a given temperature. Moreover, there must also be a shortest possible doubling time for a given temperature because we found that the S-G2-M phases have a fixed duration that is independent of ROS. We explored these "speed limits" for the duration of the cell cycle – the longest and shortest allowed doubling times – at near-freezing temperatures. We reasoned that the gene-expression machineries affect a cell's doubling time because a cell needs time to produce ROS-reducing enzymes, replace molecules that ROS damaged, and build a daughter cell. Hence, we reasoned that the speed of global gene-expression machineries (e.g., RNA polymerases, ribosomes) are likely major factors that determine the doubling time [68, 86, 87]. Therefore, we sought to measure the genome-wide transcription rate and protein-synthesis rate at near-freezing temperatures.

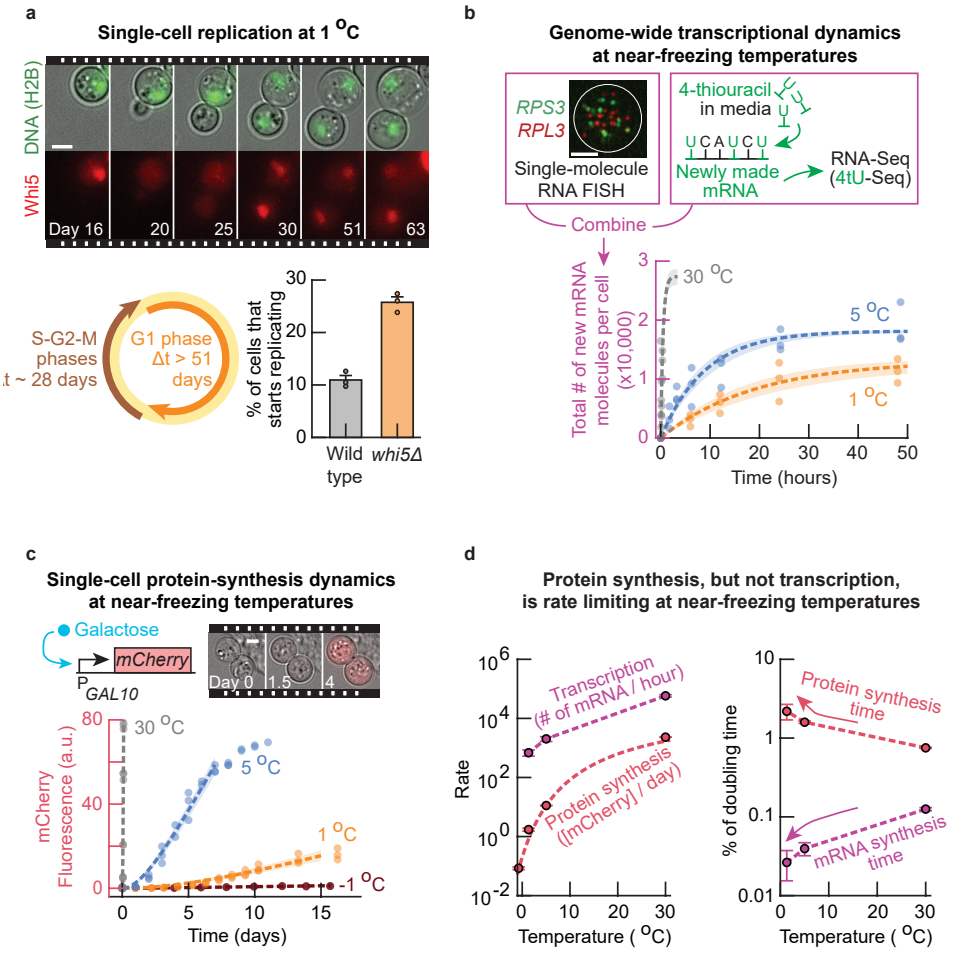

Figure 3.5: Protein synthesis, but not transcription, becomes more rate limiting for cell proliferation as temperature approaches 0 °C. (a) Time-lapse movie of a cell replicating at 1.0 °C. Moviestrip shows composite of brightfield image and fluorescence of H2B-GFP (top) and Whi5-mCherry (bottom). Scale bar is 3 µm. Circle shows duration of cell-cycle phases at 1.0 °C. Average duration of S-G2-M is 28.4 ± 3.2 days (n = 10 cells, brown arrow), duration of G1 is at least 51 days (duration of time-lapse, orange arrow). Bar graph shows percentage of cells that starts replicating (i.e., forms a bud) at 1.0 °C for the *whi5*Δ strain (25.8 ± 1.0%; mean with s.e.m. – orange bar) compared with wild-type strain (10.9 ± 0.9% – grey bar). (Also see Supplementary Figs. S3.33-S3.32). **(b)** Quantifying transcriptional dynamics by combining metabolically labelled RNA-sequencing using 4-thiouracil (4tU) and single-molecule RNA FISH. Graph shows the number of newly synthesized transcripts over time at 30.0 °C (grey curve), 5.0 °C (blue curve) and 1.0 °C (orange curve). Image shows RNAs in a single cell as visualized by RNA FISH, with a composite of *RPS3* (green) and *RPL3* (red) at 1.0 °C. White circle indicates cell outline from brightfield image. Scale bar is 2 µm. (Also see Supplementary Figs. S3.35-S3.38). **(c)** Quantifying single-cell protein-synthesis dynamics. Movie strip shows expression of mCherry at 5.0 °C after 0, 1.5 and 4 days of incubation with 2% galactose (added on day 0). Images are a composite of brightfield image and mCherry fluorescence. Scale bar is 5 µm. Graph shows the mCherry fluorescence measured in single cells with a flow cytometer over time at 30.0 °C (grey curve), 5.0 °C (blue curve), 1.0 °C (orange curve) and −1.0 °C (red curve). (Also see Supplementary Figs. S3.39-S3.40 and Supplementary Theory S3.6). In **(b-c)**, the dots show raw measurements, dotted lines show a model fit with average parameter estimates, and shaded areas represent s.e.m. of fitted parameters, having n = 3 biological replicates per condition. ***(caption continues on the next page)***

Figure 3.5 ***(caption continued from the previous page):*** **(d)** Summarizing (b-c): *Left:* Transcription rate (# of mRNA / hour, pink curve) and protein-synthesis rate ([mCherry] a.u. / day; red curve) as function of temperature. Red dotted line shows fit of Arrhenius-type equation to protein-synthesis rate. (also see Supplementary Figs. S3.41-S3.44 and Supplementary Theory S3.6). *Right:* Characteristic time for protein synthesis (red curve) and transcription (pink curve) relative to the doubling time at each temperature. Characteristic time is the time to synthesize 1 a.u. of mCherry or the time to synthesize 100 mRNAs. Doubling time is the average single-cell doubling time at each temperature. In both graphs, the error bars show mean with s.e.m. of $n = 3$ biological replicates.

Measuring genome-wide transcription rate and protein-synthesis rate at near-freezing temperatures. To determine the genome-wide transcription rates, we incubated high-density populations at a desired temperature (1 °C, 5 °Cand 30 °C) in a minimal medium and added a nucleotide analogue, 4-thiouracil (4tU). The 4tU incorporated into every newly synthesized RNA during incubation in this medium. We then identified and quantified the abundance of all newly made transcripts at different times by using next-generation sequencing of the 4tU-labelled mRNA ("4tU-seq"; Supplementary Figs. S3.35-S3.36). Additionally, we used single-molecule RNA FISH on endogenous yeast genes to measure the integer copy-number of transcripts during their steady-state expression at each temperature. We then converted the abundance of mRNA from the 4tU-seq to an integer copy-number of transcripts per cell (Supplementary Fig. S3.37). This yielded genome-wide transcription dynamics for each temperature (in "# of mRNA / cell / hour") (Fig. 3.5b – points). A rate equation for transcriptional dynamics [88, 89],

$$N_{\mathrm{mRNA}}(t) = \frac{\mu}{\lambda} \cdot \Big[1 - \exp(-\lambda \cdot t)\Big], \tag{3.1}$$

with constitutive synthesis rate μ (in "# of mRNA / hour") and first-order degradation rate λ (in "1 / hour") closely matched the data at all temperatures (Fig. 3.5 – curves). We found that cells synthesized mRNA at an average rate of 700 mRNA per hour at 1 °C, 2,000 mRNA per hour at 5 °C, and 58,000 mRNA per hour at 30 °C. We also found that, on average, mRNA has a half-life of 14 hours at 1 °C, 7 hours at 5 °C, and 20 minutes at 30 °C. We additionally measured the dynamics of transcription for a single-gene at near-freezing temperatures using RNA FISH and found the same timescales (Supplementary Fig. S3.38). Moreover, our measurements at 30 °C closely resemble those of recent studies (~60,000 mRNA synthesized per hour and an average half-life of ~20 minutes [89–93]). These measurements establish that transcription occurs on the order of hours to days at near-freezing temperatures.

To determine the time-scale for making a functional protein, starting from transcription initiation, we used a strain in which galactose induced mCherry expression. Af-

ter adding galactose to the growth medium of high-density populations, we measured mCherry protein abundance (fluorescence per cell area) in single cells for up to two weeks at various temperatures (−1 °C, 1 °C, 5 °C, and 30 °C) (Fig. 3.5c). We found that the growth medium froze at −2 °C. The global (gene-independent) machineries for gene expression, such as RNA polymerases and ribosomes, must function at least as rapidly as the time-scale of mCherry synthesis in cells. A rate equation for protein synthesis (Supplementary Theory S3.6),

$$N_{\text{protein}}(t) = m \cdot t - \frac{m}{\gamma} \cdot \Big[1 - \exp(-\gamma \cdot t)\Big], \tag{3.2}$$

for which we fitted the protein-synthesis rate m (in "fluorescence a.u. / day") and then the protein-maturation rate γ, recapitulated the data at all temperatures (Fig. 3.5c – curves; Supplementary Figs. S3.39-S3.40). We found that cells synthesized mCherry at an average rate of 2,300 a.u. per day at 30 °C, 11 a.u. per day at 5 °C, 1.7 a.u. per day at 1 °C and negligibly at −1 °C (i.e., less than 0.1 a.u. per day). By comparing these values to the value at 30 °C, we can obtain a fold-reduction in the mCherry-synthesis rate ("protein-synthesis rate") which represents a slowing down of global gene-expression machineries (e.g., RNA polymerases, ribosomes).

Protein synthesis, but not transcription, becomes more rate limiting for cell replication as the environment freezes. By also measuring the rates of genome-wide transcription and protein synthesis with an ample amount (250 μM) of added GSH, we discovered that ROS did not affect either of the rates at any temperature (Supplementary Figs. S3.41-S3.43). We plotted the ROS-independent rates of th gene expression machinery (from Fig. 3.5b-c) as a function of temperature (Fig. 3.5d – left). An Arrhenius-type function recapitulated the protein-synthesis rate decreasing with temperature (fitted curve in Fig. 3.5d; Supplementary Theory S3.6). This revealed that the protein-synthesis rate decreases faster compared to the genome-wide transcription rate as the temperature decreases towards 0 °C. This was more evident when we compared how the inverse of each rate changes as a percentage of the doubling time at each temperature. The inverse of these rates yield characteristic times for transcription and protein synthesis. By plotting these characteristic times as percentages of the doubling time at each temperature, we found that mRNA synthesis takes smaller fractions of the doubling time, while protein synthesis takes larger fractions of the doubling time as the temperature decreases (Fig. 3.5d – right; Supplementary Fig. S3.44). This result establishes that the speeds of translational and post-translational machineries become more rate-limiting for cell replication as temperature approaches 0 °C, whereas transcription becomes less rate-limiting for cell replication. Hence, we can use the protein-synthesis rate together

with ROS to study the "speed limits" for the duration of the cell cycle.

Stochastic model establishes speed limits for completing the cell cycle in frigid environments. Knowing how ROS and the protein-synthesis rate together control the duration of the cell cycle, we built a model that reproduced the measured distribution of single-cell doubling times at near-freezing temperatures (details in Supplementary Theory S3.6). The main idea of the model is that to replicate, a cell must remove sufficiently many ROS molecules, replace biomolecules that ROS damaged, and build the components of its daughter cell. These processes require gene expression whose timescale, as we determined, is largely that of protein-synthesis. More ROS would mean a longer time for a cell to replicate because there would be more ROS to remove, more damages to repair and more biomolecules to replace. Hence, as our measurements showed, a cell with minimal ROS would have the shortest doubling time t, which would depend only on the timescale of protein-synthesis and which is not affected by ROS. In addition to t, the cell would need additional time Δt to remove intracellular ROS, with more ROS leading to a longer time Δt. Thus, our model describing a cell's doubling time τ is given by (Fig. 3.6a),

$$\tau = t + \Delta t. \tag{3.3}$$

Like the protein-synthesis rate (Fig. 3.5d – left panel), we found that an Arrhenius-type function could fit the measured doubling times for cells that had the least amount of ROS at each temperature. Consequently, we found a power-law relationship between the shortest doubling time t and the average protein-synthesis rate r (Fig. 3.6b – green line; Supplementary Theory S3.6), $t \sim r^{-0.77}$. This power law means that a fold-change in the protein-synthesis rate r corresponds to an appropriate fold-change in the shortest possible doubling time t, regardless of the absolute value of either parameter [94] (i.e., the power-law preserves proportionality across temperatures). For example, a 10-fold increase in the average protein-synthesis rate decreases the shortest possible doubling time by ~6-fold, regardless of the original values of t and r. To obtain the additional time Δt, we use single-cell ROS levels and the time required for building proteins to remove this ROS and for replacing molecules that the ROS damaged. Specifically, we used the fact that the measured distributions of single-cell ROS levels roughly follow a log-normal distribution. Thus, the additional time Δt is dependent on the protein-synthesis rate r and the abundance of intracellular ROS given by stochastic, normally distributed variable [ROS]. From these two observations, we found that $\Delta t \sim (1/r) \cdot \exp([\mathrm{ROS}])$ (Fig. 3.6b – red; Supplementary Theory S3.6). Using the doubling time τ described by the sum of t and Δt defined here, we simulated whether or not a cell divided and its doubling time

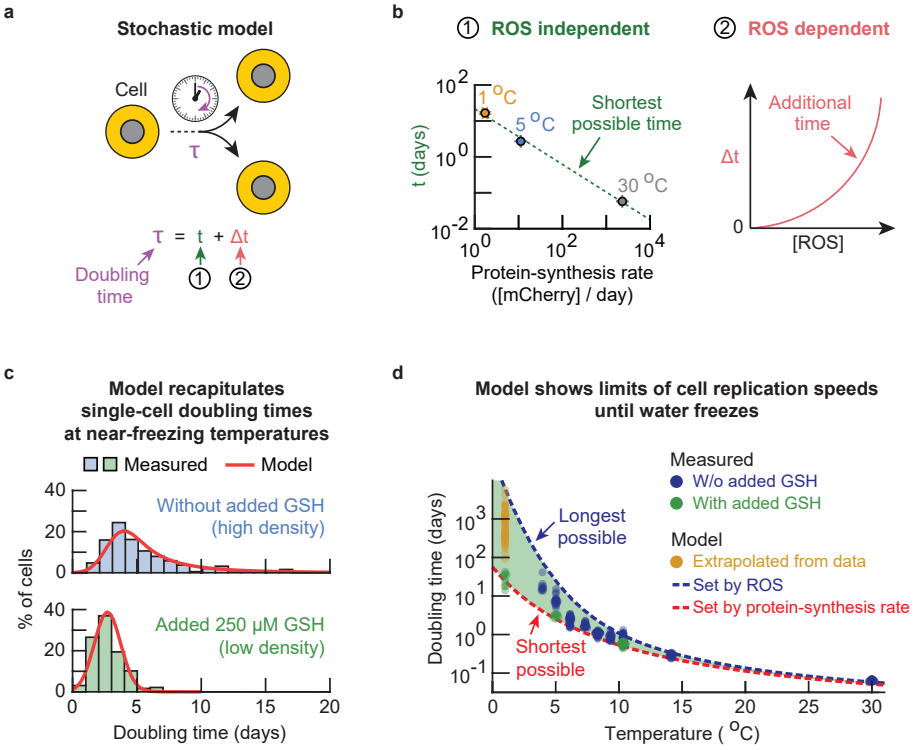

Figure 3.6: Mathematical model reproduces data and reveals fastest and slowest possible cell-replication speed at every temperature. **(a)** Description of the stochastic model. Doubling time τ of a cell (yellow circle) is dictated by a ROS-independent shortest duration t (labelled "1") and a stochastic, ROS-dependent duration Δt (labelled "2"). (Also see Supplementary Theory S3.6). **(b)** *Left:* The shortest doubling time t is limited by the protein-synthesis rate at each temperature and is the same for all cells in the population. Log-log plot shows the measured "minimum" single-cell doubling time as function of the protein-synthesis rate for populations at 30 °C, at 5 °C (with 250 μM added GSH), and at 1 °C (the duration of S-G2-M phases). Error bars show mean with s.e.m., having $n = 3$ biological replicates. Dotted green line shows a power-law fit (exponent is 0.77 ± 0.05 (mean with s.e.m.), Pearson correlation-coefficient $\beta = 0.9979$). *Right:* The additional time Δt varies between cells, is proportional to the time to synthesize proteins and increases exponentially with the intracellular ROS concentration (red solid line). **(c-d)** Results generated by the model described in (a-b) with a single fixed set of parameters. **(c)** The model recapitulates the single-cell doubling times at 5.0 °C with and without added GSH. Histograms show the experimentally measured values (Supplementary Fig. S3.13). Red solid line shows distribution of doubling times generated by the model. **(d)** The model also predicts the shortest and longest possible doubling times at each temperature. The shortest possible doubling time (red dotted line) is limited by the protein synthesis rate. The longest possible doubling times (blue dotted line) are the doubling times of cells with threshold ROS abundance below which cells replicate and above which cells die (98.5-th percentile). Cells can have any doubling time in between these bounds (green shaded area). Experimentally measured data are populations without any added GSH (blue dots), with 250 μM added GSH (green dots, > 5 °C) or the duration of S-G2-M phases in single cells (green dots, 1 °C). Yellow dots are single-cell doubling times (including G1) simulated by the model at 1 °C. Almost all experimentally measured doubling times fall in between these two bounds. (Also see Supplementary Fig. S3.45 and Supplementary Theory S3.6).

by incorporating the measured, threshold concentration of ROS for cells to be able to replicate (Fig. 3.3b; Supplementary Theory S3.6). This model has one free parameter, the average concentration of intracellular ROS among cells.

The stochastic model reproduced the experimentally measured distribution of single-cell doubling times (shown for 5 °C in Fig. 3.6c; Supplementary Fig. S3.45). Indeed, the doubling times for every temperature lay between the shortest possible and longest possible doubling times that the model predicts (Fig. 3.6d). Cells are unable to complete their cell cycles any faster than the shortest doubling time τ_{min} or any slower than the longest doubling time τ_{max}. Both speed limits depend on the temperature through the temperature-dependent protein-synthesis rate r. Specifically, the average protein-synthesis rate sets the shortest possible doubling time,

$$\tau_{\text{min}} \propto r^{-0.77}. \tag{3.4}$$

As the intracellular ROS concentration increases, a cell becomes less likely to replicate and, if it replicates, has a longer doubling time. This reveals a trade-off between the speed and possibility of replications (Supplementary Theory S3.6). The longest possible doubling time is determined by the protein-synthesis rate and a threshold concentration of ROS, $[\text{ROS}]_{\text{threshold}}$, which we observed experimentally (Fig. 3.3b). Cells with below-threshold ROS abundance can divide whereas cells with above-threshold ROS abundance have virtually no chance of dividing,

$$\tau_{\text{max}} \propto r^{-0.77} + \frac{1}{r} \cdot \exp[\text{ROS}]_{\text{threshold}}. \tag{3.5}$$

This equation shows the origin of the longest possible doubling time. At a given temperature, ROS can increase the doubling time only by so much without killing the cell. Cells that progress through their cell cycle more slowly than the speed limit dictated by τ_{max} are unable to replicate and eventually die by bursting. This low-speed limit corresponds to an extremely long doubling time at temperatures near 0 °C. For example, both the experimentally measured and simulated distributions of single-cell doubling times – these distributions closely match each other – establish that a cell could take over a year to complete a cell cycle at 1 °C. However, while such ultra-slow cell replication may be possible, the same distribution of single-cell doubling times shows that observing such replicating cells is extremely unlikely (Supplementary Fig. S3.33).

3.3. DISCUSSION

Temperature is a universal parameter for life that controls the speed of cellular processes in every habitat. With budding yeast as a model organism, our work quantitatively revealed design principles and fundamental limits of eukaryotic cellular life at near-freezing temperatures. Although one can argue that a cell cannot complete its cell cycle at an arbitrarily fast pace at a temperature, it is not obvious that there exists a slowest possible, non-zero speed at which a cell can complete its cell cycle. We discovered that an interplay between the protein-synthesis rate and ROS establishes such speed limits for yeast cell replication and explains how these limits change as temperature approaches 0 °C. Specifically, a cell remains in G1 and grows in size while it repairs ROS-induced damages [95, 96]. A cell that is unable to reduce enough ROS without external help, such as being given ample glutathione, keeps growing in size until it bursts and dies [97, 98]. Thus, a cell must exit the G1 phase and replicate within a certain window of time, or die otherwise.

Finding quantitative "growth laws", in which a cell's doubling time is expressed in terms of intracellular processes such as gene expression, has attracted much attention in several organisms [86, 99–102]. Moreover, studies have examined how temperature affects gene expression in yeast [17, 103] and measured genome-wide transcriptional rates at various temperatures [104, 105]. But little is known about how varying temperature quantitatively tunes the relationships among the genome-wide transcription rate, protein-synthesis rate, and proliferation rate. By using near-freezing temperatures and yeast, our study is one of the first to establish these rates and the quantitative relationships among them. These relationships led to our discovery that speed limits exist for the cell cycle in frigid environments: a cell's life cannot progress at an arbitrarily slow speed at any temperature above 0 °C. Moreover, our work provides insights outside the context of temperature given that ROS and antioxidants are generally associated with cellular aging [106–118]. By establishing the quantitative interplay among temperature, gene-expression speed and the harmful byproducts of biochemical reactions that are unavoidable (e.g. ROS), the design principles revealed here can be used to engineer yeast and potentially other organisms so that they can live faster and longer in frigid environments. More broadly, these principles and the approach presented here may guide future studies that aim to find limits to slowing down life, slowing aging, and extending lifespans for other microbes and cells of organisms.

3.4. METHODS

Yeast strains. The "wild-type", haploid yeast strain that we used is from Euroscarf with the official strain name "20000A". It is isogenic to another laboratory-standard haploid yeast "W303a", and has the following genotype: *MATa; his3-11_15; leu2-3_112; ura3-1; trp1Δ2; ade2-1; can1-100*. For engineering the strains that express a fluorescent protein, we first engineered a strain that has a functional *ADE2* gene and thus synthesizes adenine ("*ADE2*" strain). This strain therefore no longer accumulates red pigments that would accumulate without the functional *ADE2* [36] and that would interfere with detecting fluorescent proteins. To build this strain, we inserted the functional *ADE2* gene into the locus of the defective *ade2* gene in the wild-type strain by homologous recombination. To obtain the strain that we used for protein-synthesis rate measurements, we started from the *ADE2* strain and constructed a "mCherry-inducible" strain. Specifically, the mCherry expression is controlled by the *GAL10* promotor, located on a yeast-integration plasmid that constitutively expressed *URA3* (from *C. albicans*). This construct was integrated into the non-functional *his3* locus of the *ADE2* strain by homologous recombination. To express mCherry, the "mCherry-inducible" strain was grown on the trisaccharide raffinose (2% w/v) and expressed mCherry upon addition of galactose (2% w/v) to the growth medium.

To detect whether cells secrete glutathione to their extracellular environment, we used a mutant (*gsh1*Δ strain) that we had previously constructed [119]. This mutant lacks the *GSH1* gene for glutathione biosynthesis, and therefore must import glutathione from the extracellular environment for survival and replication. In short, we amplified the HygB selection marker (hygromycin B phosphotransferase) by PCR using primers whose ends were homologous to the flanking regions of the *GSH1* gene. We then used this PCR product to knock out *GSH1* via homologous recombination. Mutants were selected on YPD selection plates containing hygromycin B and the knockout was verified by PCR.

To follow the cell-cycle progression in live cells, we constructed a strain that had several cell-cycle markers tagged with a fluorescent protein. Specifically, we fused the *GFP* gene to *HTB2* and then fused mCherry to *WHI5*. To do so, we started from the *ADE2* strain and replaced the stop codons of the genes of interest with a cassette coming from yeast integration plasmids (pkt127, [120]). In short, for *HTB2*, the cassette contained a linker sequence followed by the *GFP* gene without a start codon and followed by the KanMX selection marker. We amplified this construct by PCR using primers whose ends were homologous to the flanking regions of the stop codon of the *HTB2* gene. We then used this PCR product to replace the stop codon of *HTB2* with the linker-*GFP* and KanMX construct by homologous recombination. This created a *HTB2*-linker-*GFP* fusion gene. Mutants were selected on YPD plates containing Geneticin (G418) and were verified by

PCR and microscope. Next, we used the *HTB2-GFP* mutant to analogously construct the *WHI5*-linker-*mCherry* fusion gene, except that the integration cassette contained the NatMX selection marker and mutants were selected using YPD plates that contained nourseothricin. The resulting "cell-cycle marker" strain contained two fluorescent fusion proteins encoded by *HTB2-GFP* and *WHI5-mCherry*.

Growth media. We cultured all yeasts in defined, minimal medium (SC) that consisted of (all from Formedium): Yeast Nitrogen Base (YNB) medium (Cat. No. CYN0410), Complete Supplement Mixture (CSM, Cat. No. DCS0019) containing all the essential amino acids and vitamins, and glucose at a saturating concentration (2% = 2 g per 100 mL, Melford Biolaboratories Ltd., Cat. No. G32040). The agar pads, which we used for growing yeast colonies, contained 2%-agar (VWR Chemicals), Yeast Extract and Peptone (YEP) (Melford Biolaboratories Ltd., Cat. No. Y20020 and P20240 respectively), and 2% (w/v) glucose.

Flow cytometry. We used a BD FACSCelesta with a High-Throughput Sampler and lasers with the following wave lengths: 405 nm (violet), 488 nm (blue) and 561 nm (yellow / green). We calibrated the FSC and SSC gates to detect only yeast cells (FSC-PMT = 681 V, SSC-PMT = 264 V, GFP-PMT = 485 V, mCherry-PMT = 498 V. As a control, flowing dPBS yielded no detected events). The number of cells per mL that we plotted in our growth experiments is proportional to the number of events (yeast cells) that the flow cytometer measured in an aliquot of cells with a defined volume. We measured the GFP fluorescence with a FIT-C channel and the mCherry fluorescence with a mCherry channel. We analysed the flow cytometer data with a custom MATLAB script (MathWorks).

Growth experiments. In a typical growth experiment, we first picked a single yeast colony from an agar plate and then incubated it at 30 °C for ~14 hours in 5 mL of minimal medium. Afterwards, we took a 20 µL aliquot from the 5 mL culture, diluted it to a known volume and then flowed it through a flow cytometer to determine the 5 mL culture's population-density (# of cells / mL). We then serially diluted the culture into fresh minimal medium to a desired initial population-density for a growth experiment at the desired temperature. Specifically, we distributed 5 mL of diluted cells to individual wells in a "brick" with twenty-four 10 mL wells (Whatman, "24-well x 10mL assay collection & analysis microplate"). We sealed each brick with a breathable film (Diversified Biotech: Breathe-Easy), covered it with a custom-made Styrofoam-cap for insulation, and incubated it in a compressor-cooled, high-precision thermostatic incubators (Memmert ICP260) that stably maintained their target temperature throughout the course of our growth experiments, with a typical standard deviation of 0.052 °C over time (devia-

tion measured over several days; Supplementary Fig. S3.1). Throughout the incubation, the cultures in the brick were constantly shaken at 400 rpm on a plate shaker (Eppendorf MixMate) that we kept in the incubator. To measure their population-densities, we took a small aliquot (typically 250 µL) from each well, diluted it with dPBS (Fisher Bioreagents) into a 96-well plate (Sarstedt, Cat. No. 9020411), and then flowed it through the flow cytometer which gave us the # of cells / mL. Alternatively, the cultures were distributed into glass tubes, that were kept in the incubator and constantly mixed using a rotator set to 40 rpm.

Measuring the percentage of dead cells. Cells were incubated as described in the paragraph "growth experiments". After ~2 weeks of incubation, we took aliquots of each culture at each time point, and then stained the cells for 20 min with 1 µg / mL of propidium iodide (Thermo Fisher Scientific, Cat. No. P3566). We then flowed these (stained) cells through a flow cytometer, and measured the number of cells that were unstained by propidium iodide – these cells have intact membranes, and are assumed to be alive (conversely, stained cells have lost membrane integrity and are assumed dead [66]). We then used the total number of cells and the number of dead and alive cells over time to extract the growth rate and death rate using a growth model that we fitted to our data (Supplementary Theory S3.6).

Microscope sample preparation. All microscopy imaging was performed with 96-well glass-bottom imaging plates (Zell-Kontact, Cat. No. 5221-20). Before each sample preparation, the glass bottom of the wells was pre-treated with 0.1 mM concanavalin A for 20 min at room temperature (conA, Sigma Aldrich, Cat. No. C2010). We then removed the conA and added an appropriate amount of cells to each well. Typically, we added an aliquot containing ~7,500 cells and supplemented with sufficient dPBS (Gibco, Life Technologies Limited, Cat. No. 14190-144) such that the volume of each well was 200 µL. The plate was then centrifuged at 1,000 rpm for 5 min using a centrifuge (Eppendorf, 5810R) that was pre-cooled at the desired temperature (e.g., 5 °C).

Microscope data acquisition and time-lapse. We used an Olympus IX81 inverted, epi-fluorescence, wide-field microscope. Temperature was kept constant during imaging by an incubator cage (OKO Lab) that enclosed the microscope. Fluorescent proteins or fluorescent probes were excited using a wide-spectrum lamp (AMH-600-F6S, Andor) and images were acquired with an EM-CCD Luca R camera (Andor) and IQ3 software (Andor). For time-lapse movies of cells, we prepared yeast cells as described in the paragraph "growth experiments" and kept them at the desired temperature for two weeks. Aliquots were then transferred to 96-well imaging plates as described in the paragraph

"microscope sample preparation", except that the cultures were not diluted with dPBS. The imaging plates that contained yeast samples were subsequently incubated at the desired temperature throughout the time-lapse (e.g., at 5 °C for typically ~3 weeks), and were transported and kept on ice for imaging (typically once every day). We checked that the transport and microscopy – usually less than 10 min during which the imaging plate and samples inevitably warm up – had no observable influence on the samples. To do this, we compared two imaging plates that contained aliquots of the same samples. One plate was imaged once every day for three weeks as described above. The other plate was only imaged at the start and at the end of the time-lapse. We found no difference between the cultures in the two plates – in terms of cell density, intracellular ROS concentrations or cell size – after three weeks of incubation.

Microscope data analysis. We processed the microscope data using ImageJ (1.53c) and MATLAB. Specifically, we segmented the cells by creating oval masks containing the cells, and extracted fluorescence values or the cell size from the area inside these masks. We computed the fluorescence for each cell by taking the maximum intensity of 20 images spaced 0.2 µm apart in a z-stack. Finally, we corrected for the background fluorescence by subtracting the average (maximum) background fluorescence in the field-of-view from the value obtained for each cell.

Measuring extracellular reduced and oxidized glutathione. To quantify extracellular glutathione concentrations, we isolated the growth media from liquid cultures by flowing the liquid cultures through a 0.2 µm pore filter (VWR). We verified that no cells remained in the filtered media by flowing an aliquot through a flow cytometer. We then measured the total concentration glutathione in the filtered media as described in the manufacturers' protocol ("quantification kit for oxidized and reduced glutathione", Sigma Aldrich, Cat. No. 38185). To quantify both the concentration of oxidized and reduced glutathione, we took two 200 µL aliquots of the filtered media. To one of the aliquots we added 4 µL of masking agent provided with the kit (most likely 2-vinylpyridine in ethanol at a final concentration of ~3 mM). All aliquots were then incubated for 1 hour at 37 °C together with a standard curve for reduced glutathione ("GSH", Sigma Aldrich, Cat. No. G4251) without added masking agent, and a standard curve for oxidized glutathione ("GSSG", Sigma Aldrich, Cat. No. G4376) with added masking agent. We then used a spectrophotometer (Spectrostar nano, BMG labtech) to measure the optical absorbance at 415 nm. For all conditions, we measured and averaged the absorbance of three technical replicates. As a background for all measurements, we subtracted the absorbance measured with the assay on fresh SD medium that did not contain any glutathione. Glutathione concentrations were determined via the

kinetics method and by interpolating the samples onto the standard curves.

(During incubation, the masking agent irreversibly binds and thereby removes reduced glutathione. The assay subsequently only detects oxidized glutathione in the samples. We verified that this protocol indeed quantifies the amount of oxidized and reduced glutathione. We found that the masking agent removed ~90% of the reduced glutathione during incubation).

Measuring the concentration of intracellular ROS. We prepared yeast cells as described in the paragraph "growth experiments" and incubated the cultures for two weeks at the desired temperature. We then transferred aliquots to 96-well imaging plates as described in the paragraph "Microscope sample preparation", except that the cultures were not diluted with dPBS. We next removed the supernatant and washed the cells twice with pre-cooled dPBS to remove thiols from the growth media (e.g., cysteine). We then added an indicator dye and incubated the cells for 30 min at the desired temperature. As indicator dye, we used either "mitoSOX red" to stain intracellular superoxide (at 5 μM final concentration, Thermo Fisher Scientific, Cat. No. M36008) or "cellROX orange" to stain intracellular ROS (at 5 μM final concentration, Thermo Fisher Scientific, Cat. No. C10443). Finally, we removed the excess dye by washing the cells twice with dPBS and imaged the cells with a microscope as described in the paragraph "microscope data acquisition and time-lapse". For time-lapse movies of cells stained with the indicator dyes, we followed the above protocol with the following modifications. After preparing the cells and washing away the excess dye, we placed back the supernatant (growth media) that we took away before and kept at the desired temperature when incubating the cells with the dye. We then proceeded with the microscopy time-lapse as described in "microscope data acquisition and time-lapse".

Measuring extracellular ROS production rate. To measure the extracellular oxidation rate, we used a probe called dihydroethidium (DHE, Thermo Fischer Scientific, Cat. No. D11347) that becomes fluorescent upon oxidation by ROS (superoxide). DHE is usually used to detect intracellular ROS, and it intercalates with DNA giving a bright signal in the nucleus. Instead, we used DHE to detect extracellular ROS where no cellular components were present. To still facilitate the fluorescent signal of DHE, we added herring sperm DNA (Promega, Cat. No. D1816) to our samples with a 0.2 mg / mL final concentration. Right before measuring fluorescence, we added DHE to our samples at a 20 μM final concentration. We then transferred the samples to a flat-bottom 96-well plate (Sarstedt, Cat. No. 82.1581.001) using 150 μL per well. Directly after, fluorescence was measured every 3 minutes for 2 hours using a plate reader (Synergy HTX Multi-Mode Microplate Reader, Biotek). Fluorescence was measured with excitation at 500 nm and

emission at 620 nm. For measuring the oxidation rate at 30 °C, we pre-warmed all media and set our plate reader to incubate the samples at 30 °C during the measurements. For measuring the oxidation rate at 5 °C, we prepared 5 mL of each sample that we pre-cooled at 5 °C. We then kept these samples at 5 °C for the duration of the experiment. We took 150 µL aliquots of each sample every hour, and transferred these into a 96-well plate. Directly after we measured the fluorescence of these aliquots with our plate reader. For all samples, we measured and averaged the fluorescence of three technical replicates. All measurements included controls consisting of pure water or regular SD medium. The oxidation rate was determined by determining the slope (a.u. per second) of the fluorescence curve over ~1 hour (at 30 °C), typically starting after measuring at least 10 min with the plate reader. We used the following scavengers of ROS (from Sigma Aldrich): tiron (4,5-dihydroxy-1,3-benzenedisulfonic acid disodium salt monohydrate, Cat. No. 172553) and trolox ((±)-6-Hydroxy-2,5,7,8-tetramethylchromane-2-carboxylic acid, cat. no, 238813). Samples with ROS scavengers were compared to a control having the appropriate solvent (for example, a sample having trolox that is dissolved in DMSO was compared to a sample having only DMSO).

Limited nutrients experiment. To test the effect of nutrients on the growth of cells at near-freezing temperatures, we prepared fresh wild-type yeast cells as described in the paragraph "growth experiments", except that we limited the amount of nutrients in the fresh growth medium. Specifically, we diluted the minimal medium with various amounts of water, and then supplemented each media with 2% glucose. Thus, each medium contained 2% of glucose and a known percentage ($0-100\%$) of the nutrients that are in regular minimal medium. After transferring fresh populations of cells into each media, we incubated the cultures to 5 °C and measured their population density over time as described in the paragraph "growth experiments".

Measuring extracellular ROS production during nutrient depletion. To measure the extracellular oxidation rate that cells experience during their incubation at near-freezing temperatures, we prepared cultures of our wild-type yeast at various starting densities as described in the paragraph "growth experiments". We then incubated the cells at 5 °C, and measured the oxidation rate in the growth media over time. To do so, we took aliquots of the cultures that we kept at 5 °C, and flowed them through a 0.2 µm pore filter (VWR, cellulose-acetate membrane). We then directly proceeded to measure the ROS production rate in the supernatant as described in the paragraph "measuring extracellular ROS production rate".

Measuring cell-cycle progression. We used the "cell-cycle marker" strain to measure the progression of the cell cycle at near-freezing temperatures. We prepared cultures of the "cell-cycle marker" strain as described in the paragraph "growth experiments". After two weeks of incubation, we transferred aliquots of the cultures to a pre-cooled 96-well microscopy plate that we kept on ice. The microscopy plate was further prepared as described in the paragraph "microscope sample preparation". We kept the plate at the desired temperature (e.g., 5 °C) for one day, and then proceeded by taking a snapshot of each sample twice per day to create time-lapse movies as described in the paragraph "microscopy data acquisition". We analysed the time-lapse movies as described in "microscope data analysis". In short, to quantify the amount of nuclear Whi5-mCherry and H2B-GFP, we first located the nucleus by segmenting the GFP fluorescence of each cell using a threshold GFP fluorescence that we kept fixed for all cells and time points. The nucleus was then the group of pixels whose fluorescences exceeded this threshold. We then determined the total mCherry and GFP fluorescence within the cell's nucleus. From this fluorescence we subtracted the average background fluorescence in the field-of-view from the value obtained for each cell. Finally, to obtain the copy number of DNA we rescaled the nuclear GFP between the average minimum and maximum GFP fluorescence that we observed for replicating cells. To obtain the amount of nuclear Whi5 we took the ratio of the nuclear and cytoplasmic mCherry fluorescence. (Also see Supplementary fig. S3.24).

Mutant yeasts. We constructed several mutant strains in which we removed genes involved in (oxidative) stress-responses. In short, we designed primers whose ends were homologous to the flanking regions of the desired gene to be knocked out. Using these primers, we amplified a selection marker by PCR, and knocked out the desired gene in the wild-type yeast via homologous recombination. Mutants were selected on YPD selection plates and knockouts were verified by PCR. Specifically, we knocked out the genes for the stress-response transcriptional activators (*MSN2*), membrane organisation (*HSP12*), disaggregase (*HSP104*), glutathione s-transferase (*GTT2*) and glutathione peroxidase (*GPX1*) using the HygB selection marker and YPD plates containing hygromycin B. We also knocked out genes for suppression of protein aggregation (*HSP26*), glutaredoxin (*GRX2*), catalase (*CTT1*) and the transcriptional regulator for G1-to-S transition (*WHI5*) using the NatMX selection marker and YPD plates containing nourseothricin. The *MSN2,MSN4* double knockout was constructed by removing, sequentially, first the *MSN2* gene and then the *MSN4* gene. We thus obtained several mutants that lacked genes for transcriptional regulation (*msn2,msn4*Δ-strain, *whi5*Δ-strain) or that lacked genes for the oxidative stress response (*gtt2*Δ-strain, *gpx1*Δ-strain, *grx2*Δ-strain and *ctt1*Δ-strain).

FISH probes. We designed single-molecule FISH probes to detect mCherry mRNA. For this we used the Stellaris FISH probe designer (LGC Biosearch Technologies). The probes (25 probes) were designed to attach to the full length of mCherry RNA and were coupled to Quasar 670 (a Cy5 analog, LGC Biosearch Technologies). We also designed FISH probes to detect mRNA of endogenous yeast genes to convert relative transcript levels from our 4tU RNA-sequencing data to integer numbers of RNA per cell. For this, we used probes for *RPS3* (30 probes coupled to Quasar 670), *RPL3* (48 probes coupled to Quasar 570, a Cy3 analog LGC Biosearch Technologies), *RPB1* (48 probes coupled to Quasar 670) and *RPB3* (40 probes coupled to Quasar 570). The excitation and emission peaks of these fluorophores are ex. 548 / em. 566 nm (Quasar 570) and ex. 647 / em. 760 nm (Quasar 670).

Single-molecule RNA FISH. We used the standard protocol for single-molecule RNA FISH in yeast, as described in "Protocol for *S. cerevisiae* from Stellaris RNA FISH" (LGC Biosearch Technologies). Specifically, when performing FISH with multiple sets of probes, we incubated our cultures with all sets of FISH probes simultaneously during the hybridization step. Finally, we made sure to image the fluorescence of Quasar 670 probes first as this probe was the most sensitive to photo bleaching.

Measuring the single-gene transcription rate. We used the "mCherry-inducible" strain to measure the transcription rate for a single gene. We prepared liquid cultures of the mCherry-inducible strain as described in the paragraph "growth experiments", except that we used minimal medium (SC) containing 2% raffinose as the carbon source. The cultures were incubated in 500 mL Erlenmeyer flasks 5 °C for two weeks on an Eppendorf platform shaker set to 125 rpm. After two weeks, we supplemented the cultures with 2% galactose to induce expression of mCherry. After incubating the cultures at 5 °C for the desired amounts of time, we transferred aliquots of the cultures (typically ~10 mL) to 15 mL tubes containing 37% formaldehyde such that the final volume formaldehyde was 10%. We then proceeded with RNA FISH as described in the paragraph "single-molecule RNA FISH".

Measuring the single-gene protein-synthesis rate. We used the "inducible mCherry" strain to measure the protein-synthesis rate. We prepared cultures of the mCherry-inducible strain as described in the paragraph "growth experiments", except that the minimal medium (SC) contained 2% raffinose as the carbon source. We then incubated the cultures for two weeks in glass tubes at 5 °C in a rotator at 40 rpm. After two weeks, we transferred aliquots of the cultures to a pre-cooled 96-well microscopy plate that we kept on ice. The microscopy plate was further prepared as described in the

paragraph "microscope sample preparation". As medium we used fresh, pre-cooled SC containing 2% raffinose to dilute the aliquots to the desired density on the microscopy plate. We kept the plate at the desired temperature (e.g., 5 °C) for one day, and then took a snapshot of the populations as described in the paragraph "microscope data acquisition and time-lapse". Finally, we supplemented each sample on the microscopy plate with 2% galactose to induce the expression of mCherry. We continued to take a snapshot of each sample twice per day for the time-lapse movies. In parallel, we also added 2% galactose to the original cultures that were kept in the rotator at 5 °C. We then measured the average mCherry fluorescence of the population twice per day by flowing aliquots of the cultures through a flow cytometer as described in the paragraphs "growth experiments" and "flow cytometry".

Measuring genome-wide transcription rate with 4tU labelled RNA (see 1-4). (1) Sample preparation. We prepared large cultures of our wild-type yeast similarly to the description in "growth experiments". In short, we incubated single yeast colonies in Erlenmeyer flasks containing 100 mL of minimal medium at 30 °C for ~24 hours. We then took aliquots (~25 mL) of these cultures containing ~100 million cells, spun them down using a centrifuge and dissolved the yeast pellet with 250 mL fresh SD medium in 500 mL Erlenmeyer flasks. We then transferred the cultures to a shaker set to 150 rpm that we kept at (say) 5 °C. To ensure that the yeasts had sufficient nutrients, we refreshed the growth media several times during the two weeks of incubation at 5 °C (on days 7, 10 and 13). Specifically, we spun down the cultures using a pre-cooled, 5 °C centrifuge (Eppendorf, 5810R) for 5 min at 4,000 rpm, discarded the supernatant, and re-suspended the pellet into fresh, pre-cooled SD medium. We ensured that the cultures never ran out of nutrients by checking that the discarded supernatant contained sufficient nutrients to allow for growth of yeast – the supernatant contained enough nutrients to always grow the wild-type yeast to a density of $> 1,000,000$ cells / mL at 30 °C.

(2) Sample collection. Previous work suggests to prepare a 2 M solution of 4-thiouracil (4tU, Sigma Aldrich, Cat. No. 440736-1G) in DMSO, which is then added to growth medium at a final 5 mM concentration [121]. We found that the 4tU solution precipitates and does not dissolve when added to the growth media at $\leq$ 5 °C. To circumvent this problem we added the 4tU solution to growth medium at 37 °C at a final 7.5 mM concentration ("1.5x-4tU-medium"). We then cooled this 1.5x-4tU-medium overnight to 5 °C without the 4tU precipitating. After two weeks of incubation at 5 °C, we first took aliquots of the liquid cell cultures without 4tU as a control. We then added an appropriate volume of the pre-cooled 1.5x-4tU-medium to the cultures, resulting in the cultures having a final concentration of 5 mM 4tU. Samples of the cell cultures were subsequently collected after $1.5, 3, 6, 12, 24, 48$ and 96 hours of incubation with 4tU

(or 0,6,12,24,48 and 96 hours at 1 °C or 0,5,10 and 20 min at 30 °C). During sample collection at 1 °C or 5 °C, we transferred aliquots of the cultures into 50 mL falcon tubes and spun them down with a pre-cooled centrifuge for 5 min at 4,000 rpm. We discarded the supernatant and re-suspended the pellets in 1 mL RNAlater (Thermo Fischer Scientific, Cat. No. AM7021). To wash the samples, we again spun down the samples for 2 min at 4,000 rpm, removed the supernatant and re-suspended the pellets in 1 mL RNAlater. During sample collection at 30 °C, we collected aliquots of the cultures into 50 mL falcon tubes and directly flowed the aliquots through 0.2 µm bottle-top filters with a vacuum. The cells are too small to pass through the filter and remain on the membrane. We then washed the cells with 50 mL ice-cold PBS and directly removed the vacuum. The pellet on the membrane of the filter was re-suspended with ~5 mL RNAlater, and cells were collected in 50 mL falcon tubes. Finally, right before storage, we took a 20 µL aliquot of the all samples of collected cells in RNAlater, to determine the cell density with a flow cytometer (to know the total number of collected cells). All samples were stored at 5 °C for a couple of hours to ensure that RNAlater would penetrate the cells before storing the samples at −20 °C for further processing. As a spike-in of 4tU labelled RNA, we used cells from *Schizosaccharomyces pombe* (YFS110) analogously to previous work [121]. Specifically, we grew *S. pombe* cells in 300 mL YPD on a shaker set to 150 rpm at 30 °C to a density of ~5,000,000 cells / mL. We then incubated the cells with 5 mM 4tU for 15 min to label the RNA with 4tU, collected the cells as described and stored the cells in 5 mL RNA later at −20 °C.

(3) Sample processing. Before continuing with the RNA extraction we added a fixed amount of *S. pombe* cells to each sample (in a ~1 : 6 ratio). We then spun down our samples in a pre-cooled centrifuge, removed the RNAlater, and proceeded with RNA extraction. We performed RNA extractions using the RiboPure Yeast RNA extraction kit (Thermo Fischer Scientific, Cat. No. AM1926) following the kit instructions. We also performed the DNAse treatment after RNA extraction, and stored the isolated RNA in elution buffer at −80 °C before further processing. The 4tU-labelled RNA was always extracted within three days of the last samples being collected. We simultaneously extracted the RNA of all time points in a single time-lapse to minimize the effect of processing the RNA on each time-lapse. After RNA extraction, we proceeded with biotinylation and purification of the 4tU labelled RNA. Here we followed the protocol described in previous work with minor modifications [121]. Briefly, the RNA was biotinylated using a biotinylation buffer (a solution containing 100 mM Tris, 10 mM EDTA, pH 7.6 (Thermo Fischer Scientific, Cat. No. BP2475)) and biotin-HPDP (dissolved in DMSO) at a final volume of 1 mL. After incubation, the excess biotin-HPDP was removed by mixing in and washing with 1 mL of chloroform. The RNA was then precipitated with 100 µL of 5 M NaCl and 1 mL isopropanol and spun down using a pre-cooled centrifuge for 45 min

at 18,000x g (used throughout). The RNA was washed with 1 mL of 75% ethanol and re-dissolved in 100 µL DEPC treated water (Invitrogen, 750023). After biotinylation, we directly continued with purification of the 4tU labelled RNA. To do so, we incubated the biotinylated RNA with 100 µL streptavidin-coated magnetic beads (Miltenyi Biotec, Cat. No. 120-001-017) for at least 90 min at room temperature. During that time, we placed micro-columns to a magnetic stand (microMACS separator (Miltenyi Biotec, Cat. No. 130-042-602)) and pre-washed the columns with 1 mL washing buffer (a solution containing 100 mM Tris, 10 mM EDTA and 1 M NaCl, pH 8.0 (Thermo Fischer Scientific, Cat. No. BP2479), and 0.1% Tween-20 (Thermo Fischer Scientific, Cat. No. BP337-100)). After incubation we applied the RNA to the columns. We re-applied the flow-through to the columns as the columns do not capture all magnetic beads during the first flow-through. After washing the columns 5 times with 1 mL washing buffer, we eluted the 4tU labelled RNA twice with 200 µL of 0.1 M DTT (Sigma Aldrich, Cat. No. 43816). To precipitate the RNA, we then added 40 µL of 3 M NaOAc (Sigma Aldrich, Cat. No. S7899) and 1.3 mL of ice-cold 100% ethanol (Merck KGaA, Cat. No. 1.00983.1011) to the eluted RNA. Finally, we added 2 µL of 20 mg/mL RNA-grade glycogen (Thermo Fischer Scientific, Cat. No. R0551) to aid precipitation, and left the RNA to precipitate overnight (at least 15 hours) at -20 °C. Finally, the 4tU labelled RNA was re-suspended in 15 µL of DEPC-treated, RNAse-free water. We found that the RNA extracted from ~25,000,000 cells of *S. pombe* that were incubated with 5 mM 4tU for 15 min (our spike-in) was generally enough to yield ~15 µL of > 40 ng/µL 4tU labelled RNA. This 4tU labelled RNA has poor RIN numbers and rRNA ratio's (due to incomplete synthesis of the ribosomal RNA that is purified), but is enough and of sufficient quality for RNA sequencing.

(4) Data normalization. We performed a quality check of each sample with FastQC and processed all sequencing data with the Salmon tool to quantify relative transcript abundance [122]. Specifically, we obtained reference transcripts for *S. cerevisiae* and *S. pombe* from Ensembl (assemblies R64-1-1 and ASM294v2 respectively) and built a Salmon index containing the transcripts (cDNA and ncRNA) with both genomes as a decoy. We then quantified the transcript levels in each sample using this index. Finally, we converted the transcript levels for *S. cerevisiae* to gene expression levels (Transcripts Per Million, TPM) and merged all samples using the package tximport from Bioconductor [123]. We performed between-sample normalization by re-scaling the TPM values for each gene with the sum of the TPM values of all *S. pombe* genes. The same amount of cells from the culture *S. pombe* were added to each sample as a spike-in, such that the total transcript levels of *S. pombe* should be identical across samples (the spike-in thereby eliminates experimental variations between samples and ensures that each sample in the time-lapse represents the relative level of 4tU-labelled transcripts). We also rescaled the relative level of 4tU-labelled transcripts of each time point in the time-

lapses with the number of estimated alive cells in the population at that time point (to ensure that measuring higher transcript levels is not due to having more cells in the population as a result of population growth). These cell numbers were corrected for the percentage of dead cells in the population as measured by PI staining (typically between ~2% and ~20% of cells were dead). Together, this re-scaling gave us the relative level of 4tU-labelled transcripts per cell over time. Finally, we converted these relative transcript levels to "# of RNA / cell" with a calibration curve that we constructed using the stead-state transcript levels that we had also sequenced. Specifically, during the 4tU time-lapses, we took aliquots of the populations of cells that were in log-phase growth (steady-state gene expression) right before the labelling with 4tU. We then performed single-molecule RNA FISH on these aliquots for several endogenous yeast genes (*RPS3*, *RPL3*, *RPB1* and *RPB3*). We then used the measured (average) number of mRNA per cell (from RNA FISH) and the measured relative transcript levels (from RNA-seq) to create a standard curve that converts relative transcript levels to integer number of RNA per cell (Supplementary fig. S3.37). We used this standard curve to convert our 4tU time-lapses to "# of RNA / cell". The number of RNA per cell were subsequently used for further processing and analysis. (Also see Supplementary Figs. S3.35-S3.37 for further details).

Mathematical model. The derivation and a detailed description of the mathematical model and the used parameter values are in the Supplementary Theory S3.6.

S3.5. SUPPLEMENTARY FIGURES

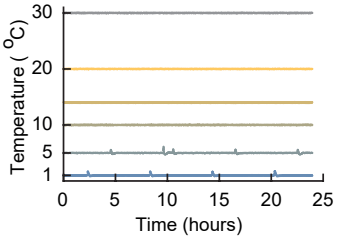

Figure S3.1: Temperature remains stable during all our growth experiments (Related to Figure 3.1a). All growth experiments were performed with liquid cultures of cells incubated in compressor-cooled, high-precision thermostatic incubators (Memmert ICPs). The ICPs had a precise temperature-recording device whose temperature readings we additionally verified using a separate thermocouple device and aligned with the temperatures of several other incubators. The temperature was monitored over the entire course of our experiments. As examples, shown here are the temperatures as recorded by the incubator's temperature sensor for 24 hours during six different growth experiments. Starting from the top, the curves show the temperature of the incubator set at 30.0 °C, 20.0 °C, 14.0 °C, 10.0 °C, 5.0 °C and 1.0 °C. Throughout our experiments, the incubators had a typical standard deviation of 0.033 °C when the incubation temperature was above 10.0 °C. The standard deviation was 0.09 °C when the incubation temperature was below 10.0 °C. This slightly larger standard deviation was due the incubator undergoing short thaw-cycles to prevent freezing of its components (deviation measured over several days).

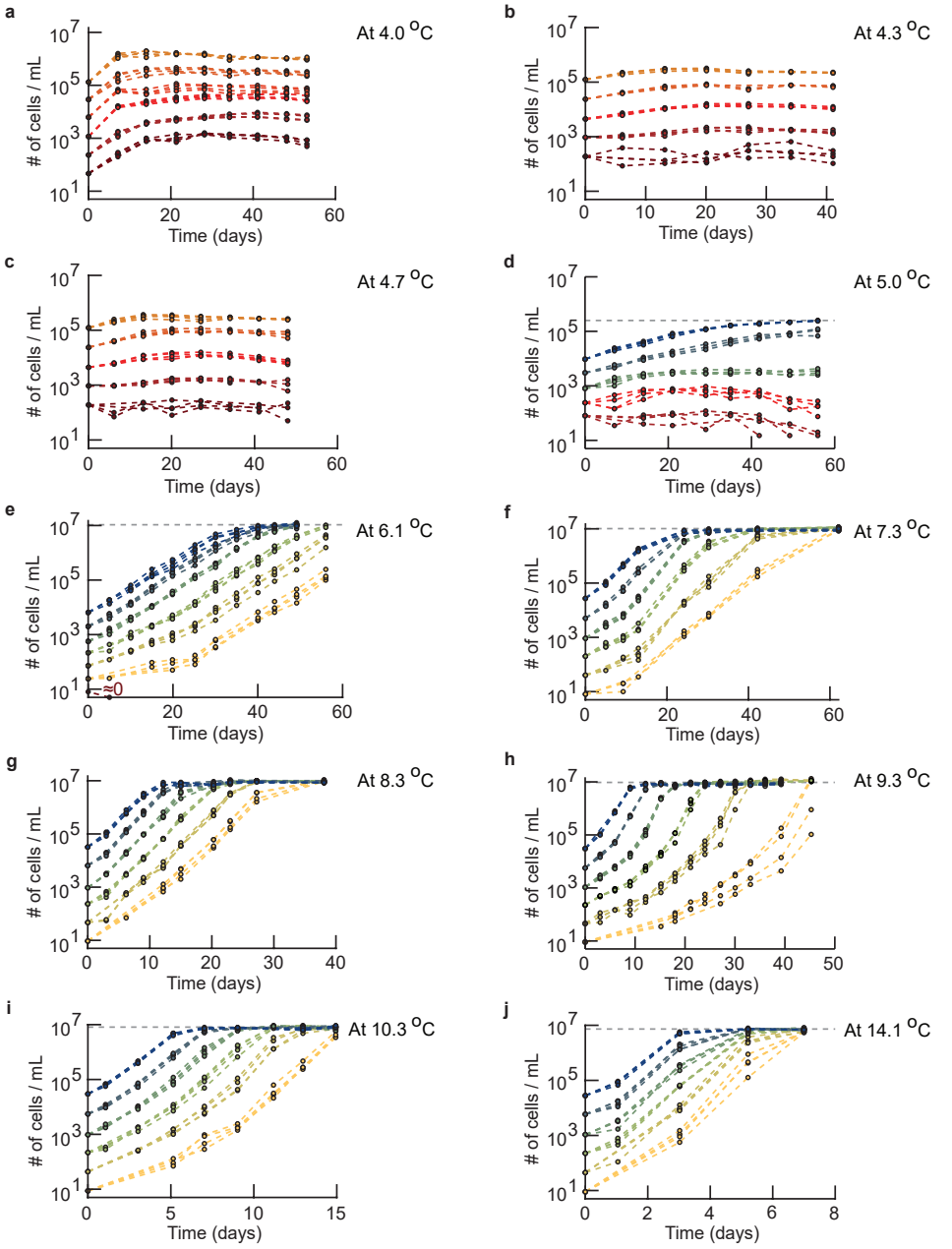

Figure S3.2: Growth curves for widely varying initial population densities and temperatures (Related to Figure 3.1a-b). Population density (number of cells / mL) measured over time with a flow cytometer. Shown are populations of wild-type yeast with differing initial densities incubated at 4.0 °C **(a)**, 4.3 °C **(b)**, 4.7 °C **(c)**, 5.0 °C **(d)**, 6.1 °C **(e)**, 7.3 °C **(f)**, 8.3 °C **(g)**, 9.3 °C **(h)**, 10.3 °C **(i)** and 14.1 °C **(j)**. Different colors represent different initial population-densities. The grey dotted lines show the carrying capacity that we estimated from the final densities of the populations. ***(caption continues on the next page)***

Figure S3.2 ***(caption continued from the previous page)*****:** To construct the phase diagram (Figure 3.1b), we used the growth-kinetics data as shown here to determine whether a population with a given initial population-density should be characterized as growing ("growth" phase) or non-growing ("no growth" phase). An initial population-density was characterized as being in the growth phase (Fig. 3.1b – blue region) if all replicate populations that started with that density exponentially grow over time and reach the carrying capacity for that temperature. An initial population-density was characterized as being in the no-growth phase (Fig. 3.1b – red region) if all replicate populations that started with that density did not grow during several weeks of incubation, except for some initial transient growth that results from the cells having been transferred from 30.0 °C. This transient growth typically lasted a few days. For example, every population in (c) belongs to the no-growth phase because no population grew during the ~6 weeks of incubation at 4.7 °C as can be seen by every population density barely increasing over time. As another example, after some lag-time, every population in (g) grew exponentially and identically over time to reach the carrying capacity at 8.0 °C. To draw the phase boundary that separates the growth phase from the no-growth phase in the phase diagram (Fig. 3.1b), we connected the maximum initial density for which a population does not grow for each temperature. This curve almost overlaps with the minimum initial density that leads to population growth for each temperature because we sampled the initial densities close to each other for each temperature. Similarly, we drew the boundary curve that separates the growth phase from the region of the phase diagram where nutrients are lacking by connecting the data points that represent, for each temperature, the measured carrying capacity (grey lines in d-j). Finally, we determined the temperature below which no population growth is possible – and thus only the no-growth phase exists below this temperature – by identifying the highest temperature (i.e., 4.7 °C (c)) where populations with different starting densities always reach differing final densities (as opposed to the common carrying capacity). In fact, these populations do not grow at all beyond the initial, transient growths (a-c). All panels show $n = 4$ replicate populations for each initial population-density (color).

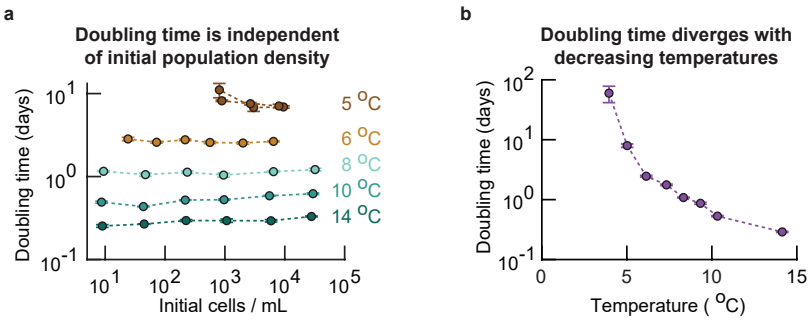

Figure S3.3: Population's doubling time is independent of its initial density at near-freezing temperatures (Related to Figure 3.1b). Summarizing Supplementary Fig. S3.2. From the growth curves of populations at various temperatures, we determined each population's doubling time. To obtain the doubling time of the populations that grew (i.e., populations in the "growth" phase of the phase diagram, Fig. 3.1b), we excluded the initial transient growth that typically lasted from a few days to one week. For non-growing populations (e.g., populations in the "no-growth" phase at 4.0 °C) we only took the growth rates that were positive and excluded the initial transient growth (i.e., transient growth in the first week of incubation). **(a)** Population doubling time as a function of initial density and temperature for growing populations. The doubling time does not depend on initial density. Error bars show the mean with s.e.m., and each data point represents at least $n = 4$ replicate populations. **(b)** Since the doubling time does not depend on initial density, we pooled all observed doubling times for each temperature. The population doubling time diverges as the temperature decreases. Error bars represent the mean with s.e.m., having at least $n = 16$ biological replicates per data point.

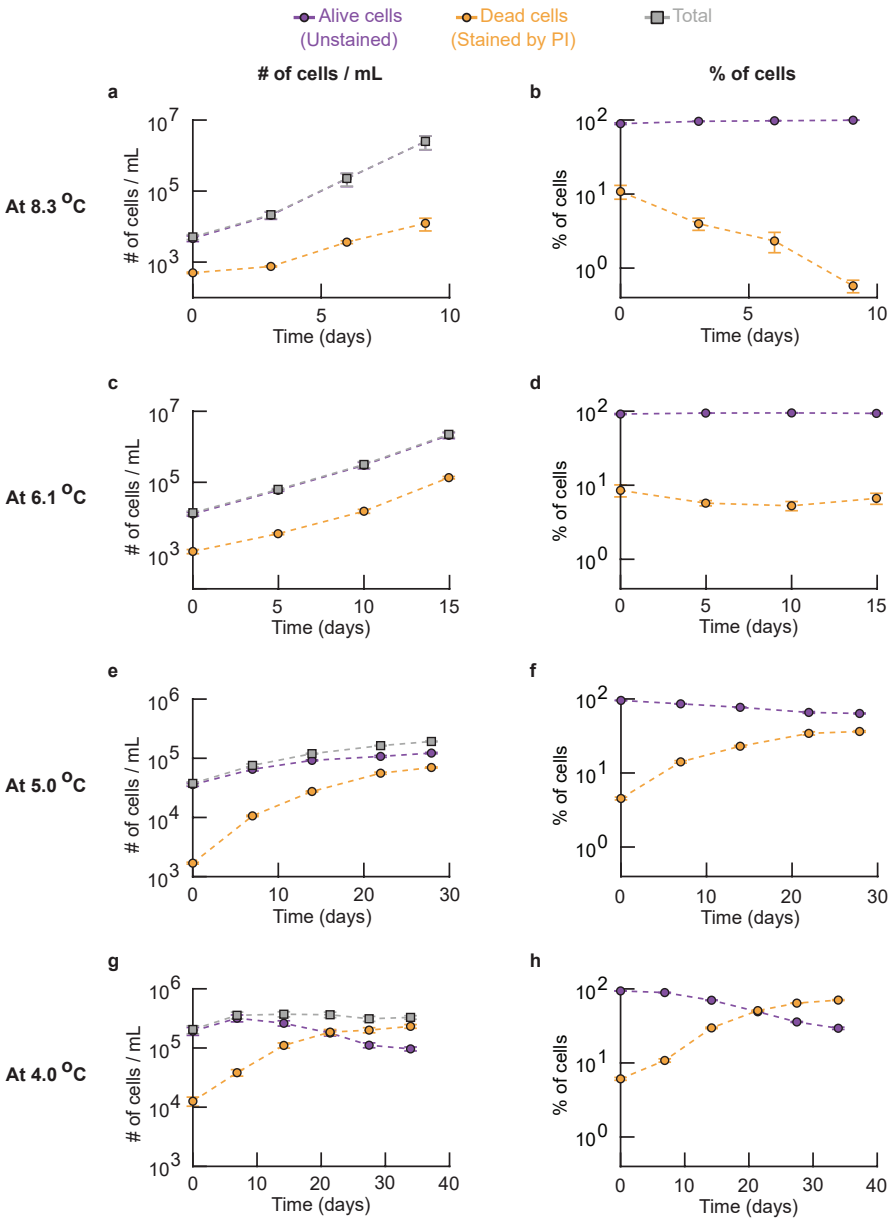

Figure S3.4: Population extinction occurs below 5 °C because as the temperature decreases, the average doubling time of a cell increases and eventually, just below ~5 °C, becomes larger than the average cell's lifespan (Related to Fig. 3.1b). Left column **(a, c, e, g)**: number of dead cells (yellow), number of alive cells (purple) and total number of cells (grey) in a population. Right column **(b, d, f, h)**: percentages of dead (yellow) and alive (purple) cells in a population. For each population, we took an aliquot of the liquid culture at various times and incubated it with 1 µg / mL of propidium iodide (PI) for 20 minutes at room temperature. ***(caption continues on the next page)***

Figure S3.4 ***(caption continued from the previous page)*****:** We then flowed this aliquot through a flow cytometer to measure the total number of cells and the number of cells that were stained (red) and unstained (yellow) by PI. PI does not stain cells with an intact membrane [66]. In contrast, PI enters cells with a damaged membrane and stains their DNA. Thus, propidium iodide stains a cell if and only if it's membrane is permeable. Hence, alive cells are commonly assumed to be impermeable to PI. Shown here are populations of wild-type yeast incubated at 8.3 °C **(a-b)**, 6.1 °C **(c-d)**, 5.0 °C **(e-f)** and 4.0 °C **(g-h)**. The curves show the total population-density and the density of stained and unstained cells over time **(a, c, e** and **f)**, together with the percentage of cells that were stained and unstained in the population **(b, d, f** and **h)**. All populations had already been incubated for at least 6 days at the respective temperature before the PI staining on day 0 in each graph (i.e., the populations had already spent ~6 days at 8.3 °C (a-b), ~10 days at 6.1 °C (c-d), and ~14 days at 5.0 °C (e-f) or 4.0 °C (g-h)). Error bars show the mean with s.e.m., with $n = 4$ replicate populations per data point. **(a-b)** Alive and dead cells over time at 8.3 °C. All populations grow exponentially over time. Both the density of alive and dead cells increase exponentially over time, with the density of alive cells increasing faster than the density of dead cells. Specifically, the percentage of dead cells in the population decreases exponentially over time. Thus, at 8.3 °C, alive cells overtake the population as cell replication occurs more frequently than cell death (purple curve in (b) stays at ~100%). **(c-d)** Alive and dead cells over time at 6.1 °C. Similar to the results at 8.3 °C. The main difference here is that the percentage of dead cells in the population remained constant over time (yellow curve in (d)), whereas the percentage of dead cells decreased over time at 8.3 °C (see (a)). Like in 8.3 °C, nearly 100% of the population consists of alive cells at 6.1 °C. **(e-f)** Alive and dead cells over time at 5.0 °C. The density of alive cells increases over time. However, the percentage of dead cells in the population increases while the percentage of alive cells decreases over time. Still, the populations consists of more alive cells than dead cells after ~6 weeks of incubation at 5.0 °C (see (f)). **(g-h)** Alive and dead cells over time at 4.0 °C. The population does not grow and the density of alive cells decreases over time (g) (i.e., less than one cells divides per cell that dies). The percentage of dead cells increases exponentially over time while the percentage of alive cells decreases, leading to the population eventually consisting mostly of dead cells (the population becomes extinct as this trend continues over time) (see (h)).
Together, (a-h) show that as the temperature decreases, the average population doubling time increases and eventually exceeds the average lifespan of a cell. Having a doubling time that is larger than the average lifespan means that the average cell does not have time to replicate before it dies. This leads to a population extinction. In other words, populations grow more slowly as temperature decreases and eventually, at around 5.0 °C, populations cannot exponentially grow because the average doubling time nearly matches the average lifespan of cells. Finally, at 4.0 °C, the doubling time exceeds the lifespan of cells and thus populations cannot grow.

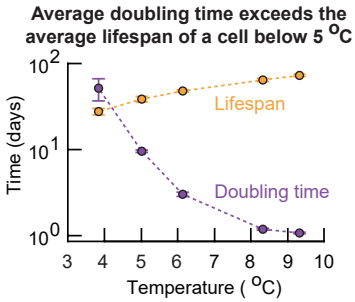

Figure S3.5: Average doubling time of a cell increases and eventually becomes larger than the average lifespan of a cell as the temperature decreases below 5 °C (Related to Figure 3.1b). Summarizing Supplementary Fig. S3.4. We used our measurements of the number of alive and dead cells in populations at each temperature to extract the average doubling time and the average lifespan of cells. Specifically, we fitted a growth model to the data that gives the expected lifespan and doubling time of cells at the population level (Supplementary Theory S3.6). Shown is the average doubling time (purple) and average lifespan (orange) at various temperatures. The average doubling time exceeds the average lifespan when the temperature is below 5.0 °C. Consequently, below 5.0 °C, the average cell dies before it has a chance to replicate and hence the population approaches extinction. Error bars represent the mean with s.e.m., having at least $n = 16$ biological replicates per data point.

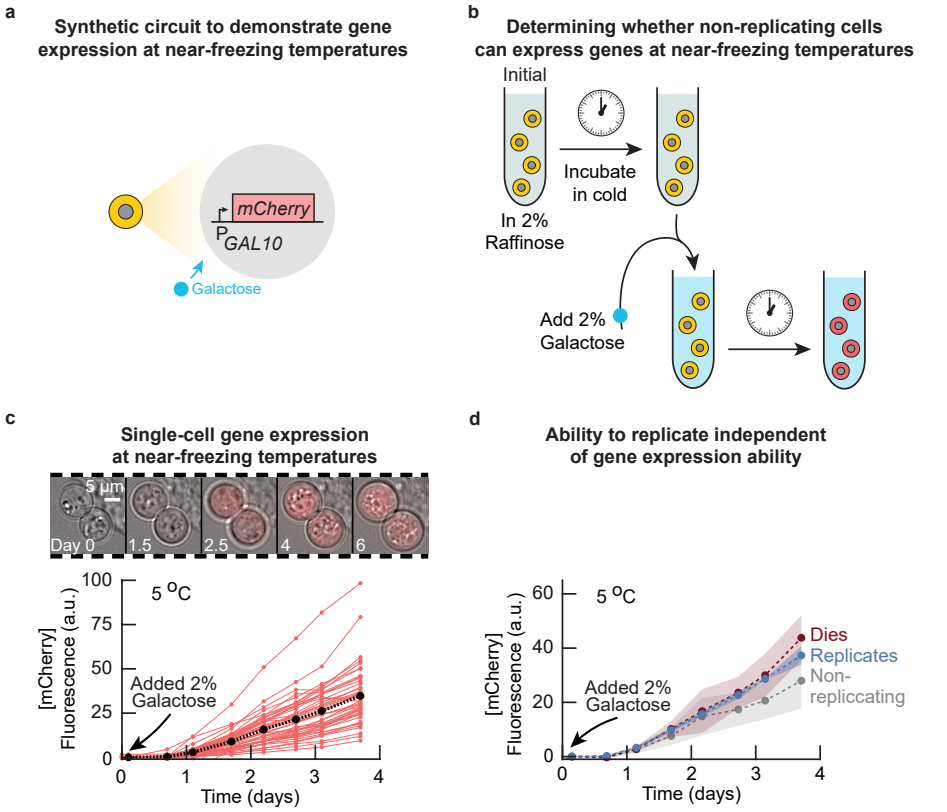

Figure S3.6: Non-replicating cells can express genes and the general machineries of gene expression (RNA polymerases and ribosomes) properly function at 5 °C (Related Figure 3.2a). **(a)** We build a synthetic gene-circuit in our wild-type yeast that makes the cells produce a red fluorescent protein, mCherry, upon induction by galactose. Expression of mCherry is controlled by an inducible promoter, *pGAL10*, which is activated by galactose. We first grow the yeast in raffinose and then add galactose to the raffinose-medium to activate the expression of mCherry. **(b)** Schematics of an example experiment to test if the engineered cells can express genes (such as mCherry) at near-freezing temperatures. We prepared cultures of the engineered strain in minimal medium that contained 2% raffinose as the carbon source (Methods 3.4). These populations were then incubated at 5 °C for two weeks, after which we induced the expression of mCherry by adding 2% galactose to the growth medium and then incubating the cells at 5 °C for the duration of the time-lapse. The expression of mCherry was then measured through microscopy or by flowing aliquots of the populations through a flow cytometer (Methods 3.4). **(c)** Time-lapse microscopy movie shows mCherry fluorescence measured in a single-cell over time. Each snapshot shown in the filmstrip is a composite of brightfield and mCherry channels. Shown are the cells on day 0 (i.e., directly after adding galactose) and after 1.5, 2.5, 4 and 6 days. Scale bar is 5 µm. Graph shows mCherry fluorescence in single cells over time from a microscopy time-lapse of a population kept at 5 °C (day 0 is the time of addition of 2% galactose). Black dotted line shows population average ($n = 44$ cells). All cells express mCherry within four days of induction with galactose. **(d)** From our microscopy time-lapses we also determined the average mCherry fluorescence over time for cells that replicated (blue), cells that died (red) and cells that grew without replicating (grey). Non-replicating cells and dying cells also express mCherry, at levels that are similar to that of replicating cells. Error bars show the mean with s.e.m. of the average fluorescence of each biological replicate ($n = 3$). With mCherry as a model gene, this experiment shows that the general machineries of transcription and translation (e.g., RNA polymerases and ribosomes) properly function to yield gene expression at 5.0 °C. Thus, being unable to express genes is not why cells do not replicate at near-freezing temperatures.

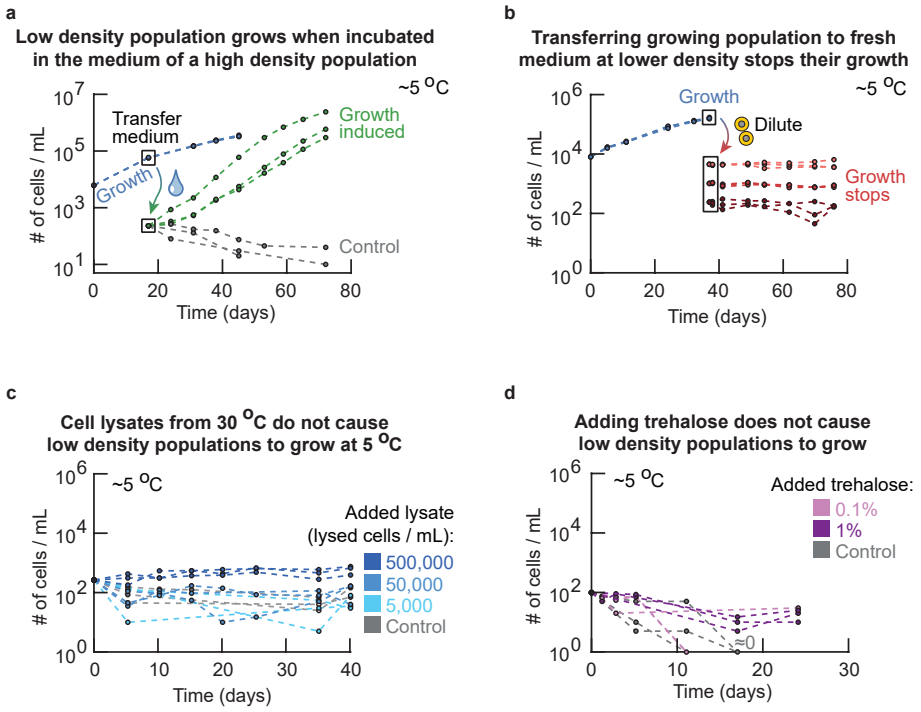

Figure S3.7: Secreted factor in extracellular medium determines whether a population grows or not at 5 °C (Related to Figure 3.2a). Testing why high-density populations grow whereas low-density populations do not grow at the same near-freezing temperature (5.0 °C). **(a)** To test whether the cell's ability to replicate at 5.0 °C is dictated by secreted factor(s) in the extracellular medium, we took the growth medium of a high-density (growing) population (blue curves, initially ~6,250 cells / mL) after several weeks of growth at 5.0 °C. Boxed data points on the blue curves show when the growth medium was taken. We flowed the high-density culture through a membrane filter with 0.2 μm pores so that growth medium taken from this culture was free of cells, which we confirmed with a flow cytometer (i.e., no cells were detected). Next, into this filtered medium, we incubated a fresh, low-density population of cells that were growing in 30 °C (green curves, initially ~250 cells / mL). As a control, we also incubated the same, low-density of cells in a fresh growth medium (grey curves, initially ~250 cells / mL). We incubated the two low-density cultures at 5.0 °C and measured their cell numbers over time. The populations of fresh cells grew in the filtered growth medium of the high-density population at 5.0 °C (green curves). But the low-density (control) populations in the fresh medium did not grow (grey curves). This experiment shows that cells change their growth medium (e.g., through secreted factor(s)) such that they can grow at 5.0 °C, and that a sufficiently high density of cells is required for the change to be sufficient for a population growth. **(b)** To test whether the ability to replicate at 5.0 °C is determined by intracellular factor(s) (e.g., a heritable trait), we took an aliquot of cells from a high-density (growing) population at 5.0 °C and diluted it by various amounts into fresh, pre-cooled media at 5.0 °C to test whether the resulting low-density population could grow. The high-density population of wild-type cells (blue curves, initially ~10,000 cells / mL) grew at 5.0 °C. After ~35 days of growth, we took an aliquot of cells from this culture and diluted it by ~50x (light red curves, initially ~10,000 cells / mL), ~250x (red curves) or ~1250x (dark red curves). Ordinarily, populations that start at these "low densities" do not grow at 5.0 °C (Fig. 3.1b). We incubated the diluted, low-density populations in fresh medium at 5.0 °C and measured their density over time (red curves). None of these populations grew at all during more than one month of incubation at 5.0 °C. This experiment shows that a population's ability to grow at 5 °C is not solely determined by intracellular factor(s). **(c)** To test whether the extracellular factors that enable population growth come from dying cells that may be bursting (lysing), we incubated populations in media with cell lysates. We obtained the cell lysates from a population of wild-type cells growing in log-phase at 30.0 °C (~5,000,000 cells / mL). ***(caption continues on the next page)***

Figure S3.7 ***(caption continued from the previous page)*****:** We added glass beads to this liquid culture and placed it on a vortex for 20 min to mechanically lyse the cells. After this, we flowed the liquid media containing the lysed cells with the beads through a 0.45 μm pore filter to remove the glass beads and any intact cells that remained. We then added the filtered cell lysate to a fresh medium in amounts dictated by the cell densities before lysis (e.g., fresh medium having 500,000 lysed cells / mL has a 90% volume of fresh medium and ~10% cell lysate that had ~5,000,000 cells / mL before the lysis). Finally, we incubated fresh cell populations in these growth media at a low density (~250 cells / mL) and at 5.0 °C. The growth curves show populations with ~500,000 lysed cells / mL (dark blue curves), ~50,000 lysed cells / mL (blue curves), ~5,000 lysed cells / mL (light blue curves) and, as control, fresh cells in a fresh medium without any cell lysate (grey curves). None of these populations grew at 5.0 °C. This experiment shows dying cells that may be bursting are not responsible for inducing population growth at 5.0 °C. **(d)** Trehalose is a common cryoprotectant that is abundant in yeasts at low temperatures and is thought to protect the cells against freezing [17]. Its precise mechanism is incompletely understood. We reasoned that yeast populations may be secreting trahalose to help them grow at 5.0 °C. To test this idea, we incubated a low-density population at 5.0 °C (initially ~100 cells / mL) with 1% trehalose (dark purple curves, percentage in weight per volume), 0.1% trehalose (light purple curves) or without trehalose (grey curves). None of the populations grew, indicating that trehalose is not one of the extracellular factor(s) that induce growth at 5.0 °C. All panels show at least $n = 3$ biological replicates per condition (color).

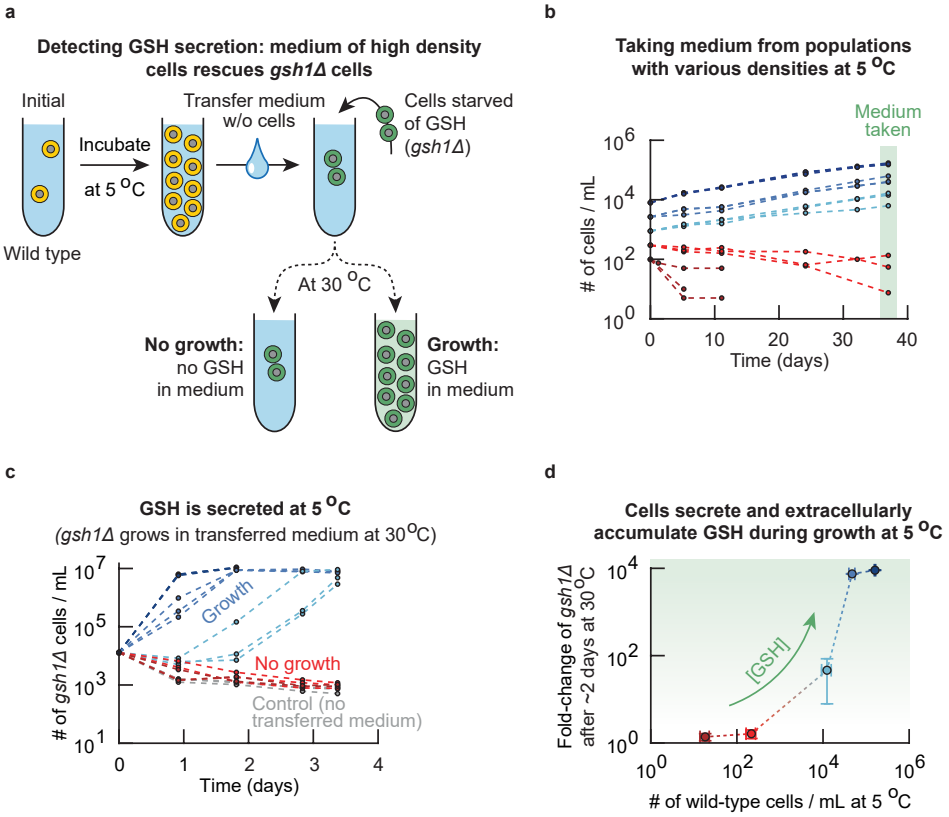

Figure S3.8: A non-viable mutant that cannot synthesize glutathione (*gsh1*Δ) is rescued by medium from high-density populations, which confirms that cells in high-density populations secrete and extracellularly accumulate glutathione at 5 °C (Related to Figure 3.2a). **(a)** Schematics of experiments in (b-d). A mutant that cannot synthesize glutathione (*gsh1*Δ-strain) cannot live without supplemented GSH even at 30 °C, because GSH is essential for life (e.g., GSH is essential for iron metabolism [48]). The only way for the mutant to survive and grow at any temperature is by supplementing GSH into its growth medium [56, 119]. To test whether cells at 5.0 °C secrete glutathione, we incubated wild-type yeast populations at 5.0 °C at different initial population-densities. After several weeks of incubation, we isolated the growth medium from the wild-type populations. Specifically, we took aliquots of the cultures at 5.0 °C and removed the cells from the growth media by spinning down the aliquot and passing the supernatant through a 0.2 µm pore filter to remove all yeasts. We checked that no cells remained in the filtered media by flowing them through a flow cytometer (no events detected). In the filtered media, we then incubated a population of *gsh1*Δ cells that we had starved of glutathione by incubating them overnight in fresh medium without GSH at 30.0 °C (these cells therefore did not grow during the overnight). If the filtered media did not contain any glutathione, then the starved *gsh1*Δ cells would not grow. If the filtered media did contain glutathione, secreted by the wild-type cells, then the *gsh1*Δ cells would be able to import the glutathione and grow. **(b)** As a first part of the experiment described in (a), we incubated wild-type yeast populations at 5.0 °C and took aliquots of their growth media after ~5 weeks of incubation. Shown is the density of wild-type populations over time for different starting densities (~300 cells / mL (red curves), ~900 cells / mL (light blue curves), ~2,700 cells / mL (blue curves) and ~8,000 cells / mL (dark blue curves)). Each color shows $n = 3$ replicate populations. **(c)** To detect extracellular glutathione, we isolated and filtered the growth media from the wild-type populations in (b). Shown is the population density over time at 30.0 °C of glutathione-starved *gsh1*Δ cells that received the filtered media (initially ~13,000 cells / mL).
(caption continues on the next page)

Figure S3.8 ***(caption continued from the previous page)*****:** The colors of the curves here match the colors used for the various densities of wild-type populations in (b) (e.g., the red populations received the filtered media from the wild-type populations whose growth curves are shown in red in (b)). As a control, we also incubated *gsh1*Δ cells in fresh medium without any glutathione (grey curves). The *gsh1*Δ cells did not grow in the medium transferred from low-density (non-growing) populations at 5.0 °C. The *gsh1*Δ cells always grew to the carrying capacity in the medium from the high-density (growing) populations at 5.0 °C. Each color shows $n = 3$ replicate populations. **(d)** Summary of the data from (b) and (c). The x-axis shows the population density of wild-type cells after ~5 weeks of incubation at 5.0 °C. The y-axis shows, after two days of incubation at 30 °C, the number of *gsh1*Δ cells in transferred media relative to the number of *gsh1*Δ cells in a fresh medium without glutathione. Populations of *gsh1*Δ cells that grew more had more glutathione in their medium (glutathione is the growth limiting factor in the transferred media, see control in (c)). Error bars represent the mean with s.e.m., having $n = 3$ biological replicates per data point. Together, (a-d) show that the amount of extracellular glutathione increases with population density for growing populations at 5.0 °C, and that barely any extracellular glutathione accumulates for non-growing populations at 5.0 °C. In summary, cells in growing populations secrete and extracellularly accumulate glutathione at near-freezing temperatures.

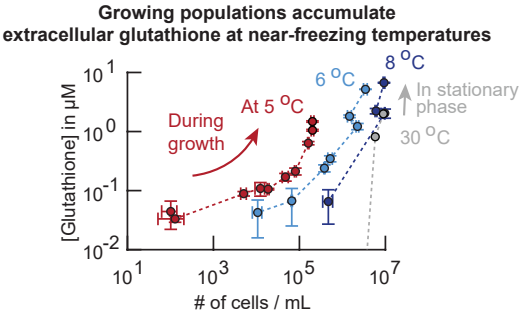

Figure S3.9: Cells secrete and accumulate glutathione during growth at near-freezing temperatures (Related to Figure 3.2a). With an enzymatic assay kit, we quantified the total glutathione concentration in the growth media of wild-type yeast populations at two different time points after at least 2 weeks of incubation at various temperatures (Methods 3.4). Shown here is the total extracellular glutathione concentration as function of population density at ~5.0 °C (red curve, one week between sampling), ~6.1 °C (light blue curve), ~8.3 °C (dark blue curve) and ~30.0 °C (grey curve). The extracellular glutathione concentration increases during population growth at near-freezing temperatures (i.e., 5.0 °C - 8.3 °C), whereas glutathione only accumulates in stationary phase at 30.0 °C (data reused [119]). Error bars show the mean with s.e.m., having $n = 3$ biological replicates per data point.

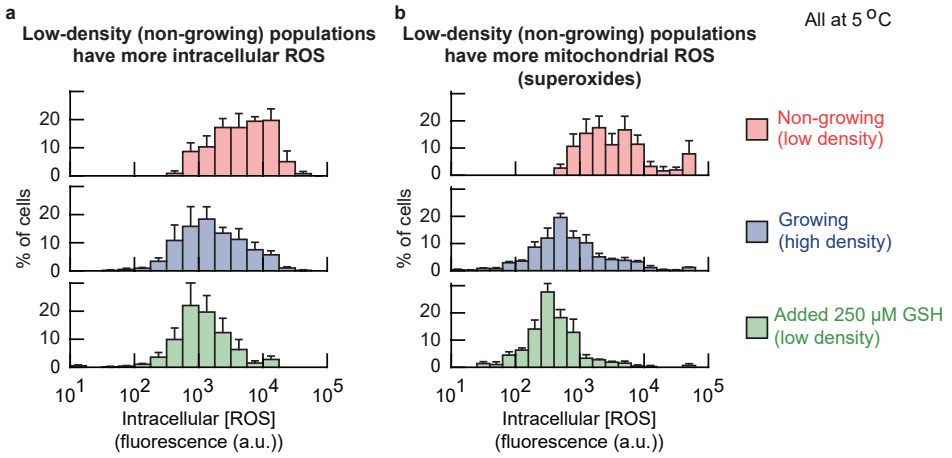

Figure S3.10: Cells of low-density (non-growing) populations at 5 °C have more intracellular Reactive Oxygen Species (ROS), including superoxides in their mitochondria, which can be removed by supplementing extracellular reduced glutathione (GSH) (Related to Figure 3.2d). (a-b) Measured intracellular ROS concentrations in single cells. We stained intracellular ROS in live, single cells with two different dyes. One dye (cellROX) measured the amount of general, cytoplasmic ROS while another dye (mitoSOX) measured the amount of superoxides in mitochondria. We incubated populations of cells at 5.0 °C for two weeks and then stained the cells with the ROS dyes (Methods 3.4). We then used fluorescence microscopy to determine the amounts of intracellular ROS in single cells, represented by the average intracellular fluorescence of the dye in each cell (after subtracting background fluorescence). **(a)** Intracellular ROS concentration for general ROS (with cellROX). **(b)** Superoxide concentrations in mitochondria (with mitoSOX). Histograms in (a-b) show cells of low-density (non-growing) populations (red bars, initially ~250 cells / mL), growing populations (blue bars, initially ~6,250 cells / mL) and low-density populations that had 250 μM GSH added to their growth media (green bars, initially ~250 cells / mL). These histograms show that the low-density (non-growing) populations have higher intracellular ROS concentrations than high-density (growing) populations. Adding extracellular GSH decreased the intracellular ROS concentrations of the low-density populations to concentrations similar to the high-density populations. Error bars show the mean with s.e.m., having $n = 3$ biological replicates per histogram.

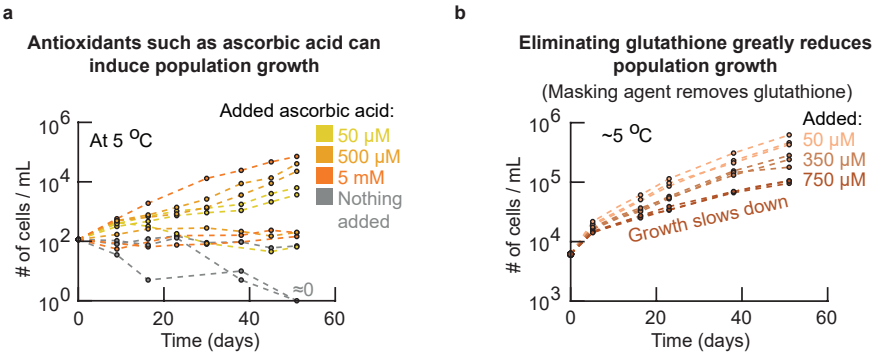

Figure S3.11: Supplementing the growth medium with an extracellular antioxidant (ascorbic acid or glutathione) is sufficient for inducing growth at 5 °C (Related to Figure 3.2d). So far, we have shown that an ample extracellular GSH can induce population growths at 5.0 °C (Fig. 3.2c) and that cells secrete and extracellularly accumulate glutathione, with a sufficient amount for growth being secreted only by sufficiently high-density populations (Fig. 3.2a, Supplementary Fig. S3.8). **(a)** To show that it is glutathione's role as an antioxidant, as opposed to its other roles (e.g., regulating iron metabolism [48]), that causes the population growths, we incubated wild-type yeast populations at 5.0 °C in medium supplemented with ascorbic acid, an antioxidant that yeasts do not synthesize [124]. Shown here is the population density measured over time for low-density populations (~100 cells / mL) incubated with 50 µM ascorbic acid (yellow curves), 500 µM ascorbic acid (orange curves), 5 mM ascorbic acid (red curves) or without any ascorbic acid (grey curves). More than half of the populations that had extracellular ascorbic acid grew at 5.0 °C, whereas the control populations without ascorbic acid did not grow at all (because the initial population-density was too low for growth according to our phase diagram, Fig. 3.1b). This result supports the idea that the antioxidant action of glutathione alone is sufficient to induce population growths since other antioxidants such as ascorbic acid can also induces population growths. **(b)** Knowing that glutathione's antioxidant role is sufficient to induce population growths, we next tested whether glutathione is absolutely necessary for growth at 5.0 °C. We used a masking agent (1M2VP) that specifically and functionally blocks extracellular glutathione in the growth medium [54, 55]. We incubated wild-type cell populations at 5.0 °C (initially ~6,250 cells / mL) with 50 µM of masking agent (beige curves), 350 µM of masking agent (light brown curves) or 750 µM of masking agent (dark brown curves). We found that the masking agent reduces population growth, with more masking agent reducing growth further. However, the masking agent does not fully prevent population growth at any concentration. Extracellular GSH is therefore sufficient for inducing growth at 5.0 °C, but does not seem to be necessary for populations to grow at 5.0 °C. Together, our results suggest that there is (are) likely additional extracellular factor(s) that control population growth. This is because we established that secreted factor(s) determine whether populations grow (Supplementary Fig. S3.7), high-density populations continue to grow without extracellular glutathione (b), and low-density populations are not able to grow at 5.0 °C (Fig. 3.1a). Each color shows $n = 3$ replicate populations in both panels.

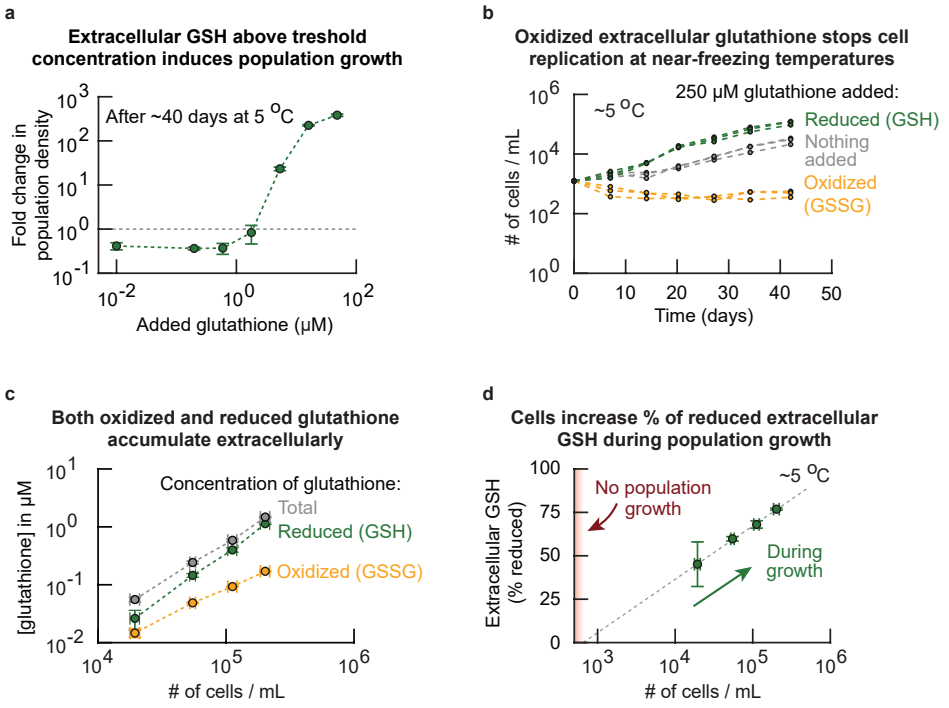

Figure S3.12: Reduced form of glutathione, not the oxidized form of glutathione, enables and accelerates replications at 5 °C above threshold concentration of ~1 μM (Related to Figure 3.2d). Unless stated otherwise, our experiments added the reduced form of glutathione (GSH). But for the experiments in this figure, we used both reduced glutathione (GSH) and oxidized glutathione (GSSG) to determine that GSSG does not induce growth at 5.0 °C. **(a)** We incubated a low-density wild-type population (initially ~260 cells / mL) at 5.0 °C with various amounts of added GSH. The GSH concentration spanned almost four orders of magnitude. Shown here is the fold-change of the population density after ~40 days of incubation. Populations expanded when the extracellular GSH concentration exceeded ~1 μM, while populations shrank if the extracellular GSH concentration was less than ~1 μM. Thus, low-density populations require at least 1 μM of GSH to grow at 5.0 °C. This threshold concentration is high compared to the ~0.1 μM of GSH that the high-density populations accumulated themselves (Fig. 3.2a). This result suggests that there are other extracellular factors that induce population growths at 5.0 °C. There are two results that support this: (1) removing extracellular GSH does not completely stop growth of high-density populations (Supplementary Fig. S3.11); and (2) the concentration of secreted GSH by high-density (growing) populations is an order of magnitude below the concentration of the GSH that must be added to cause a low-density population to grow at 5.0 °C. Error bars show the mean with s.e.m., having $n = 3$ replicate populations per data point. **(b)** So far, we established that extracellular GSH can induce population growths (a), and it is the antioxidant action of GSH that induces growth (Supplementary Fig. S3.11). Next, we wondered whether cells at 5.0 °C specifically require reduced glutathione to induce growth. The reduced form of glutathione, GSH, functions as an antioxidant whereas the antioxidant function does not exist in the oxidized form, GSSG (two oxidized glutathione molecules). We incubated cells at 5.0 °C with either oxidized or reduced glutathione in their growth medium. Shown here are the population densities over time for 250 μM reduced glutathione (GSH, green curves), 250 μM oxidized glutathione (GSSG, yellow curves) and without any glutathione added to the medium (grey curves, all initially at ~1,240 cells / mL). All populations grew when either GSH or nothing was added to the medium, with populations having added GSH growing faster. In contrast, the populations that had GSSG (oxidized glutathione) added to their medium did not grow at all. These results show that populations require GSH (reduced form of glutathione) to grow at 5.0 °C. This finding is supported by the fact that it is glutathione's antioxidant action that induces population growth (Supplementary Fig. S3.11). Each condition (color) shows $n = 3$ replicate populations. ***(caption continues on the next page)***

Figure S3.12 ***(caption continued from the previous page)*****: (c)** We next measured the concentrations of both oxidized and reduced extracellular glutathione that accumulated in the medium of high-density (growing) populations (Methods 3.4). Shown are the total (grey curve), reduced (green curve) and oxidized (yellow curve) extracellular glutathione concentrations in the same medium after 28 days at 5.0 °C for various population densities. The total extracellular glutathione concentration increases as the initial population density increases (also see Fig. 3.2a). Both the concentrations of reduced and oxidized glutathione increase with density, with the concentration of reduced glutathione increasing faster. Error bars show the mean with s.e.m., having $n = 3$ biological replicates per density. **(d)** Using the data from (c), we plotted the percentage of extracellular GSH (the percentage of all glutathione that is reduced) as a function of the population density. Grey dotted line shows a linear fit as a visual guide. The percentage of GSH increases with population density. Extrapolating the linear fit suggests that all extracellular glutathione would be oxidized in the medium of populations with a density below ~1,000 cells / mL (i.e., non-growing populations, Fig. 3.1a). Together, our data ((c-d) and Fig. 3.2a) establish that cells in high-density populations secrete and accumulate a pool of extracellular glutathione, with higher density populations having higher concentrations of glutathione that are increasingly reduced. Moreover, these results show that populations cannot grow when the entire pool of extracellular glutathione becomes oxidized (b). Error bars show the mean with s.e.m, having $n = 3$ biological replicates per data point.

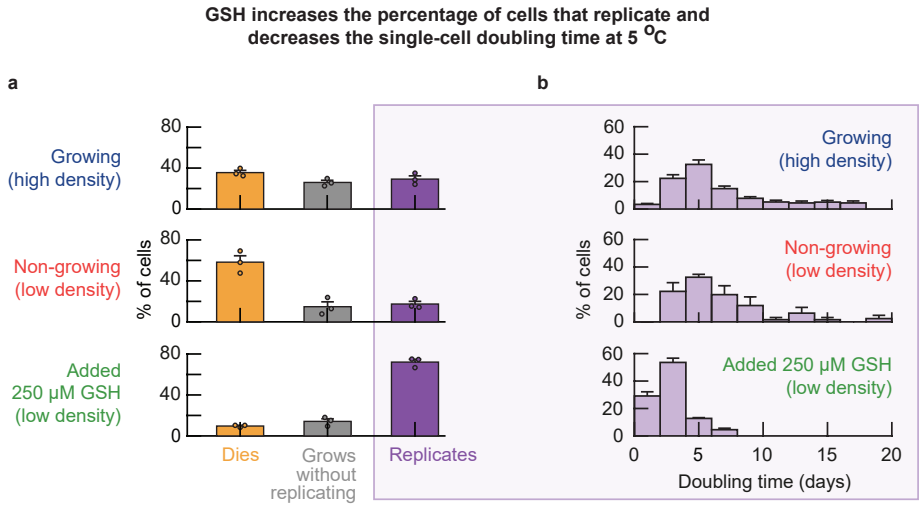

Figure S3.13: Glutathione increases the percentage of cells that replicate and decreases their doubling time at 5 °C (Related to Figure 3.2e). Comparing the behavior of single cells at near-freezing temperatures with and without reduced glutathione ("GSH") added to the growth medium. **(a)** We incubated wild-type cell populations at 5.0 °C with or without adding GSH to their growth medium. After two weeks of incubation, we followed whether individual cells replicated, grew without replicating or died with a microscopy time-lapse (Methods 3.4). Shown here are the percentages of cells that replicated (purple bar), died (orange bar) and grew without replicating (grey bar) during the ~20 days of imaging. We did these measurements for high-density (growing) populations (initially ~6,250 cells / mL), low-density (non-growing) populations (initially ~250 cells / mL), and low-density (growing) populations with 250 µM of added GSH (initially ~250 cells / mL). Note that 250 µM GSH is higher than the ~1 µM of glutathione that the high-density populations accumulate by themselves (Fig. 3.2a). The added GSH decreases the percentage of cells that die in the low-density population to 9.7 ± 0.7% (compared to ~58% in populations of the same density without added GSH). Similarly, the added GSH increases the percentage of cells that replicates in the low-density population to 72.1 ± 2.7% (compared to ~17% in the low-density populations without added GSH). Thus, extracellular GSH decreases cell deaths and increases cell replications. Bars show the mean with s.e.m., having $n = 3$ biological replicates per condition. Dots show raw data. **(b)** Doubling time for single cells in each population. Histogram shows the percentage of cells with a given doubling time. The average doubling time is 6.5 days for the high-density populations ($n = 451$ cells) and 7.1 days for the low-density populations ($n = 42$ cells). Thus, the doubling time of replicating cells is similar regardless of population density. In contrast, the average doubling time is 2.9 days for the low-density populations with added GSH ($n = 444$ cells). GSH therefore reduces the time it takes to replicate by more than half. Data shows the mean with s.e.m. for each bin, having $n = 3$ biological replicates per condition. Together (a-b) show that both high-density (growing) and low-density (non-growing) populations contain replicating cells, with nearly identical doubling time distributions. The main differences between the two populations are the percentage of cells in each population that replicate and the percentage of cells that die. Adding extracellular GSH increases the percentage of replicating cells (a) and decreases the doubling time of these cells (b). Data for populations without added GSH is reproduced here from Fig. 3.1c as a comparison.

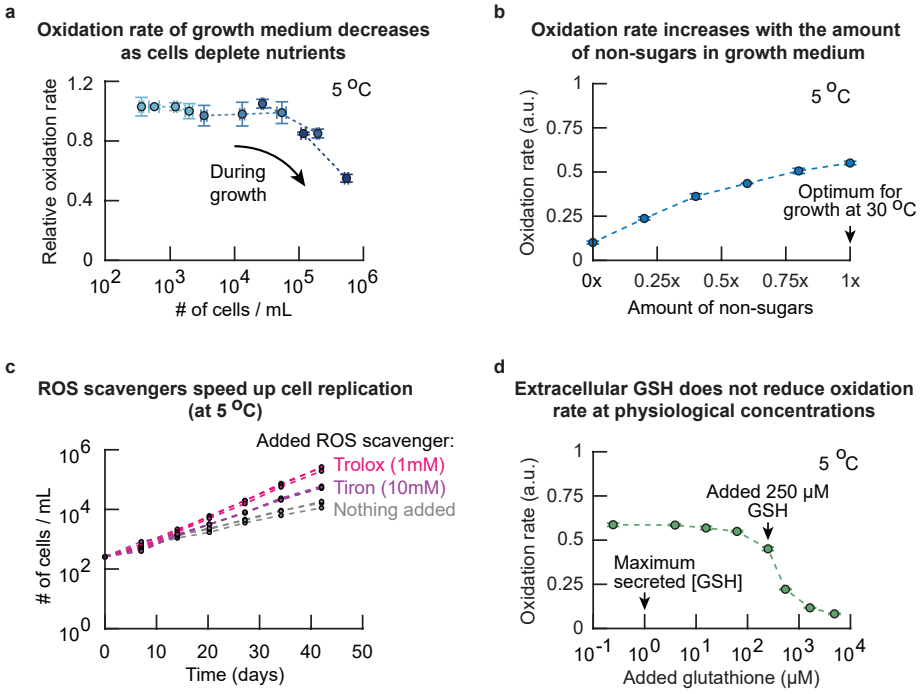

Figure S3.14: Non-sugar components of the yeast growth medium (e.g., vitamins, amino acids) and oxygen create Reactive Oxygen Species without any cells at 5 °C (Related to Figure 3.2f). Together, our results suggest that more extracellular factor(s) – besides reduced glutathione – dictate population growth at near-freezing temperatures (Supplementary Figs. S3.7 and S3.11-S3.12). Knowing that extracellular factor(s) dictate growth at near-freezing temperatures (Fig. S3.7), and that cells are stressed by ROS (Fig. 3.2a, Supplementary Fig. S3.10) and that it is the antioxidant action of GSH that induces population growth (Supplementary Figs. S3.11-S3.12), we hypothesized that the extracellular environment may also be a source of ROS. **(a)** To test whether ROS are present in the extracellular environment, we used a dye called dihydroethidium (DHE) that becomes fluorescent upon oxidation by ROS (mainly superoxides). We grew wild-type yeast populations with various starting densities at 5.0 °C, and measured the oxidation rate of their growth media relative to the oxidation rate of fresh media. Here, the oxidation rate is given by the rate at which the oxidation-responsive dye becomes fluorescent. To do so, at every time-point, we took aliquots of our liquid cultures and flowed the aliquot through a 0.2 µm pore filter. We then measured the oxidation rate in the flow-through – the growth medium without any cells – and compared with the oxidation rate in fresh medium. Shown is the relative oxidation rate as function of population density. The oxidation rate decreases when the population density exceeds ~10,000 cells / mL. This result shows that ROS are present in the extracellular environment of cells and that the oxidation rate of the medium decreases with population density. **(b)** Given that the oxidation rate decreases with population density, we further hypothesized that the components of the growth medium – which the cells consume and deplete – may be a source of ROS. We therefore tested whether the presence of any of the nutrients in medium affects the ROS production in the cell's environment. Specifically, without cells, we measured the oxidation rate of DHE at 5.0 °C in growth media having various compositions. We diluted the growth medium with water by various amounts and then supplemented these diluted media with 2% glucose (so a "0.5x-medium" contains 0.5x SC + 0.5x water, supplemented with 2% glucose). Shown is the oxidation rate in diluted media at 5.0 °C (blue curve, in steps of 0.2x non-sugars). We found that the oxidation rate increased roughly linearly with the amount of non-sugar nutrients in the medium (i.e., the concentrations of amino acids, vitamins, trace elements, salts and the nitrogen source). **(c)** Knowing that the extracellular environment may be a source of ROS through the non-sugar nutrients in the growth medium, we added chemicals to the growth medium that remove (i.e., have scavenging activity against) ROS. Specifically, we used scavengers of superoxide (10 mM tiron) or peroxyl radicals (1 mM trolox) and tested whether the scavenging agents could be beneficial for yeast growth. ***(caption continues on the next page)***

Figure S3.14 ***(caption continued from the previous page)*:** To do so, we grew populations of cells at 5.0 °C in the presence of ROS scavengers (initially ~250 cells / mL). Shown is the population density over time for populations with trolox (pink curves), tiron (purple curves) or nothing (grey curves) added to the growth medium. Both trolox and tiron increase the growth rate of populations. Thus, scavenging and removing extracellular ROS (such as superoxide and peroxyl radicals) is beneficial for population growth at near-freezing temperatures. **(d)** Finally, we tested the effect of GSH on the oxidation rate of the growth medium. Shown is the oxidation rate as a function of the GSH concentration in minimal medium without cells at 5.0 °C. Increasing the GSH concentration above a threshold concentration – at ~250 μM GSH – decreases the oxidation rate. For all panels the error bars are mean with s.e.m., with $n = 3$ replicates per condition.
In summary (a-d) show that non-sugar nutrients in the growth medium increase the oxidation rate of the environment by facilitating the generation of ROS. The oxidation rate decreases when these non-sugar nutrients are removed from the growth medium. Potential sources of ROS in the environment are oxygen (superoxide) or non-sugar nutrients themselves (peroxyl radicals), as demonstrated by scavenging of these ROS being beneficial for yeast growth at near-freezing temperatures. Finally, we found that GSH can decrease the extracellular oxidation rate at high concentrations.

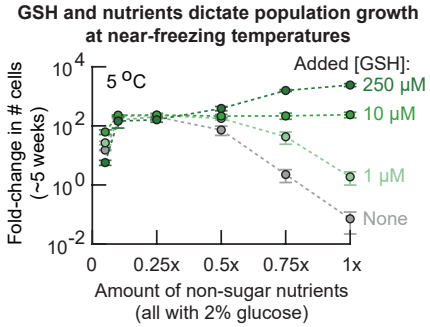

Figure S3.15: Population growth is a balance between extracellular GSH and availability of non-sugar nutrients at 5 °C (Related to Figure 3.2i). Studying the combined effect of non-sugar nutrients and extracellular GSH on population growth. We incubated cells in media that had precise amounts of non-sugar nutrients and added GSH. Specifically, for varying the amount of non-sugar nutrients, we formulated the media to contain 0.05x, 0.1x, 0.25x, 0.5x, 0.75x or 1x non-sugar nutrients. Here, 1x equals the amount of non-sugar nutrients that is in the medium for yeast grown under standard conditions (Methods 3.4). Each of these media had 2% glucose. Then, for each of these medium compositions, we added either 0 µM, 1 µM, 10 µM or 250 µM of GSH. This procedure created 24 different media (6 different amounts of non-sugar nutrients each with 4 different added GSH concentrations). In these media we incubated low-density populations of cells (initially ~210 cells / mL) at 5.0 °C. These low-density populations should not grow according to our phase diagram (Fig. 3.1b). Shown is the fold-change in population density as function of the amount of non-sugar nutrients after ~5 weeks of incubation at 5.0 °C. The curves represent 1 µM (light green curve), 10 µM (green curve), 250 µM (dark green curve) or without (grey curve) added GSH. The populations in 1x non-sugar nutrients and without added GSH did not grow at all during the 5 weeks of incubation at 5.0 °C, as expected from our phase diagram (Fig. 3.1b). Further corroborating our other data we find that at 1x non-sugar nutrients, the fold-change in population density increased with the concentration of added GSH (also see Fig. 3.2e) and that without added GSH, the fold-change in population density increased when the amount of non-sugar nutrients decreased (grey curve, also see Fig. 3.2g). Then, starting at 1x non-sugar nutrients, all curves converge to a ~100-fold change in population density as the amount of non-sugar nutrients decreased from 1x to 0.25x. Thus, adding more than 10 µM GSH is only beneficial for population growth when sufficient non-sugar nutrients are available (i.e., more than 0.5x non-sugar nutrients). Finally, populations stop growing when the amount of non-sugar nutrients decreased below 0.1x. In summary, this growth experiment shows that either sufficient extracellular GSH (> 1 µM, Supplementary Fig. S3.12) or low enough amounts of non-sugar nutrients are required for population growth at 5.0 °C. Adding glutathione or removing non-sugar nutrients induces growth by either removing ROS (Supplementary Figs. S3.10-S3.11) or decreasing the oxidation rate (Supplementary Fig. S3.14). Populations having less non-sugar nutrients require less extracellular GSH for growth, and populations having more extracellular GSH can grow with more non-sugar nutrients. The media with > 0.75x non-sugar nutrients and 250 µM added GSH are special because they permit growths that exceed the (~100-fold) growth that a population can achieve by secreting glutathione by itself (light green curve; also see Fig. 3.2a). Error bars show the mean with s.e.m., having $n = 3$ biological replicates per condition.

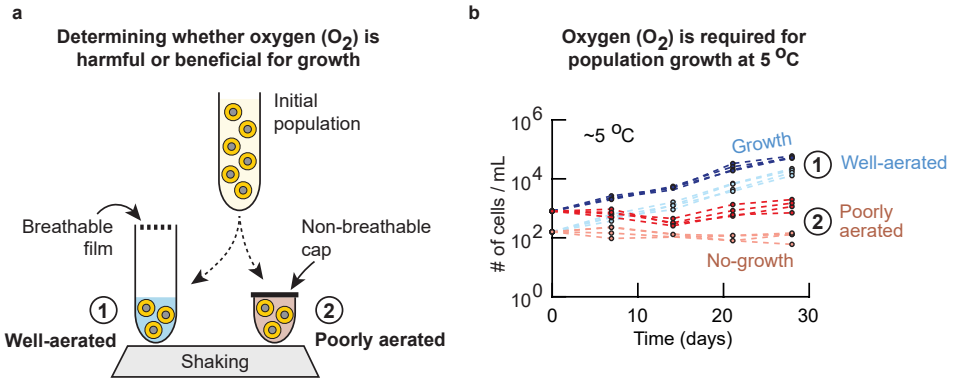

Figure S3.16: Oxygen (O_2) is required for population growth at 5 °C (Related to Figure 3.2i). Testing whether oxygen (O_2) is required or harmful for population growths at 5.0 °C. **(a)** Schematic of the experiment in (b). We incubated 5 mL of cell populations that were either well aerated or poorly aerated at 5.0 °C. For well-aerated conditions, cells were grown in tubes with a breathable film sealing the tube tops (Methods 3.4). For poorly aerated conditions, the cells were in 5 mL Eppendorf tubes that were sealed off by a non-breathable cap and parafilm. This created two populations of cells that started with the same density but one that was well-aereated (oxygen available through the air) and one that was poorly aerated (limited oxygen). Both populations were incubated at 5.0 °C and continuously shaken at 125 rpm. **(b)** Results of the experiment described in (a). Shown here are the population densities over time for populations that were well-aerated (blue curves, labelled "1") or poorly aerated (brown curves, labelled "2"), each condition having different initial densities (~350 cells / mL or ~100 cells / mL). All well-aerated populations grew exponentially over time. Poorly aerated populations barely increased in density during the experiment. These results show that aeration (sufficient availability of oxygen in the growth medium) is necessary for population growth at 5.0 °C. Thus, oxygen is both beneficial (required for cell replications) and harmful (as source of ROS, Supplementary Fig. S3.14) at 5.0 °C. This result complements our findings that non-sugar nutrients the growth medium are sources of ROS (Supplementary Fig. S3.14). Each condition (color) shows $n = 4$ biological replicates.

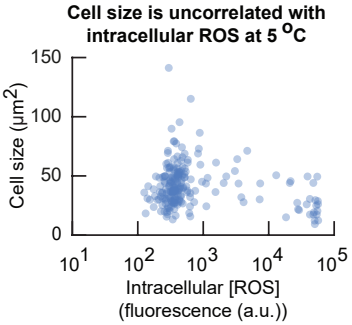

Figure S3.17: Cell size does not correlate with the intracellular ROS concentration at 5 °C (Related to Figure 3.3c). Cell size as a function of intracellular ROS concentration. We incubated populations of cells for two weeks at 5.0 °C (initially ~6,250 cells / mL). We then measured the size and intracellular ROS concentration in single cells (Methods 3.4). This result shows that the cell size is uncorrelated with intracellular ROS concentration. Dots show single-cell data aggregated from $n = 3$ biological replicates ($n = 214$ cells).

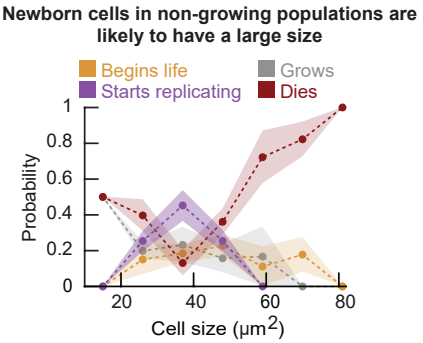

Figure S3.18: Newborn cells in low-density (non-growing) populations are larger than those in high-density (growing) populations at 5 °C (Related to Figure 3.3c). We incubated populations of wild-type cells at a low density (initially ~500 cells / mL) for two weeks at 5.0 °C and then imaged these cells in our wide-field microscope for the next several weeks (Methods 3.4). We classified individual cells in the resulting time-lapse movies as being in one of the following events (Supplementary Fig. S3.19): "begins life" (just-born daughter cell), "starts replicating", "grows" (without replicating), or "dies" (cell just before death). For every cell in each class, we measured its cell size. Specifically, for cells in the "begins life" class, we measured the daughter cell's size just after cytokinesis (when the mother's bud neck breaks). For cells in the "starts replicating" class, we measured the mother cell's size at the time the bud appears. For cells in the "grows" class, we measured their size in the first time point when the movie begins (i.e., at the first moment that they are growing without replicating). For cells in the "dies" class, we measured the size just before they die (i.e., the last time point before death). We binned the cells according to their sizes. For each bin, we determined the probability that a cell in that size bin would be in each of the four classes. Dots show average probability in each bin for the different events, shaded area represents the s.e.m. for $n = 3$ biological replicates. This graph shows that newborn cells in low-density (non-growing) populations are likely to have a large size, instead of being smallest cells in the population (Fig. 3.3c). Thus, newborn cells in low-density (non-growing) populations are less likely to replicate than the mother cells in the same population (see Supplementary Fig. S3.19).

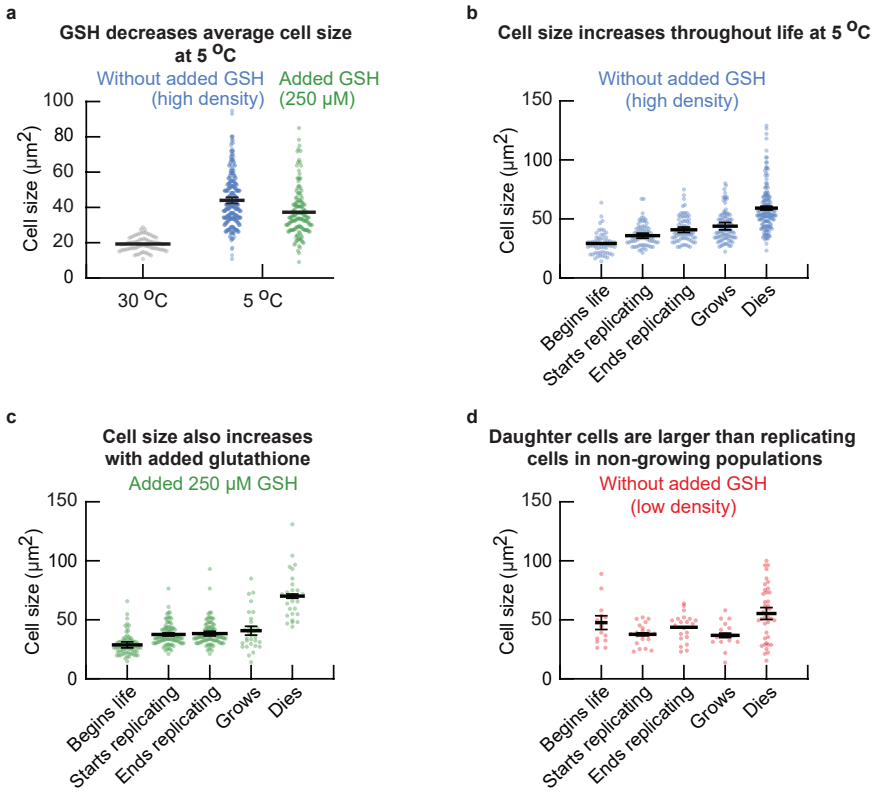

Figure S3.19: Cell size monotonically increases from birth to death at 5 °C (Related to Figure 3.3c). (a) We incubated wild-type cell populations for two weeks at 5.0 °C and then measured the cell sizes with a wide-field microsope. Shown here are the cell sizes of individual cells from high-density populations without any GSH added (blue dots, initially ~8,000 cells / mL) and sizes of individual cells from low-density populations that were incubated with 250 µM GSH (green dots, initially ~420 cells / mL). Grey dots show cells during growth at 30.0 °C as a comparison. Surprisingly, we find that cells are, on average, more than double the size (cross-sectional area) at 5.0 °C (44.0 ± 1.7 µm^2) compared to 30.0 °C (19.3 ± 0.2 µm^2). Moreover, adding GSH to the growth medium decreases the average cell size at 5.0 °C (to 37.3 ± 0.1 µm^2). Error bars represent the mean with s.e.m., having $n = 3$ biological replicates. Dots show data aggregated from the biological replicates. **(b-d)** Next, we incubated populations of wild-type cells for two weeks at 5.0 °C. After two weeks we transferred aliquots of the liquid cultures to microscopy plates that we kept chilled at 5.0 °C before the transfer and took a snapshot of the cells with a microscope every day (Methods 3.4). The resulting snapshots form time-lapse movies at 5.0 °C. From these movies, we classified the cells into one of the following events: "begins life" (the daughter cell right after the mother cell finishes cytokinesis), "start replicating" (the mother cell right after it forms a bud), "end replicating" (the mother cell right after the it cell finishes cytokinesis), "grows" (a cell that grew in size without replicating for the duration of the time-lapse movies of ~17 days) and "dies" (cells that die during the time-lapse movies). We determined the cell size for all cells in each event. Shown are the cell sizes of individual cells from populations with high initial density (~8,000 cells / mL) **(b)**, low initial density (~420 cells / mL) with 250 µM added GSH **(c)**, and low initial density (~420 cells / mL) without any GSH added **(d)**. (b) At high density, newborn cells are the smallest cells in the population (29.2 ± 0.5 µm^2), with cells increasing in size during cell replication (from 35.8 ± 2.1 µm^2 at bud formation to 40.8 ± 2.3 µm^2 at cytokinesis). Growing cells are on average 43.8 ± 3.1 µm^2. Finally, cells that die are the largest cells in the population (59.1 ± 1.6 µm^2). (c) Similarly, in populations that were incubated in growth medium to which we added 250 µM GSH, we found that newborn cells are the smallest cells in the population (at 28.7 ± 2.5 µm^2), with replicating cells increasing in size during replication (starting at 37.6 ± 1.3 µm^2 and ending with 38.3 ± 2.0 µm^2 at the end of division).
(caption continues on the next page)

Figure S3.19 ***(caption continued from the previous page)*:** Growing cells are on average $40.8 \pm 3.7\,\mu m^2$. Finally, with added GSH, cell deaths occur at larger sizes ($70.1 \pm 1.3\,\mu m^2$) compared to cells without added GSH. (d) In low-density (non-growing) populations, the newborn cells are on average larger ($47.6 \pm 5.8\,\mu m^2$) than the average size at which the cells start replicating ($37.9 \pm 1.2\,\mu m^2$), end replicating ($43.7 \pm 0.4\,\mu m^2$), or are growing ($36.8 \pm 1.9\,\mu m^2$). Finally, cells that die are smaller ($55.3 \pm 5.0\,\mu m^2$) than cells in the growing populations. For all panels, the error bar shows the mean with s.e.m., having $n = 3$ biological replicates. Dots are data aggregated from the biological replicates.
Together, these results show that, in growing populations, newborn cells have on average the smallest size of the population. In contrast, in low-density (non-growing) populations without added GSH, the newborn cells are on average larger than the replicating cells in the population. Moreover, these results show that the cell size monotonically increases from a cell's birth to its death, since the cell size increases for consecutive life events (i.e., a newborn cell either eventually replicates or will grow without replicating, and every cell eventually dies).

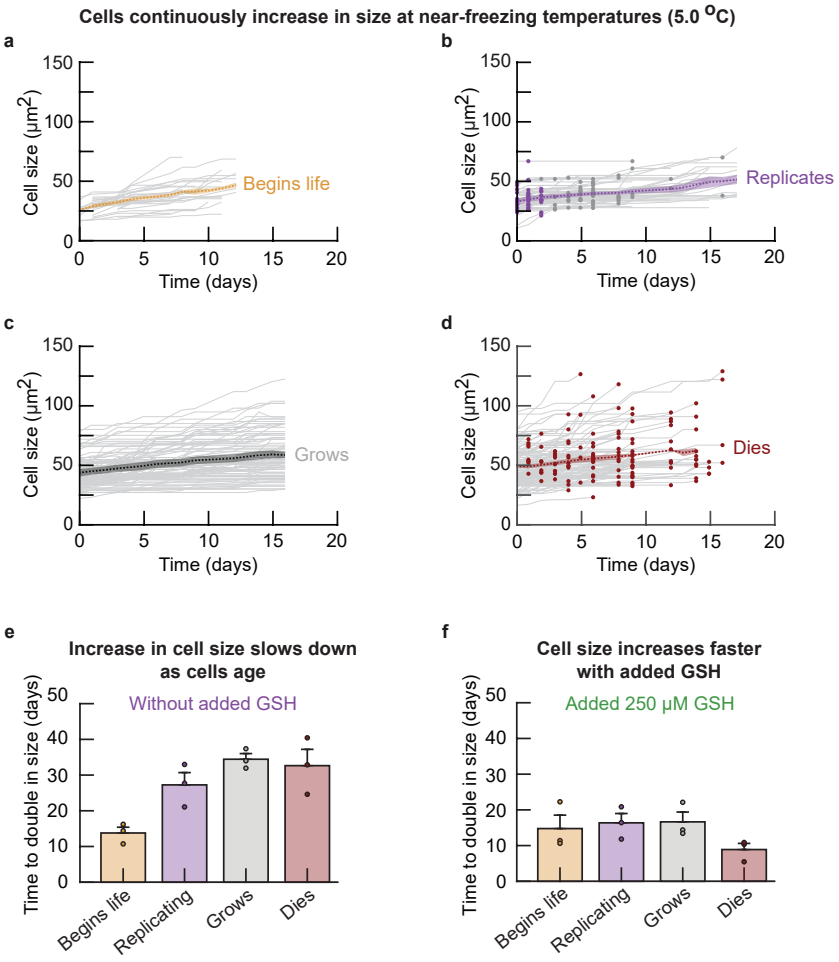

Figure S3.20: Cell size monotonically increases during all live events at 5 °C (Related to Figure 3.3c). Our data shows that the cell size monotonically increases at 5.0 °C starting with the smallest cell size at birth and ending with the largest cell size at death (including during cell replications, Supplementary Fig. S3.19). We used time-lapse microscopy to measure how the cell size changes over time in individual cells at 5.0 °C. **(a-d)** We used our time-lapse movies of cells in high-density populations (initially ~8,000 cells / mL) to track the cell size over time in single cells that were present at the start of the time-lapse movies. To reconstruct cell size growth throughout every stage of a cell's life at near-freezing temperatures, we categorized all cells in the first time point of our movies (day "0") into one of four classes (Supplementary Fig. S3.19): "begins life" (newborn daughter cells just after cytokinesis), "replicates" (cells that replicated), "grows" (cells that grew without replicating for the entire duration of the time-lapse (~17 days,) and "dies" (cells that died). We assumed that the cells in the first time point of the movies were representative samples of populations at 5.0 °C, because the populations that we imaged were pre-incubated at 5.0 °C for two weeks before the first frame of the time-lapse. As an exception, since we did not know which cells were newborn cells when the time-lapse began, we used daughter cells that were newly born within a three-day period of our time-lapse movies. Shown here is the cell size over time for cells in each event, with newborn cells **(a)**, cells that replicated (i.e., when their bud began to grow) **(b)**, cells that grew without replicating **(c)**, and cells that died (almost always by bursting open **(d)**. Grey curves show the cell size over time for individual cells. Purple and grey dots in (b) indicate the time points at which bud formation (purple dots) and cytokinesis (grey dots) occurred respectively. ***(caption continues on the next page)***

Figure S3.20 ***(caption continued from the previous page)*****:** Red dots in (d) indicate the cell size just before death. The dotted curves show the average size of cells each respective event for $n = 3$ biological replicates, and the shaded area represents the s.e.m. of the average cell size of each biological replicate. Together, (a-d) show that almost all cells continuously increase in size at 5.0 °C for the entire duration of the time-lapse movies. Given that a newborn cell will either eventually replicate or will grow without replicating and that every cell will eventually die, these data together show that cells continuously increase in their size throughout their life at 5.0 °C. **(e-f)** From the measurements in (a-d), we determined the time that cells take to double in size without added GSH **(e)** and with 250 μM added GSH **(f)**. Shown here is the time taken to double in size for cells right after cytokinesis (yellow bars), cells that begin to replicate (purple bars), cells that grow without replicating (grey bars), and cells just before they die (red bars). These measurements show that, without added GSH, cells take increasingly more time to double in size. This time is the shortest for a newborn cells (13.8 ± 1.6 days) and increases in the following order: cells that start to replicate (27.3 ± 3.4 days), cells that are growing without replicating (34.4 ± 1.6 days), and cells that are about to die (32.6 ± 4.6 days). In contrast, with added GSH, cells take approximately constant time to double in size for newborn cells (14.8 ± 3.8 days), cells that begin to replicate (16.4 ± 2.6 days), and cells that are growing without replicating (16.6 ± 2.8 days). Lastly, cells that die take the shortest time to double in size with 250 μM added GSH (8.9 ± 1.7 days). Dots show the average time for each biological replicate. Error bars show the mean with s.e.m. of $n = 3$ biological replicates. Together, (e-f) show that cells double in size more slowly as they (chronologically) age, and that adding GSH accelerates cell growth.

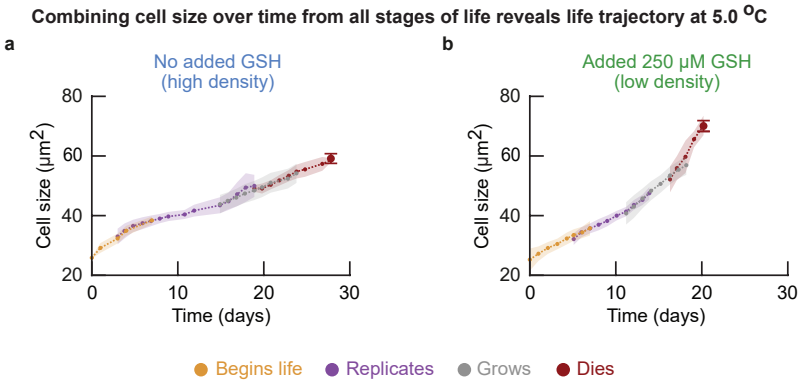

Figure S3.21: Continuous cell size growth during all life events reveals "life trajectory" of cells at 5 °C (Related to Figure 3.3d). We have now established that cells continuously increase in size throughout each life event at 5.0 °C (Supplementary Fig. S3.20). We also found that the cell size increases with consecutive life events (cells in "begins life" are smaller than cells in "replicates", followed by cells in "grows" and "dies", Supplementary Fig. S3.19). Moreover, since a newborn cell will either eventually replicate or will grow without replicating, and that every cell will eventually die, there exists a temporal order to these life events. We therefore used the cell size over time for each event to reconstruct the life of cells at 5.0 °C as function of cell size, by stitching together the cell size curves for each of the consecutive events based on the order of the average cell size (Supplementary Fig. S3.19): "begins life", "replicates", "grows" and "dies". Specifically, we connected each of the curves with its preceding curve at the time that the cell size at the respective endpoints overlapped most. Shown here are the stitched curves for populations of cells that were incubated without added GSH **(a)** and with 250 µM added GSH **(b)**. Each curve overlaps with at least three data points with neighboring curves. The colors of each curve indicates the separate life events, showing a cell that begins life (yellow curve), replicates (purple curve), grows without replicating (grey curve), and dies (red curve). Large red dot shows average cell size just before cell death. Dots show the mean cell size, with shaded areas representing the s.e.m. of $n = 3$ biological replicates.

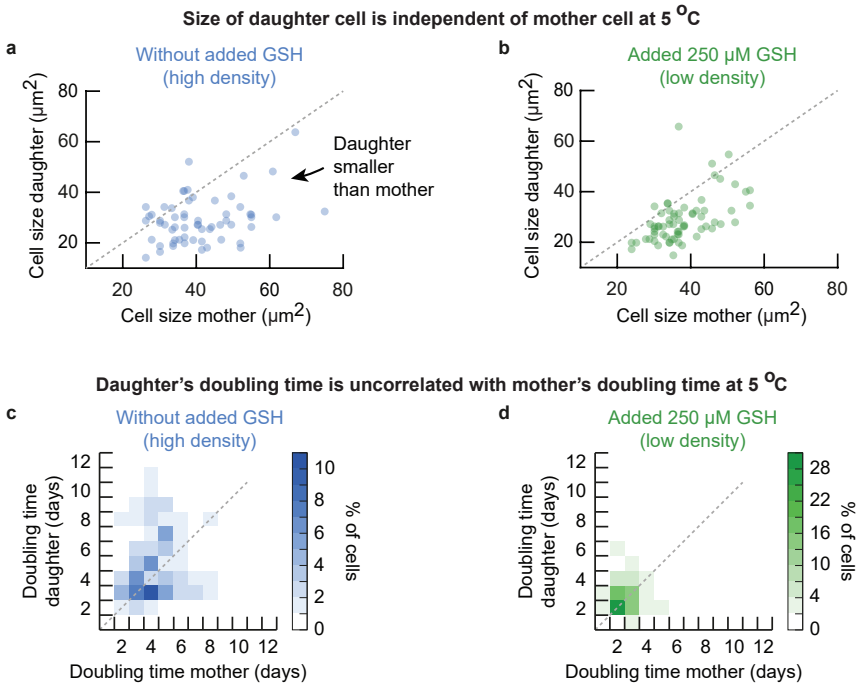

Figure S3.22: The size and doubling time of a newborn daughter cell are uncorrelated with its mother at 5 °C (Related to Figure 3.3d). Measuring how the cell size and doubling time of newborn cells depend on the size and doubling time of their mother cell. We grew populations of wild-type cells for two weeks at 5.0 °C and then began making time-lapse movies of these cells with our wide-field microscope (Methods 3.4). From these movies, we determined the cell size and doubling time of each mother-daughter pair. **(a-b)** Size of newborn daughter cells (directly after cytokinesis) compared to the cell size of the mother cell at the time she began to give birth to the daughter (i.e., when her bud started growing). Shown here are cells from populations without added GSH **(a)** or with 250 μM added GSH **(b)**. Grey diagonal line indicates locations where the mother and her newborn daughter having the same size. These graphs (a-b) show that the size of daughter cells poorly correlates with the size of their mother cells regardless of the presence of extracellular GSH. Moreover, newly born daughter cells are smaller than their mother cells as seen by the data points mostly lying below the diagonal line. **(c-d)** Doubling time of daughter cells as a function of the doubling time of their mothers in populations without added GSH **(c)** or with 250 μM of added GSH **(d)**. Heatmaps show doubling times binned into 1-day intervals. Data from the same time-lapse movies as in (a-b). Grey diagonal line indicates locations where the mother and daughter cells have the same doubling times. The doubling times of mother and daughter cells are poorly correlated. Without added GSH the doubling time of the daughter cell varies widely from two to over ten days, whereas the doubling time of mother and daughter cells are preserved at ~2.5 days with 250 μM added GSH. Together, (a-d) show that both the cell size and doubling time of a mother cell are unrelated to the cell size and doubling time of its daughter cell, with the daughter cell usually being smaller than the mother cell (also see Supplementary Fig. S3.19). These results show that the size and doubling time of the daughter cell does not depend on the traits of her mother. All panels show data aggregated from $n = 3$ biological replicates.

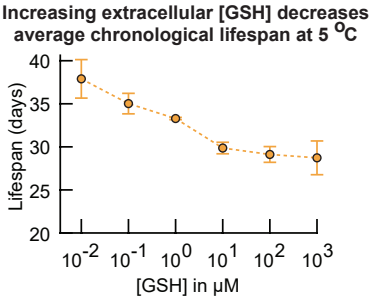

Figure S3.23: Average chronological lifespan decreases as the added GSH concentration increases at 5 °C (Related to Figure 3.3d). Cell's average chronological lifespan (average chronological age at death) as a function of added extracellular GSH concentration. We incubated wild-type cell populations at 5.0 °C with various amounts of GSH added to the growth medium (all initially at ~5,680 cells / mL). We took an aliquot of each liquid culture every week and measured the number of alive and dead cells using propidium iodide (Methods 3.4). We then fitted these measurements to the same growth model as before to determine the average chronological lifespan of cells (Supplementary Fig. S3.5; Supplementary Theory S3.6). The average chronological lifespan of cells at 5.0 °C decreases from ~37 days without added GSH to ~30 days with 100 μM added extracellular GSH. Extracellular GSH therefore decreases the chronological lifespan of cells at near-freezing temperatures. Error bars represent the mean with s.e.m., having $n = 4$ biological replicates per data point.

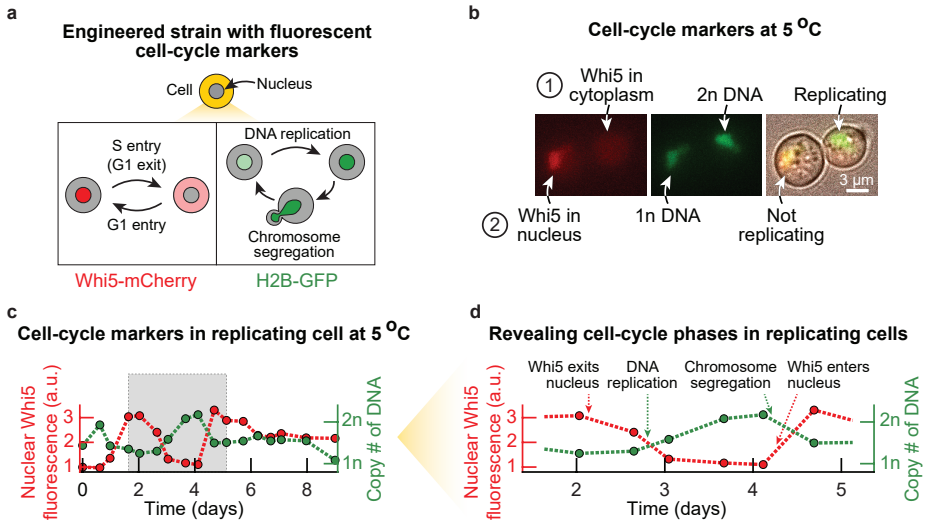

Figure S3.24: Time-lapse microscopy on engineered cells with fluorescent reporters for DNA replication (H2B histone fused to GFP) and G1-to-S transition (Whi5 protein fused to mCherry) reveals cell-cycle phases at 5 °C (Related to Figure 3.4). (a) Schematic of the engineered strain used for identifying when key cell-cycle phases occur in single cells at 5.0 °C. We engineered yeast to have the G1 transcriptional repressor Whi5 protein fused to mCherry protein (Whi5-mCherry), and the histone protein, H2B (Htb2), fused to GFP (H2B-GFP) (Methods 3.4). Both Whi5 and H2B are well-known cell-cycle markers that indicate G1 phase (Whi5 translocates to the nucleus [70, 73–76, 125]) and the S-G2-M phases (the amount of H2B is proportional to the amount of DNA [70–72]) respectively. We used this engineered strain to track the cell cycle at 5.0 °C. **(b)** Microscopy snapshots of the engineered strain. Fluorescence of Whi5-mCherry (red, left image) and H2B-GFP (green, middle) are shown for two representative cells at 5.0 °C. Also shown is the composite image that includes the brightfield image (right). Here, one cell is replicating which we can tell, aside from the brightfield image, by finding almost all of the Whi5-mCherry in the cytoplasm and a bright nucleus with H2B-GFP (contains 2n DNA, labelled "1" in the top row). In the same picture, we see that the other cell is not dividing, which we can also tell by finding almost all the Whi5-mCherry to be localized in the nucleus and a dim nucleus with H2B-GFP (contains 1n DNA, labelled cell "2" in the bottom row). The dividing cell has a bud. Scale bar is 3 μm. **(c)** Nuclear Whi5-mCherry and H2B-GFP over time shown for a replicating cell at 5.0 °C. This cell is from a population that was pre-incubated for two weeks at 5.0 °C before starting the time-lapse, after which we tracked cells in these populations with a microscope (initially at ~6,250 cells / mL). We took aliquots of our liquid cultures that we transferred to an imaging plate. We then kept this plate at 5.0 °C and imaged the cells every ~12 hours (Methods 3.4. Finally, we used this microscopy time-lapse to quantify the amount of nuclear Whi5-mCherry (left y-axis, red) and H2B-GFP (righ y-axis, green) over time. The grey area indicates a full cell-cycle, starting in G1 (Whi5-mCherry located in the nucleus). Specifically, we used the fluorescence of H2B-GFP to locate the nucleus and quantify the amount of DNA in the cells. We first located the nucleus by segmenting the GFP fluorescence of each cell using a threshold GFP fluorescence that we kept fixed for all cells and all time points when analysing this engineered strain. The nucleus was then the group of pixels whose fluorescences exceeded this threshold. To determine the copy number of DNA in a cell, we determined the total GFP fluorescence within the cell's nucleus. We subsequently rescaled the nuclear GFP between the average minimum and maximum GFP fluorescence that we observed for replicating cells. Thus, the amount of nuclear H2B was rescaled to a scale between "1n DNA" (average GFP fluorescence in the nucleus of replicating cells in G1) and "2n DNA" (average GFP fluorescence in the nucleus of replicating cells in G2). Finally, we used the fluorescence of Whi5-mCherry to quantify the relative amount of nuclear Whi5. To do so, we determined the average mCherry fluorescence in the nucleus and cytoplasm of each cell. The amount of nuclear Whi5 was then given by the ratio of measured nuclear and cytoplasmic mCherry fluorescence. **(d)** Nuclear Whi5 and H2B mark the cell-cycle phases of replicating cells. Shown is a cell during one cell cycle (from the grey box of the replicating cell in (c)). Dotted arrows indicate the end of G1 (Whi5-mCherry exits the nucleus), the S phase (the amount of H2B-GFP increases during replication of DNA), the M phase (H2B-GFP decreases during chromosome segregation) and the start of G1 (Whi5-mCherry begins to enter the nucleus).

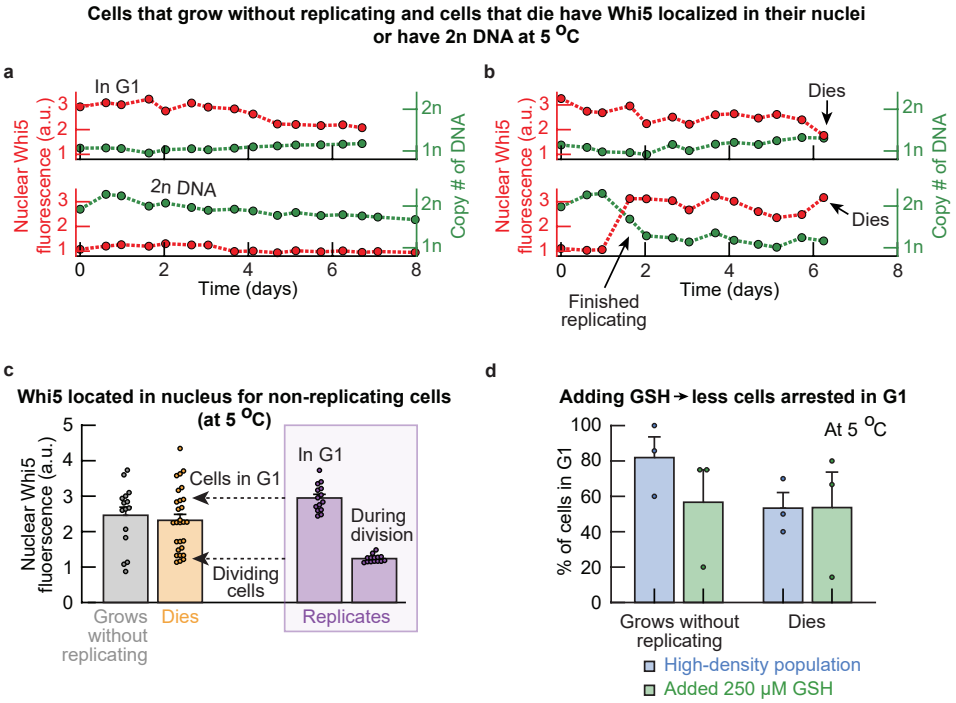

Figure S3.25: Growing cells that never replicate until dying are arrested in G1 phase at 5 °C (Related to Figure 3.4c). (a-b) Nuclear Whi5-mCherry and H2B-GFP over time in cells that grow without replicating and in dying cells at 5.0 °C (also see Supplementary Fig. S3.24). Shown are cells that did not replicate and stayed in G1 or G2 phase **(a)**, and cells just before they die **(b)**. The amount of nuclear Whi5-mCherry and the amount of DNA remained constant during many days of incubation in the cells that did not replicate. **(c)** Cells that grow without replicating and cells that die often have Whi5 located in the nucleus. Shown is the average amount of nuclear Whi5-mCherry in cells that grew without replicating (grey bar), in cells that died (orange bar) and for cells that replicated (purple box) when in G1 phase (left purple bar) or during cell division (S-G2-M phases, right purple bar). The data suggests that most cells that grow without replicating stay in G1 (their Whi5-mCherry always stays in the nucleus, in contrast to the cells in G1 that do replicate). The average amount of nuclear Whi5-mCherry in cells that grew without replicating was determined by averaging the amount of nuclear Whi5-mCherry for the entire duration of the time-lapse. The average amount of nuclear Whi5-mCherry in cells that died represents the amount of nuclear Whi5-mCherry averaged over the last three frames (~36 hours) before the cell dies. The average amount of nuclear Whi5-mCherry for cells that replicated and were in G1 and for cells that were dividing, were determined as follows: we determined when Whi5-mCherry was located in the cytoplasm or the nucleus. We then averaged the amount of nuclear Whi5-mCherry for each cell while the cell is either in G1 or S-G2-M. Dots show raw data ($n = 14$ replicating cells, $n = 15$ growing, non-replicating cells, and $n = 28$ dying cells). Bars show the mean with s.e.m. of all cells. **(d)** Cells that grow without replicating and cells that die mostly remain in G1. Shown here are the percentages of cells in G1 phase in growing populations of high-density (blue bars) and low-density populations supplemented with 250 μM GSH (green bars). This plot shows that at least 60% of non-replicating cells remained in G1 until they die. Extracellular GSH decreased the percentage of cells that remained in G1. Whether a cell is in G1 or not was determined with the average amount of nuclear Whi5-mCherry (in (c)) and the amount of DNA in the cell (a cell was in G1 when the amount of nuclear Whi5-mCherry was above 1.66 and when the amount of DNA was below 2n). Bars show the mean with s.e.m., having $n = 3$ biological replicates per condition. Dots show average percentage in each replicate.

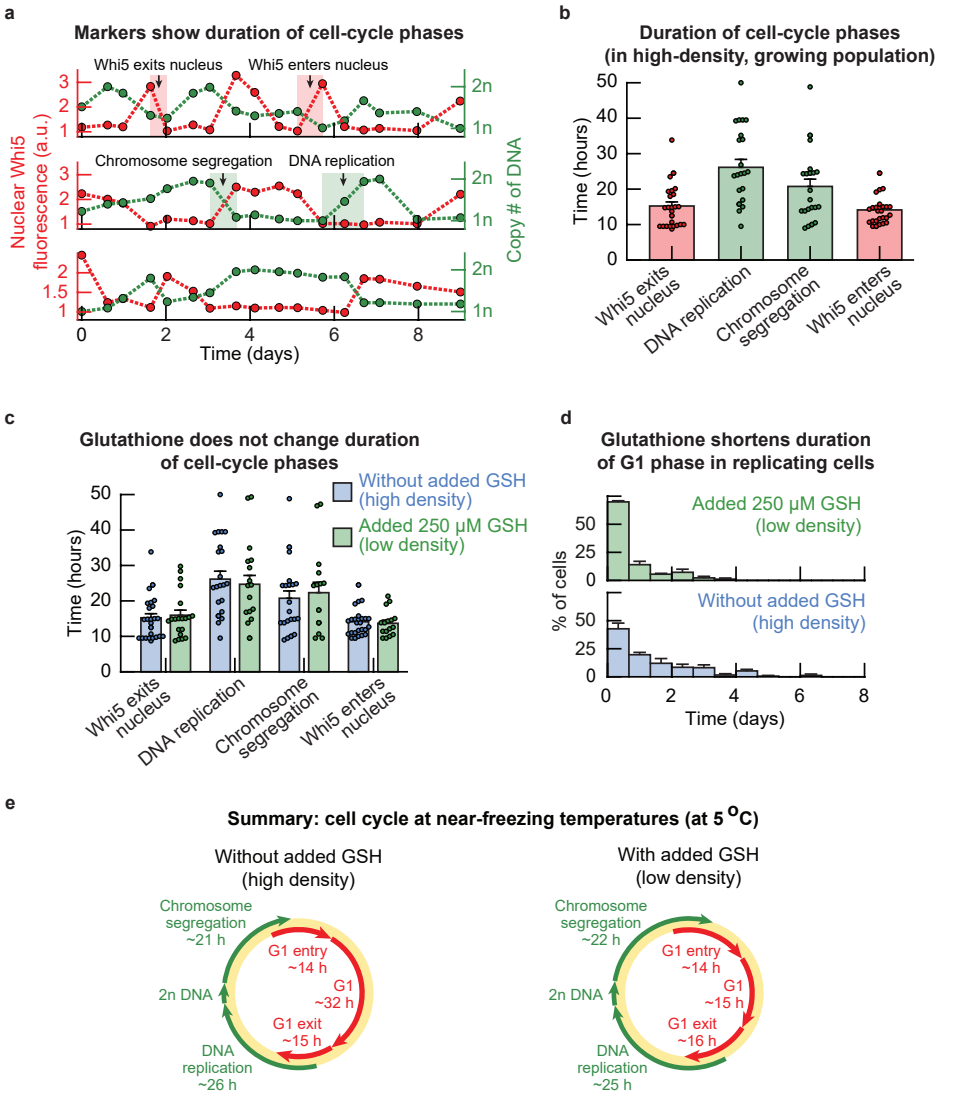

Figure S3.26: Glutathione shortens duration of G1 phase, but not S-G2-M phases, at 5 °C (Related to Figure 3.4c-d). **(a)** Nuclear Whi5-mCherry and H2B-GFP over time in replicating cells that were incubated at 5.0 °C (Supplementary Fig. S3.24). Red shaded areas indicate examples of the duration of Whi5-mCherry exiting or entering the nucleus. Green shaded areas indicate examples of the duration of DNA replication or chromosome segregation. **(b)** Using time-lapse movies that examined the amounts of Whi5-mCherry and H2B-GFP in single cells, we determined the duration of cell-cycle events in replicating cells from high-density, growing populations (following the methodology in (a)). Shown here are the durations of Whi5-mCherry exiting the nucleus (15.2 ± 1.1 hours, red bar), DNA replication (26.1 ± 2.2 hours, green bar), chromosome segregation (20.8 ± 2.1 hours, green bar), and Whi5-mCherry entering the nucleus (14.1 ± 0.8 hours, red bar). Since the time-lapse movies consists of snapshots taken every ~12 hours, this ~12 hours is a lower bound on the true duration of each event. Dots show raw data pooled from $n = 3$ biological replicates, having $n = 28$ cells for the location of Whi5-mCherry, $n = 23$ cells with DNA replication and $n = 24$ cells with DNA segregation. Bars show the mean with s.e.m. of all cells. ***(caption continues on the next page)***

Figure S3.26 ***(caption continued from the previous page)*****: (c)** Duration of cell-cycle events in cells from low-density populations that were incubated with 250 μM of GSH (green bars). Blue bars show the same data as in (b) as a comparison. Shown here are, all with the added GSH, Whi5-mCherry exiting the nucleus (16.0 ± 1.4 hours), DNA replication (24.7 ± 2.5 hours), chromosome segregation (22.3 ± 2.9 hours), and Whi5-mCherry entering the nucleus (13.7 ± 0.9 hours). There is no reason to assume that the duration of any cell-cycle event changes upon addition of extracellular GSH (p-values are 0.69 for Whi5-mCherry exiting the nucleus, 0.69 for DNA replication, 0.66 for chromosome segregation and 0.72 for Whi5-mCherry entering the nucleus). Blue dots are as in (b). Green dots show raw data from $n = 3$ biological replicates, having $n = 16$ cells for Whi5-mCherry entry and $n = 20$ cells for Whi5-mCherry exit of the nucleus, $n = 17$ cells with DNA replication and $n = 16$ cells with DNA segregation. Bars show the mean with s.e.m. of all cells. **(d)** Histograms showing the durations of G1 phase in replicating cells from populations without added GSH (blue) and with 250 μM added GSH (green). The average duration of G1 was 32 ± 3.0 hours without added GSH, and 15.0 ± 1.5 hours with added GSH (median ~24 hours without added GSH and ~9 hours with added GSH). Thus, GSH shortens the duration of G1 in replicating cells at near-freezing temperatures. With added GSH, the majority of G1 phases in replicating cells take 12 hours or less. In contrast, without added GSH, the G1 phase in replicating cells takes up to 6 days. Error bar shows mean with s.e.m. of $n = 3$ biological replicates. **(e)** Summarizing (b-d). Shown are the durations of the cell-cycle phases in replicating cells from populations without added GSH (left) and with added GSH (right). The length of the arrows is proportional to the duration of each phase. Red arrows represent Whi5 (indicating events associated to G1), green arrows represent H2B (indicating events associated to S-G2-M). Together, (b-d) show that adding GSH to the growth medium shortens the duration of G1 in replicating cells, while the duration of other cell-cycle remains unchanged upon addition of GSH.

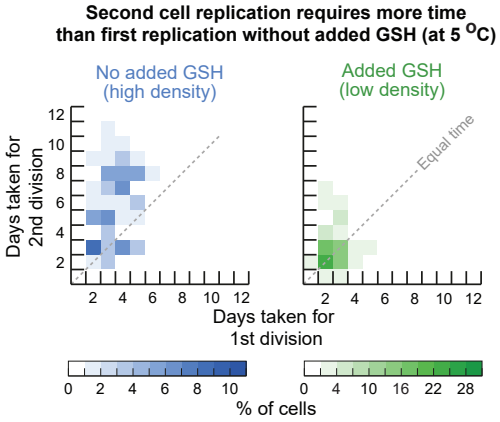

Figure S3.27: Consecutive divisions in individual cells slow down at 5 °C (Related to Figure 3.4d). We used single-cell time-lapse movies at 5.0 °C (Supplementary Fig. S3.13) to measure the doubling time of cells that replicated multiple times. Heatmaps show the durations of consecutive replications of individual cells at 5.0 °C without added GSH (blue heatmap, left) and with 250 µM added GSH (green heatmap, right). Shown is the number of days taken for a cell replication (y-axis) as function of the number of days taken for the preceding cell replication (x-axis) of each cell. Grey dotted diagonal indicates location where consecutive replications in the same cell have equal doubling times. Data is aggregated from $n = 3$ biological replicates. These measurements show that the doubling time of individual cells increases over time in populations without added GSH: the duration of a cell replication is on average larger (above the diagonal) than the duration of a preceding cell replication. With added GSH, the doubling time remains approximately constant for consecutive replications.

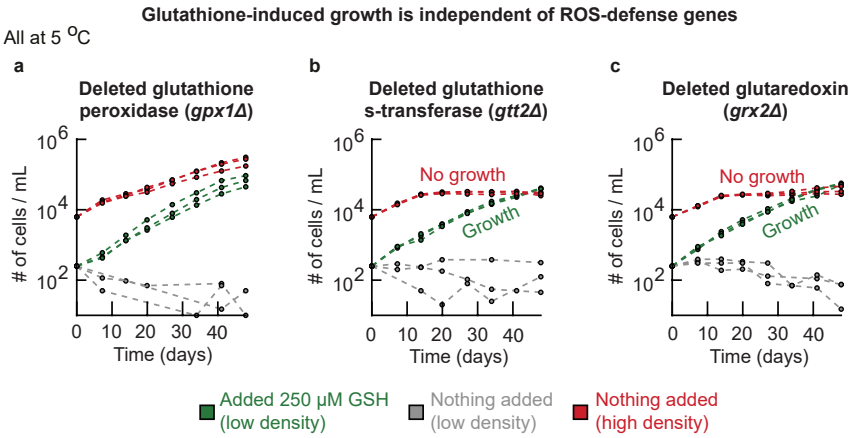

Figure S3.28: Glutathione induces population growth at 5 °C independent of ROS-defense genes (Related to Figure 3.4e). All at 5.0 °C. **(a-c)** We constructed mutants that are each lacking a gene ("ROS defense" gene) which protects the cells from oxidative stress, maintains redox state, and work with glutathione [8, 11, 14, 39]. Specifically, one strain lacks *GPX1* which encodes a glutathione peroxidase (*gpx1*Δ strain). Another strain lacks *GTT2* which encodes a glutathione s-transferase (*gtt2*Δ strain). Another strain lacks *GRX2* which encodes a glutaredoxin (*grx2*Δ strain). Shown here are the population densities over time for the *gpx1*Δ strain **(a)**, the *gtt2*Δ strain **(b)**, and the *grx2*Δ strain **(c)**. Populations of each strain started with high density (~6,250 cells / mL, red curves), low density (~250 cells / mL, grey curves), or low density with 250 μM added GSH (~250 cells / mL, green curves). Every mutant population with the added extracellular GSH grew. Surprisingly, the high-density populations of the *gtt2*Δ and *grx2*Δ strains did not sustain growth at 5.0 °C beyond an initial, transient growth of ~10 that was due to the cells being transferred from 30 °C. In contrast, at the same high density, populations of the wild type (Fig. 3.1) and the *gpx1*Δ strain grew to the carrying capacity. Hence, *GTT2* and *GRX2* are necessary for sustaining population growth at 5.0 °C, while *GPX1* is not required. Finally, both *GTT2* and *GRX2* can be substituted with reduced extracellular GSH at 5.0 °C because every population with the added extracellular GSH grew. All colors for each strain show $n = 3$ biological replicates.

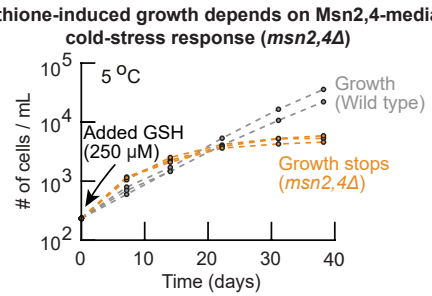

Figure S3.29: Glutathione-induced growth at near-freezing temperatures depends on Msn2,4-mediate cold-stress response (Related to Figure 3.4e). We constructed a mutant strain that lacks the major stress-response transcriptional activators, Msn2,4 (*msn2,4*Δ strain) [80–82]. Shown here is the population density over time for the *msn2,4*Δ strain at 5.0 °C with 250 μM added GSH (orange curves, initially ~250 cells / mL). Grey curves show the wild-type strain for comparison (initially ~250 cells / mL with 250 μM added GSH). The *msn2,4*Δ strain stops growing after two weeks of incubation with added GSH at 5.0 °C, whereas the wild-type strain grows exponentially over time. We already established that GSH removes intracellular ROS and thereby induces the wild-type population to grow (Fig. 3.2c). However, the *msn2,4*Δ population stops growing at 5.0 °C even with the added GSH. This means that yeasts incubated with extracellular GSH still experience a low-temperature stress, despite the added GSH reducing the intracellular ROS that inhibits cell replications. Together, our results suggest that glutathione-induced population growth at 5.0 °C depends on the Msn2,4 cold-stress response. All colors show $n = 3$ biological replicates.

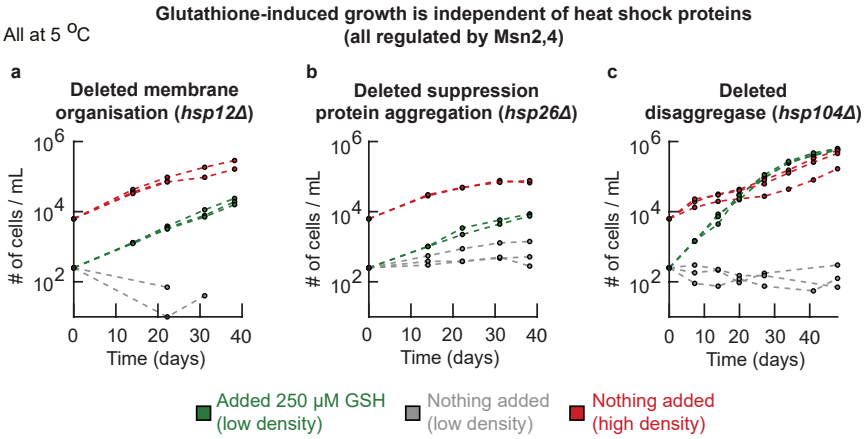

Figure S3.30: Msn2,4-regulated heat-shock proteins are not necessary for growth at 5 °C (Related to Figure 3.4e). All at 5.0 °C. **(a-c)** We constructed mutants that were lacking genes ("heat shock" genes) which are regulated by the Msn2,4 stress-response and highly expressed at low temperatures [11, 17, 39, 84, 85]. Specifically, one mutant strain lacks *HSP12* which encodes a membrane protein that helps in maintaining membrane organization (*hsp12*Δ strain). Another strain lacks *HSP26* which encodes a chaperone protein that suppresses aggregation of unfolded proteins (*hsp26*Δ strain). Another strain lacks *HSP104* which encodes a disaggregase (*hsp104*Δ strain). Shown here are the population densities over time for the *hsp12*Δ strain **(a)**, the *hsp26*Δ strain **(b)**, and the *hsp104*Δ strain **(c)**. Populations of each strain started with either a high density (~6,250 cells / mL, red curves), low density (~250 cells / mL, grey curves), or a low density with 250 μM added GSH (green curves). Every high-density population grew for all heat shock mutants. Similarly, all populations with added extracellular GSH grew, with the *hsp104*Δ strain growing fastest and the *hsp26*Δ strain growing slowest. These growth experiments show that not all Msn2,4-regulated genes are necessary for growth, even though the Msn2,4 stress-response is required for cell replications at near-freezing temperatures (Supplementary Fig. S3.29). Each condition in all panels shows $n = 3$ biological replicates.

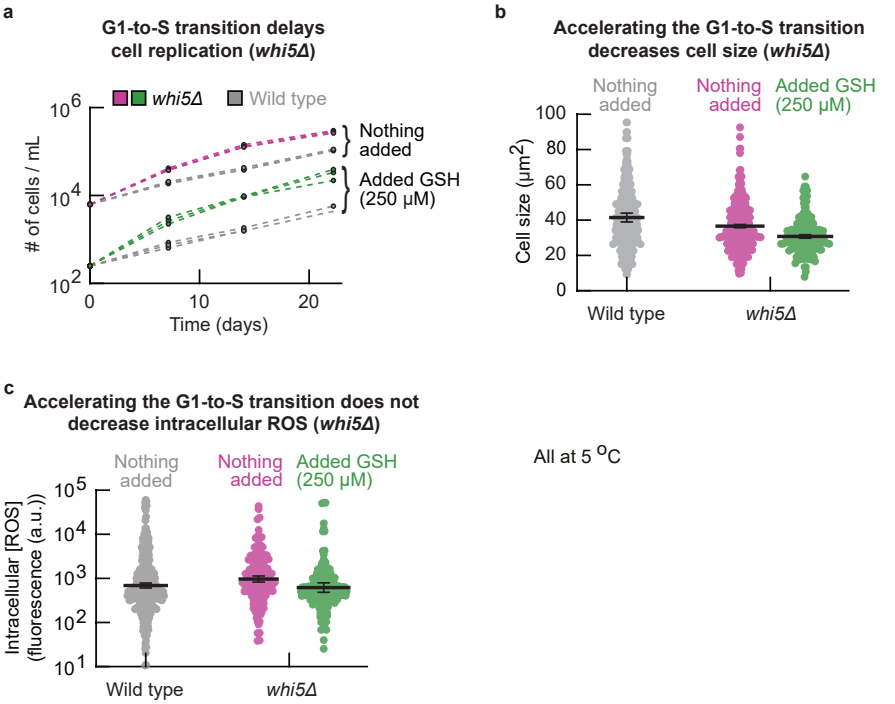

Figure S3.31: G1-to-S transition delays cell replication at 5 °C (Related to Figure 3.4e). **(a)** We constructed a mutant strain (*whi5*Δ strain) whose *WHI5* was knocked out and therefore has an accelerated G1-to-S transition at 30 °C [74]. Shown here are the population densities over time for the *whi5*Δ strain that was incubated at 5.0 °C either without added GSH (initially ~6,250 cells / mL, pink curves) or with 250 μM added GSH (initially ~250 cells / mL, green curves). Both conditions are compared with the wild-type strain (grey curves). The *whi5*Δ strain grows faster than the wild type at 5.0 °C (resulting in a 3.4 ± 0.1-fold difference in density after two weeks without added GSH, and a 5.7 ± 0.3-fold difference in density with added GSH after the same period of time). Thus, knocking out *WHI5* accelerates population growth, suggesting that the G1-to-S transition delays cell replications. Each color and initial density shows $n = 3$ replicate populations. **(b)** Cell size of the *whi5*Δ strain. Shown here are the cell sizes of the *whi5*Δ strain in populations without added GSH (pink dots) or with 250 added μM GSH (green dots). Wild-type strain without added GSH is shown as a comparison (grey). Cell sizes were measured after two weeks of incubation at 5.0 °C. The *whi5*Δ strain has a smaller average cell size compared to the wild type, with adding extracellular GSH reducing the cell size further. This suggests that accelerating the G1-to-S transition decreases the cell size at 5.0 °C (cells spend less time in the G1 (growth) phase). Error bars show mean with s.e.m., having $n = 3$ biological replicates. **(c)** Intracellular ROS concentration in the *whi5*Δ strain after two weeks of incubation at 5.0 °C (Methods 3.4). Shown here are populations that were incubated either without added GSH (pink dots) or with 250 μM added GSH (green dots). Grey dots show the wild type without added GSH as a comparison. The *whi5*Δ strain does not have less intracellular ROS compared to the wild-type strain. Error bars show mean with s.e.m., having $n = 3$ biological replicates. Together, (a-c) show that accelerating the G1-to-S transition at 5.0 °C accelerates cell replication and decreases cell size. Researchers found similar effects at 30.0 °C [74, 126]. Simultaneously, accelerating the G1-to-S transition does not decrease intracellular ROS abundance. This suggests that enabling the G1-to-S transition (G1 exit) with abundant ROS enables cell replication. Moreover, these measurements suggest that cells do not accumulate intracellular ROS during G1, since shortening the G1 duration does not decrease the intracellular ROS concentration.

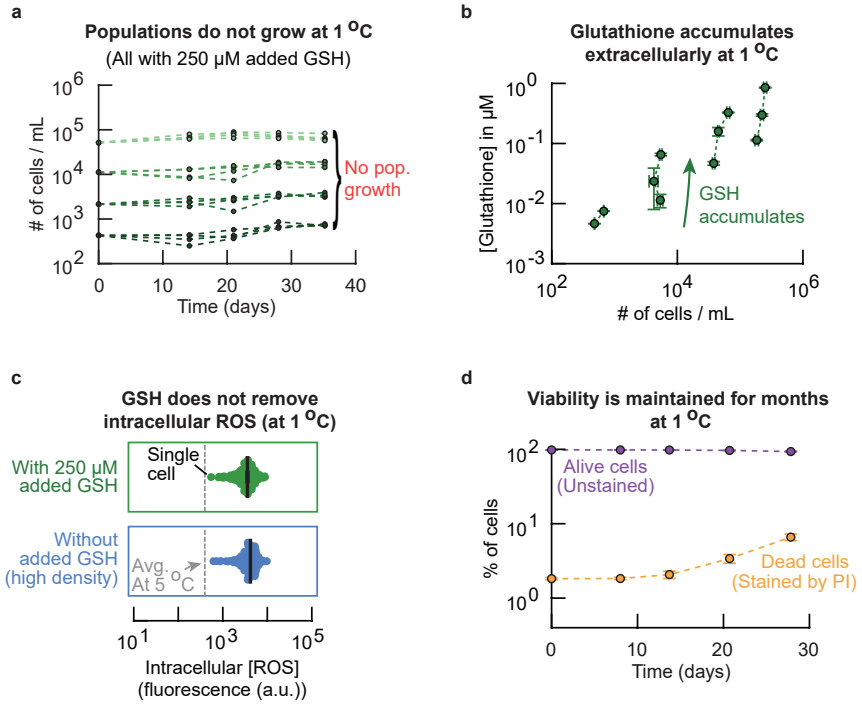

Figure S3.32: Glutathione still accumulates but does not remove intracellular ROS at 1 °C (Related to Figure 3.5). (a-c) Measuring population behavior of wild-type yeast at 1 °C. **(a)** Population-density over time for populations that were incubated with 250 μM added GSH at 1.0 °C. Colors show different initial population densities (highest density ~52,000 cells / mL, with 5-fold dilutions to lower densities). None of the populations increase appreciable in density (e.g., 10-fold) during the month long incubation. Thus, populations do not grow at 1.0 °C even with GSH added to the growth medium (also compare with Fig. 3.2c). Each color has $n = 4$ replicate populations. **(b)** We quantified the extracellular glutathione concentration for wild-type populations with an enzymatic assay kit (Methods 3.4). Shown are the concentrations of total extracellular glutathione as function of population-density after 1, 3 and 5 weeks of incubation at 1.0 °C (also see Fig. 3.2a). No glutathione was added to the growth medium (highest initial density ~156,000 cells / mL, with 5-fold serial dilutions for lower density populations). Green arrow indicates direction of time. The extracellular glutathione concentration increases over time for all populations. These measurements show that cells secrete and accumulate extracellular glutathione at 1.0 °C despite cell populations not growing (see (a)). Error bars are mean with s.e.m., having $n = 3$ biological replicates per data point. **(c)** Intracellular ROS concentration of individual cells as quantified by fluorescence of a oxidation-responsive dye for superoxides in mitochondria (Methods 3.4, also see Fig. 3.2b). Cells were stained after two weeks of incubation at 1.0 °C. Shown are intracellular ROS concentrations for individual cells from high-density populations (blue dots, initially ~30,000 cells / mL) and populations incubated with 250 μM GSH (green dots, initially 2,000 cells / mL). Grey dotted line indicates the average intracellular ROS concentration in growing populations at 5.0 °C (from Fig. 3.2b). In contrast to 5.0 °C, the intracellular ROS concentrations at 1.0 °C are identical between populations with and without added GSH (also compare with Fig. 3.2b-d). Thus, adding extracellular GSH does not remove intracellular ROS at 1.0 °C. Error bars show the mean with s.e.m. of the average ROS level of each biological replicate ($n = 3$). Together, (a-c) show that cells still secrete glutathione to their extracellular environment at near-freezing temperatures. However, populations do not grow at 1.0 °C even with large amounts of GSH added to the growth medium. Moreover, extracellular GSH also does not remove intracellular ROS. These results are in contrast to yeast populations incubated at 5.0 °C, where extracellular GSH does remove intracellular ROS and induces population growth. ***(caption continues on the next page)***

Figure S3.32 ***(caption continued from the previous page)*****: (d)** To test whether populations do not grow at 1.0 °C because the cells were dead, we determined the percentage of alive and dead cells over time in yeast populations incubated at 1.0 °C through a PI staining (Supplementary Fig. S3.4). Shown is the percentage of alive cells (purple points) and percentage of dead cells (orange points) for populations with a high density (initially ~156,000 cells / mL). The percentage of dead cells in the population increases over time, reaching ~10 % after 4 weeks of incubation at 1 °C. These measurements show that populations remain alive during months-long incubation at 1.0 °C. This result suggests that the reason populations do not grow at 1.0 °C is not because the cells were dead. Error bars show mean with s.e.m., with $n = 4$ replicate populations per data point.

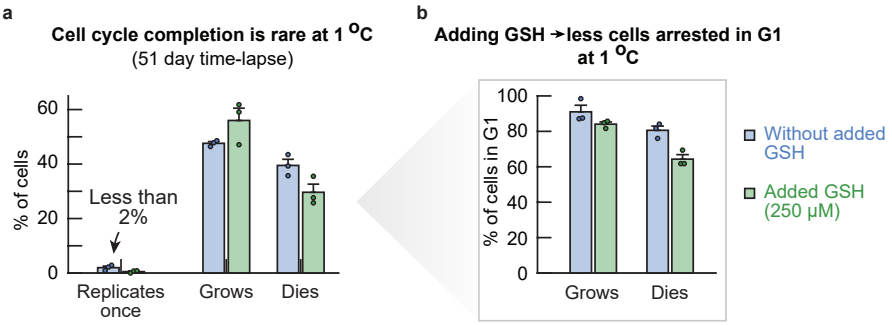

Figure S3.33: Cells are arrested in G1 and less than 2% of cells proceeds to replicate during a 51-day time-lapse at 1 °C (Related to Figure 3.5a). We incubated populations of the engineered strain with fluorescent cell-cycle markers (also see Supplementary Fig. S3.24) at 1.0 °C. After 10 days of incubation at 1.0 °C, we proceeded with tracking single cells with a microscope (initially ~30,000 cells / mL). In short, we took aliquots of the liquid cultures and transferred these to an imaging plate. We kept the plate at 1.0 °C and imaged the cells every ~4 days (Methods 3.4). **(a)** Percentage of cells that replicates, grows and dies during the 51 day microscope time-lapse at 1.0 °C. Bars show populations without added GSH (blue bars) and with 250 μM added GSH (green bars). Less than 2% of cells replicated once (no cell replicated more than once, $n = 390$ without added GSH, $n = 393$ with added GSH). **(b)** Percentages of cells that grow without replicating and cells that die while in G1 for the duration of the time-lapse. Almost all of the non-replicating cells are in G1. Similar to our measurements at 5.0 °C, we found that adding GSH decreases the percentage of cells that are in G1 (Supplementary Fig. S3.25).

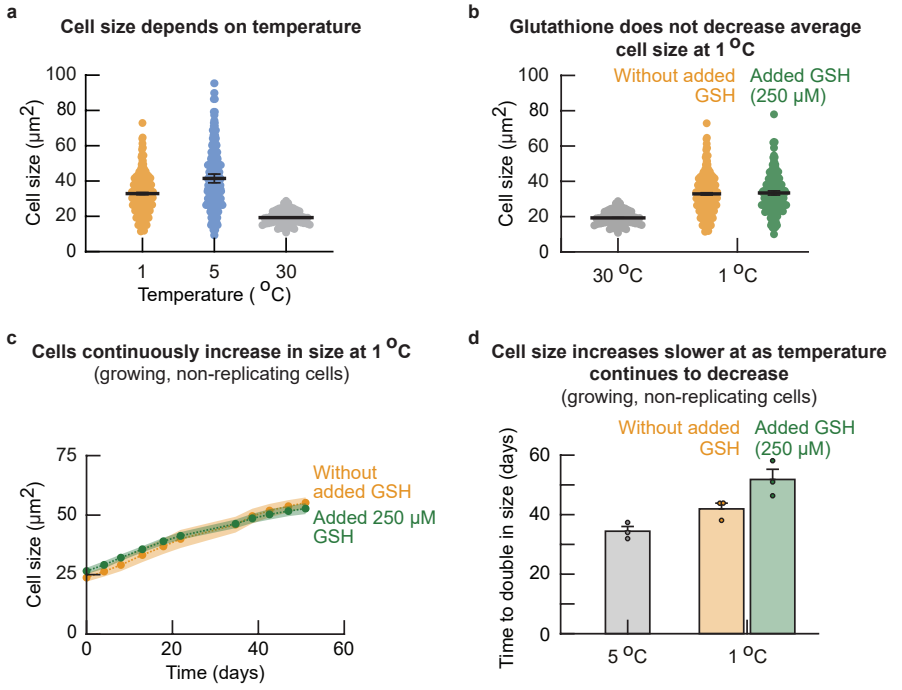

Figure S3.34: Cell size continuously increases at 1 °C, but slower than at 5 °C (Related to Figure 3.5a). (a) Cell size as function of temperature. We incubated wild-type cell populations for two weeks at 1.0 °C and then measured the cell sizes with a wide-field microscope. Shown here are the cell sizes (cross-sectional area) of individual cells from high-density populations without any added GSH at 1.0 °C (orange dots, initially ~30,000 cells / mL) and at 5.0 °C (blue dots; Supplementary Fig. S3.19). Grey dots show cells in a log-phase growth at 30.0 °C as a comparison. We find that cells at 1.0 °C are smaller in size compared to cells at 5.0 °C, but still larger in size than cells at 30.0 °C. **(b)** We also measured the cell sizes of individual cells with 250 μM added GSH after two weeks of incubation at 1.0 °C. Shown are the cell sizes of individual cells at 1.0 °C from high-density populations without any added GSH (orange dots, see (a)) and of cells from high-density populations with 250 μM added GSH (green dots). Data from 30 °C is as in (a). Here we find that cells are on average the same size with and without added GSH. This is in contrast with 5.0 °C where adding GSH decreases the average cell size. In (a-b), the error bars represent the mean with s.e.m., having $n = 3$ biological replicates. Dots show data aggregated from the biological replicates. **(c)** We used our time-lapse movies of cells in 1.0 °C to track the cell size over time for individual cells that were present at the start of the time-lapse movies (also see Supplementary Fig. S3.20). Shown here is the cell size over time for cells that did not replicate for the entire duration of the time-lapse (~50 days). Cells were from populations that were incubated without added GSH (orange curve) or with 250 μM added GSH (green curve). All populations that we imaged were pre-incubated for two weeks at 1.0 °Cbefore the first frame of the time-lapse movies. The cell size continuously increases during the entire ~50 day time-lapse. Dots show the mean with shaded representing the s.e.m., having $n = 3$ biological replicates per condition (at least $n = 16$ cells per replicate). **(d)** From the measurements in (c), we determined the time that cells take to double in size. Shown here are the time taken to double in size for cells that grow without replicating at 1.0 °C, either without added GSH (orange bar) or with 250 μM added GSH (green bar). Grey bar shows the time taken to double in size for cells that grow without replicating at 5.0 °C without added GSH as a comparison (data from Supplementary Fig. S3.20). At 1.0 °C, cells take more time to double in size with added GSH (51.8 ± 3.4 days) compared to without added GSH (41.9 ± 1.9 days). Together, (a-d) show that cells continuously grow in size at 1 °C, but do so slower compared to 5 °C. Moreover, in contrast to 5 °C, GSH does not decrease the average cell size at 1 °C (also see Supplementary Figs. S3.19-S3.20).

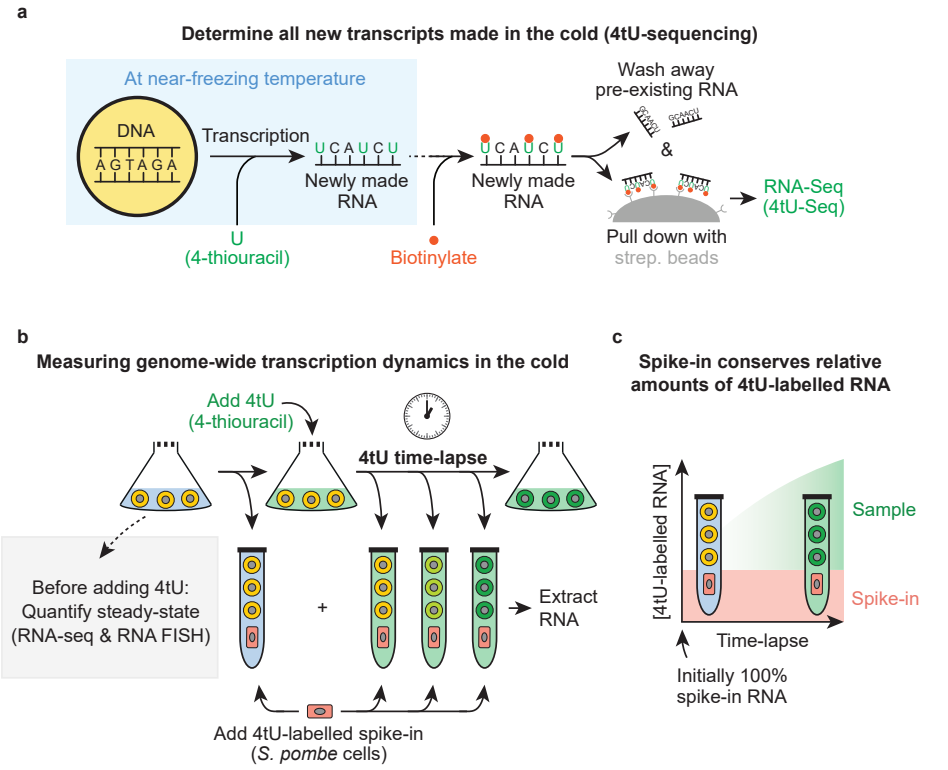

Figure S3.35: Measuring the genome-wide transcription dynamics at near-freezing temperatures (Related to Figure 3.5b). (a) Schematic demonstrating the experimental procedure for performing 4tU-sequencing on newly-made transcripts in populations of *S. cerevisiae* [89, 121, 127]. A synthetic uracil analog (4-thiouracil, 4tU) is added to the growth medium of cells. Cells incorporate the 4tU into their newly synthesized RNA. We collect cells after the desired time of incubation with 4tU and extract the total RNA. The newly synthesized RNA is linked to biotin by specifically biotinylating the 4tU ("4tU-labelled" RNA). Simultaneously, the pre-existing RNA that does not contain 4tU is not biotinylated. Finally, the 4tU-labelled RNA is separated from the pre-existing RNA without 4tU through a pull-down with magnetic beads containing streptavidin, after which the purified 4tU-labelled RNA is sequenced (see Methods 3.4 for experimental details). **(b)** Schematic illustrating the experimental procedure for measuring the genome-wide transcription dynamics at near-freezing temperatures. We incubated liquid cultures with populations of wild-type yeasts at the desired temperature (e.g., 5.0 °C). After two weeks of incubation, we first collected two aliquots of our cultures (as "time 0" hours of the time-lapse). Directly after, we supplemented the growth medium of the cultures with 4tU at a final 5 mM concentration, and collected aliquots from our cultures at the desired time-points (see 3.4 for experimental details). After collecting the time-lapse samples, we added a fixed amount of 4tU-labelled *S. pombe* (*Schizosaccharomyces pombe*) cells to all 4tU time-lapse samples as a spike-in and proceeded with RNA-extraction. Finally, we used the extra "time 0" hours aliquots to quantify the steady-state transcript levels (grey box, RNA-seq and RNA FISH). **(c)** The *S. pombe* spike-in that was added to all 4tU time-lapse samples enabled us to normalize the amount of 4tU-labelled transcripts from different time-points. Initially, all 4tU-labelled RNA in the sample is from the *S. pombe* spike-in since the cold-incubated *S. cerevisiae* cells have not initially synthesized 4tU-labelled RNA. Over time, the cold-incubated cells synthesize new 4tU-labelled RNA and degrade old (unlabelled) RNA, increasing the percentage of 4tU-labelled RNA that is from the cold-incubated cells. Normalizing with the amount of spike-in transcripts therefore ensures that the relative differences between samples in a time-lapse are conserved (since the amount of 4tU-labelled RNA from *S. pombe* cell was the same in every sample). Moreover, this procedure eliminates experimental differences between samples due processing of RNA and sequencing.

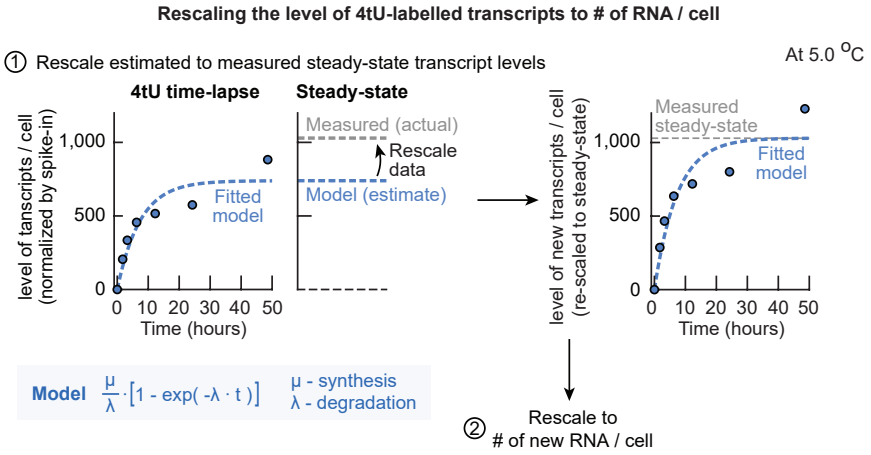

Figure S3.36: Procedure for rescaling the 4tU transcript levels using the steady-state transcript levels (Related to Figure 3.5b). First, the 4tU time-lapse samples were normalized by the transcript level of spike-in RNA and the number of alive cells in the population that we had also measured, giving the relative 4tU transcript level per cell over time (the amount of 4tU-labelled RNA normalized by the 4tU spike-in RNA). Next, these relative values are rescaled to obtain the "# of new RNA / cell". To do so, the samples are rescaled such that steady-state transcript level per cell that is estimated by the 4tU time-lapse is equal to the measured steady-state transcript level per cell that we measured through RNA-seq (Supplementary Fig. S3.35). To obtain the estimated steady-state transcript level per cell, we fitted a mathematical model to the relative 4tU transcript levels per cell over time. The conventional model to describe RNA synthesis assumes that RNA is synthesized at a constant rate and degraded at a rate that is dependent on the concentration [88, 89]. Thus, the kinetics of 4tU-labelled RNA are given by $\frac{dN}{dt} = \frac{\mu}{\lambda}\left(1 - \exp(-\lambda t)\right)$ with a RNA synthesis rate μ (in "# of RNA / cell / hour"), a RNA degradation rate λ (in "per hour") and time t. Over time, the relative 4tU transcript level per cell converges to a steady-state μ/λ (in "RNA / cell") by degradation of old RNA and synthesis of new (4tU-labelled) RNA [88, 89]. To obtain the measured steady-state transcript levels per cell we had also sequenced the steady-state transcript level (total RNA, not 4tU purified RNA) of each time-lapse together with a *S. pombe* spike-in to normalize our time-lapses across temperatures (the steady-state transcript levels can differ per temperature, and the same spike-in RNA was used for all steady-state samples). Thus, we rescaled all 4tU-samples such that the estimated steady-state transcript levels of the model matched the experimentally measured steady-state transcript levels. Shown is a representative example of such a rescaling from a 4tU time-lapse without added extracellular GSH at 5.0 °C. Note that this rescaling conserves the relative differences between all time points within each time-lapse. By applying this methodology to all time-lapses from each condition, we obtained the relative level of new transcripts (4tU-labelled RNA) over time between replicates and across temperatures. Moreover, the estimated steady-state of each time-lapse is equal to the experimentally measured steady-state of that time-lapse. As a last step, the relative levels of new transcripts per cell will be rescaled to integer number of RNA per cell using the steady-state samples and RNA FISH (Supplementary Fig. S3.37). Dots show raw (normalized) data for one replicate. Blue dotted lines shows model fit for that replicate. Grey dotted lines shows measured steady-state values.

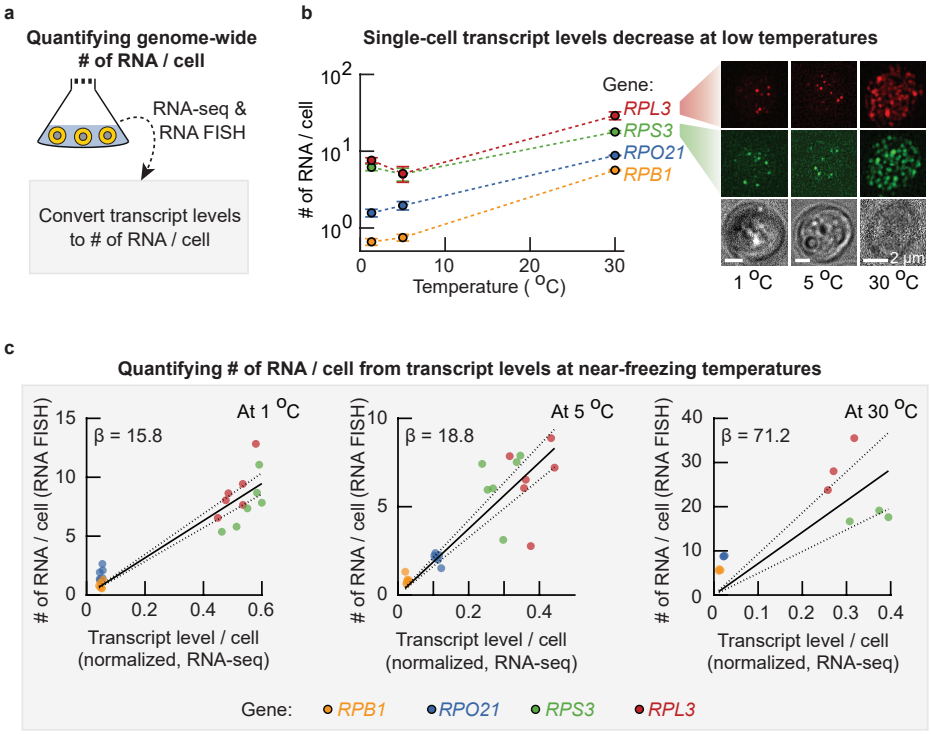

Figure S3.37: Quantifying the genome-wide number of RNA per cell from the relations between RNA-seq and RNA FISH data in steady-state (Related to Figure 3.5b). **(a)** Steady-state transcript levels were quantified in two ways. In one way, we performed regular RNA-seq on the steady-state RNA (normalized across temperatures by a spike-in of total RNA from *S. pombe*). In the other way, we quantified the number of RNA per cell for endogenous yeast genes via single-molecule RNA FISH with cells from the same aliquots on which we performed RNA-seq (Methods 3.4). These measurements were then combined to re-scale the relative transcript levels per cell (from RNA-seq) to the "# of RNA / cell" as measured by RNA FISH (Supplementary Figs. S3.35-S3.36). **(b)** The single-cell number of transcripts for several endogenous yeast genes were quantified through RNA FISH at 30 °C, 5.0 °C and 1.0 °C. Shown is the average number of RNA per cell as function of temperature for *RPL3* (red curve), *RPS3* (green curve), *RPO21* (blue curve) and *RPB1* (yellow curve). The average number of mRNA per cell decreases with temperature. Each data point shows the average of $n = 3$ biological replicates, having at least $n = 616$ cells (for *RPB1* and *RPO21*) or at least $n = 421$ cells (for *RPL3* and *RPS3*). Images show representative examples of labelled RNA in single-cells at 1.0 °C (left), 5.0 °C (middle) and 30 °C (right). Dots are labelled RNA of *RPL3* (red fluorescence, top) or *RPS3* (green fluorescence, bottom). Brightfield images are shown as a comparison. Scale bar is 2 μm. **(c)** The average number of RNA per cell from RNA FISH as a function of the relative steady-state transcript levels per cell from RNA-seq at 1.0 °C (left panel), 5.0 °C (middle panel) and 30 °C (right panel). Shown are the steady-state transcript levels for *RPB1* (yellow dots), *RPO21* (blue dots), *RPS3* (green dots) and *RPL3* (red dots). Black solid line shows a linear fit without intercept, dotted lines show 95% confidence interval of the fit. Since both RNA FISH and RNA-seq measurements were performed on the same cell populations, these linear fits yield scaling factors β that converts the relative transcript levels per cell to the "# of RNA / cell" for each temperature ($\beta = 15.8$ at 1.0 °C (Pearson-correlation coefficient $\rho = 0.94$), $\beta = 18.8$ at 5.0 °C ($\rho = 0.87$) and $\beta = 71.2$ at 30 °C ($\rho = 0.79$)). We used these scaling factors to rescale the relative level of 4tU-labelled transcripts per cell (from 4tU-seq; Supplementary Figs. S3.35-S3.36) to integer numbers of RNA per cell for all temperatures. All colors show 6 dots, having $n = 3$ biological replicates each for 250 μM added GSH and without added GSH.

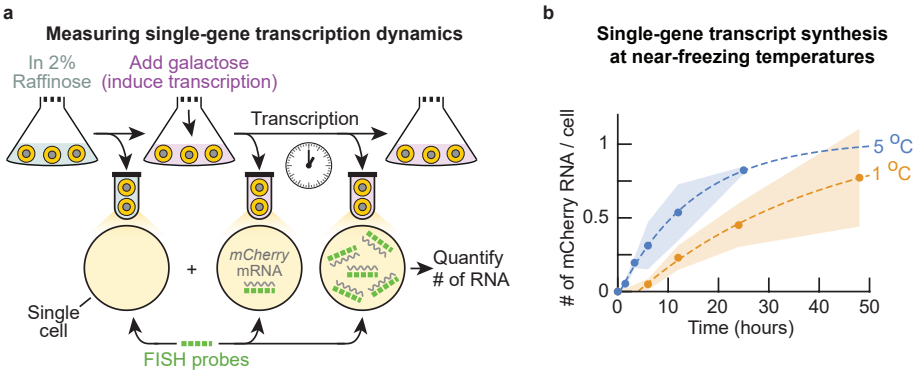

Figure S3.38: Single-gene transcription dynamics at near-freezing temperatures (Related to Figure 3.5b). We used a mCherry-inducible strain to measure the transcription dynamics for a single gene at near-freezing temperatures. **(a)** Schematic showing an experiment to measure single-gene transcription (Methods 3.4). Liquid cultures with populations of the mCherry-inducible strain were incubated at the desired temperature with 2% raffinose as the carbon source. After two weeks of incubation, we took aliquots of these liquid cultures (as a control without mCherry). Directly after, we supplemented the growth media with 2% galactose to induce the expression of mCherry, and continued to collect aliquots of these cultures at the desired time points. We then performed RNA FISH on the mCherry RNA for each aliquot, and quantified the average number of RNA per cell over time. **(b)** Single-gene transcription dynamics at near-freezing temperatures. Shown is the number of mCherry RNA per cell as function of time at 5.0 °C (blue curve) and at 1.0 °C (orange curve). Dotted line shows a model for the kinetics of RNA synthesis fitted to the average number of RNA per cell (Supplementary Fig. S3.36). The fitted model yields a RNA synthesis rate of 0.03 RNA / cell / hour and a RNA half-life of 26.0 hours at 1.0 °C, and a RNA synthesis rate of 0.07 RNA / cell / hour and a RNA half-life of 10.6 hours at 5.0 °C. These measurements show that the time-scale of transcription for mCherry (reaching half the steady-state in ~10 hours) is considerably slower than the time-scale of protein synthesis at near-freezing temperatures (no appreciable increase in fluorescence within the first day of mCherry induction, Fig. 3.5c). Dots show the average of the mean number of RNA per cell in each replicate, shaded area represents the s.e.m., having $n = 2$ (at 5.0 °C) or $n = 3$ (at 1 °C) biological replicates. Each replicate had at least $n = 92$ cells (at 5.0 °C), or at least $n = 154$ cells (at 1.0 °C).

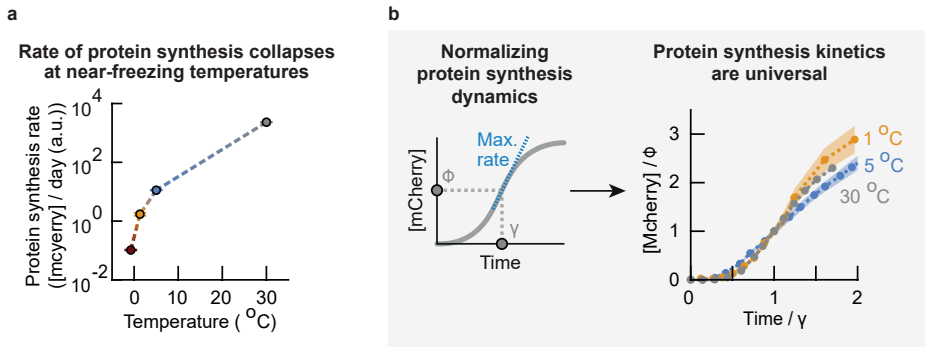

Figure S3.39: The protein-synthesis rate collapses as water freezes (0 °C) (Related to Figure 3.5c). Using a mCherry-inducible strain to the measure protein-synthesis rate across temperatures (Supplementary Fig. S3.6). **(a)** For each curve in Fig. 3.5c we determined the maximum rate of mCherry synthesis (maximum slope m of each fluorescence curve; Supplementary Theory S3.6). Shown are the protein-synthesis rates as function of temperature (the synthesis rate of general proteins can be at least as fast as the synthesis rate of mCherry measured here). **(b)** Protein-synthesis dynamics across temperatures. *Left*: Schematics of relevant parameters. At each temperature, we used a characteristic time γ and characteristic fluorescence ϕ at which the population reaches its maximum rate of protein synthesis to rescale protein-synthesis dynamics. *Right*: Normalized mCherry fluorescence over time (Fig. 3.5c). The fluorescence was normalized with the characteristic fluorescence ϕ and time was rescaled with the characteristic time γ at each temperature. The normalized curves approximately collapse onto a single master curve. These normalized curves suggest that one only needs to know the characteristic fluorescence-scale ϕ and time-scale γ for each temperature to describe expression of mCherry at that temperature. In both panels the error bars and shaded areas show the mean with s.e.m., having $n = 3$ replicate populations.

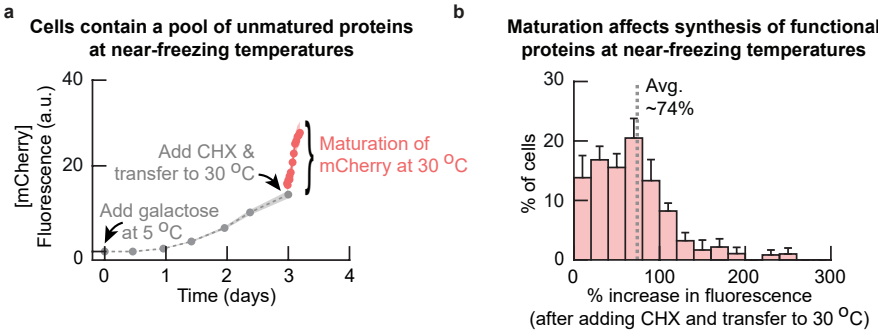

Figure S3.40: Time to synthesize a functional protein is affected by maturation (e.g., folding) time at 5 °C (Related to Figure 3.5c). Using a mCherry-inducible strain to quantify the time to synthesize functional proteins at near-freezing temperatures (also see Supplementary Figs. S3.6 and S3.39). **(a)** We incubated cells of the inducible mCherry strain for two weeks at 5.0 °C. We then added galactose to the growth media and followed the expression of mcherry at 5 °C in single cells over time with a microscope (Methods 3.4). After three days of incubation with galactose, we added cycloheximide (CHX) to the growth medium at a final 100 µg / mL concentration to instantly stop the translation machinery in the cells. We then transferred the cells to 30 °C and continued to measure the mCherry fluorescence of cells to quantify the maturation of unmatured mCherry. Shown is the fluorescence of mCherry over time at 5 °C (grey curve), and the increase in fluorescence at 30 °C after addition of CHX (red curve). The average fluorescence considerably increases after addition of CHX. Cells therefore contain a pool of unmatured mCherry at 5 °C when synthesis is induced with galactose. Dots show average fluorescence, and shaded area shows s.e.m. of the average fluorescence in $n = 5$ populations. **(b)** Histogram shows the increase in fluorescence of single cells from (a) after addition of CHX and transfer to 30 °C. The average fluorescence increases by 74% after addition of CHX, showing that roughly half of mCherry was not yet mature (fluorescent) at the time of adding CHX. Synthesis of functional proteins is therefore affected by the time required for maturation at near-freezing temperatures (Supplementary Theory S3.6). Histogram contains $n = 108$ cells, error bars show s.e.m. of $n = 5$ populations.

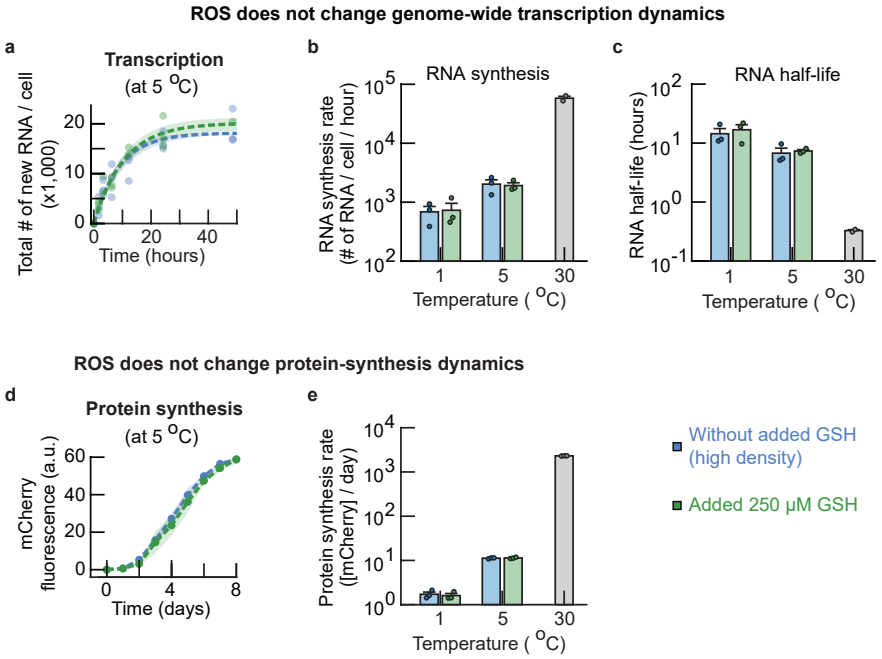

Figure S3.41: ROS does not change genome-wide transcription dynamics or protein synthesis dynamics at near-freezing temperatures (Related to Figure 3.5d). **(a-c)** ROS does not change rates of genome-wide transcription. **(a)** We used the measured number of synthesized RNA over time to fit a model for the kinetics of RNA synthesis in cells (Supplementary Figs. S3.36-S3.37). Shown are the number of newly synthesized RNA per cell over time at 5.0 °C for populations without added GSH (blue curve) or with 250 μM added GSH (green curve). Dots show measured data. Dotted lines represent fitted kinetics model using average parameter estimates, with $n = 3$ biological replicates per condition. Shaded area represents the s.e.m. for fitted model parameters. From the fitted model we obtain the RNA synthesis rates **(b)** and RNA half-lives **(c)** at 1.0 °C and 5.0 °C. Included are the rates for populations without added GSH (blue bars) and with 250 μM added GSH (green bars). Rates at 30 °C are shown as a comparison (grey bars). The RNA half-lives and RNA synthesis rates decrease with temperature. Without added GSH, the steady-state transcript levels (in # of RNA / cell) are $12,900 \pm 900$ (1.0 °C), $18,300 \pm 800$ (5.0 °C) and $27,300 \pm 1,300$ (30 °C), the RNA synthesis-rates (in # of RNA / cell / hour) are 690 ± 160 (1.0 °C), $2,020 \pm 370$ (5.0 °C) and $58,100 \pm 5,500$ (30 °C), and the RNA half-lives (in hours) are 14.4 ± 3.9 (1.0 °C), 6.7 ± 1.8 (5.0 °C) and 20 ± 1 (30 °C, in minutes). There is no reason to assume that the RNA synthesis rates are different upon addition of GSH (p-values are 0.82 at 5.0 °C and 0.89 at 1.0 °C). Error bars show mean with s.e.m., having $n = 3$ biological replicates per condition at 1.0 °C and 5.0 °C, and $n = 2$ biological replicates at 30 °C. Dots show raw data. **(d-e)** ROS does not change rate of protein synthesis. **(d)** The synthesis of mCherry over time at 5.0 °C compared for populations without added GSH (blue curve) and with 250 μM added GSH (green curve) (also see Fig. 3.5c and Supplementary Fig. S3.39). The dots show the average fluorescence, with shaded area representing the s.e.m. of $n = 3$ biological replicates. **(e)** Protein synthesis rates at 5.0 °C and 1.0 °C for populations that were incubated without added GSH (blue bars) or with 250 μM added GSH (green bars). Grey bar shows synthesis rate of mCherry at 30 °C as a comparison. The protein synthesis rate decreases with temperature. Without added GSH, the protein synthesis rates (in mCherry fluorescence / day (a.u.)) are 1.7 ± 0.2 (1.0 °C), 11.2 ± 0.2 (5.0 °C) and 2314 ± 10 (30 °C). There is no reason to assume that the protein synthesis rates are different upon addition of GSH (p-values are 0.66 at 5.0 °C and 0.69 at 1.0 °C).

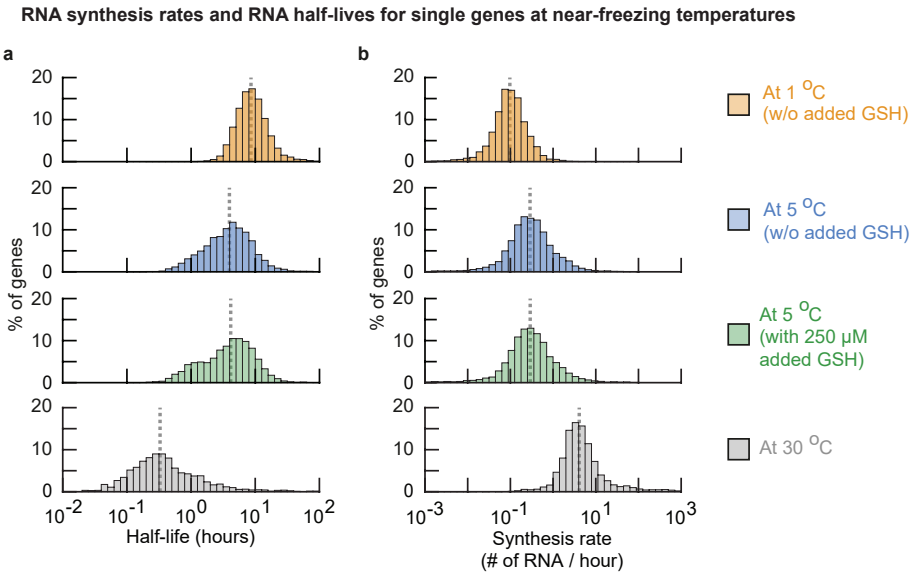

Figure S3.42: Single-gene RNA synthesis rates and RNA half-lives at near-freezing temperatures (Related to Figure 3.5d). (a-b) Using the data of freshly synthesized RNA per cell over time for the whole genome (as determined by 4tU-seq; Supplementary Figs. S3.36-S3.37), we fitted the model for the kinetics of RNA synthesis for every individual gene. Histograms show the RNA half-lives **(a)** and RNA synthesis rates **(b)** for 4,955 genes in the *S. cerevisiae* genome at 1.0 °C without added GSH (yellow bars), at 5.0 °C without added GSH (blue bars) and at 5.0 °C with 250 µM added GSH (green bars). The RNA half-lives and RNA synthesis rates at 30 °C are included as a comparison ($n = 2,135$ genes, grey bars). Grey dotted lines show the median RNA half-lives (8.57, 3.95 and 4.13 hours) and the median RNA synthesis rates (0.10, 0.29 and 0.29 RNA / hour) for each condition (at 1.0 °C, and at 5.0 °C without added GSH and with added glutathione respectively). The median RNA half-life at 30 °C is 14.3 minutes and the median RNA synthesis rate is 4.1 RNA / hour. The distribution of RNA synthesis rates and RNA half-lives remains almost unchanged upon addition of extracellular GSH, suggesting that ROS does not change the transcriptional dynamics at near-freezing temperatures.

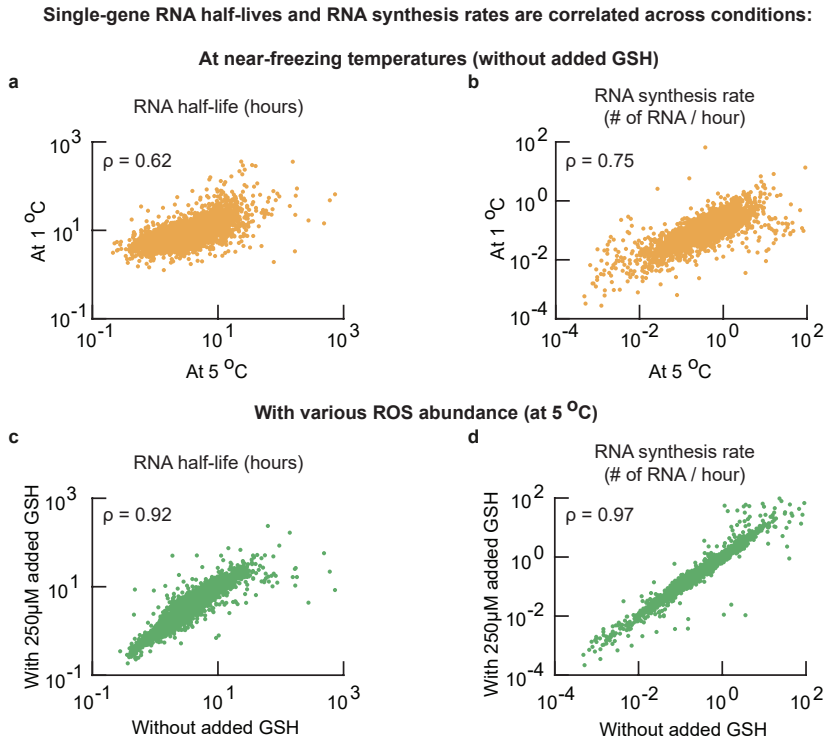

Figure S3.43: Single-gene RNA half-lives and RNA synthesis rates are correlated at various temperatures and are correlated at various ROS abundances (Related to Figure 3.5d). (a-d) Comparing single-gene transcription dynamics across near-freezing temperatures and with various ROS abundances (using the single-gene transcriptional rates determined in Supplementary Fig. S3.42). **(a-b)** Single-gene transcription rates compared between 5.0 °C (x-axis) and 1.0 °C (y-axis) without added GSH. Shown are the single-gene RNA half-lives (Pearson-correlation coefficient $\rho = 0.62$) **(a)** and the RNA synthesis rates (Pearson-correlation coefficient $\rho = 0.75$) **(b)**. The RNA half-life and RNA synthesis rate are correlated between temperatures. **(c-d)** Single-gene transcriptional rates at 5.0 °C compared without added GSH (x-axis) and with 250 μM added GSH (y-axis). Shown are the single-gene RNA half-lives (Pearson-correlation coefficient $\rho = 0.92$) **(c)** and RNA synthesis rates (Pearson-correlation coefficient $\rho = 0.97$) **(d)**. The half-lives and synthesis rates of RNA remain almost unchanged upon addition of GSH to the growth media, showing that ROS does not change the transcriptional dynamics at near-freezing temperatures. The colored dots in each panel show the rates for single genes, represented by the average rate of $n = 3$ biological replicates.

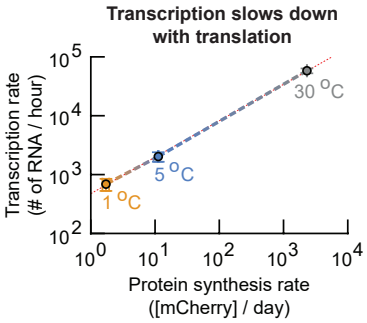

Figure S3.44: Transcription slows down with the protein synthesis rate (Related to Figure 3.5d). Using the transcription rate (# of synthesized RNA / cell / hour) and protein synthesis rate (mCherry fluorescence / day, (a.u.)) without added GSH across temperatures (Supplementary Fig. S3.41). Log-log plot shows how the transcription rate scales with the protein synthesis rate across temperatures (also see Fig. 3.5d). The red dotted line shows a power-law fit (exponent 0.62 ± 0.01, Pearson correlation-coefficient $\beta = 0.9998$). This power-law scaling confirmed that protein synthesis slows down faster than transcription as temperature decreases (exponent below 1; Supplementary Theory S3.6), such that transcription becomes more limiting for cell replications than protein synthesis as temperature continues to decrease (the fold-change in the protein synthesis rate is always larger than the fold-change in the transcription rate as temperature decreases, so that protein synthesis becomes more limiting than transcription upon a decrease in temperature). Dots show experimentally measured average values (Supplementary Fig. S3.41), error bars show s.e.m. of $n = 3$ biological replicates.

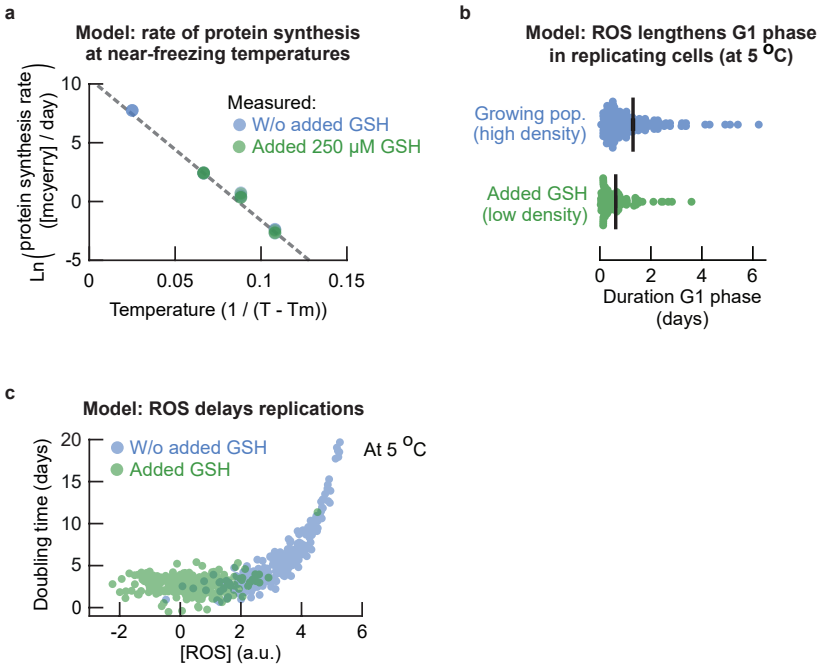

Figure S3.45: Stochastic model for the duration of single-cell replication at near-freezing temperatures (Related to Figure 3.6). **(a)** Estimating the parameter a for the model for single-cell doubling times at near-freezing temperatures (Supplementary Theory S3.6). To do so, we fitted a linear model to the protein synthesis rate $r_g(T)$ as function of temperature T using an Arrhenius-type equation ($\ln r_g(T) \propto -a/(T-T_m)$, see equation S3.13 and Supplementary Theory S3.6 for derivation). This model assumes a minimum temperature $T_m = -10\,^\circ$C below which protein synthesis does not occur. Fitting this linear model to the experimental data (Supplementary Fig. S3.41) yields $a \approx 120.72$. **(b-c)** Using the model to simulate the doubling time of individual cells and G1 phase durations (Supplementary Theory S3.6). **(b)** Simulation of the ROS-dependent G1 duration of the cell cycle at 5.0 °C (equal to the additional time Δt in the model, compare with Fig. 3.4c). The only free parameter (i.e., the average intracellular ROS concentration R of cells in the population) was chosen such that the average additional time Δt equals the average measured G1 duration for each condition respectively (Fig. 3.4c, the parameter R in equation S3.20 of Supplementary Theory S3.6). This yielded $R = 2.4$ for high-density (growing) populations (blue dots) and $R = 1.55$ for low-density populations with added GSH (green dots). Error bars show the mean with s.e.m. of $n = 3$ replicate simulations that each have $n = 50$ cells. Dots show the simulated additional time Δt for individual cells. **(c)** Simulation of the ROS-dependent doubling times of individual cells at 5.0 °C without added GSH (blue dots) and with added GSH (green dots). Initially, for relatively low ROS concentrations, the ROS-dependent additional time Δt is negligible compared to the shortest doubling time t that is set by the protein synthesis rate. Thus, at low ROS concentrations (green dots), the doubling time τ is approximated by the shortest doubling time t with noise (Supplementary Theory S3.6, equation S3.18). For relatively high ROS concentrations, the ROS-dependent additional time Δt becomes of the same size as the shortest doubling time t, such that the doubling time τ becomes dictated by ROS abundance. Each condition shows a simulation of $n = 250$ cells. The free parameter of the model was chosen to be equal to the values used to simulate the single-cell doubling times (see Fig. 3.6c; $R = 3.2$ without added GSH, $R = 0.35$ with added GSH).

S3.6. SUPPLEMENTARY THEORY

Density effect emerges from the percentage of replicating and dying cells (related to Fig. 3.1). Here we establish that the density-dependent growth at 5.0 °C does not emerge from the density-independent single-cell doubling times at 5.0 °C but instead from the percentage of cells in the population that dies and the percentage of cells that replicates (Supplementary Fig. S3.13). This is illustrated through only considering the initial population of cells in the time-lapse. For example, in high-density (growing) populations, 29% of the population at the start of the time-lapse replicates with a doubling time of ~6.5 days. These 29% of cells can therefore replicate at least 3x during the ~20 day time-lapse, thereby expanding the initial population by 88% with newborn cells. During the same ~20 days, 36% of the population at the start of the time-lapse dies. Thus, the cells within the initial high-density population that die are more than replenished by the newborn cells during the time-lapse. This leads to the high-density populations growing over time. In contrast, in low-density (non-growing) populations, 17% of the population at the start of the time-lapse replicates with a doubling time of ~7.1 days. The replicating cells in non-growing populations can therefore replicate less than 3x during the ~20 day time-lapse. The replicating cells then expand the initial population with at most 52% newborn cells, while during the same time 58% of the initial population dies. Then, the number of cells within the initial low-density population that die exceeds the number of newborn cells from this population during the time-lapse. As a consequence, more cells die than there are newborns per unit time, leading to the low-density population to go extinct. In summary, the density effect at 5.0 °C emerges from the percentage of cells that die and the percentage of cells that replicate that depend on the initial population density.

Growth model for expected lifespan and doubling time (related to Fig. 3.1). Here we derive a simple growth model that describes the expected lifespan and doubling time of cells at near-freezing temperatures. Assume that the number of cells in the population is given by $N(t)$ at time t. Of these $N(t)$ cells, $A(t)$ are alive and $D(t)$ are dead, such that $N(t) = A(t) + D(t)$. The number of alive cells changes over time through cell replications and cell deaths. The rate at which cells replicate is given by μ and the rate at which cells die is given by λ. Then, the number of alive cells changes over time according to,

$$\frac{dA}{dt} = A(t) \cdot (\mu - \lambda). \tag{S3.1}$$

Similarly, the total number of cells changes according to,

$$\frac{dN}{dt} = \mu A(t), \tag{S3.2}$$

since we add freshly born cells to the total number of cells and dead cells are not removed from the total number of cells in the population. Solving the differential equation S3.1 yields,

$$A(t+dt) = A(t) \cdot \exp\Big((\mu-\lambda)\cdot dt\Big). \tag{S3.3}$$

Using equation S3.3 to solve equation S3.2 we obtain,

$$\begin{aligned} N(t+dt) &= N(t) + \int_0^{dt} \mu A(\tau) d\tau \\ &= N(t) + \mu A(t) \int_0^{dt} \exp\Big((\mu-\lambda)\tau\Big) \\ &= N(t) + \frac{\mu}{\mu-\lambda} A(t) \Big[\exp\Big((\mu-\lambda)\tau\Big)\Big]_0^{dt} \\ &= N(t) + \frac{\mu}{\mu-\lambda}\Big(A(t+dt) - A(t)\Big) \end{aligned} \tag{S3.4}$$

In our experiments we can measure the number of alive cells and the number of dead cells and the total number of cells over time. We therefore have $A(t)$ and $N(t)$ available to fit the growth rate μ and death rate λ with our model. Taking the logarithm of equation S3.3 describing the number of alive cells in the population and rewriting yields,

$$r_1 := \frac{1}{dt}\Big(\ln A(t+dt) - \ln A(t)\Big) = \mu - \lambda \tag{S3.5}$$

Similarly, we can rewrite equation S3.4 describing the total number of cells in the population as,

$$r_2 := \frac{N(t+dt) - N(t)}{A(t+dt) - A(t)} = \frac{\mu}{\mu-\lambda}. \tag{S3.6}$$

Finally, we use the numbers r_1 (from equation S3.5) and r_2 (from equation S3.6) to find the rates μ and λ,

$$\begin{aligned} \mu &= r_1 \cdot r_2, \\ \lambda &= r_1 \cdot (r_2 - 1). \end{aligned} \tag{S3.7}$$

We used equations S3.5-S3.7 to estimate the growth rate μ and death rate λ from the total number of cells and the number of alive cells in a population. The expected lifespan of cells in the population is then given by $1/\lambda$ (cells die at a rate λ).

Model for protein synthesis rate (Related to Fig. 3.5). Here we describe a simple kinetics model for the synthesis of mCherry that we measured experimentally by following the mCherry fluorescence in cells over time. Assume that mCherry is synthesized by first being translated into an unfolded polypeptide chain, followed by folding into a fluorescent protein (Supplementary Fig. S3.40). We let u denote the amount of unfolded mCherry and f denote the amount of folded mCherry in a cell. We further assume that unfolded mCherry is synthesized at a constant rate m (a.u. / day), and that the unfolded mCherry is folded at a rate γ (day^{-1}). Then the amounts of unfolded and folded mCherry over time t are described by,

$$\frac{du}{dt} = m - \gamma \cdot u, \tag{S3.8}$$

$$\frac{df}{dt} = \gamma \cdot u. \tag{S3.9}$$

Solving equation S3.8 yields $u(t) = \frac{m}{\gamma} \cdot \Big(1 - \exp(-\gamma \cdot t)\Big)$, and substitution of $u(t)$ into equation S3.9 yields,

$$f(t) = \frac{m}{\gamma} \cdot \Big(\exp(-\gamma \cdot t) - 1\Big) + m \cdot t. \tag{S3.10}$$

Equation S3.10 describes the amount of folded mCherry over time and provides a model for the experimentally measured mCherry fluorescence in cells. Initially, synthesis of mCherry has not occurred, such that a cell does not have unfolded mCherry and no folded mCherry is being produced. At time $t = 0$ the cell starts synthesizing unfolded mCherry, whose concentration is described by $u(t) = \frac{m}{\gamma} \cdot (1 - \exp(-\gamma \cdot t))$. Thus, the amount of unfolded mCherry initially increases and eventually reaches a steady-state that is determined by an inflow from synthesis and an outflow to folded mCherry ($u(t) \to \frac{m}{\gamma}$ as $t \to \infty$). At this steady-state, the equation S3.8 for unfolded mCherry satisfies $\frac{du}{dt} = 0$, such that $\gamma \cdot u = m$ and $\frac{df}{dt} = m$ (from equation S3.9). Thus, this derivation shows that the slope of mCherry fluorescence over time converges to the synthesis rate m ($\frac{df}{dt} \approx m$ for sufficiently large t). In practice, we measured the synthesis rate $m(T)$ for each temperature T by taking the maximum slope of the increase of mCherry fluorescence over time, and then used these $m(T)$ to further fit the model in equations S3.8-S3.9 to the data.

S3.6.1. STOCHASTIC MODEL FOR SPEED LIMITS OF CELLULAR LIFE IN FRIGID ENVIRONMENTS

Here we derive a stochastic model with one free parameter for single-cell doubling times at near-freezing temperatures. The model is derived using our experimental observations. First, we motivate a description of the doubling time in terms of a ROS-independent lower limit. This lower limit is set by the protein-synthesis rate, while the doubling time increases above this minimum through an additional time that is ROS-dependent. Using our measurements, we show a power-law type scaling between the shortest doubling time and the protein-synthesis rate. Next, we describe the protein-synthesis rate as function of temperature, such that also the shortest doubling time is a function of temperature. We further use our experimental data to derive the stochastic, ROS-dependent time in addition to the shortest doubling time. Combining the ROS-independent shortest time and the ROS-dependent additional time then yields the complete stochastic model. Finally, we fit all parts of the model to our experimental data to find the value of all model parameters.

Doubling time is dictated by the protein-synthesis rate and intracellular ROS abundance. Experimentally we have found that removing ROS with GSH shortens the doubling time at a given temperature (Supplementary Fig. S3.13), and that the durations of the S-G2-M phases of the cell cycle are independent of ROS (durations of S-G2-M do not change upon addition of GSH, Supplementary Fig. S3.26). These observations suggest that removing ROS by adding GSH decreases the doubling time to a minimum value for a given temperature (compare Fig. 3.2e with Fig. 3.4c-d). We therefore assume that there is a ROS-independent, shortest doubling time t for each temperature, and that cells having minimal ROS replicate almost as fast as that shortest doubling time. Additionally, we have found that removing ROS by adding GSH shortens G1 duration (Fig. 3.4c). Furthermore, cells with high intracellular ROS concentrations are unlikely to replicate (Fig. 3.3b) and are often arrested in G1 (Supplementary Fig. S3.25). These results suggest that G1 duration is ROS-dependent, which yields an additional time Δt that increases the doubling time above the ROS-independent minimum. Together, these experimental observations suggest that the single-cell doubling time τ is the sum of a ROS-independent shortest time t and a ROS-dependent additional time Δt at each temperature T, such that,

$$\tau(T,R) = t(T) + \Delta t(R,T). \tag{S3.11}$$

where R is some environmental parameter that depends on, for example, ROS and GSH. Here, we assume that $\Delta t > 0$ such that the doubling time is at least the shortest time for

a given temperature ($\tau(T,R) > t(T)$).

Modeling the temperature dependence of the protein-synthesis rate. Recall that the protein-synthesis rate decreases as function of temperature (Supplementary Fig. S3.39). To describe protein synthesis as function of temperature with a model, we assume that there exists a lower temperature limit T_m below which the yeast protein machinery fails. Then we can describe the rate as function of temperature with a common Arrhenius-type model $r_g(T) = c \cdot \exp(-a/(T - T_m))$ for some parameters a and c, such that $r_g(T) \to 0$ as the temperature decreases to T_m. Note that the Arrhenius equation would have $T_m = -273$ °C. We can rewrite this model using the experimentally measured protein-synthesis rate at a known temperature T_0,

$$r_g(T) = r_g(T_0) \cdot \exp\Big[-a\Big(\frac{1}{T - T_m} - \frac{1}{T_0 - T_m}\Big)\Big], \tag{S3.12}$$

providing a simple equation that describes the protein-synthesis rate as function of temperature. Taking the logarithm of equation S3.12 we find that,

$$\ln r_g(T) \propto -a \cdot \frac{1}{T - T_m}, \tag{S3.13}$$

which is a model that is linear in $1/(T - T_m)$ and that we fit to the experimentally measured protein-synthesis rates at various temperatures to find the parameter a (S3.45).

Model for the protein-synthesis rate setting the shortest possible doubling time. We have experimentally measured the shortest doubling time $t(T)$ by taking away ROS with GSH (Supplementary Fig. S3.13). We have also experimentally measured the ROS-independent protein-synthesis rate $r_g(T)$ (Fig. 3.5d, Supplementary Fig. S3.41). Then both the shortest doubling time and protein-synthesis rate are independent of ROS, and we assume without loss of generality that the shortest doubling time $t(T)$ is limited by the protein-synthesis rate $r_g(T)$ at each temperature T (i.e., a cell requires a certain time to build a daughter at each temperature, regardless of ROS abundance). Here, we seek to describe the relation between the shortest doubling time and the protein-synthesis rate.

Experimentally, we have found that the observed doubling time slows down with the protein-synthesis rate via a power-law type scaling (Fig. 3.6b). One reason why the relation may be of power-law type is the following. We assume that the rate of each process depends on temperature according to an Arrhenius-type equation $r_p(T) = A_p \exp\Big(-\frac{E_p}{RT}\Big)$, where $r_p(T)$ is the rate of each process (i.e., protein synthesis or cell division) and constants E_p, R and A_p. Isolating the reciprocal temperature rewrites the Arrhenius

equation to $\frac{1}{T} = -\frac{R}{E_p}\Big(\ln(r_p) - \ln(A_p)\Big)$. Denoting the rate of cell division as $r_d(T)$ and the rate of protein synthesis with $r_g(T)$, we can express the rate of cell division in terms of the rate of protein synthesis (omitting the temperature dependence of each rate for readability),

$$\begin{aligned}\ln(r_d) &= -\frac{E_d}{R}\Big(\frac{1}{T}\Big) + \ln(A_d) \\ &= -\frac{E_d}{R}\Big(-\frac{R}{E_g}(\ln(r_g) - \ln(A_g))\Big) + \ln(A_d) \\ &= \frac{E_d}{E_g}\ln(r_g) + c_1, \end{aligned} \tag{S3.14}$$

where c_1 is a constant of aggregated rest terms. Let $k = E_d/E_g$ be some factor such that by taking the exponent of equation S3.14 we obtain, $r_d = c_2 \cdot r_g^k$. Then, by substituting the shortest doubling time $t(T)$ for the growth rate $r_d(T)$ via $t(T) = \ln(2)/r_d(T)$ we obtain,

$$t(T) = c \cdot r_g(T)^{-k}, \tag{S3.15}$$

for some constant c and exponent k. Note that the above derivation is not restricted to any choice of a temperature scale. Taking the logarithm of equation S3.15 we find that,

$$\ln t(T) \propto -k \cdot \ln r_g(T), \tag{S3.16}$$

giving a linear model that we fit to the experimentally measured shortest doubling times and protein-synthesis rates at various temperatures to find the value of the exponent k. The power law with exponent k in equation S3.15 illustrates how the doubling time changes with protein synthesis. For example, if the protein-synthesis rate changes by two-fold, then the doubling time changes by 2^{-k}-fold, such that fold-change in the doubling time is smaller than the fold-change in protein synthesis for exponents $k < 1$. Of note, with such power law, it is only the fold-change of the protein-synthesis rate that sets how the doubling time changes, irrespective of the actual values (i.e., the doubling time and protein-synthesis rate change proportionally).

In summary, with an Arrhenius-type equation describing rates as function of temperature, we can derive that cell division and protein synthesis may follow a power-law relation. We have therefore now experimentally measured and theoretically motivated a power-law type scaling of the shortest doubling time and the protein-synthesis rate. Finally, using equation S3.15, we rewrite the shortest doubling time $t(T)$ using some ob-

served shortest doubling time $t(T_0)$ at a known temperature T_0,

$$t(T) = t(T_0) \cdot \left(\frac{r_g(T)}{r_g(T_0)}\right)^{-k}. \tag{S3.17}$$

We know from our single-cell data that the experimentally measured shortest doubling time is stochastic and approximately normally distributed (e.g., the single-cell doubling times of the wild type at 5.0 °C with added GSH; Supplementary Fig. S3.13). We therefore assume that $t(T_0)$ is stochastic and equal to the experimentally measured shortest doubling time with normally distributed noise $\epsilon_m \sim N(0,1)$, such that,

$$t(T) \sim \left(t(T_0) + \epsilon_m\right) \cdot \left(\frac{r_g(T)}{r_g(T_0)}\right)^{-k}, \qquad \epsilon_m \sim N(0,1). \tag{S3.18}$$

We use $t(T)$ with $\epsilon_m = 0$ as the deterministic shortest doubling time $t_{\min}(T)$ from the model. The shortest doubling time at a given temeperature thus changes proportionally to the protein-synthesis rate as temperature changes. Cell-to-cell variability due to other factors is simulated with the normally distributed noise.

Stochastic model for the ROS-dependent duration of the doubling time. Having derived the ROS-independent shortest doubling time (equation S3.18), we here seek to describe the ROS-dependent additional time $\Delta t(R,T)$ that increases the doubling time above this shortest time. To describe this ROS-dependence, we assume that $\Delta t(R,T)$ is described by the time it takes a cell to remove sufficient intracellular ROS and repair enough damages to divide. For example, we have experimentally measured that cells with low intracellular ROS concentrations are likely to replicate whereas cells with high intracellular ROS concentrations are unlikely to replicate (Fig. 3.3b). We therefore assume that a cell has some amount of doubling time delaying tasks to perform before it can replicate and that this amount of time is proportional to the abundance of intracellular ROS. We further assume that these tasks can be performed in a time that is proportional to how fast a cell can express genes, for example to synthesize ROS-reducing enzymes and to replace damaged components. Thus, we assume that $\Delta t(R,T) \propto [\mathrm{ROS}]/r_g(T)$ (a cell synthesizes proteins at a rate $r_g(T)$ (a.u. / time) and has an ROS abundance of [ROS] (a.u.)). Moreover, we have experimentally measured the intracellular ROS concentrations in cells, which is approximately normally distributed on a log-scale (Supplementary Fig. S3.10). Finally, our measurements suggest that there is some threshold concentration of ROS above which replications become very unlikely (Fig. 3.3b). We therefore assume that we can describe the distribution of intracellular ROS concentrations according to $\ln[\mathrm{ROS}] \sim N(R,1)$, where R is some parameter describing the average ROS abundance in cells (see Fig. 3.2a,c). Thus, $\Delta t(R,T)$ is stochastic and

described by,

$$\Delta t(R,T) \sim \frac{1}{r_g(T)} \cdot \exp\Big(\epsilon_d(R)\Big), \qquad \epsilon_d(R) \sim N(R,1). \tag{S3.19}$$

The additional time that increases the doubling time above its minimum thus varies between cells because of some ROS-dependent parameter that is log-normally distributed.

Stochastic model for ROS and temperature setting the doubling time. Using the ROS-independent shortest doubling time (equation S3.18) and the ROS-dependent addition to the doubling time (equation S3.19), we obtain the single-cell doubling time τ as a function of the temperature T and average ROS abundance R,

$$\begin{aligned}\tau(T,R) &= t_{\min}(T) + \Delta t(R,T) \\ &= \Big(t(T_0) + \epsilon_m\Big) \cdot \Big(\frac{r_g(T)}{r_g(T_0)}\Big)^{-k} + \frac{1}{r_g(T)} \cdot \exp\Big(\epsilon_d(R)\Big).\end{aligned} \tag{S3.20}$$

Here, $t(T_0)$ and $r_g(T_0)$ are the experimentally observed shortest doubling time and protein-synthesis rate at a temperature T_0 respectively, k is the exponent that describes the scaling between the shortest doubling time and the protein-synthesis rate, and (from equation S3.12),

$$\begin{aligned} r_g(T) &= r_g(T_0) \cdot \exp\Big[-a \cdot \Big(\frac{1}{T-T_m} - \frac{1}{T_0 - T_m}\Big)\Big], \\ \epsilon_m &\sim N(0,1), \\ \epsilon_d(R) &\sim N(R,1). \end{aligned} \tag{S3.21}$$

The parameter a describes the protein-synthesis rate as function of temperature, and T_m represents the temperature below which protein synthesis stops for yeast. With log-normally distributed ROS, we find that the single-cell doubling times are a trade-off between the speed at which a cell replicates and the likelihood of such a cell occurring. In practice, there exists a longest possible doubling time $\tau_{\max}$ due to an experimentally observed threshold ROS concentration beyond which cells are unable to duplicate and die. The parameter R is the only free variable in the model, and all other parameters will be constrained next.

Model parameters. We choose the known temperature T_0 to be 5.0 °C, where we have experimentally measured $r_g(T_0) \approx 11.23$ a.u. / day (Supplementary Fig. S3.39) and the experimentally measured shortest doubling time $\tau(T_0) \approx 2.5$ days (with added GSH: ~25 hours DNA replication, ~22 hours DNA segregation, ~4 hours in G2, and a median G1

duration of ~9 hours; Supplementary Fig. S3.26). Here, we used the median G1 duration due to the shape of the distribution to more accurately estimate the shortest time spent in G1 with added GSH. We fitted the power-law type scaling (equation S3.15) of the shortest doubling time as function of the protein-synthesis rate to obtain an exponent $k \approx 0.77$ (Fig. 3.6b, Pearson correlation-coefficient $\beta = 0.998$). Only single-cell data was used as the experimental minimum doubling times (the average single-cell doubling time at 30 °C, the average single-cell doubling time with added GSH at 5.0 °C, and the minimum single-cell doubling times at 1.0 °C that exclude the duration of G1). As a lower temperature limit T_m for protein synthesis in yeast we took $T_m = -10$ °C, motivated by the fact that the yeast growth medium freezes at −2 °C (and thus limits protein synthesis by for example restricting access to nutrients, leading to deprivation of oxygen and limiting movement of (say) ribosomes), because important enzymes such as Catalase stop functioning at −6 °C [128], and other essential enzymes inactivate at 0 °C [12, 13]. It is therefore safe to assume that the temperature below which yeast's protein synthesis stops lies above −10 °C. Having fixed T_m, we fitted the temperature dependence of the protein-synthesis rate using equation S3.13 from which we find that $a \approx 120.72$ (Fig. S3.39, Pearson correlation-coefficient $\beta = 0.995$). Substituting the values of all known parameters into equations S3.20-S3.21 yields the model that was used for all simulations,

$$\begin{aligned} \tau(T,R) &\sim (2.5+\epsilon_m)\cdot\exp\Big(\frac{93}{T+10}-6.2\Big)+0.09\cdot\exp\Big(\frac{121}{T+10}-8+\epsilon_d(R)\Big), \\ \epsilon_m &\sim N(0,1), \\ \epsilon(R) &\sim N(R,1). \end{aligned} \tag{S3.22}$$

This model describes the doubling time for single cells as a function of temperature T, with R representing the average abundance of ROS in cells, the only free parameter in the model. Knowing the measured (average) doubling time at a given temperature thereby constrains R through the model's predicted average doubling time. We thus constrained R as follows. We measured the average single-cell doubling time with and without added GSH at 5.0 °C (Supplementary Fig. S3.13). We then chose R such that the predicted doubling time of each population was equal to its measured, experimental doubling time. At 5.0 °C, this yielded $R = 3.2$ for populations without added GSH, and $R = 0.35$ for populations with added GSH (yielding Fig. 3.6c). We simulated R for different temperatures by taking $R = 3.2$ (without added GSH) and by decreasing R with 1.5% for every 0.1 °C increase in temperature (yielding Fig. 3.6d). Finally, we note that cells are extremely unlikely to replicate for sufficiently abundant ROS (Fig. 3.3b). We therefore assume that simulated cells beyond the 98.5-th percentile of ROS concentrations ($[ROS]_{\text{threshold}}$) are unable to replicate, yielding the slowest possible doubling times of the model.

4

CONCLUSION

Temperature is perhaps the most important physical environmental factor affecting the speed at which cellular life replicates [1]. Cell replications slow down as the temperature changes to a less optimal value [1, 129], and cells stop replicating if the temperature goes beyond the range of habitable temperatures. However, the bio-molecular processes that cause cells to stop replicating upon exposure to extreme temperatures have remained poorly understood [2–5, 10, 11, 17, 18]. In this dissertation, we used the budding yeast *Saccharomyces cerevisiae*, a model for the eukaryotic cell, to study what processes enable and constrain the proliferations of cellular life at extreme temperatures. In short, the conventional views state that failure of key intracellular factors or processes prevent cells from replicating at sufficiently extreme temperatures. At high temperature, this textbook view proposes that crucial proteins unfold and heat-induced damages occur that prevent cell replications [2–6]. At low temperatures, common suggestions are that essential processes such as transcription, translation and enzymatic reactions occur too slowly to sustain growth [1, 7–9] or that low temperatures lead to growth-preventing stress from, for example, stiff membranes or oxidative damages [1, 9–16]. However, we found that the true reasons that cells cannot proliferate at extreme temperatures are more intricate and require a systems-level view of cellular life. Together, our results establish quantitative foundations for uncovering design principles of cellular life and its fundamental limits at extreme temperatures.

Collective growth and survival at high temperatures. At high temperatures (Chapter 2), we found that budding yeasts help each other and future generations of cells to repli-

cate by secreting and extracellularly accumulating glutathione. As a consequence of this behavior a yeast population can, at the same temperature, either exponentially grow, never grow, or grow after unpredictable durations (hours to days) of stasis, depending on the population density. The yeast populations that cannot grow continuously decelerate their approach to extinction, with higher population-densities stopping faster due to cells still cooperatively accumulating extracellular glutathione. We determined that exporting glutathione, but not importing glutathione, is required for yeasts to survive and replicate at high temperatures. Overall, this study demonstrates that glutathione – by eliminating harmful extracellular agents such as Reactive Oxygen Species (ROS) as an antioxidant – is both necessary and sufficient for surviving and replicating at high temperatures. Moreover, our work suggests ways to help organisms combat rising temperatures and help us understand how climate change impacts unicellular life and multicellular communities.

Speed limits of cellular life at low temperatures. At near-freezing temperatures (Chapter 3), we found that budding yeast also secretes and extracellularly accumulates glutathione, resulting in density-dependent growth similar to high temperatures. Cells die and cannot divide primarily because of having abundant intracellular ROS. Survival and cell replication can be enabled and accelerated by promoting the G1-to-S transition, either through removing intracellular ROS or by letting cells exit G1 with abundant ROS. Such interventions yielded a comprehensive view of cellular life at near-freezing temperatures through measurements of months-long lifespans, days-to-months-long cell-cycle durations, protein-synthesis rates and genome-wide transcriptional rates. This view showed that protein synthesis becomes rate-limiting for cell replication as temperature decreases to 0 °C, and that protein synthesis and ROS together establish speed limits for life at near-freezing temperatures: a cell must proliferate at a minimum speed or face death. This study provides a basis for understanding fundamental limits of cellular life, including temperature's role in setting an organism's replicative ability, lifespan and speed of aging.

Refining the conventional views of cell replications at extreme temperatures. Strikingly, our findings demonstrated that the replicative abilities of cells exposed to extreme temperatures are governed by several common principles. At both high and low temperatures, we found that *i)* yeast survival and proliferation is density-dependent, *ii)* the extracellular environment plays an essential role for a cell's replicative abilities, and *iii)* that yeast's life is enabled and constrained by an interplay between ROS and glutathione's (extracellular) role as antioxidant. The fact that yeast replication is density-dependent and controlled by a single molecule for both high and low temperatures is

fascinating given that the effect of these temperatures, and the reasons why cells stop replicating, have conventionally been considered to be very different [1–16]. Our findings integrated such conventional reasons – such as cells indeed experiencing oxidative stress at extreme temperatures [15, 42] – and demonstrate how common principles collectively determine when cells fail or succeed to replicate at extreme temperature.

Additionally, our work revealed principles that control cell proliferation at extreme temperatures on both the single-cell and population level. For example, at the single-cell level at near-freezing temperatures, the replicative ability of a cell decreases as a cell becomes older or contains more intracellular ROS. A young cell or a cell with minimal ROS is likely to replicate. As a cell ages, its probability of replicating decreases and its doubling time increases due to the cell becoming unlikely to exit G1. Eventually a cell is unable to replicate as it becomes too old or has an above-threshold amount of intracellular ROS. At the population-level, at both high and low temperatures, growth is density-dependent and controlled by ROS being removed by glutathione. High-density populations are able to secrete and accumulate extracellular glutathione above some threshold concentration, leading to population growth. In contrast, low-density populations cannot accumulate sufficient extracellular glutathione because there are less cells secreting glutathione, thereby preventing population growth. Thus, only together can cells secrete enough glutathione to sustain growth, with populations requiring more cells secreting glutathione as temperature becomes more extreme. Eventually, at sufficiently extreme temperatures, there are not enough nutrients available in the environment to sustain the required number of cells secreting glutathione, leading to only non-growing populations beyond those temperatures.

As a remarkable consequence of our findings, we demonstrated that cells can, in fact, replicate at extreme temperatures that were conventionally thought to be unlivable. For example, cells can replicate with months-long time-scales at 1 °C (instead of the conventional ~5 °C) and sustain population growth at 41 °C with ample extracellular reduced glutathione (GSH) (instead of at ~38 °C without extracellular GSH). In summary, the habitability of a temperature is not solely determined by intracellular conditions (e.g., age and ROS abundance) but also by common principles at the population level (e.g., population density controlling the extracellular glutathione concentration). Our findings thereby add to the few known examples of cooperative behaviors through shared goods in yeasts [28, 130] and other findings of positive relationships between population density and growth or survival of other microorganisms [31, 62, 131–133]. Moreover, our findings suggest ways to help yeast and other organisms to survive climate change, for example by tuning the composition of their environment or engineering organisms so

that they can live in more extreme environments [134].

The roles of reactive oxygen species at extreme temperatures. While ROS can be beneficial for intracellular signaling and regulation at physiological concentrations [135–137], we found that cells become exposed to harmful amounts of ROS that inhibit cell replication at extreme temperatures. The primary ROS that cells experience are superoxides, with half-lives of minutes to hours [108, 110]. At optimal growth temperatures, these ROS are known to damage cellular components such as nucleic acids [43, 69], proteins [44, 69], and cell membranes [45], thereby prolonging or inhibiting cell replication [95, 96, 138–143]. Thus, given their longevity and reactivity, ROS such as superoxides have the potential to diffuse across cellular scales, damage all components of a cell and prevent its proliferation, regardless of their origin [144]. It is therefore not surprising that the extracellular environment can be a main source of replication-inhibiting ROS, as we established at extreme temperatures.

Our findings add to previous reports of ROS being generated or being present in many (aquatic) habitats [144–146]. One could therefore reason that ROS are present in the extracellular environment regardless of temperature, and that these ROS could also prohibit replications at optimal growth temperatures (~30 °C). However, the effect of ROS on cells is special at extreme temperatures for two reasons. First, inactivating a certain amount of ROS per unit time requires more effort as the temperature becomes more extreme [128, 147, 148], for example because essential cellular processes slow down regardless of the presence of ROS as we have demonstrated at near-freezing temperatures. Second, the solubility of oxygen is ~3-fold higher at near-freezing temperatures compared to 30 °C [26], such that more dissolved oxygen is available to form radicals [144, 149]. Similarly, heating of aqueous solutions has been found to generate superoxides [149], potentially increasing the amount of ROS at high temperatures compared to 30 °C. Together, the increased potential for ROS generation and the reduced ability of cells to remove these ROS provide an argument why ROS become prohibitive for proliferations at sufficiently extreme temperatures.

Despite ROS being the common replication-prohibitive factor at extreme temperatures, we found that the sources of extracellular ROS and the actions of ROS on cells are not identical at high and low temperatures. For example, we found that the nutrients in the growth medium – such as metal ions that are present in all culture media and which are essential to life [146] – are one of the growth-inhibiting sources of ROS at near-freezing temperatures but not at high temperatures. Consequently, we found that removing nutrients from the growth medium (including metal ions) only induces growth

at near-freezing temperatures. These observations suggest that extracellular ROS may be generated and may act in different ways at the two temperature extremes. Finally, these ROS-generating sources cannot simply be removed entirely while still permitting cell replications. Indeed, we demonstrated that major ROS-generating sources such as nutrients and dissolved oxygen are also essential for yeast replication at near-freezing temperatures. The availability of extracellular factors such as nutrients and oxygen thereby simultaneously fuel life and, through ROS, inhibit its proliferation at extreme temperatures.

Expanding the roles of glutathione in yeast. We established that extracellular glutathione has essential functions as antioxidant at extreme temperatures. Through its function as antioxidant, glutathione enables survival and population growth at both low and high temperatures, expanding the few known extracellular roles of glutathione and other antioxidant defenses in yeast [52, 53, 150]. One advantage of secreting glutathione is that it can reduce harmful substances extracellularly before these reach the cell. Another advantage of collectively secreting glutathione is that extracellular glutathione protects not only a cell itself but also has the potential to protect other cells and future generations after the current generation of cells has died. A collective stress response is therefore beneficial for the entire population.

However, just as with ROS, the effect of extracellular glutathione on cells is very different at high and low temperatures. This is not surprising given the tight interplay between glutathione and ROS, and the differences we found in the actions and sources of ROS at low and high temperatures. For example, at high temperatures, we found that GSH enables cell replications at most as fast as cells replicate in growing populations without added GSH. Moreover, we found that the action of extracellular GSH can be fully substituted with other antioxidants at high temperatures. Furthermore, glutathione must be exported for population growth while glutathione import is not necessary. Together, these observations suggest that the action of glutathione is solely as extracellular antioxidant at high temperatures. In contrast, at near-freezing temperatures, we found that extracellular GSH enables cell replication at more than double the speed of cells in any growing population without added GSH. Moreover, GSH removes ROS that are intracellular, and its action cannot be fully substituted by other antioxidants. Furthermore, extracellular GSH can substitute the functions of some intracellular ROS-defense enzymes that are required for growth. Together, these effects of extracellular GSH lead to drastically different proliferation, aging and lifespans of cells, suggesting that GSH has additional, essential intracellular roles at near-freezing temperatures. Overall, extracellular GSH enables survival and cell replication in ways that may seem very similar on

the population level when comparing low and high temperatures, but glutathione's effects on single cells and their individual lives are very different between the temperature extremes.

Outlook. Our work on cell replication at extreme temperatures is timely in light of global warming, and encourages re-examining the cell-autonomous picture of microorganisms. Environments that are conventionally considered prohibitive for a cell because of extreme temperatures, may in fact prove habitable. For example, melting ice exposes cells to near-freezing aquatic environments that form new habitats, while the heating of existing habitats exposes cells to replication-inhibiting high temperatures. Our findings demonstrate that survival and proliferation in these conditions can emerge as collective features dictated by ROS, and that unicellular organisms such as yeasts can act as a community to extend the boundaries of life-permitting temperatures. Moreover, our studies reveal a quantitative interplay between ROS and the gene-expression rate that fundamentally limits the speed at which an organism's life progresses. Given the ubiquity of glutathione and ROS in the lives of cells [108, 137], our work raises the question whether similar principles exist for other microbes and mammalian cells.

Indeed, yeast [52, 53, 119, 150] and the cells of other organisms [151] have been found to secrete antioxidants such as glutathione in various stress conditions. Future studies may therefore show that glutathione acts as a general defense against extracellular stress. Moreover, such studies could further unravel the poorly understood relations among cellular ROS-defense systems, the transport of glutathione [58, 59, 152], the sources of extracellular ROS [146], and their dependence on temperature changes [26, 149]. Furthermore, both intracellular ROS [108–115] and glutathione [106, 107] have previously been associated with aging outside the context of temperature. Interestingly, the effect of extracellular antioxidants on the aging of yeast have been found to vary widely, with some antioxidants extending lifespan and others shortening lifespan [116–118]. Investigating the roles of ROS and antioxidants such as glutathione in an organism's life may therefore further our understanding of lifespan and theories of aging.

Finally, the quantitative relationships that we established among temperature, the extracellular environment and intracellular processes such as gene-expression machineries reveal fundamental limits and growth laws for cellular life that are of broad interest [35, 99–102, 153–158]. Such design principles can be used to engineer yeast and potentially other organisms so that they can live longer and at desired speeds in extreme environments, and may guide future studies that aim to find limits to slowing aging and extending lifespan.

REFERENCES

[1] M. T. Madigan, J. Martinko, D. Stahl, and D. Clark, *Brock Biology of Microorganisms*, 13th ed. (Pearson, 2011).

[2] K. Ghosh and K. Dill, *Cellular proteomes have broad distributions of protein stability,* Biophys. J. **99**, 3996 (2010).

[3] P. Leuenberger, S. Ganscha, A. Kahraman, V. Cappelletti, P. Boersema, C. von Mering, M. Claassen, and P. Picotti, *Cell-wide analysis of protein thermal unfolding reveals determinants of thermostability,* Science **355**, eaai7825 (2017).

[4] J. Verghese, J. Abrams, Y. Wang, and K. A. Morano, *Biology of the heat shock response and protein chaperones: budding yeast (Saccharomyces cerevisiae) as a model system,* Microbiol. Mol. Biol. Rev. **76**, 115 (2012).

[5] K. Richter, M. Haslbeck, and J. Buchner, *The heat shock response: life on the verge of death,* Mol. Cell **40**, 253 (2010).

[6] D. A. Ratkowsky, R. K. Lowry, T. A. McMeekin, A. N. Stokes, and R. E. Chandler, *Model for bacterial culture growth rate throughout the entire biokinetic temperature range,* J. Bacteriol. **154**, 1222 (1983).

[7] P. G. Jones and M. Inouye, *RbfA, a 30S ribosomal binding factor, is a cold-shock protein whose absence triggers the cold-shock response,* Mol. Microbiol. **21**, 1207 (1996).

[8] Y. Murata, T. Homma, E. Kitagawa, Y. Momose, M. S. Sato, M. Odani, H. Shimizu, M. Hasegawa-Mizusawa, R. Matsumoto, S. Mizukami, K. Fujita, M. Parveen, Y. Komatsu, and H. Iwahashi, *Genome-wide expression analysis of yeast response during exposure to 4°C,* Extremophiles **10**, 117 (2005).

[9] M. Redón, J. M. Guillamón, A. Mas, and N. Rozès, *Effect of growth temperature on yeast lipid composition and alcoholic fermentation at low temperature,* Eur. Food Res. Technol. **232**, 517 (2011).

[10] L. Ballester-Tomás, R. Pérez-Torrado, S. Rodríguez-Vargas, J. A. Prieto, and F. Randez-Gil, *Near-freezing effects on the proteome of industrial yeast strains of Saccharomyces cerevisiae,* J. Biotechnol. **221**, 70 (2016).

[11] B. Schade, G. Jansen, M. Whiteway, K. D. Entian, and D. Y. Thomas, *Cold adaptation in budding yeast,* Mol. Biol. Cell **15**, 5492 (2004).

[12] P. L. Privalov, *Cold denaturation of protein,* Crit. Rev. Biochem. Mol. Biol. **25**, 281 (1990).

[13] K. Gast, G. Damaschun, H. Damaschun, R. Misselwitz, and D. Zirwer, *Cold denaturation of yeast phosphoglycerate kinase: Kinetics of changes in secondary structure and compactness on unfolding and refolding,* Biochemistry **32**, 7747 (2002).

[14] J. Aguilera, F. Randez-Gil, and J. A. Prieto, *Cold response in Saccharomyces cerevisiae: New functions for old mechanisms,* FEMS Microbiol. Rev. **31**, 327 (2007).

[15] L. Zhang, K. Onda, R. Imai, R. Fukuda, H. Horiuchi, and A. Ohta, *Growth temperature downshift induces antioxidant response in Saccharomyces cerevisiae,* Biochem. Biophys. Res. Commun. **307**, 308 (2003).

[16] X. Du and H. Takagi, *N-Acetyltransferase Mpr1 confers freeze tolerance on Saccharomyces cerevisiae by reducing reactive oxygen species,* J. Biochem. **138**, 391 (2005).

[17] O. Kandror, N. Bretschneider, E. Kreydin, D. Cavalieri, and A. L. Goldberg, *Yeast adapt to near-freezing temperatures by STRE/Msn2,4-dependent induction of trehalose synthesis and certain molecular chaperones,* Mol. Cell **13**, 771 (2004).

[18] L. Feng, H. Jia, Y. Qin, Y. Song, S. Tao, and Y. Liu, *Rapid identification of major QTLS associated with near- freezing temperature tolerance in Saccharomyces cerevisiae,* Front. Microbiol. **0**, 2110 (2018).

[19] O. S. Venturelli, I. Zuleta, R. M. Murray, and H. El-Samad, *Population diversification in a yeast metabolic program promotes anticipation of environmental shifts,* PLoS Biol. **13**, e1002042 (2015).

[20] M. Kærn, T. C. Elston, W. J. Blake, and J. J. Collins, *Stochasticity in gene expression: from theories to phenotypes,* Nat. Rev. Genet. **6**, 451 (2005).

[21] M. Ackermann, *A functional perspective on phenotypic heterogeneity in microorganisms,* Nat. Rev. Microbiol. **13**, 497 (2015).

[22] M. Ackermann, *Microbial individuality in the natural environment,* ISME J. **7**, 465 (2012).

[23] Y. Taniguchi, P. J. Choi, G.-W. Li, H. Chen, M. Babu, J. Hearn, A. Emili, and X. S. Xie, *Quantifying E. coli proteome and transcriptome with single-molecule sensitivity in single cells,* Science **329**, 533 (2010).

[24] R. Milo and R. Phillips, *Cell Biology by the Numbers*, 1st ed. (Garland Science, 2015).

[25] L. Bruslind, *Microbiology* (Open Oregon State University, 2019).

[26] P. Doran, *Bioprocess Engineering Principles*, 2nd ed. (Academic, 2012) pp. 653–655.

[27] M. B. Miller and B. L. Bassler, *Quorum sensing in bacteria,* Annu. Rev. Microbiol **55**, 165 (2001).

[28] J. Gore, H. Youk, and A. van Oudenaarden, *Snowdrift game dynamics and facultative cheating in yeast,* Nature **459**, 253 (2009).

[29] J. H. Koschwanez, K. R. Foster, and A. W. Murray, *Sucrose utilization in budding yeast as a model for the origin of undifferentiated multicellularity,* PLoS Biol. **9**, e1001122 (2011).

[30] J. H. Koschwanez, K. R. Foster, and A. W. Murray, *Improved used of a public good selects for the evolution of undifferentiated multicellularity,* eLife **2**, e00367 (2013).

[31] C. Ratzke, J. Denk, and J. Gore, *Ecological suicide in microbes,* Nat. Ecol. Evol. **2**, 867 (2018).

[32] J. Postmus, A. B. Canelas, J. Bouwman, B. M. Bakker, W. van Gulik, M. J. Teixeira de Mattos, S. Brul, and G. J. Smits, *Quantitative analysis of the high temperature-induced glycolytic flux increase in Saccharomyces cerevisiae reveals dominant metabolic regulation,* J. Biol. Chem. **283**, 23524 (2008).

[33] R. M. Walsh and P. A. Martin, *Growth of Saccharomyces cerevisiae and Saccharomyces uvarum in a temperature gradient incubator,* J. Inst. Brew. **83**, 169 (1977).

[34] E. Dekel and U. Alon, *Optimality and evolutionary tuning of the expression level of a protein,* Nature **436**, 588 (2005).

[35] M. Scott and T. Hwa, *Bacterial growth laws and their applications,* Curr. Opin. Biotechnol. **22**, 559 (2011).

[36] V. Bharathi, A. Girdhar, A. Prasad, M. Verma, V. Taneja, and P. K. Patel, *Use of ade1 and ade2 mutations for development of a versatile red/white colour assay of amyloid-induced oxidative stress in Saccharomyces cerevisiae,* Yeast **33**, 607 (2016).

[37] N. Q. Balaban, *Persistence: mechanisms for triggering and enhancing phenotypic variability,* Curr. Opin. Genet. Dev. **21**, 768 (2011).

[38] H. C. Causton, B. Ren, S. S. Koh, C. T. Harbison, E. Kanin, E. G. Jennings, T. I. Lee, H. L. True, E. S. Lander, and R. A. Young, *Remodeling of yeast genome expression in response to environmental changes,* Mol. Biol. Cell **12**, 323 (2001).

[39] A. P. Gasch, P. T. Spellman, C. M. Kao, O. Carmel-Harel, M. B. Eisen, G. Storz, D. Botstein, and P. O. Brown, *Genomic expression programs in the response of yeast cells to environmental changes,* Mol. Biol. Cell **11**, 4241 (2000).

[40] K. Sugiyama, A. Kawamura, S. Izawa, and Y. Inoue, *Role of glutathione in heat-shock-induced cell death of Saccharomyces cerevisiae,* Biochem. J. **352**, 71 (2000).

[41] K. Sugiyama, S. Izawa, and Y. Inoue, *The Yap1p-dependent induction of glutathione synthesis in heat shock response of Saccharomyces cerevisiae,* J. Biol. Chem. **275**, 15535 (2000).

[42] J. F. Davidson, B. Whyte, P. H. Bissinger, and R. H. Schiestl, *Oxidative stress is involved in heat-induced cell death in Saccharomyces cerevisiae,* Proc. Natl Acad. Sci. USA **93**, 5116 (1996).

[43] F. M. Yakes and B. van Houten, *Mitochondrial DNA damage is more extensive and persists longer than nuclear DNA damage in human cells following oxidative stress,* Proc. Natl Acad. Sci. USA **94**, 514 (1997).

[44] E. Cabiscol, E. Piulats, P. Echave, E. Herrero, and J. Ros, *Oxidative stress promotes specific protein damage in Saccharomyces cerevisiae,* J. Biol. Chem. **275**, 27393 (2000).

[45] T. Bilinski, J. Litwinska, M. Blaszczynski, and A. Bajus, *Superoxide dismutase deficiency and the toxicity of the products of autooxidation of polyunsaturated fatty acids in yeast,* Biochim. Biophys. Acta **1001**, 102 (1989).

[46] D. J. Jamieson, *Oxidative stress responses of the yeast Saccharomyces cerevisiae,* Yeast **14**, 1511 (1998).

[47] B. Zechmann, L.-C. Liou, B. E. Koffler, L. Horvat, A. Tomašić, H. Fulgosi, and Z. Zhang, *Subcellular distribution of glutathione and its dynamic changes under oxidative stress in the yeast Saccharomyces cerevisiae,* FEMS Yeast Res. **11**, 631 (2011).

[48] C. Kumar, A. Igbaria, B. D'Autreaux, A.-G. Plansons, C. Junot, E. Godat, A. K. Bachhawat, A. Delaunay-Moisan, and M. B. Toledano, *Glutathione revisited: a vital function in iron metabolism and ancillary role in thiol-redox control,* EMBO J. **30**, 2044 (2011).

[49] M. B. Toledano, C. Kumar, N. Le Moan, D. Spector, and F. Tacnet, *The system biology of thiol redox system in Escherichia coli and yeast: differential functions in oxidative stress, iron metabolism and DNA synthesis,* FEBS Lett. **581**, 3598 (2007).

[50] M. T. Elskens, C. J. Jaspers, and M. J. Penninckx, *Glutathione as an endogenous sulfur source in the yeast Saccharomyces cerevisiae,* J. Gen. Microbiol. **137**, 637 (1991).

[51] K. Mehdi and M. J. Penninckx, *An important role for glutathione and γ-glutamyltranspeptidase in the supply of growth requirements during nitrogen starvation of the yeast Saccharomyces cerevisiae,* Microbiology **143**, 1885 (1997).

[52] M. Thorsen, T. Jacobson, R. Vooijs, C. Navarrete, T. Bliek, H. Schat, and M. J. Tamás, *Glutathione serves an extracellular defence function to decrease arsenite accumulation and toxicity in yeast,* Mol. Microbiol. **84**, 1177 (2012).

[53] G. G. Perrone, C. M. Grant, and I. W. Dawes, *Genetic and environmental factors influencing glutathione homeostasis in Saccharomyces cerevisiae,* Mol. Biol. Cell **16**, 218 (2005).

[54] D. Giustarini, D. Tsikas, G. Colombo, A. Milzani, I. Dalle-Donne, P. Fanti, and R. Rossi, *Pitfalls in the analysis of the physiological antioxidant glutathione (GSH) and its disulphide (GSSG) in biological samples: an elephant in the room,* J. Chromatogr. B Analyt. Technol. Biomed. Life Sci. **1019**, 21 (2016).

[55] A. R. T. S. Araujo, L. M. F. S. Saraiva, and J. L. F. C. Lima, *Determination of total and oxidized glutathione in human whole blood with a sequential injection analysis system,* Talanta **74**, 1511 (2008).

[56] C. M. Grant, F. H. MacIver, and I. W. Dawes, *Glutathione is an essential metabolite required for resistance to oxidative stress in the yeast Saccharomyces cerevisiae,* Curr. Genet. **29**, 511 (1996).

[57] A. Bourbouloux, P. Shahi, A. Chakladar, S. Delrot, and A. K. Bachhawat, *Hgt1p, a high affinity glutathione transporter from the yeast Saccharomyces cerevisiae,* J. Biol. Chem. **275**, 13259 (2000).

[58] M. Dhaoui, F. Auchère, P.-L. Blaiseau, E. Lesuisse, A. Landoulsi, J.-M. Camadro, R. Haguenauer-Tsapis, and N. Belgareh-Touzé, *Gex1 is a yeast glutathione exchanger that interferes with pH and redox homeostasis,* Mol. Biol. Cell **22**, 2054 (2011).

[59] K. Kiriyama, K. Y. Hara, and A. Kondo, *Extracellular glutathione fermentation using engineered Saccharomyces cerevisiae expressing a novel glutathione exporter,* Appl. Microbiol. Biotechnol. **96**, 1021 (2012).

[60] L. Dai, D. Vorselen, K. S. Korolev, and J. Gore, *Generic indicators for loss of resilience before a tipping point leading to population collapse,* Science **336**, 1175 (2012).

[61] S. H. Strogatz, *Nonlinear dynamics and chaos: with applications to physics, biology, chemistry, and engineering* (Westview, 1994).

[62] M. Mojtahedi, A. Skupin, J. Zhou, I. G. Castaño, R. Y. Y. Leong-Quong, H. Chang, K. Trachana, A. Giuliani, and S. Huang, *Cell fate decision as high-dimensional critical state transition,* PLoS Biol. **14**, e2000640 (2016).

[63] J. Garcia-Ojalvo, J. M. Sancho, and L. Ramirez-Piscina, *A nonequilibrium phase transition with colored noise,* Phys. Lett. A **168**, 35 (1992).

[64] H. Youk and W. A. Lim, *Secreting and sensing the same molecule allows cells to achieve versatile social behaviors,* Science **343**, 1242782 (2014).

[65] C. Trapnell, A. Roberts, L. Goff, G. Pertea, D. Kim, D. R. Kelley, H. Pimentel, S. L. Salzberg, J. L. Rinn, and L. Pachter, *Differential gene and transcript expression analysis of RNA-seq experiments with TopHat and Cufflinks,* Nat. Protoc. **7**, 562 (2012).

[66] C. Riccardi and I. Nicoletti, *Analysis of apoptosis by propidium iodide staining and flow cytometry,* Nat. Protoc. **1**, 1458 (2006).

[67] T. Homma, H. Iwahashi, and Y. Komatsu, *Yeast gene expression during growth at low temperature,* Cryobiology **46**, 230 (2003).

[68] L. T. Siew, P. Daran-Lapujade, M. C. Walsh, J. T. Pronk, and J. M. Daran, *Acclimation of Saccharomyces cerevisiae to low temperature: A chemostat-based transcriptome analysis,* Mol. Biol. Cell **18**, 5100 (2007).

[69] E. R. Stadtman and R. L. Levine, *Free radical-mediated oxidation of free amino acids and amino acid residues in proteins,* Amino acids **25**, 207 (2003).

[70] C. Garmendia-Torres, O. Tassy, A. Matifas, N. Molina, and G. Charvin, *Multiple inputs ensure yeast cell size homeostasis during cell cycle progression,* eLife **7**, e34025 (2018).

[71] S. Morlot, J. Song, I. Léger-Silvestre, A. Matifas, O. Gadal, and G. Charvin, *Excessive rDNA transcription drives the disruption in nuclear homeostasis during entry into senescence in budding yeast,* Cell Rep. **28**, 408 (2019).

[72] G. Perrino, S. Napolitano, F. Galdi, A. La Regina, D. Fiore, T. Giuliano, M. di Bernardo, and D. di Bernardo, *Automatic synchronisation of the cell cycle in budding yeast through closed-loop feedback control,* Nat. Commun. **12**, 1 (2021).

[73] G. Charvin, C. Oikonomou, E. D. Siggia, and F. R. Cross, *Origin of irreversibility of cell cycle start in budding yeast,* PLoS Biol. **8**, e1000284 (2010).

[74] P. Jorgensen, J. L. Nishikawa, B.-J. Breitkreutz, and M. Tyers, *Systematic identification of pathways that couple cell growth and division in yeast,* Science **297**, 395 (2002).

[75] M. Costanzo, J. L. Nishikawa, X. Tang, J. S. Millman, O. Schub, K. Breitkreuz, D. Dewar, I. Rupes, B. Andrews, and M. Tyers, *CDK activity antagonizes Whi5, an inhibitor of G1/S transcription in yeast,* Cell **117**, 899 (2004).

[76] P. Palumbo, M. Vanoni, V. Cusimano, S. Busti, F. Marano, C. Manes, and L. Alberghina, *Whi5 phosphorylation embedded in the G1/S network dynamically controls critical cell size and cell fate,* Nat. Commun. **7**, 1 (2016).

[77] H. X. Chao, C. E. Poovey, A. A. Privette, G. D. Grant, H. Y. Chao, J. G. Cook, and J. E. Purvis, *Orchestration of DNA damage checkpoint dynamics across the human cell cycle,* Cell Syst. **5**, 445 (2017).

[78] L. Teufel, K. Tummler, M. Flöttmann, A. Herrmann, N. Barkai, and E. Klipp, *A transcriptome-wide analysis deciphers distinct roles of G1 cyclins in temporal organization of the yeast cell cycle,* Sci. Rep. **9**, 1 (2019).

[79] P. Dong, C. Zhang, B.-T. Parker, L. You, and B. Mathey-Prevot, *Cyclin D/CDK4/6 activity controls G1 length in mammalian cells,* PloS one **13**, e0185637 (2018).

[80] F. Estruch and M. Carlson, *Two homologous zinc finger genes identified by multicopy suppression in a SNF1 protein kinase mutant of Saccharomyces cerevisiae,* Mol. Cell. Biol. **13**, 3872 (1993).

[81] M. T. Martínez-Pastor, G. Marchler, C. Schüller, A. Marchler-Bauer, H. Ruis, and F. Estruch, *The Saccharomyces cerevisiae zinc finger proteins Msn2p and Msn4p are required for transcriptional induction through the stress response element (STRE).* EMBO J. **15**, 2227 (1996).

[82] F. Estruch, *Stress-controlled transcription factors, stress-induced genes and stress tolerance in budding yeast,* FEMS Microbiol. Rev. **24**, 469 (2000).

[83] C. M. Grant, S. Luikenhuis, A. Beckhouse, M. Soderbergh, and I. W. Dawes, *Differential regulation of glutaredoxin gene expression in response to stress conditions in the yeast Saccharomyces cerevisiae,* Biochim. Biophys. Acta, Gene Struct. Expression **1490**, 33 (2000).

[84] M. Amorós and F. Estruch, *Hsf1p and Msn2/4p cooperate in the expression of Saccharomyces cerevisiae genes HSP26 and HSP104 in a gene- and stress type-dependent manner,* Mol. Microbiol. **39**, 1523 (2001).

[85] M. R. Grably, A. Stanhill, O. Tell, and D. Engelberg, *HSF and Msn2/4p can exclusively or cooperatively activate the yeast HSP104 gene,* Mol. Microbiol. **44**, 21 (2002).

[86] M. Scott, C. W. Gunderson, E. M. Mateescu, Z. Zhang, and T. Hwa, *Interdependence of cell growth and gene expression: Origins and consequences,* Science **330**, 1099 (2010).

[87] M. Basan, *Resource allocation and metabolism: the search for governing principles,* Curr. Opin. Microbiol. **45** (2018), 10.1016/j.mib.2018.02.008.

[88] K. Kawata, H. Wakida, T. Yamada, K. Taniue, H. Han, M. Seki, Y. Suzuki, and N. Akimitsu, *Metabolic labeling of RNA using multiple ribonucleoside analogs enables the simultaneous evaluation of RNA synthesis and degradation rates,* Genome Res. **30**, 1481 (2020).

[89] B. Neymotin, R. Athanasiadou, and D. Gresham, *Determination of in vivo RNA kinetics using RATE-seq,* RNA **20**, 1645 (2014).

[90] F. Miura, N. Kawaguchi, M. Yoshida, C. Uematsu, K. Kito, Y. Sakaki, and T. Ito, *Absolute quantification of the budding yeast transcriptome by means of competitive PCR between genomic and complementary DNAs,* BMC Genet. **9**, 574 (2008).

[91] U. Nagalakshmi, Z. Wang, K. Waern, C. Shou, D. Raha, M. Gerstein, and M. Snyder, *The transcriptional landscape of the yeast genome defined by RNA sequencing,* Science **320**, 1344 (2008).

[92] V. Pelechano, S. Chávez, and J. E. Pérez-Ortín, *A complete set of nascent transcription rates for yeast genes,* PLoS Biol. **5**, e15442 (2010).

[93] S. E. Munchel, R. K. Shultzaberger, N. Takizawa, and K. Weis, *Dynamic profiling of mRNA turnover reveals gene-specific and system-wide regulation of mRNA decay,* Mol. Biol. Cell **22**, 2787 (2011).

[94] M. Adler and U. Alon, *Fold-change detection in biological systems,* Curr. Opin. Syst. Biol. **8**, 81 (2018).

[95] J. Chiu, C. M. Tactacan, S.-X. Tan, R. C. Y. Lin, M. A. Wouters, and I. W. Dawes, *Cell cycle sensing of oxidative stress in Saccharomyces cerevisiae by oxidation of a specific cysteine residue in the transcription factor Swi6p,* J. Biol. Chem. **286**, 5204 (2011).

[96] J. Chiu and I. W. Dawes, *Redox control of cell proliferation,* Trends Cell Biol. **22**, 592 (2012).

[97] G. E. Neurohr, R. L. Terry, J. Lengefeld, M. Bonney, G. P. Brittingham, F. Moretto, T. P. Miettinen, L. P. Vaites, L. M. Soares, J. A. Paulo, J. W. Harper, S. Buratowski, S. Manalis, F. J. van Werven, L. J. Holt, and A. Amon, *Excessive cell growth causes cytoplasm dilution and contributes to senescence,* Cell **176**, 1083 (2019).

[98] G. E. Neurohr, R. L. Terry, A. Sandikci, K. Zou, H. Li, and A. Amon, *Deregulation of the G1/S-phase transition is the proximal cause of mortality in old yeast mother cells,* Genes Dev. **32**, 1075 (2018).

[99] S. Klumpp, M. Scott, S. Pedersen, and T. Hwa, *Molecular crowding limits translation and cell growth,* Proc. Natl Acad. Sci. USA **110**, 16754 (2013).

[100] M. Kafri, E. Metzl-Raz, G. Jona, and N. Barkai, *The Cost of Protein Production,* Cell Rep. **14**, 22 (2016).

[101] E. Metzl-Raz, M. Kafri, G. Yaakov, and N. Barkai, *Gene transcription as a limiting factor in protein production and cell growth,* G3: Genes Genomes Genet. **10**, 3229 (2020).

[102] Q. Zhang, E. Brambilla, R. Li, H. Shi, M. C. Lagomarsino, and B. Sclavi, *A decrease in transcription capacity limits growth rate upon translation inhibition,* mSystems **5** (2020), 10.1128/mSystems.00575-20.

[103] D. A. Charlebois, K. Hauser, S. Marshall, and G. Balázsi, *Multiscale effects of heating and cooling on genes and gene networks,* Proc. Natl Acad. Sci. USA **115**, E10797 (2018).

[104] K. Sidaway-Lee, M. J. Costa, D. A. Rand, B. Finkenstadt, and S. Penfield, *Direct measurement of transcription rates reveals multiple mechanisms for configuration of the Arabidopsis ambient temperature response,* Genome Res. **15**, 1 (2014).

[105] L. Castells-Roca, J. García-Martínez, J. Moreno, E. Herrero, G. Bellí, and J. E. Pérez-Ortín, *Heat shock response in yeast involves changes in both transcription rates and mRNA stabilities,* PLoS Biol. **6**, e17272 (2011).

[106] P. Maher, *The effects of stress and aging on glutathione metabolism,* Ageing Res. Rev. **4**, 288 (2005).

[107] R. V. Sekhar, S. G. Patel, A. P. Guthikonda, M. Reid, A. Balasubramanyam, G. E. Taffet, and F. Jahoor, *Deficient synthesis of glutathione underlies oxidative stress in aging and can be corrected by dietary cysteine and glycine supplementation,* Am. J. Clin. Nutr. **94**, 847 (2011).

[108] M. Valko, D. Leibfritz, J. Moncol, M. T. D. Cronin, M. Mazur, and J. Telser, *Free radicals and antioxidants in normal physiological functions and human disease,* Int. J. Biochem. Cell Biol. **39**, 44 (2007).

[109] A. Ayer, C. W. Gourlay, and I. W. Dawes, *Cellular redox homeostasis, reactive oxygen species and replicative ageing in Saccharomyces cerevisiae,* FEMS Yeast Res. **14**, 60 (2014).

[110] M. T. Aung-Htut, A. Ayer, M. Breitenbach, and I. W. Dawes, *Aging Research in Yeast. Subcellular biochemistry*, Vol. 57 (Subcell Biochem, 2011) pp. 13–54.

[111] M. Breitenbach, P. Laun, J. R. Dickinson, A. Klocker, M. Rinnerthaler, I. W. Dawes, M. T. Aung-Htut, L. Breitenbach-Koller, A. Caballero, T. Nyström, S. Büttner, T. Eisenberg, F. Madeo, and M. Ralser, *Aging Research in Yeast. Subcellular Biochemistry*, Vol. 57 (Springer, Dordrecht, 2011) pp. 55–78.

[112] P. Laun, A. Pichova, F. Madeo, J. Fuchs, A. Ellinger, S. Kohlwein, I. Dawes, K. U. Fröhlich, and M. Breitenbach, *Aged mother cells of Saccharomyces cerevisiae show markers of oxidative stress and apoptosis,* Mol. Microbiol. **39**, 1166 (2001).

[113] Y. T. Lam, M. T. Aung-Htut, Y. L. Lim, H. Yang, and I. W. Dawes, *Changes in reactive oxygen species begin early during replicative aging of Saccharomyces cerevisiae cells,* Free Radic. **50**, 963 (2011).

[114] P. Fabrizio, L. Battistella, R. Vardavas, C. Gattazzo, L.-L. Liou, A. Diaspro, J. W. Dossen, E. B. Gralla, and V. D. Longo, *Superoxide is a mediator of an altruistic aging program in Saccharomyces cerevisiae,* J. Cell Biol. **166**, 1055 (2004).

[115] E. Herker, H. Jungwirth, K. A. Lehmann, C. Maldener, K.-U. Fröhlich, S. Wissing, S. Büttner, M. Fehr, S. Sigrist, and F. Madeo, *Chronological aging leads to apoptosis in yeast,* J. Cell Biol. **164**, 501 (2004).

[116] A. Owsiak, G. Bartosz, and T. Bilinski, *Oxidative stress during aging of the yeast in a stationary culture and its attenuation by antioxidants,* Cell Biol. Int. **34**, 731 (2010).

[117] Y. T. Lam, R. Stocker, and I. W. Dawes, *The lipophilic antioxidants α-tocopherol and coenzyme Q10 reduce the replicative lifespan of Saccharomyces cerevisiae,* Free Radic. **49**, 237 (2010).

[118] H. J. Shields, A. Traa, and J. M. Van Raamsdonk, *Beneficial and detrimental effects of reactive oxygen species on lifespan: A comprehensive review of comparative and experimental studies,* Front. Cell Dev. Biol. **9**, 181 (2021).

[119] D. S. Laman Trip and H. Youk, *Yeasts collectively extend the limits of habitable temperatures by secreting glutathione,* Nat. Microbiol. **5**, 943 (2020).

[120] M. A. Sheff and K. S. Thorn, *Optimized cassettes for fluorescent protein tagging in Saccharomyces cerevisiae,* Yeast **21**, 661 (2004).

[121] T. Baptista and D. Devys, *Saccharomyces cerevisiae metabolic labeling with 4-thiouracil and the quantification of newly synthesized mRNA as a proxy for RNA polymerase II activity,* J. Vis. Exp. , e57982 (2018).

[122] R. Patro, G. Duggal, M. I. Love, R. A. Irizarry, and C. Kingsford, *Salmon provides fast and bias-aware quantification of transcript expression,* Nat. Methods **14**, 417 (2017).

[123] C. Soneson, M. I. Love, and M. D. Robinson, *Differential analyses for RNA-seq: Transcript-level estimates improve gene-level inferences,* F1000Research **4**, 1521 (2015).

[124] D. J. Jamieson, *Saccharomyces cerevisiae has distinct adaptive responses to both hydrogen peroxide and menadione,* J. Bacteriol. Res. **174**, 6678 (1992).

[125] K. M. Schmoller, J. J. Turner, M. Kõivomägi, and J. M. Skotheim, *Dilution of the cell cycle inhibitor Whi5 controls budding-yeast cell size,* Nature **526**, 268 (2015).

[126] J. Zhang, C. Schneider, L. Ottmers, R. Rodriguez, A. Day, J. Markwardt, and B. L. Schneider, *Genomic scale mutant hunt identifies cell size homeostasis genes in S. cerevisiae,* Curr. Biol. **12**, 1992 (2002).

[127] J. D. Barrass, J. E. A. Reid, Y. Huang, R. D. Hector, G. Sanguinetti, J. D. Beggs, and S. Granneman, *Transcriptome-wide RNA processing kinetics revealed using extremely short 4tU labeling,* Genome Res. **16**, 1 (2015).

[128] K. Shikama and T. Yamazaki, *Denaturation of catalase by freezing and thawing,* Nature **190**, 83 (1961).

[129] M. Vanoni, M. Vai, and G. Frascotti, *Effects of temperature on the yeast cell cycle analyzed by flow cytometry,* Cytometry **5**, 530 (1984).

[130] L. Dai, K. S. Korolev, and J. Gore, *Relation between stability and resilience determines the performance of early warning signals under different environmental drivers,* Proc. Natl Acad. Sci. USA **112**, 10056 (2015).

[131] K. Drescher, C. D. Nadell, H. A. Stone, N. S. Wingreen, and B. L. Bassler, *Solutions to the public goods dilemma in bacterial biofilms,* Curr. Biol. **24**, 50 (2014).

[132] T. Artemova, Y. Gerardin, C. Dudley, N. M. Vega, and J. Gore, *Isolated cell behavior drives the evolution of antibiotic resistance,* Mol. Syst. Biol. **11**, 822 (2015).

[133] P. A. Stephens, W. J. Sutherland, and R. P. Freckleton, *What Is the Allee Effect?* Oikos **87**, 185 (1999).

[134] S. Schink, Z. Gough, E. Biselli, M. G. Huiman, Y.-F. Chang, M. Basan, and U. Gerland, *MetA is a 'thermal fuse' that arrests growth and protects Escherichia coli at elevated temperatures,* bioRxiv , 2021.06.14.448417 (2021).

[135] J. T. Hancock, R. Desikan, and S. J. Neill, *Role of reactive oxygen species in cell signalling pathways,* Biochem. Soc. Trans. **29**, 345 (2001).

[136] H. Sauer, M. Wartenberg, and J. Hescheler, *Reactive oxygen species as intracellular messengers during cell growth and differentiation,* Cell. Physiol. Biochem. **11**, 173 (2001).

[137] G. Poli, G. Leonarduzzi, F. Biasi, and E. Chiarpotto, *Oxidative stress and cell signalling,* Curr. Med. Chem. **11**, 1163 (2004).

[138] J. Lee, A. Romeo, and D. J. Kosman, *Transcriptional remodeling and G1 arrest in dioxygen stress in Saccharomyces cerevisiae,* J. Biol. Chem. **271**, 24885 (1996).

[139] V. Wanke, K. Accorsi, D. Porro, F. Esposito, T. Russo, and M. Vanoni, *In budding yeast, reactive oxygen species induce both RAS-dependent and RAS-independent cell cycle-specific arrest,* Mol. Microbiol. **32**, 753 (1999).

[140] N. Alic, V. J. Higgins, and I. W. Dawes, *Identification of a Saccharomyces cerevisiae gene that is required for G1 arrest in response to the lipid oxidation product linoleic acid hydroperoxide,* Mol. Biol. Cell **12**, 1801 (2001).

[141] C. S. Fong, M. D. Temple, N. Alic, J. Chiu, M. Durchdewald, G. W. Thorpe, V. J. Higgins, and I. W. Dawes, *Oxidant-induced cell-cycle delay in Saccharomyces cerevisiae: the involvement of the SWI6 transcription factor,* FEMS Yeast Res. **8**, 386 (2008).

[142] J. A. Flattery-O'Brien and I. W. Dawes, *Hydrogen peroxide causes RAD9-dependent cell cycle arrest in G2 in Saccharomyces cerevisiae whereas menadione causes G1 arrest independent of RAD9 function,* J. Biol. Chem. **273**, 8564 (1998).

[143] M. Shapira, E. Segal, and D. Botstein, *Disruption of yeast forkhead-associated cell cycle transcription by oxidative Stress,* Mol. Biol. Cell **15**, 5659 (2004).

[144] A. L. Rose, *The influence of extracellular superoxide on iron redox chemistry and bioavailability to aquatic microorganisms,* Front. Microbiol. **3**, 124 (2012).

[145] J. K. Lee, K. L. Walker, H. S. Han, J. Kang, F. B. Prinz, R. M. Waymouth, H. G. Nam, and R. N. Zare, *Spontaneous generation of hydrogen peroxide from aqueous microdroplets,* Proc. Natl Acad. Sci. USA **116**, 19294 (2019).

[146] B. Halliwell, *Oxidative stress in cell culture: an under-appreciated problem?* FEBS Lett. **540**, 3 (2003).

[147] V. L. Arcus, E. J. Prentice, J. K. Hobbs, A. J. Mulholland, M. W. Van Der Kamp, C. R. Pudney, E. J. Parker, and L. A. Schipper, *On the temperature dependence of enzyme-catalyzed rates,* Biochemistry **55**, 1681 (2016).

[148] M. E. Peterson, R. M. Daniel, M. J. Danson, and R. Eisenthal, *The dependence of enzyme activity on temperature: determination and validation of parameters,* Biochem. J **402**, 331 (2007).

[149] K. Matsumoto, M. Nyui, M. Kamibayashi, T. Ozawa, I. Nakanishi, and K. Anzai, *Temperature-dependent free radical reaction in water,* J. Clin. Biochem. Nutr. **50**, 40 (2012).

[150] D. Cruz-Garcia, N. Brouwers, V. Malhotra, and A. J. Curwin, *Reactive oxygen species triggers unconventional secretion of antioxidants and acb1,* J. Cell Biol. **219** (2020), 10.1083/jcb.201905028.

[151] S. A. Golladay, S. H. Park, and A. E. Aust, *Efflux of reduced glutathione after exposure of human lung epithelial cells to crocidolite asbestos,* Environ. Health Perspect. **105**, 1273 (1997).

[152] N. Ballatori, S. M. Krance, R. Marchan, and C. L. Hammond, *Plasma membrane glutathione transporters and their roles in cell physiology and pathophysiology,* Mol. Aspects Med. **30**, 13 (2009).

[153] S. Iyer-Biswas, C. S. Wright, J. T. Henry, K. Lo, S. Burov, Y. Lin, G. E. Crooks, S. Crosson, A. R. Dinner, and N. F. Scherer, *Scaling laws governing stochastic growth and division of single bacterial cells,* Proc. Natl Acad. Sci. USA **111**, 15912 (2014).

[154] M. Kafri, E. Metzl-Raz, F. Jonas, and N. Barkai, *Rethinking cell growth models,* FEMS Yeast Res. **16**, 81 (2016).

[155] S. Iyer, D. Le, B. R. Park, and M. Kim, *Distinct mechanisms coordinate transcription and translation under carbon and nitrogen starvation in Escherichia coli,* Nat. Microbiol. **3**, 741 (2018).

[156] M. Basan, T. Honda, D. Christodoulou, M. Hörl, Y. Chang, E. Leoncini, A. Mukherjee, H. Okano, B. R. Taylor, J. M. Silverman, C. Sanchez, J. R. Williamson, J. Paulsson, T. Hwa, and U. Sauer, *A universal trade-off between growth and lag in fluctuating environments,* Nature **584**, 470 (2020).

[157] N. M. Belliveau, G. Chure, C. L. Hueschen, H. G. Garcia, J. Kondev, D. Fisher, J. A. Theriot, and R. Phillips, *Fundamental limits on the rate of bacterial growth and their influence on proteomic composition,* Cell Syst. **12**, 924 (2021).

[158] A. R. Zomorrodi and D. Segrè, *Genome-driven evolutionary game theory helps understand the rise of metabolic interdependencies in microbial communities,* Nat. Commun. **8**, 1 (2017).

ACKNOWLEDGMENTS

I am grateful to my family, friends and colleagues for their support for my scientific passion. I particularly thank my colleagues for the memorable and exciting time at BN. Hyun, I am thankful for our insightful discussions, your guidance, continued support and belief in my ideas. I thoroughly enjoyed our original and exciting projects. Théo, thanks for our countless coffees and discussions, your patience with me and your dedication to our time-consuming experiments. Without your contributions our cool project would not have come to fruition. Yaroslav and Greg, I am grateful for your support throughout my time at BN. Finally, I express my gratitude to Anke, Jan, Jérémie, Sasha and the rest of the support staff for their chats, help and readiness to keep BN running smoothly.

To my friends, I am thankful for our chats, drinks, dinners, trips and time together. Finally, I thank Christine and my family for their continued patience, support and encouragements throughout the years.

Curriculum Vitæ

Diederik Scato Laman Trip

2017–2022	PhD in Biophysics Kavli Institute of Nanoscience, Delft University of Technology
2013–2017	Master in Mathematics *(with distinction)* Leiden University
2012–2016	Bachelor in Life Science & Technology *(with distinction)* Leiden University and Delft University of Technology
2010–2013	Bachelor in Mathematics Leiden University
2004–2010	Gymnasium Lyceum Sancta Maria, Haarlem
09-08-1992	Born in Haarlem, The Netherlands *Thesis:* Enabling yeast replication in extreme cold and heat *Promotors:* Prof. dr. H. Youk and prof. dr. Y. M. Blanter *Copromotor:* Dr. G. E. Bokinsky

LIST OF PUBLICATIONS

In this dissertation

5. D. S. Laman Trip, T. Maire, H. Youk, *Fundamental limits to progression of cellular life in frigid environments*, In review (2022).

4. D. S. Laman Trip, H. Youk, *Yeasts collectively extend the limits of habitable temperatures by secreting glutathione*, **Nature Microbiology**, 5, 7, p. 943-954 (2020).

Other

3. D. S. Laman Trip, W. N. van Wieringen, *A parallel algorithm for ridge-penalized estimation of the multivariate exponential family from data of mixed types*, **Statistics and Computing**, 31, 41 (2021).

2. D. S. Laman Trip, T. Maire, H. Youk, *Evaluation of Schink et al.: Having the Gem Shine through a Fog*, **Cell Systems**, 9, 1, p. 3-7 (2019).

1. P. Ketterer, A. N. Ananth, D. S. Laman Trip, A. Mishra and E. Bertosin and M. Ganji and J. van der Torre and P. Onck and H. Dietz and C. Dekker, *DNA origami scaffold for studying intrinsically disordered proteins of the nuclear pore complex*, **Nature Communications**, 9, 902 (2018).